

University of Bath



**PHD**

## **Quantification and Control of Cohesive and Adhesive Forces in Dry Powder Inhaler Formulations**

Begat, Philippe Michel

*Award date:*  
2004

*Awarding institution:*  
University of Bath

[Link to publication](#)

### **General rights**

Copyright and moral rights for the publications made accessible in the public portal are retained by the authors and/or other copyright owners and it is a condition of accessing publications that users recognise and abide by the legal requirements associated with these rights.

- Users may download and print one copy of any publication from the public portal for the purpose of private study or research.
- You may not further distribute the material or use it for any profit-making activity or commercial gain
- You may freely distribute the URL identifying the publication in the public portal ?

### **Take down policy**

If you believe that this document breaches copyright please contact us providing details, and we will remove access to the work immediately and investigate your claim.

Download date: 13. May. 2019

# Quantification and Control of Cohesive and Adhesive Forces in Dry Powder Inhaler Formulations

Submitted by

**Philippe Michel Begat**

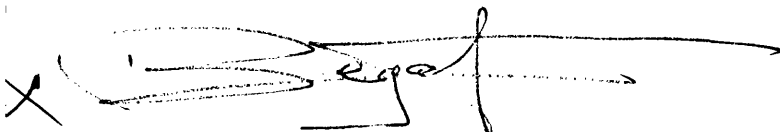
For the degree of Doctor of Philosophy

of the University of Bath

November 2004

## COPYRIGHT

Attention is drawn to the fact that copyright of this thesis rests with its author. This copy of the thesis has been supplied on condition that anyone who consults it is understood to recognise that its copyrights rests with its author and that no quotation from the thesis and no information derived from it may be published without the prior written consent of the author.

A handwritten signature in black ink, appearing to read 'Philippe Michel Begat', with a long horizontal flourish extending to the right.

UMI Number: U193851

All rights reserved

INFORMATION TO ALL USERS

The quality of this reproduction is dependent upon the quality of the copy submitted.

In the unlikely event that the author did not send a complete manuscript and there are missing pages, these will be noted. Also, if material had to be removed, a note will indicate the deletion.



UMI U193851

Published by ProQuest LLC 2013. Copyright in the Dissertation held by the Author.  
Microform Edition © ProQuest LLC.

All rights reserved. This work is protected against  
unauthorized copying under Title 17, United States Code.



ProQuest LLC  
789 East Eisenhower Parkway  
P.O. Box 1346  
Ann Arbor, MI 48106-1346

UNIVERSITY OF BATH  
LIBRARY  
40 23 AUG 2005  
Ph.D.



This thesis may be made available for consultation within the University Library  
and may be photocopied or lent to other libraries for the purpose of  
consultation.

*To my wife.*

## Acknowledgments

The author wishes to express his gratitude and utmost appreciation for the guidance, inspiration, suggestions, criticism and support that Dr Robert Price and Dr David Morton have given throughout the course of this investigation. The author is also grateful to Professor John Staniforth, who organised this project in the first place. Sincere appreciations are given to past and present members of the Pharmaceutical Technology Research Group. Special thanks are given to Kevin Smith and Ade Olatokun for their technical support. Special thanks to Louise Pettit for reading the manuscript.

The author would like to express his gratitude for his whole family for their years of patience, affection and encouragement. Finally, the author would like to express his deepest appreciation to his wife, Cecile, for her continuing encouragement, patience, understanding and love, which played a critical part in the realisation of this thesis.

## Scientific Publications

P. Begat, P. M. Young, S. Edge, J. S. Kaerger, and R. Price. The effect of mechanical processing on surface stability of pharmaceutical powders: Visualization by atomic force microscopy. *J. Pharm. Sci.* **92**: 611-620 (2003).

P. Begat, D. A. V. Morton, J. N. Staniforth, and R. Price. The cohesive-adhesive balances in dry powder inhaler formulations I: Direct quantification by atomic force microscopy. *Pharm. Res.* **21**: 1591-1597 (2004).

P. Begat, D. A. V. Morton, J. N. Staniforth, and R. Price. The cohesive-adhesive balances in dry powder inhaler formulations II: Influence on fine particle delivery characteristics. *Pharm. Res.* **21**: 1826-1833 (2004).

P. Begat, D. A. V. Morton, J. N. Staniforth, and R. Price. The influence of force control agents on the adhesive-cohesive balance in dry powder inhaler formulations. *Pharm. Res.* **Submitted**: (2005).

# Quantification and Control of Cohesive and Adhesive Forces in Dry Powder Inhaler Formulations

By P. Begat

Department of Pharmacy, University of Bath

## Abstract

Dry powder inhaler (DPI) formulations are commonly based on a mixture of coarse carrier, typically lactose, and micronised drug. The de-aggregation and dispersion properties of respirable particles, as well as the stability of the formulation, are associated with a delicate balance of the cohesive and adhesive interaction forces within the powder blend. This study describes the development of a novel atomic force microscopy (AFM) based technique to assess the dominant particulate interactions governing behaviour of such systems, and the optimisation and control of these interaction forces by the selective introduction of force control agents (FCAs) together with a mixing procedure capable of producing effective nano-layer coating within DPI formulations.

The atomic force microscope (AFM) colloid probe technique was used to measure the adhesive and cohesive force characteristics of dry powder systems containing an active component (budesonide, salbutamol sulphate) and the alpha-lactose monohydrate excipient. To minimise variations in contact area between colloid probes and substrates, nanometre smooth crystal surfaces of the drugs and

the excipient were prepared. A cohesive-adhesive balance (CAB) graphs was developed to allow direct comparison of the interaction forces occurring in model carrier-based formulations.

Aerodynamic particle analyses together with *in vitro* characterisation of model DPI formulations revealed a paradoxical relationship between particle cohesive strength and de-agglomeration efficiencies of drug only formulations, where an increase in cohesive strength led to a higher fine particle fraction. A possible explanation for the variation in the fluidisation and aerosolisation properties between low and high cohesive particles was modelled on the relationship between cohesion, metastable agglomerate size and the resulting aerodynamic drag force acting on the fluidised agglomerates. The addition of a fine particle lactose carrier influenced the drug deposition patterns in different ways depending on the relative cohesive and adhesive force balances within the formulation.

In order to improve dry powder formulation delivery characteristics, the influence of force control agents (FCAs) on the properties and performances of model DPI formulations was investigated. Three FCAs were chosen for their low surface energetic properties: leucine, lecithin and magnesium stearate. The cohesive and adhesive dependencies were controlled by conditioning either the drug or the carrier with an FCA before mixing in order to create selective modifications of the inter-particulate interactions within the dry powder formulation. This was achieved by first using a high energetic process (mechanofusion) following a low energetic process (Turbula). Radical modifications in the behaviour of the formulation performances, anticipated by CAB-graph analyses, were subsequently observed.

This work emphasised that the CAB analysis method can be utilised for pre-formulation studies in the design of new formulation systems for dry powder

inhalers. The work also confirmed the potential value of the use of force control agents together with the Mechanofusion process in the preparation of DPI formulations.

# Contents

List of Figures.....	vi
List of Tables.....	xii
<b>Chapter 1 Introduction .....</b>	<b>1</b>
1.1. General Introduction.....	1
1.2. Particle Interaction Fundamentals.....	4
1.2.1. Forces Contributing to Particle Interaction.....	4
1.2.1.1. Lifshitz-van der Waals Forces.....	5
1.2.1.2. Electrostatic Forces .....	13
1.2.1.3. Capillary Forces .....	15
1.2.2. Factors Influencing Adhesions.....	16
1.2.2.1. Particle Size .....	16
1.2.2.2. Particle Shape and Roughness .....	17
1.2.2.3. Surface Energy .....	19
1.2.2.4. Relative Humidity.....	19
1.3. Particle Physical State .....	21
1.3.1. The Crystalline State.....	21
1.3.2. Crystal Habit .....	22
1.3.3. Polymorphism .....	22
1.3.4. The Amorphous State.....	23
1.4. DPI Formulation Development .....	24
1.4.1. Particle Engineering Techniques.....	25
1.4.2. The Use of Coarse Carrier Particles .....	27
1.4.3. Addition of Fine Excipient Particles.....	29

1.4.4.	Force Control Agent (FCA) .....	30
1.5.	Aim of the Study .....	31
1.6.	References.....	32
<b>Chapter 2</b>	<b>Materials and Methods.....</b>	<b>47</b>
2.1.	Materials .....	47
2.1.1.	Pharmaceutical Ingredients .....	47
2.1.2.	Liquids .....	50
2.2.	Particle Size Analysis .....	50
2.2.1.	Light Scattering Analysis .....	50
2.2.2.	Time-of-Flight Analysis .....	51
2.3.	Particle Shape Analysis .....	52
2.3.1.	Scanning Electron Microscopy (SEM) .....	52
2.3.2.	Atomic Force Microscopy (AFM) .....	52
2.4.	True Density.....	53
2.5.	Formulation Performance Analysis.....	53
2.5.1.	Twin-Stage Impinger (TSI).....	54
2.5.2.	Next Generation Impactor (NGI).....	55
2.6.	Drug Analysis.....	56
2.6.1.	Solubility Analysis .....	56
2.6.1.1.	Solubility of Budesonide as a Function of Temperature .....	57
2.6.1.2.	Solubility of Budesonide as a Function of Solvent/Anti-Solvent Ratio .....	58
2.6.1.3.	Solubility of Salbutamol Sulphate as Function of Solvent/Anti-Solvent Ratio .....	59
2.6.2.	HPLC Analyses .....	60
2.6.2.1.	Methods .....	60
2.6.2.2.	Preparation of Standards and HPLC Calibration .....	60
2.7.	Atomic Force Microscope .....	62
2.7.1.	General Description of the Apparatus .....	62
2.7.2.	Surface Topography Analysis .....	64



2.7.3.	Solid-Solid Interaction Measurements.....	66
2.7.4.	Materials and Methods.....	68
2.7.4.1.	Particle Attachment onto Tipless AFM Cantilevers.....	68
2.7.4.2.	Substrate Sample Preparation.....	68
2.7.4.3.	Control of Relative Humidity.....	70
2.8.	Surface Energy Characterisation.....	70
2.8.1.1.	Principles and Methods.....	70
2.8.1.2.	Results.....	72
2.9.	Statistical analyses.....	73
2.10.	References.....	74

### **Chapter 3 Quantification of the Interaction Force Balance in Dry Powder**

<b>Formulations .....</b>	<b>78</b>
3.1. Introduction .....	78
3.2. Methods.....	80
3.3. Results .....	81
3.3.1. Morphological Characterisation .....	81
3.3.2. Interaction Force Measurements.....	85
3.4. Discussion.....	87
3.5. Conclusions .....	93
3.6. References.....	93

### **Chapter 4 Influence of the Cohesive-Adhesive Balance on DPI Formulation**

<b>Behaviour .....</b>	<b>97</b>
4.1. Introduction .....	97
4.2. Methods.....	98
4.3. Results and Discussion.....	99
4.3.1. General Physical Characterisation .....	99
4.3.2. Influence of Particle Cohesiveness on Powder Behaviour .....	102

4.3.3.	Influence of Drug-Excipient Interactions on Formulation Behaviour .....	108
4.4.	Conclusions .....	115
4.5.	References .....	115
<b>Chapter 5</b>	<b>The Use of Force Control Agents in Model Salbutamol Sulphate DPI Formulations .....</b>	<b>118</b>
5.1.	Introduction .....	118
5.2.	Methods .....	120
5.3.	Results and Discussion .....	122
5.3.1.	Model Formulations with Conditioned Lactose .....	123
5.3.2.	Model Formulations with Conditioned Salbutamol Sulphate ....	132
5.4.	Conclusions .....	141
5.5.	References .....	142
<b>Chapter 6</b>	<b>The Use of Force Control Agents in Model Budesonide DPI Formulations .....</b>	<b>144</b>
6.1.	Introduction .....	144
6.2.	Methods .....	145
6.3.	Results and Discussion .....	147
6.3.1.	Model Formulations with Conditioned Budesonide .....	148
6.3.2.	Model Formulations with Conditioned Lactose .....	156
6.4.	Conclusions .....	164
<b>Chapter 7</b>	<b>Optimisation of the Fluidisation and Aerosolisation of Drug Only Formulations .....</b>	<b>165</b>
7.1.	Introduction .....	165
7.2.	Methods .....	167
7.3.	Results .....	169
7.3.1.	General Powder Morphology .....	169

7.3.2.	<i>In Vitro</i> Aerosol Deposition Studies .....	172
7.3.3.	Laser Diffraction Analyses .....	174
7.4.	Discussion .....	179
7.5.	Conclusions .....	186
7.6.	References .....	187
<b>Chapter 8</b>	<b>General Conclusions .....</b>	<b>190</b>
8.1.	Introduction .....	190
8.2.	Summary .....	191
8.3.	Future Work.....	193

## List of Figures

Figure 1- 1: Description of the lungs.....	2
Figure 1- 2: Capillary interaction between a particle and a surface .....	16
Figure 1- 3: Schematic representation of roughness parameter determination.....	18
Figure 1- 4: Diagrammatic representation of a material water affinity.....	20
Figure 1- 5: Representative scanning electron micrograph of a coarse lactose particle.....	28
Figure 1- 6: Representative scanning electron micrograph of a smooth lactose particle.....	28
Figure 2- 1: Chemical structure of budesonide.....	47
Figure 2- 2: Chemical structure of salbutamol .....	48
Figure 2- 3: Chemical structure of $\alpha$ -Lactose monohydrate.....	48
Figure 2- 4: Chemical structure of L-leucine .....	49
Figure 2- 5: Chemical structure of lecithin.....	49
Figure 2- 6: Chemical structure of magnesium stearate.....	49
Figure 2- 7: Schematic representation of a Twin-stage liquid impinger.....	54
Figure 2- 8: Next Generation Impactor.....	56

Figure 2- 9: Solubility of budesonide as a function of temperature.....	57
Figure 2- 10: Solubility of budesonide as a function of solvent/anti-solvent ratio	58
Figure 2- 11: Solubility of salbutamol as a function of solvent/anti-solvent ratio	59
Figure 2- 12: Calibration curves for budesonide and salbutamol sulphate. ....	61
Figure 2- 13: Photograph and schematic representation of multimode™ AFM....	62
Figure 2- 14: Feedback loop controlling tip sample distance.....	64
Figure 2- 15: Diagrammatic representation of tapping mode™ method .....	65
Figure 2- 16: Diagrammatic representation of phase imaging method .....	66
Figure 2- 17: Schematic representation of a force curve .....	67
Figure 2- 18: Schematic representation of the anti-solvent re-crystallisation step. . .....	69
Figure 2- 19: Diagrammatic representation of contact angle measurement.....	71
Figure 3- 1: Representative SEM images and 3D morphologies (ii) of crystals of budesonide (A), salbutamol sulphate (B) and $\alpha$ -lactose monohydrate (C)....	82
Figure 3- 2: Representative AFM amplitude images of the surface of re-crystallised budesonide (A), salbutamol sulphate (B) and $\alpha$ -lactose monohydrate (C)....	84
Figure 3- 3: Interaction forces between budesonide (A), salbutamol sulphate (B) and lactose (C) probes and D-lactose monohydrate, salbutamol sulphate and budesonide crystal substrates.....	86
Figure 3- 4: Description of a CAB-graph for a theoretical binary system. ....	90
Figure 3- 5: Comparison between forces of cohesion and force of adhesion in a binary lactose/budesonide system. ....	91

Figure 3- 6: Comparison between forces of cohesion and force of adhesion in a binary lactose/salbutamol sulphate system. ....	92
Figure 4- 1: Representative SEM images of ‘as supplied’ lactose Sorbalac 400 (A), salbutamol sulphate (B) and budesonide (C).....	101
Figure 4- 2: Apparent agglomerate volume versus cohesion ratio dependency of salbutamol sulphate, budesonide and lactose.....	104
Figure 4- 3: In vitro deposition of salbutamol sulphate (A) and budesonide (B) from a Rotahaler® and a Turbuhaler® DPI. ....	105
Figure 4- 4: Schematic representation of the possible de-agglomeration and dispersion mechanisms of weakly cohesive (salbutamol sulphate) and highly cohesive (budesonide) particles.....	107
Figure 4- 5: Representative micrographs of blends of salbutamol sulphate-lactose (A), and budesonide-lactose (B).....	111
Figure 4- 6: <i>In vitro</i> deposition of salbutamol sulphate-lactose (A) and budesonide-lactose (B) carrier-based formulation from a Rotahaler® and a Turbuhaler® DPI.....	112
Figure 5- 1: Schematic representation of mechanofusion particle mixing mechanisms. ....	119
Figure 5- 2: CAB-graph of a salbutamol sulphate lactose binary system .....	123
Figure 5- 3: Influence of the mechanofusion of lactose with leucine on the cohesive-adhesive balances of a salbutamol sulphate-lactose system.....	125
Figure 5- 4: Influence of the mechanofusion of lactose with lecithin on the cohesive-adhesive balances of a salbutamol sulphate-lactose system.....	126
Figure 5- 5: Influence of the mechanofusion of lactose with lecithin on the cohesive-adhesive balances of a salbutamol sulphate-lactose system.....	127

- Figure 5- 6: Representative scanning electron micrographs of ternary mixtures of salbutamol sulphate and lactose pre-conditioned with leucine (A), lecithin (B) and magnesium stearate (C). ..... 130
- Figure 5- 7: In-vitro deposition of salbutamol sulphate carrier-based formulations with conditioned lactose..... 132
- Figure 5- 8: Influence of the mechanofusion of salbutamol sulphate with leucine on the cohesive-adhesive balances of a salbutamol sulphate-lactose system. .... 134
- Figure 5- 9: Influence of the mechanofusion of salbutamol sulphate with lecithin on the cohesive-adhesive balances of a salbutamol sulphate-lactose system. .... 135
- Figure 5- 10: Influence of the mechanofusion of salbutamol sulphate with lecithin on the cohesive-adhesive balances of a salbutamol sulphate-lactose system. .... 136
- Figure 5- 11: Representative scanning electron micrographs of ternary mixtures of lactose and salbutamol sulphate pre-conditioned with leucine (A), lecithin (B) and magnesium stearate (C). ..... 139
- Figure 5- 12: In-vitro deposition of carrier-based formulations with conditioned salbutamol sulphate. .... 140
- Figure 5- 13: Fine particle fraction and emission efficiency of salbutamol sulphate carrier-based formulations. .... 142
- Figure 6- 1: CAB-graph of a budesonide lactose binary system ..... 147
- Figure 6- 2: Influence of the coating of budesonide with leucine on the cohesive-adhesive balances of a budesonide-lactose system..... 149

Figure 6- 3: Influence of the coating of budesonide with lecithin on the cohesive-adhesive balances of a budesonide-lactose system.....	150
Figure 6- 4: Influence of the coating of budesonide with magnesium stearate on the cohesive-adhesive balances of a budesonide-lactose system. ....	151
Figure 6- 5: Representative scanning electron micrographs of ternary mixtures of lactose and budesonide pre-conditioned with leucine (A), lecithin (B) and MgST (C).....	154
Figure 6- 6: In-vitro deposition of budesonide carrier-based formulations with conditioned budesonide.....	156
Figure 6- 7: Influence of the coating of lactose with leucine on the cohesive-adhesive balances of a budesonide-lactose system.....	158
Figure 6- 8: Influence of the coating of lactose with lecithin on the cohesive-adhesive balances of a budesonide-lactose system.....	159
Figure 6- 9: Influence of the coating of lactose with magnesium stearate on the cohesive-adhesive balances of a budesonide-lactose system. ....	160
Figure 6- 10: In-vitro deposition of budesonide carrier-based formulations with conditioned lactose.....	161
Figure 6- 11: Representative scanning electron micrographs of ternary mixtures of budesonide and lactose pre-conditioned with leucine (A), lecithin (B) and magnesium stearate (C).....	162
Figure 6- 12: Fine particle fraction and emission efficiency of budesonide carrier-based formulations. ....	163
Figure 7- 1: Scanning electron micrographs of unprocessed salbutamol sulphate (A) and salbutamol sulphate mechanofused with leucine (B), lecithin (C) and MgST (D).....	170



Figure 7- 2: Scanning electron micrographs of unprocessed budesonide (A) and budesonide mechanofused with leucine (B), lecithin (C) and MgST (D)...	171
Figure 7- 3: In-vitro deposition of micronised salbutamol sulphate and FCAs formulations.....	172
Figure 7- 4: In-vitro deposition of micronised budesonide and FCAs formulations .....	173
Figure 7- 5 Cumulative salbutamol sulphate formulation emissions as a function of actuation time at a flow rate of 30L.min <sup>-1</sup> (A), 60L.min <sup>-1</sup> (B), and 90L.min <sup>-1</sup> (C). .....	175
Figure 7- 6: Cumulative budesonide formulation emissions as a function of actuation time at a flow rate of 30L.min <sup>-1</sup> (A), 60L.min <sup>-1</sup> (B), and 90L.min <sup>-1</sup> (C). .....	176
Figure 7- 7: Plume duration and density of salbutamol sulphate formulations. .	180
Figure 7- 8: Plume duration and density of budesonide formulations. ....	181
Figure 7- 9: Fine particle fraction and emission efficiency of salbutamol sulphate formulations.....	183
Figure 7- 10: Fine particle fraction and emission efficiency of budesonide formulations .....	184

## List of Tables

Table 2- 1: Surface tension contributions (in $\text{mJ.m}^{-2}$ ) of liquids used in direct contact angle measurements. ....	72
Table 2- 2: Contact angle measurements of powders assessed by sessile drop techniques.....	72
Table 2- 3: Powder surface energy contributions and resulting Gibbs surface free energy of cohesion.....	73
Table 3- 1: Roughness properties of budesonide, salbutamol sulphate and $\alpha$ -lactose monohydrate. ....	83
Table 3- 2: Cohesive-adhesive balance dependencies between salbutamol sulphate, lactose and budesonide interaction combinations. ....	93
Table 4- 1: Particle size distribution characteristics of lactose Sorbalac 400, micronised salbutamol sulphate and micronised budesonide by laser scattering .....	100
Table 4- 2: Particle size distribution characteristics of lactose Sorbalac 400, micronised salbutamol sulphate and micronised budesonide by time of flight measurements at high (5psi) and low (1psi) shear forces.....	102
Table 4- 3: Reduced intermixing coefficient of salbutamol sulphate, budesonide and lactose .....	109

Table 4- 4: Fine particle fraction and emission efficiency of salbutamol sulphate and budesonide carrier-based formulations from a Rotahaler® and Turbuhaler® DPI .....	114
Table 5- 1: Contact angle measurements of mechanofused lactose with FCAs..	128
Table 5- 2: Surface energy contributions and resulting Gibbs interfacial free energy of interaction of mechanofused lactose with FCAs. ....	128
Table 5- 3: Mixing sequences of salbutamol sulphate carrier-based formulations with conditioned lactose and reduced intermixing coefficients and content uniformities. ....	131
Table 5- 4: Contact angle measurements of mechanofused salbutamol sulphate with leucine, lecithin and MgST.....	137
Table 5- 5: Surface energy contributions and resulting interfacial Gibbs free energy of cohesion of mechanofused salbutamol sulphate with FCAs. ....	137
Table 5- 6: Mixing sequences of salbutamol sulphate carrier-based formulations with conditioned drug and reduced intermixing coefficients and content uniformities. ....	140
Table 6- 1: Contact angle measurements of mechanofused budesonide with leucine, lecithin and MgST. ....	152
Table 6- 2: Surface energy contributions and resulting interfacial Gibbs free energy of cohesion of mechanofused budesonide with FCAs .....	152
Table 6- 3: Mixing sequences of budesonide carrier-based formulations with conditioned budesonide and reduced intermixing coefficients and content uniformities. ....	153

Table 6- 4: Mixing sequences of budesonide carrier-based formulations with conditioned lactose and reduced intermixing coefficients and content uniformities. .... 157

Table 7- 1: Summary of recovered dose in device and capsule, and subsequent device retention for salbutamol and budesonide formulations at 30, 60 and 90L.min<sup>-1</sup> ..... 178

Table 7- 2: Variations in drug cohesiveness by co-processing drug and force control agent by mechanofusion. .... 182

# Chapter 1

## Introduction

### 1.1. General Introduction

The majority of drug formulations are delivered to the body in a solid dosage form. A variety of routes are used to transport the solid drug particulates for systemic delivery, including oral, rectal, intra-venous, intra-muscular and sub-cutaneous suspension injections [1]. However, with the exception of local treatment of airway diseases, the respiratory tract has, until now, been largely overlooked as a potential portal entry of therapeutic agents for systemic delivery. The lung offers several key advantages over other established routes. These advantages include rapid absorption of therapeutic agents via the alveoli and respiratory bronchioles and rapid distribution of the drug to active sites, whilst reducing unwanted side effects encountered with first pass metabolism via the liver and unwanted reactions within the gastric system [2, 3].

The major function of a lung is the exchange of large volumes of gaseous material between the atmosphere and blood capillaries. This process occurs in the peripheral regions of the lungs. To maximize the degree of gaseous exchange, these regions exhibit an impressive surface area of about  $100\text{m}^2$  in humans [2]. As a result, they potentially offer a target of choice for delivery of drugs for various pathologies. A diagrammatic picture of human lungs and related descriptions is shown in Figure 1.1 (dimensions correspond to the size requirements for particle delivery to the corresponding sites).

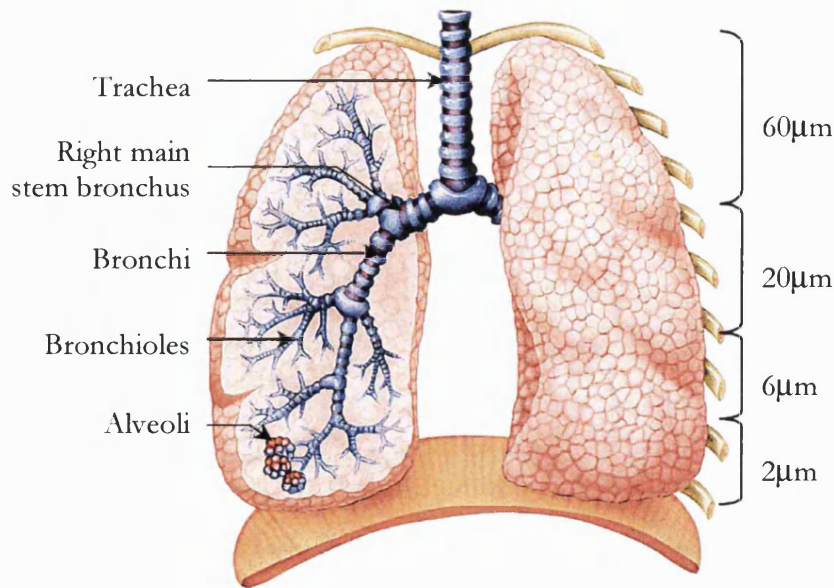


Figure 1- 1: Description of the lungs

The internal structure of the lung consists of a series of branching airways starting from the trachea and dividing into two smaller bifurcations for 24 generations, finishing with the alveolar sacs [2]. Thus, for systemic delivery, inhaled particles have to circumvent a tortuous path to reach the peripheral regions of the lung, while constantly being subjected to various deposition mechanisms, which are influenced by the physico-chemical properties of the aerosol particles and related physiological factors. The major mechanism responsible for deposition in the upper airways is inertial impaction [4]; while in the conducting airways, gravitational sedimentation dominates due to the decreased velocity and larger relaxation times for the aerosol particles in the lower bronchi and bronchioles. Other modes of deposition include diffusion, interception and electrostatic precipitation [5].

Minimisation of impaction and sedimentation in the respiratory tract is achievable for particles of low aerodynamic diameter. For systemic delivery, aerosol particles exhibiting an average diameter in the range of 0.5 to 5 μm are generally regarded as suitable to reach the deeper airways [4, 6]. Nevertheless, the majority of pharmaceutical

powder particles are not spherical and show rather irregular shapes. In order to address these variations and to characterise the key feature which affects transport and deposition in the lung, aerosol particles are defined in terms of their aerodynamic diameter. The mass median aerodynamic diameter (MMAD) is defined as the diameter of a sphere with unit density ( $1\text{g/cm}^3$ ) that has the same terminal settling velocity as the aerosol particle [4].

Delivery of therapeutic agents to the lung is mainly achieved via three different types of devices: nebuliser, pressure metered dose inhaler (pMDI), and dry powder inhaler (DPI) [7]. In the first two cases, the active drug is aerosolised as either a solution or a solid suspension. Drug delivery by a nebuliser is achieved by supplying the active ingredient in the form of aerosolised droplets over a considerable duration. The subsequent aerosol is generally passed through a face mask and delivered to the lung by the patient natural tidal breathing.

In the case of a pMDI device, the formulation is contained within a pressurised liquid propellant. Currently, hydro-fluoroalkane (HFA) is the propellant of choice after the signing of the Montreal protocol in 1986, where the environmental issue of ozone depletion resulted in the banning of the use of chloro-fluorocarbon (CFC) propellants. Although cheap to manufacture, the major disadvantages of pMDIs include the administration of low drug doses (generally limited to 1mg), the relatively high velocity of the delivered droplets resulting in considerable drug loss in the oropharynx upon impaction and the requirement of synchronisation between discharge activation and patient inhalation [8, 9].

In comparison, all current passive DPIs work on the principle of generating a turbulent airflow to disperse a powder formulation by optimising the energy supplied by the patient inhalation. The fluidisation, de-aggregation and dispersion of a dry powder formulation are achieved via the patient's inspiratory action. In contrast to other drug delivery platforms, the characteristic properties of the dry powder formulation are critically important to the effective performance of a DPI system [7, 10]. Thus, the development of a dry powder formulation is highly specialised and a complex

operation. A formulation is typically required to go through several iterative and optimisation steps before a product specification can be achieved.

However, despite technological improvements in inhalation systems and developments in formulation science over recent years, there are still difficulties in delivering the optimum therapeutic dose to specific target regions of the respiratory tracts. As the mechanisms involved in particle-particle interactions are still not fully understood, more detailed investigations are necessary in order to comprehend and control these mechanistic processes. Additionally, the complex fluid dynamic environment within the device upon actuation and formulation behaviour in that environment need to be more clearly understood.

## 1.2. Particle Interaction Fundamentals

Particle-particle interactions are due to long-range interactions not including covalent bonds. Covalent forces bring two atoms together to form a molecule, having an energy of formation usually comprised between 300 and 900kJ.mol<sup>-1</sup> (i.e.  $D_{C-C}=346\text{kJ.mol}^{-1}$ ,  $D_{C=C}=835\text{kJ.mol}^{-1}$ ). Particle interactions, however, are due to much weaker physical bonding, having energies of formation inferior to 40kJ.mol<sup>-1</sup>. These forces, although inferior to covalent bonds, have a significant influence over relatively large distances.

Interactive forces responsible for the interaction between particles can be broadly differentiated into two groups: adhesion or cohesion, depending on the nature of the two interacting materials. Particle adhesion is the result of forces existing between particles of different chemical nature. Cohesion is referred to interaction between particles of the same material.

### 1.2.1. Forces Contributing to Particle Interaction

Long-range forces can establish an interaction between two particles before they come into contact, the degree of interaction is critically dependant on the separation distance [11]. Particle interactions in pharmaceutical systems are a result of a combination of different interactive forces; namely the van der Waals forces, electrostatic (Coulombic) forces and capillary forces. The contribution of each of these



forces will be dependent on various factors including: physical properties of the material, the degree of processing, and environmental conditions. For example, if particles get charged during handling as a result of contact or triboelectrification, electrostatic forces will arise and may dominate inter-particulate adhesions [12]. Similarly, if the material is kept at high relative humidity, the condensation of water vapour between the contiguous bodies may lead to the dissipation of the electrostatic charges due to increased conductance. However, the presence of the physisorbed water may induce capillary interactions with the formation of stable meniscus bridge between the two surfaces [13]. A more detailed overview of each of these physical forces is described below.

Nevertheless, such interactions are dominant only for very small particles, as gravity tends to overcome these physical forces with increasing particle mass (size). Particle adhesion occurs when the interaction forces applying between a particle and a surface exceed the separation forces exerted on the particle. Adhesive (or cohesive) forces become significant enough to overcome gravitational forces when the particles size of the material is reduced to less than  $10\mu\text{m}$  [14]. As a result, gravitational forces play a negligible role in the behaviour of respirable particles.

#### 1.2.1.1. Lifshitz-van der Waals Forces

Van der Waals forces, which occur between all solid particles, are extremely strong at short range and decline rapidly with increasing separation distance. These electro-dynamic interactions consist of three main types of forces [15]:

- **Keesom-orientation forces (permanent moment interactions)**

If two molecules have a dipolar moment, they will orientate themselves so that the negative pole of one molecule is directed toward the positive pole of the other.

- **Debye-induction forces (permanent moment/induced moment interactions)**

A molecule which has a permanent dipole can induce an electrical dipole in an apolar molecule only if the latter is polarizable.

- **Dispersion forces (instantaneous moment/ induced moment interactions)**

Commonly known as London-van der Waals interactions, these forces provide the main contribution of the interactions between macroscopic bodies. These forces arise due to the random movement of electrons within an electron cloud with respect to the nuclear proton, inducing the formation of a temporary dipole. In turn, these instantaneous moments generate an electrical field, which induce a dipole to the nearby neutral molecules by polarizing them. According to London theory, the energy of interaction between two molecules can be described by the following expression:

$$U = \frac{-1}{(4\pi\epsilon_0)^2} \cdot \frac{3h\nu_0\alpha^2}{4d^6} \quad [1.1]$$

where  $U$  is the potential energy (J),  $\alpha$  is the polarisability ( $\text{C}^2\cdot\text{m}^2\cdot\text{J}^{-1}$ ),  $\epsilon_0$  is the dielectric permittivity ( $8.854\cdot 10^{-12} \text{ C}^2\cdot\text{m}^{-1}\cdot\text{J}^{-1}$ ),  $\nu_0$  is the characteristic frequency ( $\text{s}^{-1}$ ),  $h$  is the Planck's constant ( $6.626\cdot 10^{-34} \text{ J}\cdot\text{s}$ ) and  $d$  is the distance separating the two objects (m).

However, it must be noted that the interaction energy does not become infinite when the separating distance tends to zero, as the formula would suggest. This manifestation of a very short-range repulsive energy is due to the impenetrability of the electronic clouds [16]. The value of this energy is proportional to  $d^{12}$ , thus overcoming any attractive interaction at very short separation distance.

In 1937, Hamaker based his theory on the assumption that the interaction between a couple of atoms are not influenced by the neighbouring ones. By integrating on the whole pairs of the microscopic objects, Hamaker was able to calculate the interaction energy between macroscopic bodies [17].

The Hamaker constant,  $A_{ii}$  is commonly used to estimate the dispersion interaction at short distance between two microscopic bodies of the same material and is expressed below.

$$A_{ii} = \pi^2 q_i^2 \beta_{ii} \quad [1.2]$$

where  $q_i$  is the number of atoms per unit volume and  $\beta_{ii}$  is the London constant related to atom interaction, i.e.,  $\beta_{ii} = \frac{3h\nu_0\alpha^2}{4(4\pi\epsilon_0)^2}$  obtained from Equation [1.1].

According to Berthelot's principle, the interaction constant between two particles of different materials is equal to the geometric mean of the interaction constant of the individual materials [18]. The combining rules describing the different types of interaction between two bodies are expressed below:

- between two materials 1 and 2 *in vacuo*:

$$A_{12} = \sqrt{A_{11}A_{22}} \quad [1.3]$$

- between two particles of a material 1 immersed in a medium 3:

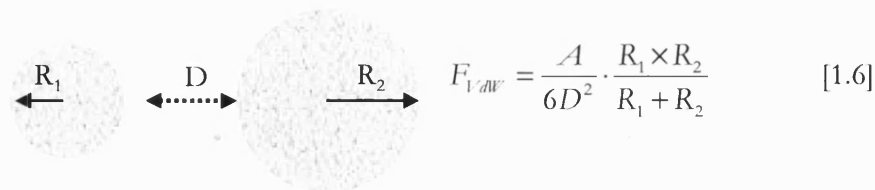
$$A_{131} = \sqrt{A_{11}} - \sqrt{A_{33}} \quad [1.4]$$

- between two materials 1 and 2 immersed in a medium 3:

$$A_{132} = (\sqrt{A_{11}} - \sqrt{A_{33}})(\sqrt{A_{22}} - \sqrt{A_{33}}) \quad [1.5]$$

By using Hamaker's pair-wise summation, the free energy of interaction between particles can be assessed. In turn, interaction forces can be calculated by differentiating the energy with respect to distance:

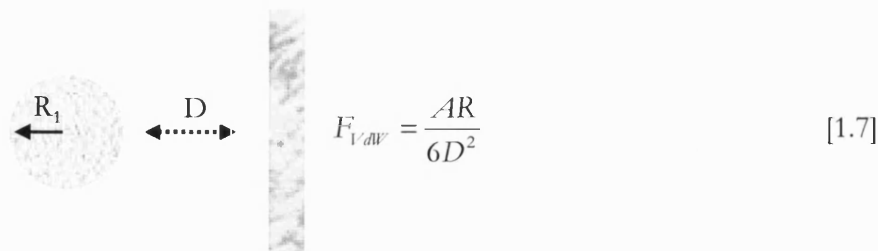
- Sphere-sphere (equivalent sized particles):



The diagram shows two spheres of radii  $R_1$  and  $R_2$  separated by a distance  $D$ . The force equation is given as:

$$F_{VdW} = \frac{A}{6D^2} \cdot \frac{R_1 \times R_2}{R_1 + R_2} \quad [1.6]$$

- Sphere-plan surface (small-large particles):



The diagram shows a sphere of radius  $R_1$  separated from a plan surface by a distance  $D$ . The force equation is given as:

$$F_{VdW} = \frac{AR}{6D^2} \quad [1.7]$$

where  $A$  is the Hamaker constant, related to the Lifshitz-Van der Waals constant  $\bar{\omega}$  by:

$$A = \frac{3}{4\pi} b \bar{\omega} \quad [1.8]$$

As shown in the formulae, the separation distance  $D$  is a critical parameter. The latter parameter being at the square power in the denominator, the forces will considerably reduce as the separation distance increases. Hence, the Lifshitz-Van der Waals forces can be influenced by the presence of large asperities that would maintain a greater separation distance between the cores of two interacting bodies

#### 1.2.1.1.1. Lifshitz Dispersive Interactions

In contrast to Hamaker's approach, Lifshitz calculated the interaction energy considering quantum mechanic and electromagnetic field fluctuations in a continuous media, thereby treating the problem from a purely macroscopic framework [19].

Israelachvili demonstrated the applicability of the Lifshitz approach to estimate the Hamaker constant and corresponding surface tension of different liquids using the following equation [20]:

$$\gamma_i^{LW} = \frac{A_{ii}}{24\pi d^2} \quad [1.9]$$

where  $\gamma_i^{LW}$  is the apolar component of the surface tension of material (i). LW refers to the Lifshitz-van der Waals contribution to the total surface tension.

Good, Girifalco and Fowkes determined that the interfacial tension,  $\gamma_{12}^{LW}$ , between two materials 1 and 2 can be expressed as a function of their respective intrinsic surface energy and is given in the following equation [21, 22]:

$$\gamma_{12}^{LW} = \left( \sqrt{\gamma_1^{LW}} - \sqrt{\gamma_2^{LW}} \right)^2 \quad [1.10]$$

The change in Gibbs free energy,  $\Delta G_{12}^{LW}$  is concomitant with the interfacial surface energy of the interacting materials. The relationship was established by Dupré and is illustrated in the equation below:

$$\Delta G_{12}^{LW} = \gamma_{12}^{LW} - \gamma_1^{LW} - \gamma_2^{LW} \quad [1.11]$$

Substituting Eq. [1.10] into Eq. [1.11] yields:

$$\Delta G_{12}^{LW} = -2\sqrt{\gamma_1^{LW}\gamma_2^{LW}} \quad [1.12]$$

It can be discerned from Eq. [1.9] that as the free energy of interaction is strictly negative, the interaction between two condensed phases *in vacuo* will always be attractive.

From Eq. [1.12], various scenarios can be envisaged in determining particle interactions between similar or different materials, *in vacuo* or immersed in a third media:

- free energy of cohesion of material 1 *in vacuo*:

$$\Delta G_{11}^{LW} = -2\gamma_1^{LW} \quad [1.13]$$

- free energy of cohesion of material 1 immersed in a medium 3:

$$\Delta G_{131}^{LW} = -2\gamma_{13}^{LW} \quad [1.14]$$

- free energy between material 1 and 2 immersed in a medium 3:

$$\Delta G_{132}^{LW} = \gamma_{12}^{LW} - \gamma_{13}^{LW} - \gamma_{23}^{LW} \quad [1.15]$$

The Lifshitz-van der Waals interactions can be closely approximated by measuring the dispersive surface free energy properties of the relevant materials. These characteristics can be determined by a variety of different techniques. One of the most accurate methods for determining surface free energy is contact angle measurement [22-25]. This method is based on measuring the angle of repose of a droplet of liquid with known surface tension on a solid surface. Other methods, such as inverse gas chromatography and capillary intrusion technique are increasingly becoming popular in studying the characteristic energies of pharmaceutical powders [26-30].

#### 1.2.1.1.2. Polar or Lewis Acid-Base Interactions

For many years, intermolecular forces were assessed in dense gases, where the measurement of dispersion forces (London), the dipole-dipole interactions (Keesom) and dipole-induced dipole interactions (Debye) were sufficient to elucidate most of the intermolecular interactions between pair of atoms or molecules. These considerations

were subsequently extended to macroscopic bodies for the measurements of interactions between solids and liquids.

However, significant advances in interfacial tension measurements via thermodynamic techniques have revealed a deviation from such an approach. It is now widely accepted that polar interactions are of significant importance in the determination of interaction forces, especially when occurring in a polar media [31, 32]. Fowkes proposed that the surface tension of a material  $i$  can be divided into subclass components, namely the non-polar Lifshitz-van der Waals (LW) contribution and the polar Lewis acid-base (AB) contribution [21]:

$$\gamma_i = \gamma_i^{LW} + \gamma_i^{AB} \quad [1.16]$$

Since  $\Delta G_{ii} = -2\gamma_i$ , the total free Gibbs energy can be written as:

$$\Delta G = \Delta G^{LW} + \Delta G^{AB} \quad [1.17]$$

where  $\Delta G^{LW}$  and  $\Delta G^{AB}$  are the free energy changes due to Lifshitz-van der Waals interactions and acid-base interactions, respectively.

Fowkes further investigated the importance of acid-base interactions by determining the work of adhesion ( $W_{SL}$ ) between polymer surfaces and liquids of various acidities as a function of acidity of the polymer [32]. He showed that the polar contribution to the total work of adhesion is strictly dependent upon the acidity (basicity) of the polymer of interest. Polar interactions arise from the interaction between electron-acceptor (acid of Lewis) and electron-donor (base of Lewis) sites in molecules. The polar contribution of the surface energy of a material can be expressed as:

$$\gamma_1^{AB} = 2\sqrt{\gamma_1^+ \gamma_1^-} \quad [1.18]$$

where  $\gamma_1^+$  and  $\gamma_1^-$  are the electron-acceptor and electron-donor surface tension parameters, respectively.

Based on Fowkes' approach, Van Oss *et al* showed that the interaction between two polar materials 1 and 2 is essentially asymmetrical; i.e. the electron-acceptor site of one material interacts with the electron-donor site of the other and *vice versa* [33]. The acid-base Gibbs free energy between two materials  $i$  and  $j$  can therefore be expressed as:

$$\Delta G_{ij}^{AB} = -2\left(\sqrt{\gamma_i^+ \gamma_j^-} - \sqrt{\gamma_i^- \gamma_j^+}\right) \quad [1.19]$$

Adapting the Dupré equation [1.11] to acid-base parameters, and substituting Eq. [1.18] and [1.19], the acid-base surface tension  $\gamma_{ij}^{AB}$  can subsequently be written as:

$$\gamma_{ij}^{AB} = 2\left(\sqrt{\gamma_i^+} - \sqrt{\gamma_j^+}\right)\left(\sqrt{\gamma_i^-} - \sqrt{\gamma_j^-}\right) \quad [1.20]$$

### 1.2.1.1.3. Interaction Predictions by Combining the Interfacial Energy Contributions

Using the Dupré equation in the form of:

$$\Delta G_{132} = \gamma_{12} - \gamma_{13} - \gamma_{23} \quad [1.21]$$

to describe the interaction between material 1 and 2 in a media 3 and combining the apolar contribution (Equ. [1.10]) with the polar contribution (Equ. [1.20]) yields:

$$\Delta G_{132} = 2 \left[ \begin{array}{l} \left(\sqrt{\gamma_1^{LW}} - \sqrt{\gamma_3^{LW}}\right)\left(\sqrt{\gamma_2^{LW}} - \sqrt{\gamma_3^{LW}}\right) \\ + \sqrt{\gamma_3^+} \left(\sqrt{\gamma_1^-} + \sqrt{\gamma_2^-} - \sqrt{\gamma_3^-}\right) + \sqrt{\gamma_3^-} \left(\sqrt{\gamma_1^+} + \sqrt{\gamma_2^+} - \sqrt{\gamma_3^+}\right) \\ - \sqrt{\gamma_1^+ \gamma_2^-} - \sqrt{\gamma_1^- \gamma_2^+} \end{array} \right] \quad [1.22]$$



Similarly, the interaction between molecules of substance 1 immersed in a media 3 can be expressed as:

$$\Delta G_{131} = -2\left(\sqrt{\gamma_1^{LW}} - \sqrt{\gamma_3^{LW}}\right)^2 - 4\left(\sqrt{\gamma_1^+ \gamma_1^-} + \sqrt{\gamma_3^+ \gamma_3^-} - \sqrt{\gamma_1^+ \gamma_3^-} - \sqrt{\gamma_1^- \gamma_3^+}\right) \quad [1.23]$$

The resulting interaction between material 1 and 2 *in vacuo* therefore is:

$$\Delta G_{12} = -2\left(\sqrt{\gamma_1^{LW} \gamma_2^{LW}} + \sqrt{\gamma_1^+ \gamma_2^-} + \sqrt{\gamma_1^- \gamma_2^+}\right) \quad [1.24]$$

Interestingly, Eq. [1.24] states that  $\Delta G_{12}$  is always negative and cannot be nought since the van der Waals contribution of all materials has a finite value. Hence, the interaction between two substances *in vacuo* is always attractive. This is of particular interest when considering a material hydrophobicity, as water is always attracted to the most hydrophobic material. Polytetrafluoroethylene (Teflon), for example, is one of the most hydrophobic material known although exhibiting an interfacial surface free energy of  $40\text{mJ}\cdot\text{m}^{-2}$ .

### 1.2.1.2. Electrostatic Forces

Electrostatic charges develop as a result of contact and separation of two different surfaces. According to theory, contact and friction electrifications are two different phenomena. However, they are both usually described as triboelectrification. The major processing of pharmaceutical powders, such as micronisation, high shear mixing or spray drying may induce triboelectrification of particulate surfaces [34]. As all these processes involve very violent collisions between particles, high electrical charges can arise on the surfaces of processed particles. The generation of electrostatic forces onto solid surfaces occurs for various reasons. The simplest case occurs when two charged particles come into contact. The electrostatic force can be either attractive or repulsive, depending on the respective charges on the surfaces of the particles.

The resulting electrostatic force can be described by Coulomb's law:

$$F_e = \frac{q_1 q_2}{4\pi\epsilon_0 d^2} \quad [1.25]$$

where  $q_1$  and  $q_2$  are the respective electrical charges,  $\epsilon_0$  is the permittivity and  $d$  the separation distance.

When an uncharged particle encounters a charged particle, either positively or negatively charged, electrons will transfer between the particles. Thus, if a particle of charge  $q$  approaches an uncharged particle of radius  $r$ , the first particle will induce what is called an image charge on the second particle. The interaction force due to the formation of an image charge can be described by:

$$F_e = \frac{q^2 \left( 1 - \frac{d}{\sqrt{r^2 + d^2}} \right)}{16\pi\epsilon_0 d^2} \quad [1.26]$$

When the uncharged particle is a flat surface ( $r \rightarrow \infty$ ), the previous equation becomes:

$$F_e = \frac{q^2}{16\pi\epsilon_0 d^2} \quad [1.27]$$

Finally, the contact between two uncharged particles can result in the induction of electrostatic charges. Charge transfer between the two surfaces can be explained in terms of difference in work function of the materials. The work function is defined as the minimum energy required to emit one electron from a particle surface to infinity. As two solids are separated from a distance  $d$ , the material with the lower work function will transfer electrons to the material with the higher work function until equilibrium is reached. The resulting force is given by:

$$F_v = \pi\epsilon_0 r \frac{(\Delta U)^2}{d} \quad [1.28]$$

Electrostatic forces are of considerable importance when considering pharmaceutical powders [34]. Generally, pharmaceutical excipients have a low conductivity, behaving as insulators, precluding effective surface charges to dissipate into the particle core. Thus, electrostatic interactions are considered to be significant during the initial attraction and adhesion between particles, while the van der Waals forces are responsible for maintaining the ordered unit, once the electrostatic charges have dissipated. Staniforth and Rees demonstrated that the stability of ordered mixes depended upon the electrostatic charges developed on the materials during mixing [35]. It is even considered that the presence of electrostatic forces may be beneficial for ordered mixing and minimising the segregation tendency of the blends [36].

### 1.2.1.3. Capillary Forces

As opposed to van der Waals forces and electrostatic forces, capillary forces arise when particles come into intimate contact. Capillary interactions are highly dependant on the partial water vapour pressure of the surrounding atmosphere and the physico-chemical properties of the materials, in particular its hydrophilic/hydrophobic nature [37]. Upon raising the relative humidity, the condensation of water vapour onto the surface of solids generally increases. With sufficient condensation, the formation of a liquid bridge between two contacting surfaces may be induced, resulting in significant interaction energy [38]. A diagrammatic representation of capillary interaction between a particle and a surface is shown in Figure 1.2.

This capillary condensation only occurs at high relative humidity [39]. When a meniscus is formed between a sphere and a larger flat surface, the corresponding capillary force (to be added to the already existing interaction forces) is described by [40]:

$$F_c = 2\pi\gamma_L r(\cos \alpha + \cos \beta) \quad [1.29]$$

where  $\alpha$  is the contact angle of the liquid with the surface,  $\beta$  is the contact angle of the liquid,  $r$  is the particle radius and  $\gamma_L$  is the surface tension of the liquid.

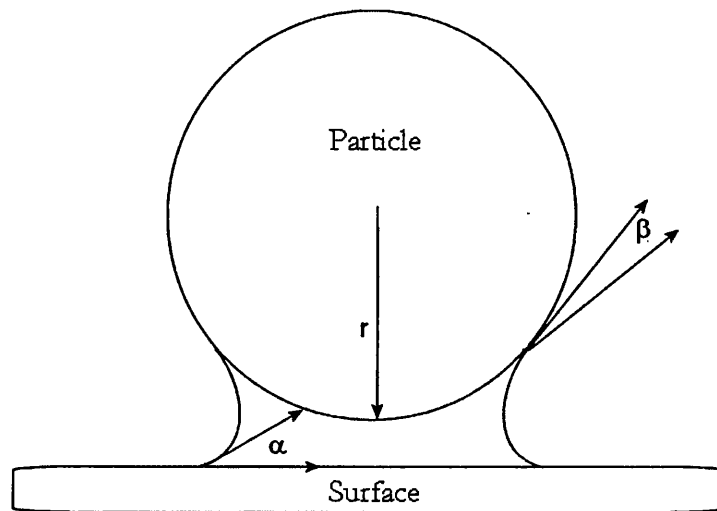


Figure 1- 2: Capillary interaction between a particle and a surface

## 1.2.2. Factors Influencing Adhesions

Given the number of discrete mechanisms in particle interactions, it can be expected that a large amount of factors will influence interaction forces. Surface roughness may alter the separation distance between two particles and thus the overall interaction forces. Particle size, shape and rugosity may modify the surface energy and thus the cohesiveness (or adhesiveness) of interacting particles. Staniforth reported that an increase in the surface area to mass ratio resulted in maximum adhesion [41]. This can be achieved by two methods, namely size reduction or through the production of macroporous particles [42]. Environmental parameters must be taken into account as well, such as relative humidity affecting the hygroscopicity or the charge of a material. The main factors influencing particles adhesion are described in greater detail below.

### 1.2.2.1. Particle Size

It has been shown previously that particle size has a great effect on interaction forces [43]. For example, Lifshitz-van der Waals forces are directly proportional to the

radius of the particle. Capillary forces and electrostatic forces are, in some cases, also dependent upon particle radius. It is reasonable then to assume that the bigger the particle, the greater the overall interaction forces. However, external forces such as gravitational or centrifugal forces are acting as separation forces on the particles. Since gravitational or centrifugal forces are a direct function of the cubic radius of the particle, there is a critical radius when separation forces overcome adhesion forces [44]. However, as gravitational forces decrease more rapidly with decreasing particle size in comparison to the Lifshitz-van der Waals, capillary and electrostatic forces at a critical particle size the influence of the gravitational force is insignificant. As a result very fine material tend to form cohesive agglomerates [10] or adhere to solid surfaces [45].

#### 1.2.2.2. Particle Shape and Roughness

One of the most important parameters affecting inter-particulate forces is the macroscopic and microscopic geometry of particles, which defines the true contact area between particles. While a perfect sphere sitting on top of a perfectly flat surface will have a very small contact, a cubic object on top of the same surface will have a contact area equal to the square of its side. Meanwhile, regular microscopic (even nanoscopic) protrusions or asperities on particle surfaces would dramatically decrease the effective contact area of contiguous surfaces, resulting in a concomitant reduction in particle interactions.

In the case of a carrier-based dry powder inhalation formulation, the dispersion and de-aggregation of drug particles adhering to surface with nanometre asperities will be more readily removed from the carrier than those attached to smoother surfaces [46]. On the other hand, if the size of the asperities matches the drug particle size, a phenomenon of entrapment or mechanical interlocking may occur, leading to a significant increase in particle-particle adhesion. Greater energy would hence be required to dislodge the particles [47]. The direct measurement of surface roughness is difficult to quantify and several parameters, such as rugosity and root mean square deviation of surface protrusions have been utilised [48]. In all surface roughness measurements, surfaces are normalized by defining the centre line, representing the general profile direction of the sampling length, as illustrated in Figure 1.3.

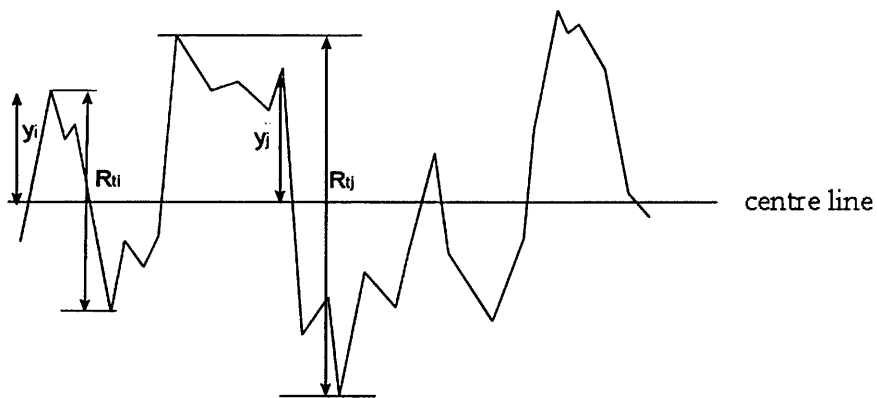


Figure 1- 3: Schematic representation of roughness parameter determination

The rugosity  $R_a$  is the arithmetic mean average distance value of all points  $R_i$  (Figure 1.3) of the profile from the centre line:

$$R_a = \frac{1}{n} \sum_{i=1}^n |y_i| \quad [1.30]$$

where  $y_i$  is the distance between the point and the centre line,  $n$  is the number of points of the profile. This value is the average height from the centre line.

The root mean square deviation of the surface roughness characterises the variability of the profile from the centre line:

$$R_q = \sqrt{\frac{1}{n} \sum_{i=1}^n y_i^2} \quad [1.31]$$

These values are very useful to quantify surface roughness for pharmaceutical powder surfaces.

### 1.2.2.3. Surface Energy

The surface energy of a solid ( $\gamma_s$ ) is defined as the free energy change during the increase of the surface area by one unit in vacuo. By definition this value is always positive. The excess energy is due to force imbalances arising at the surface of the material. As molecules at the surface of a solid are not as free to move as in a liquid, the surface energy is not evenly distributed over the surface. For example, surface energies will differ depending on the region of the solid, whether it is at an edge or a planar surface. Adsorption of contaminants on a surface generally reduces adhesive forces. In general, solids with a high surface energy exhibit a high adsorbing power, leading to stronger inter-surface forces.

Directly related to surface energy, the work of adhesion ( $W_{ad}$ ) plays a crucial role in solid-solid contact. The work of adhesion is defined as the free energy change required to separate unit areas of two surfaces from contact to infinity under vacuum, and can be written as:

$$W_{13}^{ad} = -\Delta G_{13} \quad [1.32]$$

As a result, differences between work of adhesion and work of cohesion between drug-excipient and drug-drug, respectively, are of critical importance in pharmaceutical formulations, and will directly influence mixing homogeneity as well as particle segregation and preferential agglomeration [23].

### 1.2.2.4. Relative Humidity

As previously, discussed, the presence of adsorbed water onto pharmaceutical dry powders may have a significant influence on the resulting adhesion forces. The magnitude of its effect is dependent upon environmental conditions (i.e. relative humidity) and the nature of the material. (hydrophilic/hydrophobic, hygroscopic) [49].

Despite the ubiquitous attraction between water and a surface in vacuo, a material actually presents hydrophobic properties when its adhesive surface free energy with the

water is actually lower than the cohesive energy of adsorbed water molecules ( $78.2\text{mJ}\cdot\text{m}^{-2}$ ) [31]. For example, although water is attracted to the surfaces of low surface free energy polymers, the cohesive energy of the water molecules prevents the spreading of the water on the polymer surface.

A diagrammatic representation of the behaviour of hydrophobic and hydrophilic surfaces with a water droplet is shown in Figure 1.4. The hydrophobic/hydrophilic properties of a surface are measured by the contact angle ( $\theta$ ) of the liquid with the substrate surface. The higher the value of contact angle the more hydrophobic the material.

Hygroscopicity is defined as the capacity of a material to absorb water. However, the two concepts of hydrophilic and hygroscopic are very different. For example, while salbutamol sulphate is a highly hydrophilic material and readily water soluble, its mass uptake under high relative humidity is very low, suggesting a non-hygroscopic material [50]. These properties would have a direct affect on particle interaction forces [51]. If the material is very hygroscopic, (i.e. disodium cromoglycate), adsorbed water tends to diffuse into the bulk of the particle [52]. This process is known as absorption.

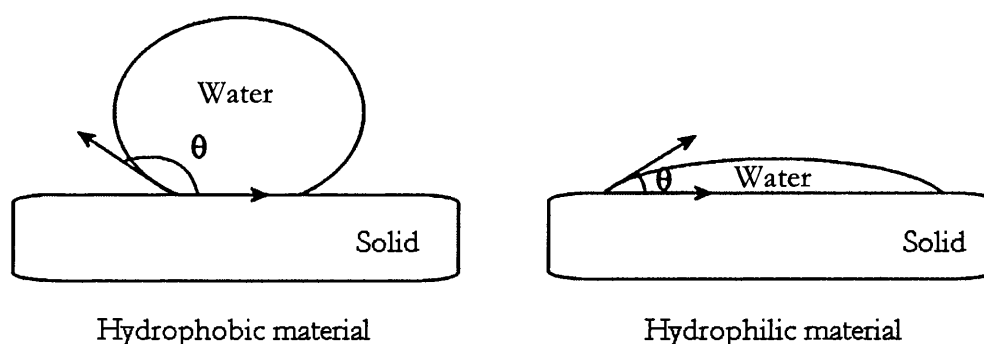


Figure 1- 4: Diagrammatic representation of a material water affinity



The increased adsorption of water on a particle surface may also increase the conductivity of the particle surface, which may lead to the dissipation of any electrostatic charges that may have build-up on the particle surface during frictional contact, reducing electrostatic induced forces [13]. Electrostatic forces would therefore be more significant at low relative humidity since surface charge dissipation would be limited [53].

Numerous studies have investigated the influence of relative humidity on the adhesive forces between particles [13, 51, 53-57]. Results have indicated that particle adhesion increased as a function of relative humidity, which would contribute to macroscopic repercussions over the general formulation performances. Several investigations related significant deterioration in the stability, de-aggregation and dispersion properties of dry powder formulations to exposure to elevated relative humidity [58-63].

### **1.3. Particle Physical State**

Every powder or solid ingredient used in pharmaceutical industries is initially crystallised from solution. To meet the required functionality, crystals are commonly subjected to different processes (i.e. micronisation, spray-drying, mechanofusion). Hence, the knowledge of crystal behaviour, surface and physical properties is of critical importance in order to understand the implications of crystallisation have over particle interactions.

#### **1.3.1. The Crystalline State**

Crystals are nucleated and grown from supersaturated solutions. A saturated solution is a thermodynamic equilibrium between the solid phase and the liquid phase at a specified temperature. This requirement for a supersaturated solution is critical for nucleation and crystal growth. Ostwald defined different areas (labile, metastable) around the solubility curve in which spontaneous nucleation would or would not occur [64].

Nucleation can occur spontaneously in a homogenous solution or induced artificially by a heterogeneous method. These processes are called primary homogeneous nucleation and primary heterogeneous nucleation, respectively. Young and Berkeley have shown that agitation, mechanical shock, friction extreme pressures and temperature cooling can increase the degree of nucleation [65, 66].

A supersaturated solution may nucleate at a lower supersaturation, when crystals of the solute are already present, or intentionally added. These crystals, more commonly described as seeds, act as nucleation centres for crystal growth. Such a process is referred as secondary nucleation [67].

### 1.3.2. Crystal Habit

Crystal habit, also known as crystal morphology, refers to the external appearance of a crystal. A complete description of the morphology of a crystal requires the characterisation of each crystal face present, their relative dominance, specific angles between the faces, relative areas and shape factors. These are used to describe the macroscopic geometry of a crystal. However, knowing the internal structure of a crystal unit cell is not sufficient to model the external habit of the resulting crystals formed. External habit is not only controlled by its internal structure, but by the conditions in which the crystal has been grown. The rate of growth, the solvent used, and the impurities present in the solution may have a critical influence on the crystal habit [68, 69].

### 1.3.3. Polymorphism

Polymorphism is the term used to describe the phenomenon of a chemical species having more than one crystal structure. When a material crystallises into different polymorphs, the chemical nature of the species remains identical, however due to the alteration in the crystal unit cell, physical properties such as density, melting point, solubility and hygroscopicity may differ [70]. This phenomenon raises a delicate issue. During the crystallisation of a material, inhibiting polymorphism may be particularly crucial. This can sometimes be achieved by optimising and controlling the

crystallisation conditions (e.g. solution temperature, solvents) as well as storage conditions (e.g. temperature and relative humidity), in preventing the formation of undesired polymorphs. For example, cimetidine, a specific competitive histamine H<sub>2</sub>-receptor antagonist, has seven known polymorphs [71]. Two of them are of particular interest to the pharmaceutical industry, with one being used in tableting (form A) and the other in suspensions (form B). While form A can be re-crystallised from non-aqueous solvents at room temperature, form B requires slow cooling from a hot aqueous solution. Lactose is known to have two anomeric forms, namely  $\alpha$  and  $\beta$ . Both are simultaneously present in aqueous solution with a  $\alpha/\beta$  ratio close to 40/60 but only the  $\alpha$ -lactose monohydrate crystallises spontaneously below 93.5°C [72, 73].

### 1.3.4. The Amorphous State

An amorphous state is characterised by the absence of three-dimensional long-range order which exists in a crystalline material. Rapid cooling, fast evaporation or precipitation may result in the formation of amorphous solids in a glassy or rubbery state. Amorphous areas on solids particles may also be produced from mechanical treatments. The differences in physical properties between crystalline and amorphous material have been shown to have a profound affect on the stability and performance of dry powder formulations [74, 75]. Molecules within an amorphous region are arranged randomly, and exhibit a higher surface energy than the respective crystalline material. This results in a higher solubility and lower melting point. Moreover, amorphous materials have different plastic properties than the crystalline material, usually softer and subject to deformation. The degree of molecular mobility within a particular amorphous material will be dependent on a number of factors, including temperature and solvent vapour pressure. The vapour pressure is defined as the pressure at which a liquid and a gas phase are in equilibrium. For example, sorption of a solvent into an amorphous region would increase molecular mobility, thus, lowering the glass transition temperature ( $T_g$ ) [76]. If the partial pressure of the solvent is high enough to lower the  $T_g$  below the experimental temperature the region may re-crystallise and expel the solvent [77]. It is important, however, to note that such a system is a thermodynamic process and not a kinetic process. It will not reach a true equilibrium until the system re-crystallises, but the process may take considerable time.

In most pharmaceutical applications, dosage forms must exhibit a specific functionality that requires a high-energy processing, such as milling or micronisation. This inevitably leads to the formation of molecular defects and dislocation and the creation of amorphous areas within the crystalline material. In general, such amorphous materials are thermodynamically unstable and will undergo re-crystallisation if the right conditions and the kinetics is favourable [78]. The presence of amorphous regions will directly affect the stability of a formulation, as the surface energetics will become unpredictable, leading to batch-to-batch variations in the stability and aerosolisation properties of the powder blend [79].

## 1.4. DPI Formulation Development

Dry powder inhalation (DPI) formulations offer many advantages over other routes of drug delivery for inhalation. In comparison with conventional pressurised metered dose inhalers (pMDIs), the volatile propellants, such as CFC or HFA, are not required thereby avoiding potential detrimental affect on the environment. Secondly, for passive DPI devices, the powder is delivered automatically when the patient inhales, thereby avoiding coordination problems usually encountered with propellant driven systems. In addition, DPIs offer the possibility of delivering high drug doses.

As mentioned previously, the active drug must exhibit a specific particle size ( $\leq 5\mu\text{m}$ ) to reach the conducting airways and peripheral regions of the lung. This leads to a well-known paradox, that respirable sized particles tend to be highly cohesive, which causes entrainment problems due to their poor flowability [10]. In addition, strong cohesion forces hinder the handling of the powder during the manufacturing process (pouring, filling). These constraints play a critical role in the processing and design of powder formulations and inhalation devices, respectively.

To overcome the highly cohesive nature of respirable powders, the drug is commonly co-processed (blended) with larger carrier particles of an inert excipient to aid flowability and drug re-dispersion. However, the carrier-based formulation approach is severely limited by the restrictive availability of excipient materials. The only approved excipients hitherto are lactose and glucose [80].

By blending a micronised drug with a carrier, sufficient adhesive bonds between the two ingredients may be generated to form an interactive mixture. Thus, the balance of inter-particulate forces within the interactive mixture is critically important. The drug particles need to be attracted to the carrier during mixing to aid blend homogeneity, device filling and formulation stability during storage and handling. Yet the active ingredient must be easily detached from the carrier upon activation to form a fine particle cloud.

Numerous techniques have been applied to modify particulate interactions in dry powder formulations. The majority have targeted the use of carrier and the control of its physical properties or the use of a ternary agent, such as fine lactose. Other methods involve the manufacture of more uniform respirable particles by particle engineering technology such as spray drying or supercritical fluid precipitation.

#### 1.4.1. Particle Engineering Techniques

In order for drug particles to be of a desired ultra-fine particle size for respiratory tract delivery, the active material must undergo high energy processing. The most common technique for obtaining the optimum particle size range for inhalation is mechanical micronisation. This process involves the use of high shear forces, which results in the continuous fracturing of large particles into the desired particle size range. One drawback of this processing is the lack of control in the size or shape homogeneity [81]. Moreover, particles produced by mechanical micronisation tend to exhibit increased surface rugosity, residual electrostatic charges and significant levels of crystalline disorder [82-84]. These modifications will typically be present on the surface of the processed material [85]. Furthermore, micronised powders generally exhibit a high surface free energy [86]. Under favourable conditions of temperature and/or humidity, these amorphous regions may undergo a re-crystallisation process, possibly inducing solid crystal bonding and subsequent aggregation. Moreover, Feeley *et al.* showed that the micronisation of crystalline particles resulted in a significant increase in their surface free energy [81, 87]. Since both van der Waals and capillary forces are functions of this latter parameter, dramatic alterations in the stability and performances of drug particles during storage and handling may be expected upon micronisation.

Other methods such as spray drying or supercritical fluids have been developed as an alternative means of generating particles suitable for inhalation. Spray drying involves solubilization of the active ingredient in a suitable solvent, and spraying the solution into a heated air stream [75, 88]. The resulting particles are often spherical and hollow due to the rapid drying process of the aerosolised droplets [89, 90]. However, the rapid solidification of the particles generally leads to an amorphous structure [88, 91]. It has been reported that *in vitro* studies of spherical spray-dried cromoglycate particles gave a higher fine particle fraction than for the crystalline micronised material [92]. It was suggested that the hollowed structure of the spray-dried particles significantly reduced their overall density, allowing larger particles to exhibit the required aerodynamic size range for inhalation. However, the stability issues related to amorphous materials have precluded their wider use in dry powder formulations. Due to the metastable nature of these amorphous particles, the use of spray-drying is currently limited to producing particles with stable glass properties, such as proteins or peptides.

A more recent development in obtaining crystalline particles within a well-defined particle size involves the use of supercritical fluids, typically carbon dioxide [93, 94]. By increasing pressure and temperature to a critical point, there is no distinction between the gaseous and liquid phase. This offers a media with interesting properties for re-crystallisation purposes. The active drug is first dissolved in a solvent and then injected with a supercritical fluid in a high pressure chamber. As the supercritical fluid evaporates, the rapid increase in supersaturation within the droplets eventually induces precipitation. More recently, the SEDS-process (Solution Enhanced Dispersion by Supercritical fluids) was introduced [94]. This technique involves a continuous flow of a solution of drug co-introduced into a particle formation vessel with a supercritical fluid. The mixing and dispersion of the drug solution leads to rapid supersaturation, subsequent nucleation and particle formation. The resulting particles are usually highly crystalline, thereby exhibiting lower surface free energies and increased stability in comparison to micronised products [87, 95]. Studies performed with inverse gas chromatography (IGC) indicated that while the dispersive surface free energy of micronised salbutamol sulphate was  $58.6\text{mJ}\cdot\text{m}^{-2}$ , SEDS-produced salbutamol sulphate exhibited a surface free energy of  $38.5\text{mJ}\cdot\text{m}^{-2}$ . However, particles produced by SEDS techniques typically exhibit smooth and planar crystal faces, resulting in a significant

increase in the contact area of contiguous surfaces. Despite the reduction in interfacial surface free energy, the particle adhesion may therefore generally be increased and reduce particle flowability [95, 96].

### 1.4.2. The Use of Coarse Carrier Particles

Carriers are mainly utilised as a bulking agent to improve the flowability of the active ingredient. It must be chemically and physically stable, and not chemically interact with the active material [41]. A large number of solid materials have been investigated as possible candidates, although lactose and lactose derivatives are the most commonly employed, mainly because of their history as a safe excipient [3, 97-99].

Lactose carrier particles are mostly prepared by crystallisation, and can be obtained in a wide variety of shapes and sizes [72, 100-102]. A specific structure of lactose,  $\alpha$ -lactose monohydrate, is preferred among others and is shown in Figure 1.5. This type of crystal particles exhibit excellent flowing properties and its particular “tomahawk” shape provides a significant area for drug-excipient interaction.

Investigations on the influence of the carrier size over formulation performance revealed that drug emission tended to increase with particle size of the carrier whilst fine particle fraction, fine particle dose and drug dispersibility appeared to increase with decreasing particle size of the carrier particles [103, 104]. Bell *et al.* have shown that optimal flowability and aerosolisation properties are obtained within a 63-90 $\mu$ m particle size range [105].

As mentioned previously, carrier morphology such as shape and roughness can play an important role in determining the particulate interaction between the drug and the carrier, thereby influencing powder properties such as flowability, mixing uniformity and de-aggregation [106, 107]. Variations in rugosity may be obtained by specific re-crystallisation techniques. Zeng *et al.* showed that the re-crystallisation of lactose from Carbopol gel or supersaturation at high temperatures (40°C) in the presence of glycerine induced the formation of smoother and more regular crystals [102, 108]. More recently, a novel technique of controlled surface etching was developed on the

partial but controlled surface re-dissolution of lactose crystals by subtle changes of temperatures around the supersaturation curve [109]. An illustration of engineered smooth lactose is shown in Figure 1.6.

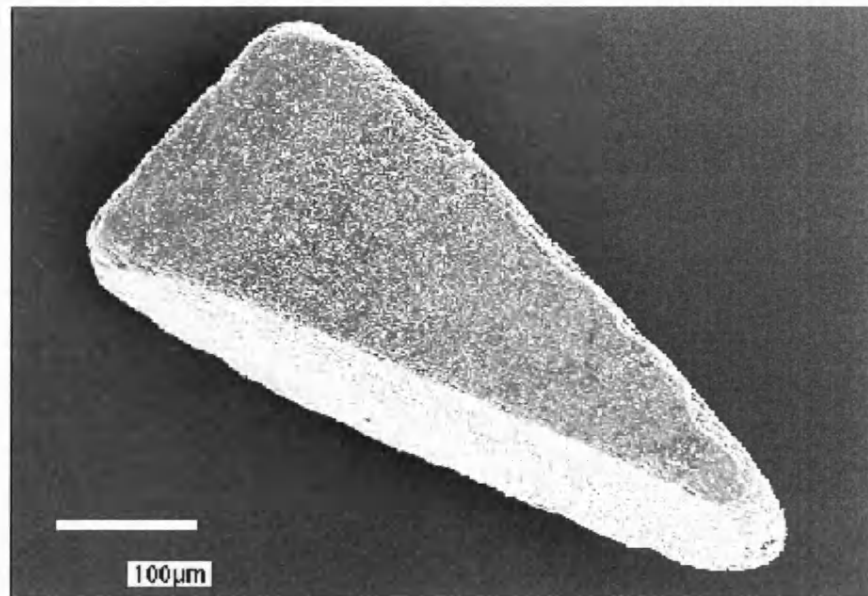


Figure 1- 5: Representative scanning electron micrograph of a coarse lactose particle

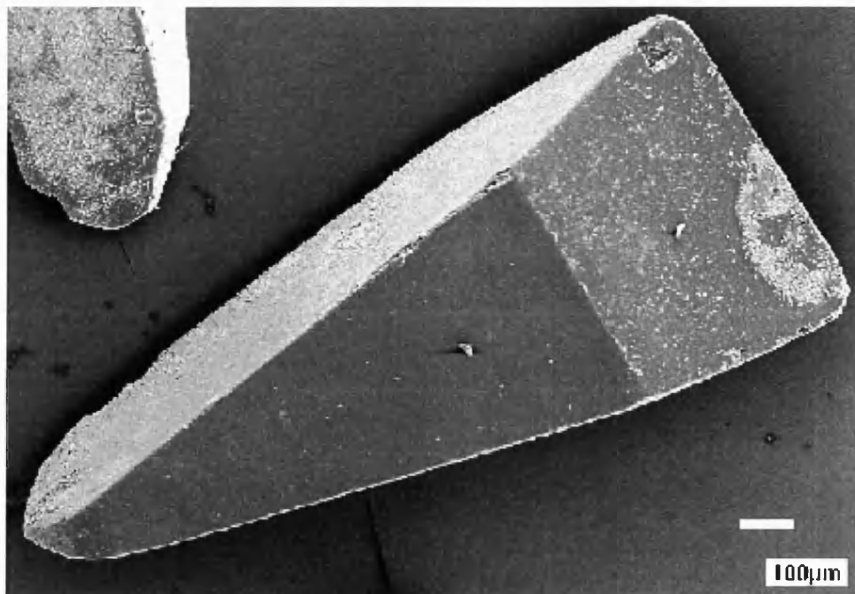


Figure 1- 6: Representative scanning electron micrograph of a smooth lactose particle



Lactose crystals of various shapes and roughness have been shown to significantly influence the *in vitro* deposition profiles of salbutamol sulphate particles [100, 110, 111]. Kawashima *et al.* showed that lactose particles with higher surface roughness resulted in a reduction in the respirable fraction due to strong adhesion between drug and carrier [107]. Similar conclusions were recently reached by Chan *et al.* who immobilised fine particles on lactose carrier by precision coating and assessed its effect on the performance of dry powder formulations [112].

### 1.4.3. Addition of Fine Excipient Particles

One of the most successful advances in optimising drug delivery performance of dry powder formulations is the addition of small amounts of fine excipient particles. Such systems are usually referred to as ternary formulations. Extensive work on the use of fines in dry powder formulations and their influence on delivery performances has been published in the scientific literature [99, 111, 113-116]. Without exception, the addition of fine particles of lactose was found to increase the fine particle fraction of the drug. A number of these studies investigated the influence of the concentration of fines within dry powder formulations. The inclusion of 1.5% to 10% of ternary agent resulted in a general increase in fine particle dose [114].

Various theories on the possible mechanisms by which additional fine excipient particles may enhance carrier-based formulations have been reported [117-120]. It is generally believed that particles of the ternary agent occupy higher energetic sites on the surface of the coarse carrier. As a consequence, only the lower energetic sites remain available for the drug to adhere to the carrier. The resulting reduced adhesion forces would thereby facilitate the more efficient drug detachment upon patient actuation. This theory was supported by several studies investigating the effect of the order in which the coarse carrier, fine excipient and drug particles were mixed. Zeng *et al.* found that formulations produced by first blending the coarse carrier and fine excipient yielded greater fine particle fractions than formulations produced by first blending the coarse carrier and the drug [111, 113].

Conversely, work by Lucas *et al.* revealed that for certain active ingredients the order of blending had no apparent effect on the performances of a ternary formulation. It was suggested that during the blending process, fine excipient and drug particles were redistributed over the coarse carrier surface to form satellite aggregates or fine particle multiplets [121]. These agglomerates could exhibit the desirable effect of being more readily detached from the large coarse carrier than individual particles, and subjected to higher drag forces and kinetic energies upon de-agglomeration and dispersion [114].

#### 1.4.4. Force Control Agent (FCA)

The primary role of these low surface free energy materials is to change the surface chemistry of the guest particles and decrease their intrinsic cohesion. In the early eighties, Staniforth *et al.* reported that the addition of magnesium stearate in a lactose and salicylic acid blend decreased drug-carrier interactions [122]. Previous studies suggested that the ternary agent preferentially adheres to the high-energy active sites of the carrier, “stripping” the active ingredient from the lactose surfaces, leading to a passivation of the carrier surfaces [123].

The use of force control agents as a possible means of increasing the aerosolisation efficiencies of dry powder inhaler formulations is more recent and mostly industrially driven. As a result, most of the relevant information regarding FCAs can be obtained via patent literature, while very little is available in the scientific literature [46, 114, 124, 125]. The initial concept of modifying the adhesive interactions in a carrier-based DPI formulation with an additive was invented by Staniforth and filed in 1996 (patent WO9623485). A force control agent preferably exhibits an anti-adherent and/or anti-friction aptitude, thereby increasing the flow properties of pharmaceutical compositions. These FCAs include conventional lubricants used in powder compression technology, and include amino acid such as leucine, phospholipids such as lecithin or fatty acids like magnesium stearate (MgST) [126]. The processing of FCAs has since been enhanced by various methodologies including the co-processing of fine lactose with the additive (patent WO0178695) or the specific coating of host particles by high energetic mixing processes (patent WO09703639). Claims indicate

that the quantity of force control agent shouldn't exceed 40% (w/w) of the total powder mixture, with a preferred interval comprised between 0.25 to 5%.

## 1.5. Aim of the Study

In order to manufacture a suitable inhalation formulation with an effective and reproducible dose delivery, the physico-chemical properties of the drug must be stable and predictable. However, many mechanical processes used in the pharmaceutical industry to produce an inhalation formulation often lead to the generation of particles with haphazard physico-chemical properties. This may inevitably lead to substantial variations in particle interactions and undesired repercussions on powder mixing, stability and drug delivery performance.

It has been previously discussed that the general properties of a dry powder inhaler formulation (stability, handling, and fluidisation) are associated with a delicate balance between the cohesive and adhesive interaction forces within the powder blend. As a result, these forces and the factors which affect them will directly influence the overall characteristics and performance of the formulation. Thus, optimisation of the formulation performance requires an efficient control of these particulate interactions. A more fundamental knowledge of particle interactions is therefore necessary to effectively understand the mechanistic processes which control and modify dry powder inhaler formulations.

In this study, the initial work was dedicated to the development of a novel AFM-based technique and analysis procedure to quantify the relative cohesive and adhesive interactions within model dry powder formulations. This subsequent analysis procedure was then used to investigate the specific role of the cohesive and adhesive force balances on the de-agglomeration efficiencies and deposition characteristics of drug only and model drug-lactose formulations in predicting blending, segregation and dispersion properties of active pharmaceutical ingredients in dry powder systems. The knowledge gained from these analyses was subsequently used to try and optimise dry powder formulation performances by specifically introducing a force control agent into a dry powder formulation to selectively target the desired interaction to be controlled.

The in-vitro deposition profiles of model drug-lactose and drug only formulations were investigated to establish a possible correlation between the cohesive and adhesive nature of the modified formulations with aerosol delivery performance.

## 1.6. References

- [1] S. R. Byrn. *Solid State Chemistry of Drugs*, Academic Press, New York, 1982.
- [2] J. S. Patton. Mechanisms of Macromolecule Absorption by the Lungs. *Adv. Drug Deliv. Rev.* **19**: 3-36 (1996).
- [3] M. P. Timsina, G. P. Martin, C. Marriott, D. Ganderton, and M. Yianneskis. Drug-delivery to the respiratory tract using Dry Powder Inhalers. *Int. J. Pharm.* **01**.: 1-13 (1994).
- [4] W. C. Hinds. *Aerosol technology: Properties, Behaviour and measurements of airborne particles*, Wiley, New York, 1999.
- [5] X. M. Zeng, G. P. Martin, and C. Marriott. *Particulate Interactions in Dry Powder Formulations for Inhalation*, Taylor & Francis, London, 2001.
- [6] D. Ganderton and T. Jones. *Drug Delivery to the Respiratory Tract.*, Camelot Press, Southampton, 1987.
- [7] A. R. Clark. Medical Aerosol Inhalers - Past, Present, and Future. *Aerosol Sci. and Tech.* **22**: 374-391 (1995).
- [8] M. T. Vidgren. Factors influencing lung deposition of inhaled aerosols. *European Respiratory Review* **4**: 69-70 (1994).
- [9] G. Brambilla, D. Ganderton, R. Garzia, D. Lewis, B. Meakin, and P. Ventura. Modulation of aerosol clouds produced by pressurised inhalation aerosols. *Int. J. Pharm.* **186**: 53-61 (1999).

- [10] D. Ganderton and N. M. Kassem. *Advances in Pharmaceutical sciences.*, Academic Press, London, 1992.
- [11] B. V. Deryaguin, N. A. Krotova, and V. P. Smilga. *Adhesion of Solids*, Consultants Bureau, New York., 1978a.
- [12] P. R. Byron, J. Peart, and J. N. Staniforth. Aerosol electrostatic I: Properties of fine powders before and after aerosolisation by dry powder inhalers. *Pharm. Res.* **14**: 698-705 (1997).
- [13] R. Price, P. M. Young, S. Edge, and J. N. Staniforth. The influence of relative humidity on particulate interactions in carrier-based dry powder inhaler formulations. *Int. J. Pharm.* **246**: 47-59 (2002).
- [14] J. Visser. Particle adhesion and removal: a review. *Particulate science and Technology* **13**: 169-196 (1995).
- [15] J. N. Israelachvili. *Intermolecular and Surface Forces. 2nd edn*, Academic Press, London, 1992.
- [16] B. V. Deryaguin. The force between particles. *Scientific American* 3-9 (1960).
- [17] E. M. Lifshitz. The theory of molecular attraction forces between solid bodies. *Sov. Phys. JETP* 73-83 (1956).
- [18] D. Berthelot. *Comp. Rend. Acad. Sci.* **126**: 1703 (1898).
- [19] E. M. Lifshitz. *J. Exp. Theor. Phys.* **29**: 94 (1955).
- [20] J. N. Israelachvili. *Q. Rev. Biophys.* **6**: (1974).

- [21] F. M. Fowkes. Additivity of intermolecular forces of interfaces. i determination of the contribution of surface and interfacial tension of dispersion forces in various liquids. *J. Phys. Chem.* **64**: 2538-2541 (1963).
- [22] R. J. Good and L. A. Girifalco. A theory for the estimation of surface and interfacial energies. iii estimation of surface energies of solids from contact angle measurements. *Journal of Physical Chemistry* **64**: 561-565 (1960).
- [23] N. M. Ahfat, G. Buckton, R. Burrows, and M. D. Ticehurst. Predicting mixing performance using surface energy measurements. *Int. J. Pharm.* **156**: 89-95 (1997).
- [24] J. M. Douillard, J. Zajac, H. Malandrini, and F. Clauss. Contact angle and film pressure: Study of a talc surface. *J. Colloid Interface Sci.* **255**: 341-351 (2002).
- [25] C. J. Vanoss, R. J. Good, and M. K. Chaudhury. Additive and Nonadditive Surface-Tension Components and the Interpretation of Contact Angles. *Langmuir* **4**: 884-891 (1988).
- [26] N. M. Ahfat, G. Buckton, R. Burrows, and M. D. Ticehurst. An exploration of inter-relationships between contact angle, inverse phase gas chromatography and triboelectric charging data. *Eur. J. Pharm. Sci.* **9**: 271-276 (2000).
- [27] D. Cline and R. Dalby. Predicting the quality of powders for inhalation from surface energy and area. *Pharmaceutical Research* **19**: 1274-1277 (2002).
- [28] M. Ohta and G. Buckton. The use of inverse gas chromatography to assess the acid-base contributions to surface energies of cefditoren pivoxil and methacrylate copolymers and possible links to instability. *International Journal of Pharmaceutics* **272**: 121-128 (2004).

- [29] O. Planinsek, A. Trojak, and S. Srcic. The dispersive component of the surface free energy of powders assessed using inverse gas chromatography and contact angle measurements. *Int. J. Pharm.* **221**: 211-217 (2001).
- [30] C. H. Sun and J. C. Berg. The effective surface energy of heterogeneous solids measured by inverse gas chromatography at infinite dilution. **260**: 443-448 (2003).
- [31] C. J. van Oss. *Interfacial Forces in Aqueous Media*, Marcel Decker Inc., New York, 1994.
- [32] F. M. Fowkes. *Physicochemical aspects of Polymer Surfaces*, Plenum Press, New York, 1983.
- [33] C. J. van Oss, M. K. Chaudhury, and R. J. Good. Monopolar Surfaces. *Adv. Colloid Interface Sci.* **28**: 35-64 (1987).
- [34] J. N. Staniforth. The importance of electrostatic measurements in aerosol formulation and preformulation., *Respiratory Drug Delivery IV*, 1994, pp. 303-311.
- [35] J. N. Staniforth and J. E. Rees. Electrostatic charge interactions in ordered powder mixes. *Journal of Pharmacy and Pharmacology* **34**: 69-76 (1982).
- [36] C. L. Tucker and N. P. Suh. Electrostatic powder mixing. *Polymer Science and Engineering* **16**: 657-663 (1976).
- [37] J. T. Cartensen. *Pharmaceutical Principles of Solid Dosage Forms. Pennsylvania*, Technomic Publishing Company, Inc., Lancaster, 1993.
- [38] H. Schubert. Haftung Zwischen Feststoffteilchen aufgrund von Flüssigkeitsbrücken. *Chemie Ingenieur Technik* **46**: 333-334 (1974).

- [39] E. N. Hiestand. Powders:particle-particle interactions. *J. Pharm. Sci.* **55**: 1325-1344 (1966).
- [40] W. J. O'Brien and J. J. Hermann. Strength of liquid bridges between dissimilar materials. *Journal of Adhesion* **5**: 91-103 (1973).
- [41] J. N. Staniforth. Ordered Mixing of Drugs with Particulate Excipients., *Pharmacy and Pharmacology*, Bath, Bath,, 1980.
- [42] J. N. Staniforth. "Order out of chaos". *J. Pharm. Pharmacol.* **39**: 329-334 (1987).
- [43] F. Podczeck, J. M. Newton, and M. B. James. Assessment of adhesion and auto adhesion forces between particles and surfaces I: The investigation of autoadhesion phenomena of salmeterol xinofoate and lactose monohydrate particles using compacted powder surfaces. *J. Adhes. Sci. Technol.* **8**: 1459-1472 (1994).
- [44] A. D. Zimon. *Adhesion of Dust and Powder. 2nd edn.*, Consultants Bureau, New York, 1982.
- [45] J. N. Staniforth. Pre-formulation aspects of dry powder aerosols., *Respiratory Drug Delivery V*, 1996.
- [46] P. M. Young, D. Cocconi, P. Colombo, R. Bettini, R. Price, D. F. Steele, and M. J. Tobyn. Characterization of a surface modified dry powder inhalation carrier prepared by "particle smoothing". *J. Pharm. Pharmacol.* **54**: 1339-1344 (2002).
- [47] A. Otsuka, K. Lidia, and H. Sunada. Measurement of the adhesive forces between particles of powdered materials and a glass substrate by means of the impact separation method. III. Effect of shape and surface asperity. *Chemical and Pharmaceutical Bulletin* **36**: 741-749 (1988).



- [48] F. Podczec. *Particle-Particle Adhesion in Pharmaceutical Powder Handling*, Imperial College Press, London, 1998.
- [49] R. N. Jashnani and P. R. Byron. Dry powder aerosol generation in different environments: Performance comparisons of albuterol, albuterol sulfate, albuterol adipate and albuterol stearate. *International Journal of Pharmaceutics* **130**: 13-24 (1996).
- [50] A. Columbano, G. Buckton, and P. Wikeley. A study of the crystallisation of amorphous salbutamol sulphate using water vapour sorption and near infrared spectroscopy. *Int. J. Pharm.* **237**: 171-178 (2002).
- [51] P. Kulvanich and P. J. Stewart. Influence of relative humidity on the adhesive properties of a model interactive system. *Journal of Pharmacy and Pharmacology* **40**: 453-458 (1988).
- [52] L. R. Chen, V. G. Young Jr, D. Lechuga-Ballesteros, and D. J. W. Grant. Solid-state behaviour of cromolyn sodium hydrates.. *J. Pharm. Sci.* **88**: 1191-1199 (1999).
- [53] R. Price, M. Tobyn, and J. N. Staniforth. Variation in Particle Adhesion Due to Capillary and Electrostatic Forces. *Respiratory Drug Delivery VII* (2000).
- [54] Y. Ando. The effect of relative humidity on friction and pull-off forces measured on submicron-size asperity arrays. *Wear* **238**: 12-19 (2000).
- [55] V. Berard, E. Lesniewska, C. Andres, D. Pertuy, C. Laroche, and Y. Pourcelot. Dry powder inhaler: influence of humidity on topology and adhesion studied by AFM. *Int. J. Pharm.* **232**: 213-224 (2002).
- [56] A. Meurk, J. Yanez, and L. Bergstrom. Silicon nitride granule friction measurements with an atomic force microscope: effect of humidity and binder concentration. *Powder Technol.* **119**: 241-249 (2001).

- [57] S. T. Patton, K. C. Eapen, and J. S. Zabinski. Effects of adsorbed water and sample aging in air on the mu N level adhesion force between Si(100) and silicon nitride. *Tribol. Int.* **34**: 481-491 (2001).
- [58] M. A. Braun, R. Oschmann, and P. C. Schmidt. Influence of excipients and storage humidity on the deposition of disodium cromoglycate (DSCG) in the Twin Impinger. *Int. J. Pharm.* **135**: 53-62 (1996).
- [59] M. J. Clarke, M. J. Tobby, and J. N. Staniforth. Physicochemical factors governing the performance of nedocromil sodium as a dry powder aerosol. *J. Pharm. Sci.* **89**: 1160-1169 (2000).
- [60] E. R. M. Geuns, J. S. Toren, D. M. Barends, and A. Bult. Decrease of the stage-2 deposition in the twin impinger during storage of beclomethasone dipropionate dry powder inhalers in controlled and uncontrolled humidities. *Eur. J. Pharm. Biopharm.* **44**: 187-194 (1997).
- [61] R. N. Jashnani, P. R. Byron, and R. N. Dalby. Testing of Dry Powder Aerosol Formulations in Different Environmental-Conditions. *Int. J. Pharm.* **113**: 123-130 (1995).
- [62] R. N. Jashnani and P. R. Byron. Dry powder aerosol generation in different environments: Performance comparisons of albuterol, albuterol sulfate, albuterol adipate and albuterol stearate. *International Journal of Pharmaceutics* **130**: 13-24 (1996).
- [63] F. Podczeck, J. M. Newton, and M. B. James. Variations in the adhesion force between a drug and carrier particles as a result of changes in the relative humidity of the air. *Int. J. Pharm.* **149**: (1997).
- [64] W. Ostwald. Studien uber die Bildung und Umwandlung fester Körper. . *Zeitschrift fur Physikalische Chemie* **22**: 289-330 (1897).

- [65] T. E. Berkeley. Solubility and supersolubility from the osmotic standpoint. *Philosophical magazine* **24**: 254-268. (1912).
- [66] S. W. Young. Mechanical stimulus to crystallization in supercooled liquids. *J. Am. Chem. Soc.* **33**: 148-162 (1911).
- [67] G. D. Botsaris. Secondary nucleation: a review. In J. W. M. (ed.) (ed), *Industrial Crystallization (6th Symposium, Usti nad Labem)* (J. W. M. (ed.), ed), Plenum Press, 1976, pp. 3-22.
- [68] R. A. Laudise. *The Growth of Single Crystals.*, Prentice-Hall, Englewood Cliffs, 1970.
- [69] R. F. Strickland-Constable. *Kinetics and Mechanism of Crystallization.*, Academic Press, New York, 1968.
- [70] J. Halebian and W. McCrone. Pharmaceutical applications of Polymorphism. *Journal of Pharmaceutical Sciences* **58**: 911-929 (1969).
- [71] A. Danesh, X. Chen, M. C. Davies, C. J. Roberts, G. H. W. Sanders, S. J. B. Tendler, P. M. Williams, and M. J. Wilkins. Polymorphic discrimination using atomic force microscopy: Distinguishing between two polymorphs of the drug cimetidine. *Langmuir* **16**: 866-870 (2000).
- [72] S. Garnier, S. Petit, and G. Coquerel. Influence of supersaturation and structurally related additives on the crystal growth of alpha-lactose monohydrate. *J. Cryst. Growth* **234**: 207-219 (2002).
- [73] T. A. Nickerson. *Fundamentals of Dairy Chemistry.*, Avi Publishing Co. Inc, Westport, 1974.

- [74] G. Buckton. Characterisation of small changes in the physical properties of powders of significance for dry powder inhaler formulations. *Adv. Drug Deliv. Rev.* **26**: 17-27 (1997).
- [75] L. Yu. Amorphous pharmaceutical solids: preparation, characterization and stabilization. *Adv. Drug Deliv. Rev.* **48**: 27-42 (2001).
- [76] G. Buckton and P. Darcy. Water mobility in amorphous lactose below and close to the glass transition temperature. *International Journal of Pharmaceutics* **136**: 141-146 (1996).
- [77] B. C. Hancock and G. Zografi. The relationship between the glass-transition temperature and the water-content of amorphous pharmaceutical solids. *Pharmaceutical Research* **11**: 471-477 (1994).
- [78] G. Buckton, P. Darcy, D. Greenleaf, and P. Holbrook. The Use of Isothermal Microcalorimetry in the Study of Changes in Crystallinity of Spray-Dried Salbutamol Sulfate. *Int. J. Pharm.* **116**: 113-118 (1995).
- [79] A. C. Williams, V. B. Cooper, L. Thomas, L. J. Griffith, C. R. Petts, and S. W. Booth. Evaluation of drug physical form during granulation, tableting and storage. *Int. J. Pharm.* **275**: 29-39 (2004).
- [80] B.P.C. British Pharmacopoeia, Vol. II, London (1993).
- [81] J. C. Feeley, P. York, B. S. Sumby, and H. Dicks. Determination of surface properties and flow characteristics of salbutamol sulphate, before and after micronisation. *Int. J. Pharm.* **172**: 89-96 (1998).
- [82] G. H. Ward and R. K. Schultz. Process-induced crystallinity changes in albuterol sulphate and its effect on powder physical stability. *Pharmaceutical Research* **12**: 773-779 (1995).

- [83] A. K. Schellinger. Calorimetric method for the determination of the surface energy of a brittle crystalline solid. *Science* **111**: 693-694 (1950).
- [84] J. C. Feeley, P. York, B. S. Sumbly, and H. Dicks. Processing effects on the surface properties of alpha-lactose monohydrate assessed by inverse gas chromatography (IGC). *J. Mater. Sci.* **37**: 217-222 (2002).
- [85] P. Begat, P. M. Young, S. Edge, J. S. Kaerger, and R. Price. The effect of mechanical processing on surface stability of pharmaceutical powders: Visualization by atomic force microscopy. *J. Pharm. Sci.* **92**: 611-620 (2003).
- [86] G. Buckton, A. Choularton, A. Beezer, and S. Chatham. The effect of the comminution technique on the surface energy of a powder.. *Int. J. Pharm.* **47**: 121-128 (1988).
- [87] J. C. Feeley, B. Y. Shekunov, A. H. L. Chow, and P. York. Surface and aerodynamic characteristics of particles for inhalation produced using supercritical fluid technology., *Drug Delivery to the Lung XI*, London, 2000.
- [88] J. Broadhead, S. K. Edmont Rouan, and C. T. Rhodes. The spray drying of pharmaceuticals. *Drug Dev. Ind. Pharm.* **18**: 1169-1206 (1992).
- [89] A. Gurav, T. Kudas, T. Pluym, and Y. Xiong. Aerosol processing of materials. *Aerosol Sci. and Tech.* **19**: 411-452 (1993).
- [90] J. O. H. Sham, Y. Zhang, W. H. Finlay, W. H. Roa, and R. Lobenberg. Formulation and characterization of spray-dried powders containing nanoparticles for aerosol delivery to the lung. *Int. J. Pharm.* **269**: 457-467 (2004).
- [91] A. Millqvist-Fureby, M. Malmstem, and B. Bergensthal. Spray-drying of trypsin surface characterisation and activity preservation. *Int. J. Pharm.* **188**: 243-253 (1999).

- [92] M. T. Vidgren, P. A. Vidgren, and T. P. Paronen. Comparison of physical and inhalation properties of spray-dried and mechanically micronised disodium-cromoglycate. *Int. J. Pharm.* **35**: 139-144 (1987).
- [93] S. Bristow, T. Shekunov, B. Y. Shekunov, and P. York. Analysis of the supersaturation and precipitation process with supercritical CO<sub>2</sub>. *J. Supercrit. Fluids* **21**: 257-271 (2001).
- [94] P. York, M. D. Ticehurst, J. C. Osborn, R. J. Roberts, and R. C. Rowe. Characterisation of the surface energetics of milled dl-propranolol hydrochloride using inverse gas chromatography and molecular modelling. *Int. J. Pharm.* **174**: 179-186 (1998).
- [95] H. Schiavone, S. Palakodaty, A. R. Clark, P. York, and S. T. Tzannis. Evaluation of SCF-engineered particle-based lactose blends in passive dry powder inhalers. *Int. J. Pharm.* **281**: 55-66 (2004).
- [96] P. York. Strategies for particle design using supercritical fluid technology. *Pharm. Sci. Techn. T.* **2**: 430-440 (1999).
- [97] C. Bosquillon, C. Lombry, V. Preat, and R. Vanbever. Influence of formulation excipients and physical characteristics of inhalation dry powders on their aerosolization performance. *J. Control. Release* **70**: 329-339 (2001).
- [98] H. Steckel and N. Bolzen. Alternative sugars as potential carriers for dry powder inhalations. *International Journal of Pharmaceutics* **270**: 297-306 (2004).
- [99] S. K. Tee, C. Marriott, X. M. Zeng, and G. P. Martin. The use of different sugars as fine and coarse carriers for aerosolised salbutamol sulphate. *Int. J. Pharm.* **208**: 111-123 (2000).

- [100] H. Larhrib, X. M. Zeng, G. P. Martin, C. Marriott, and J. Pritchard. The use of different grades of lactose as a carrier for aerosolised salbutamol sulphate. *Int. J. Pharm.* **191**: 1-14 (1999).
- [101] S. Garnier, S. Petit, and G. Coquerel. Dehydration mechanism and crystallisation behaviour of lactose. *J. Therm. Anal.* **68**: 489-502 (2002).
- [102] X. M. Zeng, G. P. Martin, C. Marriott, and J. Pritchard. The influence of crystallization conditions on the morphology of lactose intended for use as a carrier for dry powder aerosols. *J. Pharm. Pharmacol.* **52**: 633-643 (2000).
- [103] X. M. Zeng, G. P. Martin, C. Marriott, and J. Pritchard. The effects of carrier size and morphology on the dispersion of salbutamol sulphate after aerosolization at different flow rates. *J. Pharm. Pharmacol.* **52**: 1211-1221 (2000).
- [104] B. H. J. Dickhoff, A. H. de Boer, D. Lambregts, and H. W. Frijlink. The effect of carrier surface and bulk properties on drug particle detachment from crystalline lactose carrier particles during inhalation, as function of carrier payload and mixing time. *Eur. J. Pharm. Biopharm.* **56**: 291-302 (2003).
- [105] J. H. Bell, P. S. Hartley, and J. S. Cox. Dry Powder Aerosol I: A New Powder Inhalation Device. *J. Pharm. Sci.* **60**: 1559-1563 (1971).
- [106] M. P. Flament, P. Leterme, and A. Gayot. The influence of carrier roughness on adhesion, content uniformity and the in vitro deposition of terbutaline sulphate from dry powder inhalers. *Int. J. Pharm.* **275**: 201-209 (2004).
- [107] Y. Kawashima, T. Serigano, T. Hino, H. Yamamoto, and H. Takeuchi. Effect of surface morphology of carrier lactose on dry powder inhalation property of pranlukast hydrate. *Int. J. Pharm.* **172**: 179-188 (1998).

- [108] X. M. Zeng, G. P. Martin, C. Marriott, and J. Pritchard. The use of lactose recrystallised from carbopol gels as a carrier for aerosolised salbutamol sulphate. *Eur. J. Pharm. Biopharm.* **51**: 55-62 (2001).
- [109] D. El-Sabawi, P. M. Young, S. Edge, and R. Price. Modification of lactose carriers for dry powder inhalers using novel temperature controlled surface etching., *Respiratory Drug Delivery IX*, Palm Desert, 2004.
- [110] X. M. Zeng, G. P. Martin, C. Marriott, and J. Pritchard. The influence of carrier morphology on drug delivery by dry powder inhalers. *Int. J. Pharm.* **200**: 93-106 (2000).
- [111] X. M. Zeng, K. H. Pandhal, and G. P. Martin. The influence of lactose carrier on the content homogeneity and dispersibility of beclomethasone dipropionate from dry powder aerosols. *Int. J. Pharm.* **197**: 41-52 (2000).
- [112] L. W. Chan, L. T. Lim, and P. W. S. Heng. Immobilization of fine particles on lactose carrier by precision coating and its effect on the performance of dry powder formulations. *J. Pharm. Sci.* **92**: 975-984 (2003).
- [113] X. M. Zeng, G. P. Martin, S. K. Tee, A. Abu Ghoush, and C. Marriott. Effects of particle size and adding sequence of fine lactose on the deposition of salbutamol sulphate from a dry powder formulation. *Int. J. Pharm.* **182**: 133-144 (1999).
- [114] X. M. Zeng, G. P. Martin, S. K. Tee, and C. Marriott. The role of fine particle lactose on the dispersion and deaggregation of salbutamol sulphate in an air stream in vitro. *Int. J. Pharm.* **176**: 99-110 (1998).
- [115] S. K. Tee, G. P. Martin, A. R. Leeds, C. Walker, A. Kicman, D. A. Cowan, and C. Marriott. The influence of a tertiary component on the in vivo disposition of salbutamol isomers aerosolised from a dry powder inhaler formulation. *Thorax* **56**: P51 (2001).



- [116] N. Islam, P. J. Stewart, I. Larson, and P. G. Hartley. Lactose surface modification by decantation: Are drug-fine lactose ratios the key to better dispersion of salmeterol xinafoate from lactose interactive mixtures? *Pharm. Res.* **21**: 492-499 (2004).
- [117] D. Ganderton. The generation of respirable clouds from coarse powder aggregates. *J. Biopharm. Sci.* **3**: 101-105 (1992).
- [118] J. D. Lord and J. N. Staniforth. Particle size effects on packing and dispersion of powders, *Respiratory Drug Delivery V*, Interpharm Press. Inc., 1996, pp. 75-84.
- [119] J. A. Hersey. Ordered mixing: A new concept on powder mixing practice. *Powder Technol.* **11**: 41-44 (1975).
- [120] T. Srichana, G. P. Martin, and C. Marriott. On the relationship between drug and carrier deposition from dry powder inhalers in vitro. *Int. J. Pharm.* **167**: 13-23 (1998).
- [121] P. Lucas, K. Anderson, and J. N. Staniforth. Protein deposition from dry powder inhalers: Fine particle multipllets as performance modifiers. *Pharm. Res.* **182**: 562-569 (1998).
- [122] J. N. Staniforth, J. E. Rees, F. K. Lai, and J. A. Hersey. Interparticle Forces in Binary and Ternary Ordered Powder Mixes. *J. Pharm. Pharmacol.* **34**: 141-145 (1982).
- [123] F. K. Lai and J. A. Hersey. A cautionary note on the use of ordered powder mixtures in pharmaceutical dosage forms. *Journal of Pharmacy and Pharmacology* **31**: 800 (1979).
- [124] M. J. Clarke, M. J. Tobby, and J. N. Staniforth. The formulation of powder inhalation systems containing a high mass of nedocromil sodium trihydrate. *J. Pharm. Sci.* **90**: 213-223 (2001).

- 
- [125] M. D. Louey and P. J. Stewart. Particle interactions involved in aerosol dispersion of ternary interactive mixtures. *Pharmaceutical Research* **19**: 1524-1531 (2002).
- [126] L. Roblottlepel and F. Puisieux. Distribution of Magnesium Stearate On the Surface of Lubricated Particles. *International Journal of Pharmaceutics* **31**: 131-136 (1986).

## Chapter 2

### Materials and Methods

#### 2.1. Materials

##### 2.1.1. Pharmaceutical Ingredients

- Budesonide
  - Supplier: Sicor, Rho, Italy; Batch N°: 6157/MI
  - Group: Corticosteroids

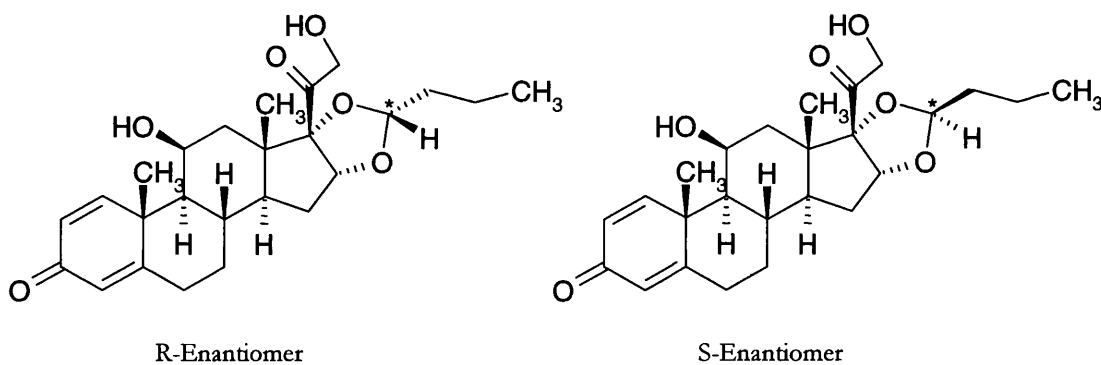


Figure 2- 1: Chemical structure of budesonide

- Salbutamol sulphate
  - Supplier: Becpharm Ltd, Harlow, UK; Batch N°: 940077
  - Group: Bronchodilators,  $\beta_2$ -agonists

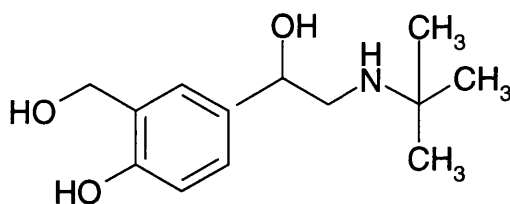


Figure 2- 2: Chemical structure of salbutamol

- Sorbalac 400 ( $\alpha$ -Lactose monohydrate)
  - Supplier: Meggle, Wasserburg, Germany
  - Group: Sugars

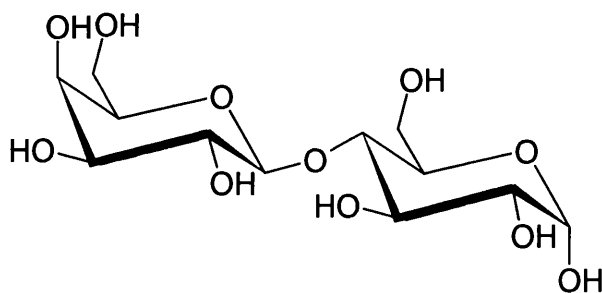


Figure 2- 3: Chemical structure of  $\alpha$ -Lactose monohydrate

- L-Leucine
  - Supplier: Ajimoto Co., Tokyo, JAPAN; Batch N°: 601FK72
  - Group: Amino-acids

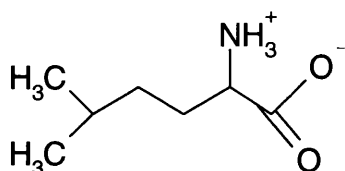


Figure 2- 4: Chemical structure of L-leucine

- Lecithin
  - Supplier: Lipoid GmbH, Ludwigshafen, Germany; Batch N°: 25661113-1/14
  - Group: Phospholipids

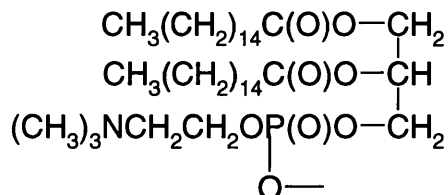


Figure 2- 5: Chemical structure of lecithin

- Magnesium stearate
  - Supplier: Avocado, Heysham, UK; Batch N°: H1028A
  - Group: Fatty acids

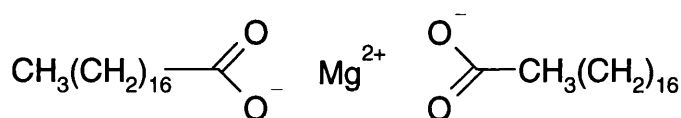


Figure 2- 6: Chemical structure of magnesium stearate

### 2.1.2. Liquids

Denomination	Supplier	Address	Batch number
Methanol	Fisher Chemicals	Loughborough, UK	N/A
Ethanol	Fisher Chemicals	Loughborough, UK	N/A
Acetonitrile	Fisher Chemicals	Loughborough, UK	N/A
Diodomethane	Acros Organics	Geel, Belgium	169835
Ethylene Glycol	Aldrich	Gillingham, UK	N/A
Acetic acid glacial 100%	BDH	Poole, UK	N/A
Water (reverse osmosis)	MilliQ, Millipore	Molsheim, France	N/A

## 2.2. Particle Size Analysis

Various techniques are available to determine the size range of powder samples. These include sieve analysis, time-of-flight determination, sedimentation, low angle laser light scattering (LALLS) or impaction based techniques. The techniques chosen for this study were namely low angle laser light scattering, time-of-flight technique and impaction analysis using two different impingers. It is important to stress that the former method determines the actual geometrical particle size, whereas the others elucidate the aerodynamic particle diameter. Nevertheless, the two parameters can easily be related via a simple equation [1]. It has been shown that lung sedimentation behaviour is closely related to the aerodynamic diameter [1], ensuing the wide use of impinger techniques to characterise formulation and inhaler device performances. These are described in greater detail in section 2.5.

### 2.2.1. Light Scattering Analysis

The LALLS technique is based on the diffraction of a monochromatic, collimated light by a particle or group of particles. The diffracted light caused by the powder dispersion traversing the laser forms a scattering pattern, which is specific to an individual particle size. The latter parameter is then calculated by Fourier transformation, using Fraunhofer diffraction theory, which allows correlation between

particle size and diffraction pattern. In the case of micron-sized particles, the Mie theory is applied to elucidate the scattering patterns, as the optical properties of the material to be analysed have to be considered [2].

In essence, the scattering pattern is obtained by integration over the whole range of single scatters caused by each particle present in the sample. Particle size distributions are then calculated by matching experimental and theoretical diffractograms [3].

Analyses were performed using a Mastersizer X (Malvern Instruments Ltd, Malvern, UK) with a 300mm lens. Prior to analysis, powders were dispersed in a mixture of lecithin (0.1% w/w) and cyclohexane before being sonicated for 5 minutes to facilitate dispersion. Samples were then stirred with the dispersant in a large volume cell inside the Mastersizer, using a magnetic stirrer in order to obtain an obscuration level of 20-30%. All samples were prepared and analysed in triplicate.

### **2.2.2. Time-of-Flight Analysis**

Aerodynamic Time-of-Flight (TOF) of airborne particles can be measured by detecting their velocity between two laser beams. Essentially, a powder sample is dispersed in air, creating an aerosol beam which is accelerated by the drag forces generated in the air stream. As particles pass through two laser beams in the measuring region spaced at a pre-set distance, the time required for individual particles to pass between the beams is detected and converted by two photomultiplier tubes into particle size.

Analyses were performed using an Aerosizer<sup>®</sup> (Amherst Process Instruments, Hadley, USA). The amount of shear forces applied to the powder sample is adjusted by monitoring the pressure drop across the annular gap between the disperser pin and the pin bowl. Therefore, subsequent shear forces are expressed as the corresponding pressure drop, varying from 0 to 5psi. After each measurement, the sample cup and the disperser unit were thoroughly cleaned.

## 2.3. Particle Shape Analysis

General morphology of the pharmaceutical ingredients was investigated by both scanning electron microscopy (SEM) for particle shape study and atomic force microscope (AFM) for surface topography analysis.

### 2.3.1. Scanning Electron Microscopy (SEM)

A scanning electron microscope creates a high resolution image of a sample *in vacuo* by the use of a collimated beam of electrons instead of light waves. An electron gun emits a beam of focused electrons which is scanned back and forth over a conductive sample. As the electron continuously sweeps across the specimen at high speed, secondary electrons are knocked loose from its surface due to the local irradiation. The signal produced by the secondary electrons emitted from the specimen is detected and interpreted to form the final image.

Representative powder samples were mounted on aluminium stubs using carbon coated adhesive tabs. A thin film of gold was vaporised onto the sample surface using a sputter coater (Model S150B, Edwards High Vacuum, Sussex, UK). Specimens were examined using a JEOL 6310 SEM (Japanese Electron optics Ltd, Tokyo, Japan).

### 2.3.2. Atomic Force Microscopy (AFM)

The atomic force microscope is a very accurate apparatus allowing the discernment of solid surfaces at the nanometre scale. However, as this surface topography analysis is only one of the AFM techniques used in this study, a fully detailed section is therefore dedicated to the description of the apparatus in section 2.7.



## 2.4. True Density

True density analyses were determined by helium pycnometry (Accupyc 1330 Gas Pycnometer, Micromeritics, Norcross, USA). Measurements were performed by determining the pressure change of helium of a calibrated sealed volume containing a powder sample of known mass and unknown volume [4].

Samples were first dried in opened pans at 40°C for 24 hours to remove any adsorbed water. Temperature was kept constant at 25°C throughout experiments. Each sample density was measured ten times for reproducibility.

True density measurements for salbutamol sulphate, budesonide and lactose were determined as 1.248 g.cm<sup>-3</sup> ( $\pm$  0.001g.cm<sup>-3</sup>), 1.473 g.cm<sup>-3</sup> ( $\pm$  0.001g.cm<sup>-3</sup>) and 1.532 g.cm<sup>-3</sup> ( $\pm$  0.001g.cm<sup>-3</sup>), respectively.

## 2.5. Formulation Performance Analysis

The most important physico-chemical parameter influencing the deposition of aerosols in the lung is particle size. However, aerodynamic diameter is often preferred to geometric diameter when considering the behaviour of fluidised particles. Hitherto, inertial impaction is the most commonly used methodology to determine the aerodynamic particle size of aerosols.

Two different apparatus were employed in this study. An impinger (impaction on liquid) or impactor (impaction on a solid surface) usually consists of a series of stages of different cut-off diameters mounted as a cascade. The desired particle cut-off size of an impinger is relative to the airflow velocity passing through the apparatus.

### 2.5.1. Twin-Stage Impinger (TSI)

The twin-stage liquid impinger (TSI) apparatus was the first device operating on inertial impaction to assess drug delivery to be adopted by the British Pharmacopoeia [5]. A representative TSI apparatus (Copley Scientific Ltd, Nottingham, UK) is shown in Figure 2.7. The TSI apparatus was operated at  $60\text{L}\cdot\text{min}^{-1}$  ( $\pm 2\text{L}\cdot\text{min}^{-1}$ ), corresponding to a cut-off diameter of  $6.4\mu\text{m}$  between the first and second stage. Flow rate was calibrated using a flowmeter (SCR2, Glass precision, Eng. Ltd., UK).

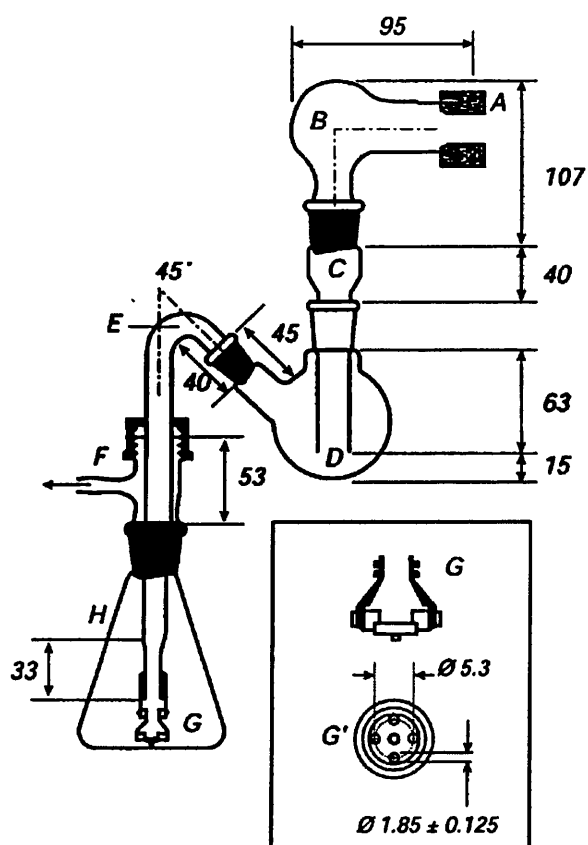


Figure 2- 7: Schematic representation of a Twin-stage liquid impinger, reproduced from British Pharmacopoeia, 2001, Volume II.

### 2.5.2. Next Generation Impactor (NGI)

The amount of time required in the testing of pharmaceutical inhalers by existing cascade impactors has encouraged the development of a novel impactor, specifically designed for pharmaceutical aerosols. This resulted in the creation of the next generation impactor (NGI), which was launched in 2000 (Figure 2.8). It is a high performance particle-classifying cascade impactor for testing pressurised metered dose or dry powder devices.

The NGI is composed of seven stages plus a Micro-Orifice Collector (MOC). The effective cut-off diameters at  $60\text{L}\cdot\text{min}^{-1}$  are as follows:

- Stage 1:  $>8.06\mu\text{m}$
- Stage 2:  $4.46 - 8.06\mu\text{m}$
- Stage 3:  $2.82 - 4.46\mu\text{m}$
- Stage 4:  $1.66 - 2.82\mu\text{m}$
- Stage 5:  $0.94 - 1.66\mu\text{m}$
- Stage 6:  $0.55 - 0.94\mu\text{m}$
- Stage 7:  $0.34 - 0.34\mu\text{m}$
- Stage 8 (MOC)  $<0.34\mu\text{m}$

The air flow passes through the impactor in a saw-tooth pattern. Particle separation and sizing is achieved by successively increasing the velocity of the air stream as it passes through each stage by forcing it through a series of nozzles containing progressively reducing jet sizes. Drug particles are collected on plates, which can be individually removed from the NGI core to collect the drug particles. Advantageously, no liquid is necessary for the *in vitro* testing. After each experiment, each stage plate can be readily removed and quickly rinsed with an adequate solvent for analytical analyses.

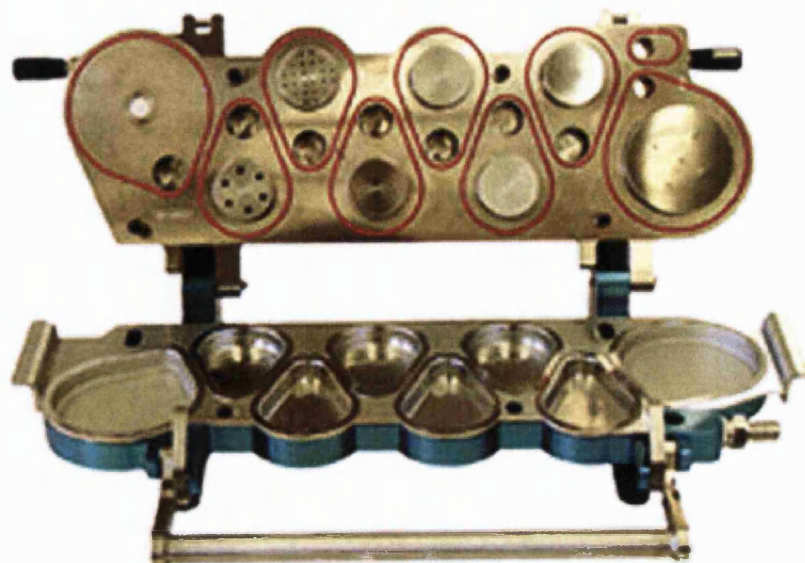


Figure 2- 8: Next Generation Impactor (Open View showing nozzles & collection cups), reproduced from Copley web site.

## 2.6. Drug Analysis

### 2.6.1. Solubility Analysis

Drug solubility analyses were measured by gravimetric technique. This method was chosen over methods like UV/VIS-spectroscopy, fluorescence spectroscopy or high performance liquid chromatography (HPLC) in order to avoid any solvent effect on the quantifying method. Solubility studies of budesonide and salbutamol sulphate in different conditions were conducted in order to determine the required conditions for satisfying re-crystallisation.

### 2.6.1.1. Solubility of Budesonide as a Function of Temperature

Saturated solutions of budesonide in ethanol and in methanol were shaken for 12 hours at different temperatures from 25 to 40°C (G76, Gyrotory water bath shaker, New Brunswick Scientific, Edison, USA) in sealed volumetric flasks. The saturated solutions were filtered and dried at 40°C before calculating solubility by mass. The solubility curves are expressed graphically in Figure 2.9. It can be noticed that the two curves followed the same trend, the solubility in methanol being slightly higher than in ethanol. However, the difference of solubility between 25 and 40°C was just about 1-1.5% (w/w) in both cases. It would therefore appear that temperature did not have a great effect on drug solubilization.

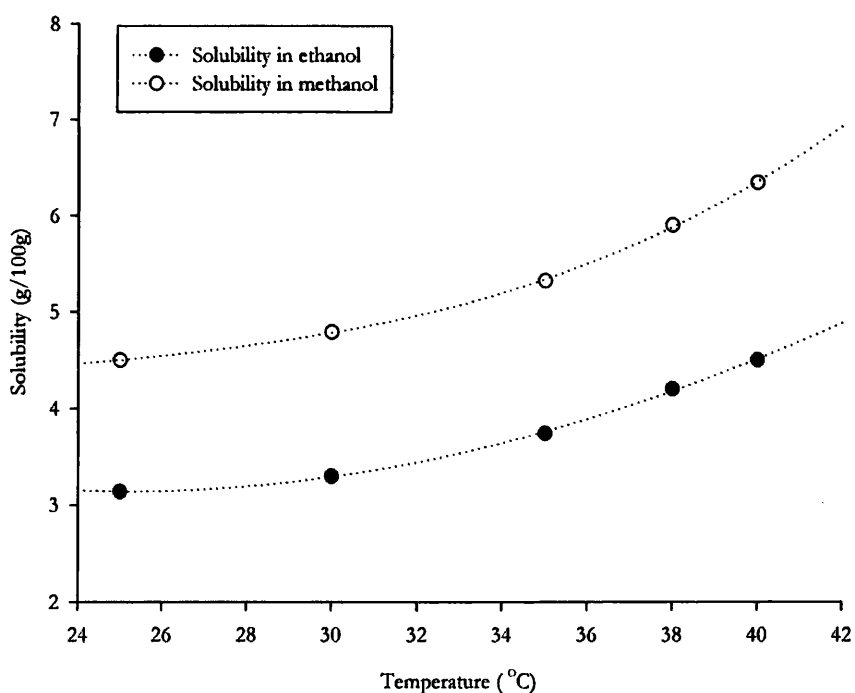


Figure 2- 9: Solubility of budesonide as a function of temperature

### 2.6.1.2. Solubility of Budesonide as a Function of Solvent/Anti-Solvent Ratio

Solubility of budesonide in mixtures of organic solvent and water was determined by saturating the drug in ethanol/water mixtures or methanol/water mixtures. The solubility curves for budesonide in mixtures of ethanol/water and methanol/water are expressed graphically in Figure 2.10. Budesonide, like most corticosteroids, is practically insoluble in water. As expected, the solubility decreased with increase of water percentage in the mixtures. However, the solubility of budesonide in ethanol/water mixtures seemed to reach a maximum at a 20:80 water/ethanol ratio. Similar trends have been observed with other materials in ethanol/water mixtures, but the phenomenon is still not well understood. Interestingly, the maximum of solubility was obtained with ethanol as the organic solvent. Moreover, the solubility dropped from 5.3% (w/w) at a 20:80 water/ethanol ratio to virtually naught at a 80:20 water/ethanol ratio.

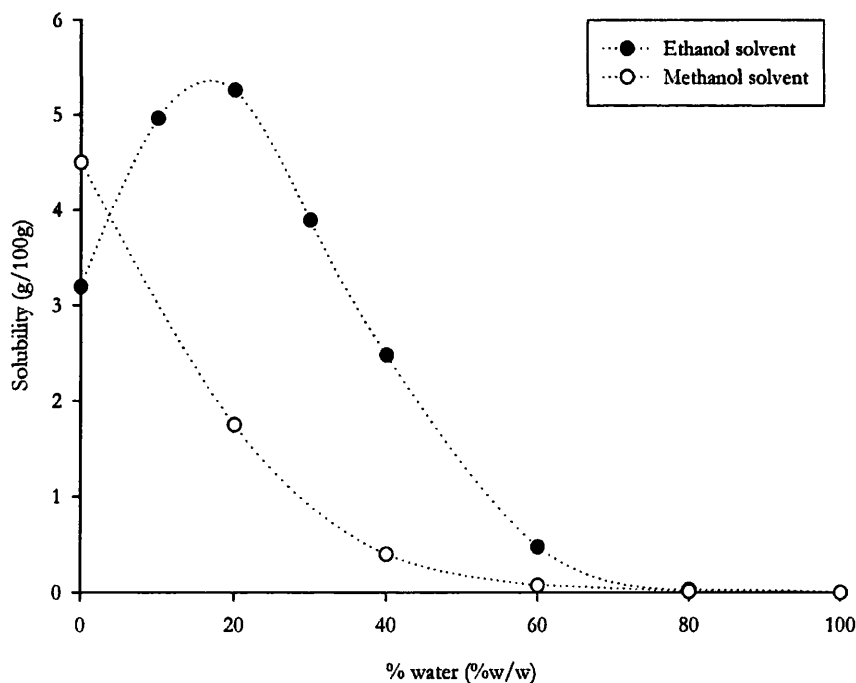


Figure 2- 10: Solubility of budesonide as a function of solvent/anti-solvent ratio

### 2.6.1.3. Solubility of Salbutamol Sulphate as Function of Solvent/Anti-Solvent Ratio

Solubility of salbutamol sulphate in mixtures of ethanol and water at a constant temperature of 20°C was determined using the conditions described previously. The solubility curve is expressed graphically in Figure 2.11. The solubility curve showed high solubility of salbutamol sulphate in water, corroborating its hydrophilic properties and affinity with water. However, salbutamol sulphate was virtually insoluble in ethanol. The resulting drop of solubility was quite significant, being around 40%.

Given the excellent solubility patterns of salbutamol sulphate in ethanol/water mixtures, it was decided not to investigate further the change of solubility of salbutamol sulphate depending on other parameters (e.g. temperature).

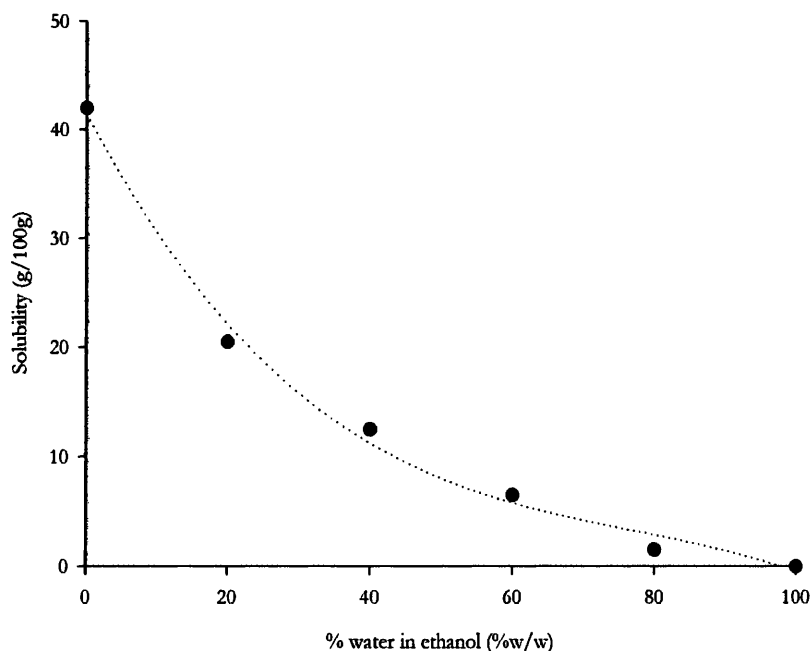


Figure 2- 11: Solubility of salbutamol as a function of solvent/anti-solvent ratio

## 2.6.2. HPLC Analyses

### 2.6.2.1. Methods

Drug concentrations collected from the various device components and TSI sampling stages during *in vitro* studies were analysed by high performance liquid chromatography (HPLC). Succinctly, the HPLC operates by separating the organic compounds relative to their affinity for the solid phase in the HPLC column. The liquid chromatograph system was equipped with an autosampler (AS-950, Jasco, Tokyo, Japan), a pump (PU-980, Jasco, Tokyo, Japan), a column oven (CO-866, Jasco, Tokyo, Japan), and a UV/VIS-detector (UV-975, Jasco, Tokyo, Japan). Data were analysed by computer (Borwin, JMBS Developments, Grenoble, France). Each value was determined by comparing the peak area of the sample to reference peaks of standard solutions of known concentration. Each sample concentration was determined in duplicate.

- **Budesonide**

A 5 $\mu$ m Hypersil column (Hypersil MOS C8, Jones Chromatography Ltd, UK) was used. The HPLC pump was operated at 1.5ml.min<sup>-1</sup> and the UV detection wavelength set at 248nm. The mobile phase consisted of 60% of water and 40% of acetonitrile (%v/v).

- **Salbutamol sulphate**

A Spherisorb<sup>®</sup> 5 $\mu$ m ODS1 column (Waters, Milford, MA, USA) was used for salbutamol sulphate. Salbutamol sulphate was analysed using a mobile phase consisting of methanol and water in a 60:40 ratio (%v/v) with 0.1% (%v/v) of acetic acid. The HPLC pump was operated at 1.25ml.min<sup>-1</sup> and the UV detection wavelength set at 276nm.

### 2.6.2.2. Preparation of Standards and HPLC Calibration

Standards for each of the micronised drugs were prepared prior to HPLC analysis. Duplicate stock standard solutions were prepared by accurately weighing 25mg aliquots of material into two 100ml volumetric flasks. Solutions were sonicated



for approximately 10 minutes to ensure complete dissolution and left to cool to room temperature. Standard solutions were prepared by serial dilution of the stock solutions using calibrated (class A) laboratory pipettes. A series of working standard with concentrations comprised between  $0.1\mu\text{g.ml}^{-1}$  and  $10\mu\text{g.ml}^{-1}$  were subsequently prepared for each drug substance.

In order to correlate UV-absorbance response to drug concentration, the concentration-peak area response for budesonide and salbutamol sulphate in their respective mobile phase was investigated through linear regression analysis and is shown in Figure 2.12. The coefficient of determination ( $R^2$ ) of 1 for both curves inferred a direct linear response between peak area and concentration over the range of  $0.05\mu\text{g.ml}^{-1}$  to  $10\mu\text{g.ml}^{-1}$ .

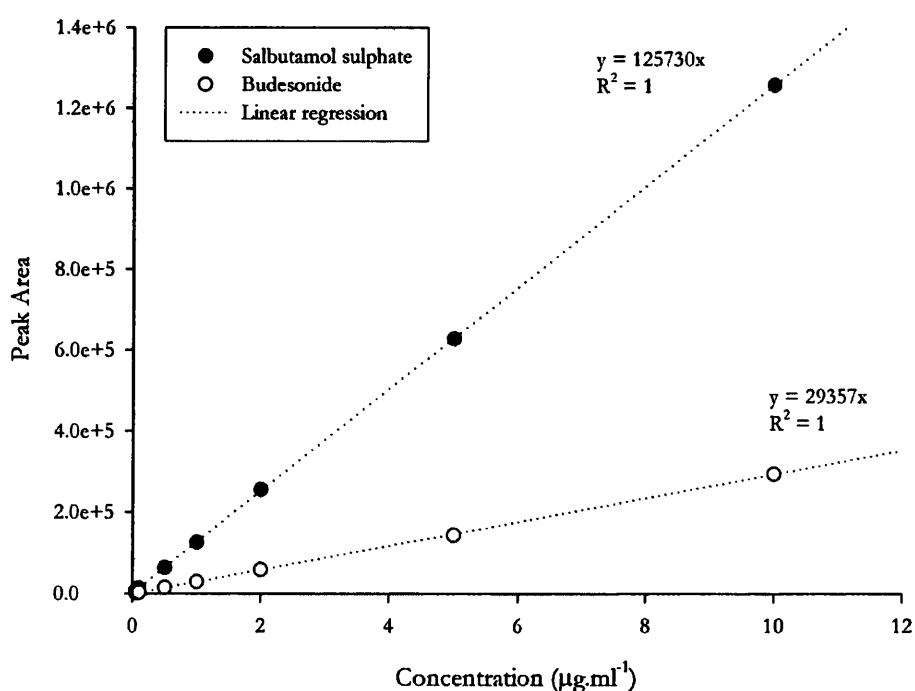


Figure 2- 12: Calibration curves for budesonide and salbutamol sulphate.

## 2.7. Atomic Force Microscope

The Atomic Force Microscope was originally an innovative development of the Scanning Tunneling microscope (STM) invention [6]. The STM technique relies on measuring the “tunnelling current” between a sharp conducting probe and a sample, and reconstructing the topography of the sample surface. However, the STM requires a conducting tip and sample, which limited quite significantly the broader use of the technique. In contrast, the Atomic Force Microscope (AFM) technique, developed by Binnig *et al.* in 1986 provided a means of characterizing the surface morphology of non-conducting surfaces to the atomic scale [7].

### 2.7.1. General Description of the Apparatus

The AFM used throughout the study was a DI Multimode™ AFM with a Nanoscope IIIa controller and extender module, (DI Instruments, Cambridge, UK). A schematic of the apparatus is given in Figure 2.13. The major components of the AFM system are described in great detail below:

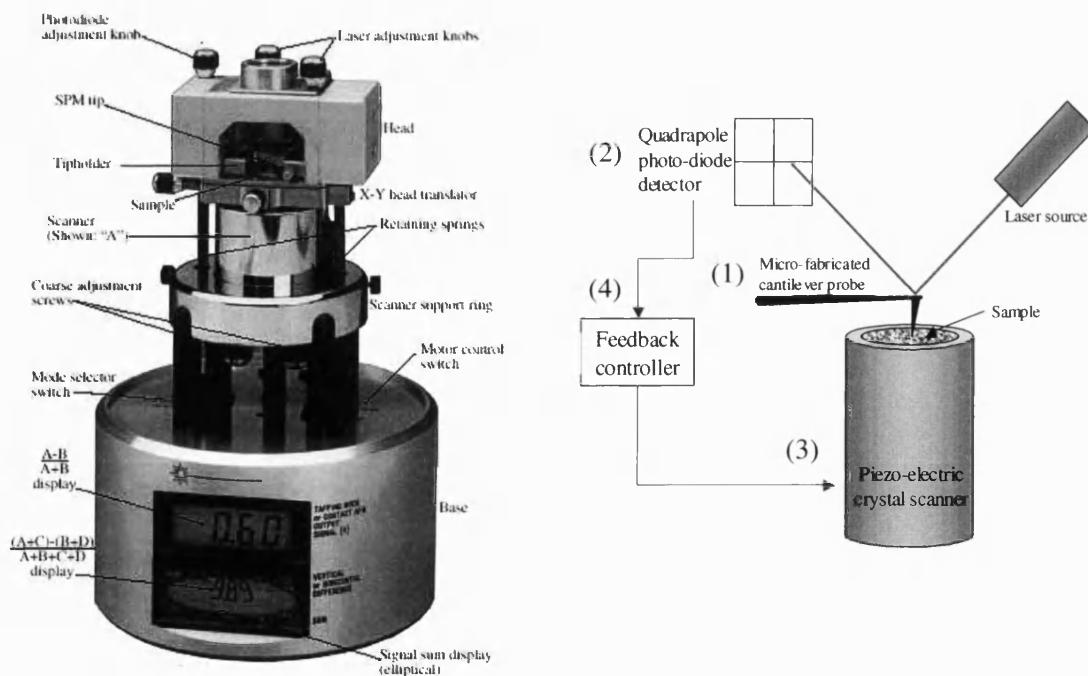


Figure 2- 13: Photograph and schematic representation of multimode™ AFM

- **Micro-fabricated cantilever probe (1)**

The AFM probe is typically a sharp proximal tip positioned at the free end of a spring-like cantilever. The probe is generally made of silicon nitride using well documented techniques used in the semiconductor industry. The spring constant of the cantilever, which is dependant on its shape and thickness, is application dependent.

- **Detector (2)**

In the case of the multimode AFM, a laser is positioned at the apex of the cantilever and reflected to a four quadrant photodiode detector. Early detectors used an STM probe to determine cantilever deflection [7]. However, more recent designs have incorporated piezoelectric sensors in the cantilever construct allowing direct deflection measurement.

- **Piezoelectric scanner (3)**

The scanner is a polycrystalline piezo cylinder constructed of doped zirconium titanate. The application of a high voltage to any one of the 3 axes will induce scanner movement. The amount of applied voltage can be calibrated to scanner movement allowing sub-Angstrom ( $\text{\AA}$ ) control. In the case of the multimode AFM, the sample is mounted on the scanner, which is moved relative to a stationary cantilever.

- **Feedback Loop Controller (4)**

The controller is a sensitive feedback data collection system between the photodiode analyser and the movement of the piezo scanner. It operates by attempting to maintain a set parameter (i.e. cantilever deflection, amplitude, etc...) monitored through the detector (Figure 2.14) by varying the position of the sample relative to the probe via the piezo scanner.

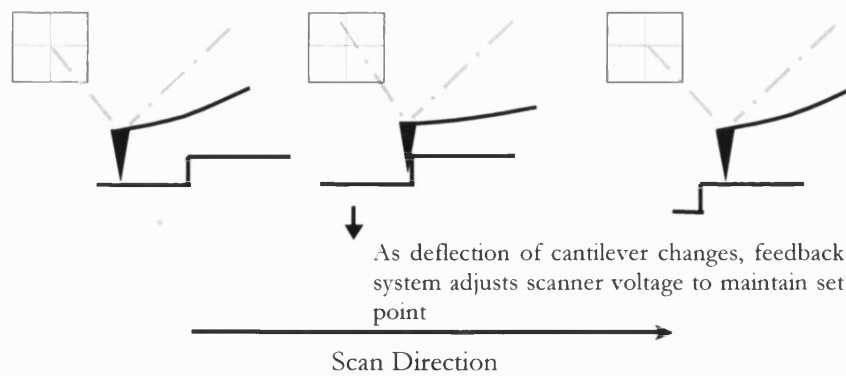


Figure 2- 14: Feedback loop controlling tip sample distance.

### 2.7.2. Surface Topography Analysis

Nanometre surface topography analyses were first operated by contact mode [8-11]. This scanning probe method involves the continuous contact between the tip and the substrate. When the probe encounters protrusions or surface deformations, the bending of the cantilever is identified by the laser deflection on the photodiode detector. The signal is then interpreted by a computer to reconstruct the substrate surface in a 3D image. A major drawback of this technique is the significant load and resulting frictional forces applied to the substrate that may potentially be destructive for soft samples [12].

Recent alterations of this AFM technique have allowed an intermittent contact of the tip with the sample surface reducing the lateral forces which may disrupt the surface of particularly fragile substrates during imaging. This intermittent mode, commonly known as Tapping mode, is based on measuring the change in amplitude of a tip oscillating at its resonance frequency, as it comes into contact with the underlying substrate surfaces. Variations in the amplitude of the oscillating tip are recorded by measuring the deflection of the laser. As the distance between the tip and the sample changes, a variation in the amplitude will occur. The feedback loop maintains the height of the scanner in order to keep the amplitude of the tip constant. A diagrammatic representation of Tapping mode method is shown in Figure 2.15.

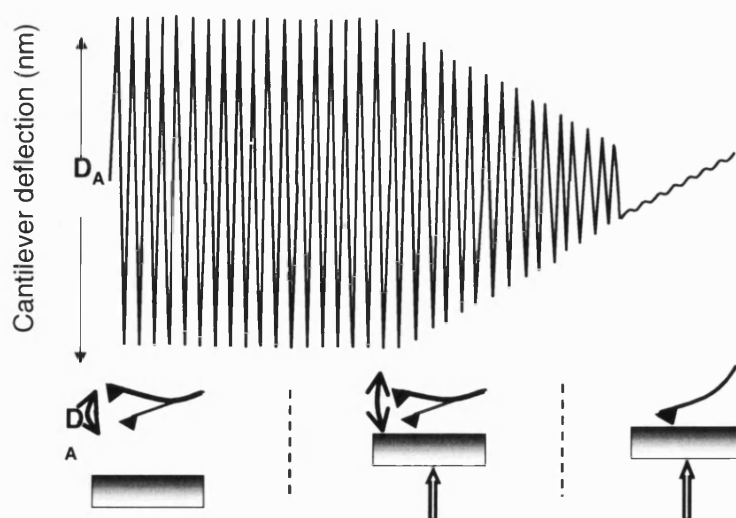


Figure 2- 15: Diagrammatic representation of tapping mode<sup>TM</sup> method

Although originally developed as a tool for surface topography analysis, numerous auxiliary uses of the AFM techniques have been developed providing a very powerful and versatile tool. Lateral friction microscopy, for example, allows measurement of the torsion of a tip as it is dragged across a sample surface. These measurements of lateral forces encountered along the surface yields a map of high/low friction sites [9, 13, 14].

A novel technique, “phase shift” imaging is an auxiliary method to Tapping mode AFM which measures the degree of phase shift in the oscillation of the tip upon encountering areas of different physico-mechanical properties [15-17]. As the oscillating cantilever tip encounters regions on a surface containing different physical properties, such as hardness or elasticity, a shift in phase will occur (lag in oscillation). A diagrammatic representation of phase imaging method is shown in Figure 2.16.

The phase lag of the drive of the cantilever-tip assembly oscillation is constantly measured. Since it is expected that crystalline regions will have a low surface free energy and a high packing density, the phase difference upon interaction with the scanning tip is expected to be very small. However, for disordered or amorphous regions, a high phase lag is expected due to a high surface free energy (large adhesion) and high deformation of the contact.

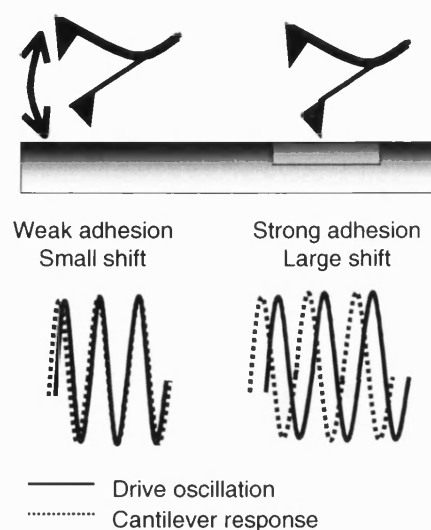


Figure 2- 16: Diagrammatic representation of phase imaging method

By measuring the degree of phase shift in unison with topography it becomes possible to identify variations in surface structure. Phase imaging has been considered as a possible tool for the visualisation of amorphous/crystalline regions on pharmaceutical material surfaces [18].

### 2.7.3. Solid-Solid Interaction Measurements

One of the most significant advances in AFM technology in term of pharmaceutical applications is Force Imaging. By affixing a particle on the apex of a tipless cantilever, it is possible to quantify the interaction forces between a particle and a substrate, at a Pico-Newton scale ( $10^{12}$ N). This technique consists of moving the piezo-scanner vertically in a sinusoidal pattern, while the cantilever is kept in a fixed position. By plotting the measured deflection as a function of displacement, a complete picture of the interactive behaviour between an individual particle and a substrate surface can be elucidated upon contact and removal of a particle from a substrate surface. Such a plot is known as a force-distance plot or more commonly as a force curve. A diagrammatic representation of an ideal force curve in which a non-deformable tip interacts with a hard surface is shown in Figure 2.17.

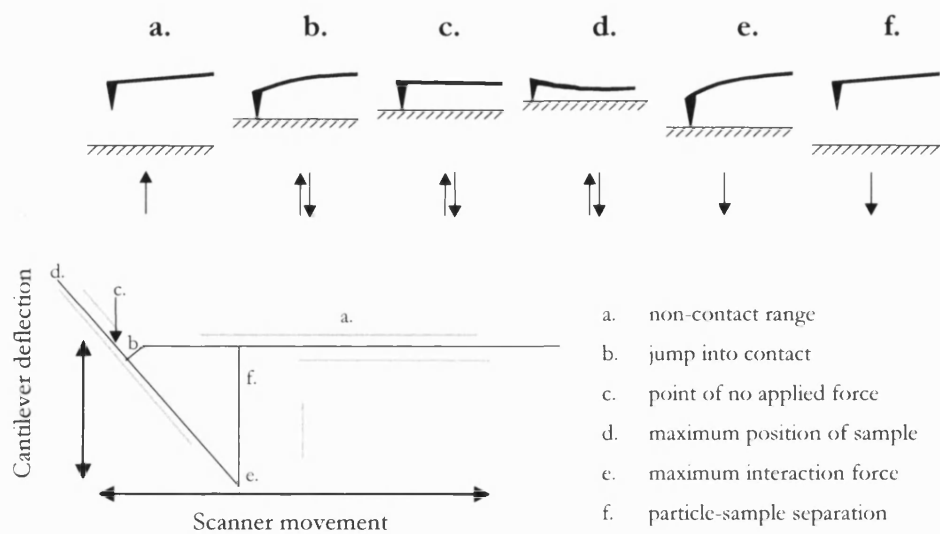


Figure 2- 17: Schematic representation of a force curve

Initially, although the scanner is moving up in the approach cycle (a), the tip is too far away to be influenced by any long-range forces and no deflection is therefore visible. At the short range (b), attractive van der Waals forces overcome the resistance of the cantilever spring and the tip jumps onto the sample surface. Scanner extension is then pursued until a pre-set compressive loading is applied between the particle and the substrate surfaces (d). This region is referred to as the region of constant compliance. Upon retraction of the tip, the same linear response is observed until the restoring force of the cantilever equals the interaction forces between sample and particle, and the maximum of the interaction forces is reached (e). Beyond this critical point, the retraction force overcomes the interaction forces and the tip separates abruptly from the surface of the sample (f). The scanner then keeps moving downward and no deflection is observable.

When the system is in equilibrium (e), the following equation is applicable:

$$F_{\text{retraction}} = F_{\text{adhesion}} \quad [2.1]$$

The retraction force can be determined using Hooke's law:

$$F_{\text{retraction}} = -kz \quad [2.2]$$

where  $k$  is the spring constant,  $z$  is the extent of the cantilever deflection, and the minus sign expresses the fact that the force is acting against the causes of its creation. It is then possible to determine  $F_{\text{adhesion}}$  as  $z$  can be calculated by means of laser deflection.

## 2.7.4. Materials and Methods

### 2.7.4.1. Particle Attachment onto Tipless AFM Cantilevers

Prior to force volume experiments, particles were affixed onto tipless cantilevers. The process can be divided into two distinctive steps. First, the apex of the standard V-shaped tipless cantilever (DNP-020, Digital Instruments, CA, USA) was coated with a thin layer of epoxy resin glue (Araldite, Bostik Ltd, Leicester, UK). The apex was then gently brought into contact with a particle. In order to achieve such a precise task, a high-resolution microscope (Zeiss, Leiptzig, Germany) was used throughout the procedure, thus allowing a control of the cantilever cleanliness as well as the particle attachment integrity. The spring constant ( $k$ ) of the cantilevers was determined by the thermal noise method ( $k = 0.282 \pm 0.039 \text{ N/m}$ ) [19-21]

### 2.7.4.2. Substrate Sample Preparation

Two techniques were developed for the preparation of sample substrates for AFM experiments: the use of model compacts formed by direct compression and the preparation of crystalline substrates with uniform flat surfaces by controlled re-crystallisation.

- ***Preparation of crystal substrates***

Large planar surfaces of the various powder materials were produced by controlled crystallisation techniques. The precise method of crystallisation was dependent on



the sample solubility profile. Saturated solutions were first prepared and shaken for 12 hours at 20°C (G76, Gyrotory water bath shaker, New Brunswick Scientific, Edison, USA) in sealed volumetric flasks prior to filtration via a 0.22  $\mu\text{m}$  membrane filter (Whatman Inc., Clifton, USA).

Powder samples were crystallised by primary nucleation, using an anti-solvent as a precipitating agent. A schematic representation of the crystallisation apparatus is shown in Figure 2.18. A microscope cover slip (12 mm x 12 mm) was supported on a vertical post in a crystallisation dish, which contained the anti-solvent. A droplet (~1 ml) of the filtered saturated solution was placed on the cover slip via a glass pipette. The system was sealed by inverting a suitable glass beaker within a crystallisation dish containing the anti-solvent. Upon equilibration of the vapour phases of the miscible solvents, nucleation and crystal growth within the solution droplet occurred. The glass cover slip was subsequently removed and fixed onto a magnetic stub with glass bond glue (Loctite, UK) for AFM studies.

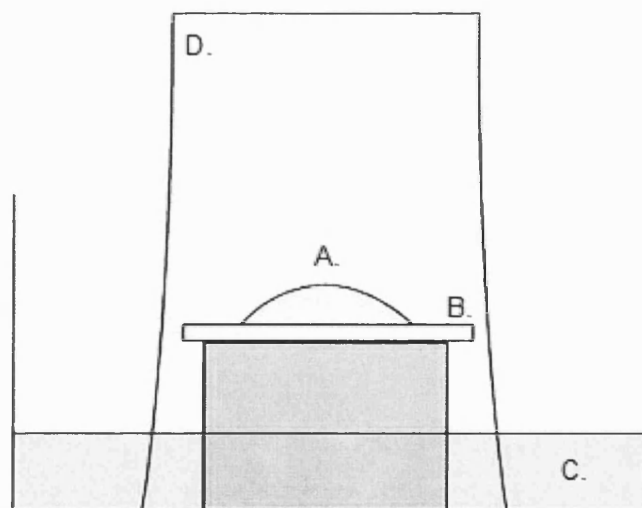


Figure 2- 18: Schematic representation of the anti-solvent re-crystallisation step. Where A: saturated solution droplet, B. glass slide, C. crystalline dish containing the anti-solvent, D. Beaker.

- **Preparation of compressed powder substrates**

Model surfaces of the various powders were prepared by high-pressure compression (TA HDI Texture analyser, Stable Micro Systems, Surrey, UK). Approximately 250mg of material was weighed into a 10mm stainless steel die and compacted during 3min, with a load of 500kg.

### 2.7.4.3. Control of Relative Humidity

A stream of dry nitrogen gas is divided into two, one of which humidified at 100% by bubbling into a bottle filled with water, while the other is maintained at 0%RH. The two streams were then recombined prior to insertion in the AFM head. By varying the flow rates of the wet and dry gases, it was possible to change the humidity from 0% up to 100% with a precision of  $\pm 1\%$ .

## 2.8. Surface Energy Characterisation

### 2.8.1.1. Principles and Methods

Several methods are available for calculating the dispersive and polar contributions to the total surface energy of a solid [22-25]. However, given the nature of the materials to be analysed, the preferred route was to calculate solid surface energy from contact angle measurements, using the sessile drop method [26-29]. This technique involves the measurement of the angle of contact between a liquid droplet and the surface of a solid of interest, as illustrated in Figure 2.19. The estimate of the contact angle,  $\theta$ , is made from the tangential vector formed between the solid surface and the sessile drop profile. The contact angle is a measure of the competing tendencies of the liquid to spread over the solid surface or rounds up to minimise its contact area. For instance, if the molecular adhesion between solid and liquid is greater than the cohesion between the molecules of liquid, wetting will occur. In contrast, liquids with high surface tension will generate a finite contact angle.

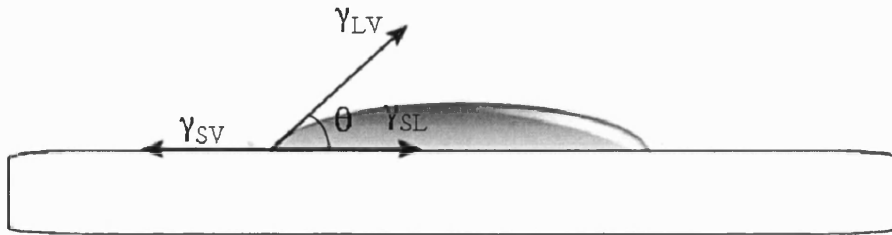


Figure 2- 19: Diagrammatic representation of contact angle measurement by sessile drop technique

Equilibrium of the surface forces is expressed mathematically by Young's equation:

$$\gamma_{LV} \cos \theta = \gamma_{SV} - \gamma_{SL} \quad [2.3]$$

where  $\gamma_{LV}$  is the interfacial tension between the liquid and vapour phase,  $\gamma_{SV}$  is the interfacial tension between the solid and vapour phase and  $\gamma_{SL}$  is the interfacial tension between the solid and liquid phase. The interfacial energy between two phases may be expressed as a function of their respective dispersive and acid-base contributions, as shown in Eq. [1.24] given in Chapter 1. Substituting this equation with Eq. [2.3] yields to:

$$(1 + \cos \theta) \gamma_L = \left( \sqrt{\gamma_S^{LW} \gamma_L^{LW}} + \sqrt{\gamma_S^+ \gamma_L^-} + \sqrt{\gamma_S^- \gamma_L^+} \right) \quad [2.4]$$

which is known as the Van Oss-Chaudhury-Good thermodynamic approach to determine the contributions of the total surface free energy of solids [30, 31]. The characterisation of the three components of the solid surface tension ( $\gamma_S^{LW}$ ,  $\gamma_S^+$  and  $\gamma_S^-$ ) from Eq. [2.4] requires therefore the use of a minimum of three liquids; one apolar and two polars. This results in a series of equations with three unknowns that can be mathematically resolved [23].

Contact angle measurements were performed using a Goniometer (Ramé-hart Inc., New Jersey, USA). Diiodomethane was used as an apolar liquid whereas ethylene glycol and glycol were used as polar liquids. Surface tension contributions of the various liquids are summarised in Table 2.1.

Liquid	$\gamma_L$	$\gamma_L^{LW}$	$\gamma_L^{AB}$	$\gamma_L^+$	$\gamma_L^-$
Diiodomethane	50.8	0.0	0.0	0.0	0.0
Ethylene glycol	48.0	29.0	19.0	1.9	47.0
Water	72.8	21.8	51.0	25.5	25.5

Table 2- 1: Surface tension contributions (in  $\text{mJ}\cdot\text{m}^{-2}$ ) of liquids used in direct contact angle measurements.

### 2.8.1.2. Results

Contact angles measured on tablets of the various materials used in this study are summarised in Table 2.2. Resulting surface energy contributions and Gibbs surface free energy of cohesion of these powders are summarised in Table 2.3.

Sample	Contact angle ( $\theta$ )		
	Diiodomethane	Ethylene glycol	U.P. water
Salbutamol sulphate	$40.00 \pm 1.00$	$15.00 \pm 1.00$	$21.67 \pm 1.53$
Budesonide	$8.00 \pm 1.00$	$45.67 \pm 7.23$	$30.33 \pm 2.08$
Sorbalac 400	$17.33 \pm 1.53$	$14.67 \pm 2.52$	$7.67 \pm 1.53$
leucine	$62.33 \pm 1.53$	$71.33 \pm 2.08$	$63.66 \pm 1.53$
lecithin	$69.67 \pm 2.51$	$13 \pm 2.64$	$20.00 \pm 0.5$
Magnesium stearate	$69.67 \pm 2.08$	$73.33 \pm 3.05$	$94.67 \pm 2.51$

Table 2- 2: Contact angle measurements of powders assessed by sessile drop techniques

Sample	$\gamma^{LW}$	$\gamma^+$	$\gamma^-$	$\gamma^{tot}$	$\Delta G^{tot}$
Salbutamol sulphate	43.94	0.01	55.59	45.58	-91.19
Budesonide	50.40	2.77	72.68	78.74	-157.51
Sorbalac 400	48.51	0.05	66.29	52.28	-104.65
leucine	27.23	0.59	40.20	36.87	-73.88
lecithin	23.07	2.29	64.43	47.38	-94.77
Magnesium stearate	23.06	0.15	3.32	24.42	-48.92

Table 2- 3: Powder surface energy contributions and resulting Gibbs surface free energy of cohesion (in  $\text{mJ}\cdot\text{m}^{-2}$ ).

## 2.9. Statistical analyses

The average and deviation of populations were expressed as arithmetic mean ( $\bar{x}$ ) and standard deviation (SD) for normal distributions, median ( $x_{50}$  corresponding to the 50<sup>th</sup> percentile) and geometric standard deviations (GSD) for lognormal distributions.

Arithmetic mean was calculated by:

$$\bar{x} = \frac{1}{n} \sum_{i=1}^n x_i \quad [2.5]$$

The standard deviation of a pool of numbers was calculated using:

$$SD = \sqrt{\frac{1}{n-1} \sum_{i=1}^n (\bar{x} - x_i)^2} \quad [2.6]$$

The relative standard deviation (RSD) was calculated by:

$$RSD = \frac{SD \times 100}{\bar{x}} \quad [2.7]$$

Geometric standard deviation was expressed as a function of the 16<sup>th</sup> and 84<sup>th</sup> percentile of the population as follow:

$$GSD = \left( \frac{x_{84\%}}{x_{16\%}} \right)^{1/2} \quad [2.8]$$

Statistical analyses between different populations were carried out by one-way ANOVA. A population was regarded as significantly different if the assumption of similarity was rejected with a probability greater than 95%. Comparison of the means was performed by Fisher pair wise comparison.

## 2.10. References

- [1] W. C. Hinds. *Aerosol technology: Properties, Behaviour and measurements of airborne particles*, Wiley, New York, 1999.
- [2] T. Allen. *Particle size measurement*, Chapman & Hall, London, 1990.
- [3] BSI. Particle size analysis laser diffraction methods, part 1: general principles, British standard institute, BS ISO number 13320-1:1999, 1999.
- [4] P. A. Webb and C. Orr. *Analytical methods in fine particle echnology*, Micromeritics Instruments Corp., Norcross, USA, 1997.
- [5] B.P.C. British Pharmacopoeia, Vol. II, London (1993).
- [6] H. J. Scheel, G. Binnig, and H. Rohrer. Atomically flat LPE-grown facets seen by scanning tunneling microscope. *J. Cryst. Growth* **60**: 199-202 (1982).
- [7] G. Binnig, C. F. Quate, and C. Gerber. Atomic force microscopy. *Phys. Rev. Let.* **56**: 930-933 (1986).

- [8] Y. Ando and J. Ino. The Effect Of Asperity Array Geometry On Friction And Pull-Off Force. *Journal of Tribology* **119**: 781-787 (1997).
- [9] Y. Ando. The effect of relative humidity on friction and pull-off forces measured on submicron-size asperity arrays. *Wear* **238**: 12-19 (2000).
- [10] Y. Ando and J. Ino. Friction and pull-off forces on submicron-size asperities. *Wear* **216**: 115-122 (1998).
- [11] S. H. Kim, C. Marmo, and G. A. Somorjai. Friction studies of hydrogel contact lenses using AFM: non- crosslinked polymers of low friction at the surface. *Biomaterials* **22**: 3285-3294 (2001).
- [12] C. J. P. Boonaert, V. Toniazzo, C. Mustin, Y. F. Dufrene, and P. G. Rouxhet. Deformation of *Lactococcus lactis* surface in atomic force microscopy study. *Colloid Surf. B-Biointerfaces* **23**: 201-211 (2002).
- [13] Y. Ando and J. Ino. Friction and pull-off forces on submicron-size asperities. *Wear* **216**: 115-122 (1998).
- [14] B. Bhushan and S. Sundararajan. Micro/nanoscale friction and wear mechanisms of thin films using atomic force and friction force microscopy. *Acta Materialia* **46**: 3793-3804 (1998).
- [15] H. S. Ahn, S. A. Chizhik, A. M. Dubravin, V. P. Kazachenko, and V. V. Popov. Application of phase contrast imaging atomic force microscopy to tribofilms on DLC coatings. *Wear* **249**: 617-625 (2001).
- [16] G. Bar, R. Brandsch, and M. H. Whangbo. Correlation between frequency-sweep hysteresis and phase imaging instability in tapping mode atomic force microscopy. *Surf. Sci.* **436**: L715-L723 (1999).

- [17] G. Bar, R. Brandsch, and M. H. Whangbo. Effect of tip sharpness on the relative contributions of attractive and repulsive forces in the phase imaging of tapping mode atomic force microscopy. *Surf. Sci.* **422**: L192-L199 (1999).
- [18] P. Begat, P. M. Young, S. Edge, J. S. Kaerger, and R. Price. The effect of mechanical processing on surface stability of pharmaceutical powders: Visualization by atomic force microscopy. *J. Pharm. Sci.* **92**: 611-620 (2003).
- [19] T. J. Senden and W. A. Ducker. Experimental-Determination of Spring Constants in Atomic-Force Microscopy. *Langmuir* **10**: 1003-1004 (1994).
- [20] J. L. Hutter and J. Bechhoefer. Calibration of Atomic-Force Microscope Tips. *Review of Scientific Instruments* **64**: 1868-1873 (1993).
- [21] D. A. Walters, J. P. Cleveland, N. H. Thomson, P. K. Hansma, M. A. Wendman, G. Gurley, and V. Elings. Short cantilevers for atomic force microscopy. *Rev. Sci. Instrum.* **67**: 3583-3590 (1996).
- [22] V. Medout-Marere, H. Malandrini, T. Zoungrana, J. M. Douillard, and S. Partyka. Thermodynamic investigation of surface of minerals. *J. Pet. Sci. Eng.* **20**: 223-231 (1998).
- [23] R. J. Good. Contact-Angle, Wetting, and Adhesion - a Critical-Review. *J. Adhes. Sci. Technol.* **6**: 1269-1302 (1992).
- [24] I. Yildirim. Surface Free Energy Characterization of Powders, *Minig and Minerals engineering*, Faculty of the Virginia Polytechnic Institute, Blacksburg, 2001.
- [25] J. Kiesvaara and J. Yliruusi. The Use of the Washburn Method in Determining the Contact Angles of Lactose Powder. *International Journal of Pharmaceutics* **92**: 81-88 (1993).



- [26] P. M. Costanzo, W. Wu, R. F. Giese, and C. J. van Oss. Comparison Between Direct-Contact Angle Measurements and Thin-Layer Wicking On Synthetic Monosized Cuboid Hematite Particles. *Langmuir* **11**: 1827-1830 (1995).
- [27] Z. Li, R. F. Giese, and C. J. van Oss. Surface Thermodynamic Properties of Synthetic Hydrotalcite Compounds. *Langmuir* **10**: 330-333 (1994).
- [28] C. J. van Oss. *Interfacial Forces in Aqueous Media.*, Marcel Decker Inc., New York, 1994.
- [29] W. Wu, R. F. Giese, and C. J. van Oss. Evaluation of the Lifshitz-Van Der Waals Acid-Base Approach to Determine Surface-Tension Components. *Langmuir* **11**: 379-382 (1995).
- [30] C. J. van Oss, M. K. Chaudhury, and R. J. Good. Interfacial Lifshitz-van der Waals and polar interactions in macroscopic systems. *Chem. Rev.* **86**: 927-941 (1988).
- [31] C. J. van Oss, R. J. Good, and M. K. Chaudhury. The Role of Van der Waals Forces and Hydrogen-Bonds in Hydrophobic Interactions between Bio-Polymers and Low-Energy Surfaces. *J. Colloid Interface Sci.* **111**: 378-390 (1986).

## Chapter 3

# Quantification of the Interaction Force Balance in Dry Powder Formulations

### 3.1. Introduction

The adhesion between a micron-sized particle and a solid surface is a result of a complex combination of physical forces. These include the ubiquitous van der Waals forces, as well as possible influences from electrostatic and capillary forces [1]. The contribution of each of these forces to the overall adhesion is dependant on various factors, including the physical properties of the contiguous surfaces as well as environmental conditions. However, direct characterisation of the specific influence of these individual forces is difficult, as is their dependence on physico-mechanical and environmental conditions. Well-established techniques for measuring particle adhesion include centrifugal particle detachment, fluid dynamic and vibration methods [2-4]. These techniques provide quantitative information concerning the integrated effect of physical and environmental variations on particle adhesion. They are, however, severely limited when the properties that influence the adhesion of an individual particle and a substrate surface are required. With the advent of the atomic force microscope (AFM) and the development of the colloid probe technique, quantification of the total interaction force between an individual drug particle and a substrate surface can be determined [5].

Measurements of the pull-off forces between pharmaceutical particles with irregular morphologies and varying degree of surface roughness have previously been reported [6]. Although the effects of surface roughness on variations in adhesion forces are acknowledged, direct quantification of true contact area between two contiguous surfaces remains difficult [7]. More recently, however, a method for characterising the contact area between a micronised particle and a substrate surface has been developed [8, 9]. This AFM based approach involves scanning a colloidal drug probe over a grid composed of very sharp asperities. Due to a limitation in the Villarrubia algorithm utilised to reconstruct the substrate topography, a reverse surface image of the tip is recorded. Although an estimate of the area of contact of a micron sized particle can subsequently be discerned, the approach is limited when considering the surface deformation of the interacting materials and the variations between two substrate surfaces of different rugosities.

Model substrate surfaces for AFM colloid probe investigations are commonly prepared by high-pressure compaction tableting [8, 10]. It is speculated that the high loading pressures required are sufficient to induce local defects and dislocations, and potentially significant areas of amorphous disorder [11, 12]. The presence of these amorphous domains may alter the surface free energy properties of the substrate material and subsequently modify the associated mechanical properties and thermodynamic work of cohesion/adhesion upon interaction.

In this study, model drug and carrier particles were crystallised directly from solution to obtain well-defined and highly reproducible single crystals with characteristically smooth and planar surfaces. Although the contact area between an interacting probe and substrate would remain unknown, the uniform texture of substrate surfaces should allow direct comparison of interactions between a specific colloid probe and an array of substrate materials. This AFM based approach may provide a novel means of quantifying the cohesive and adhesive interactions within a dry powder formulation and ultimately provide a critical understanding of the force balance, which directly influence the overall characteristics and performance of a dry powder formulation.

## 3.2. Methods

General methods of each technique or apparatus used in this study are described in detail in Chapter 2.

- **Crystallisation of material substrates**

Saturated solutions of budesonide in ethanol, salbutamol sulphate in water and lactose in water were prepared prior to re-crystallisation. Samples were shaken for 12 hours at 20°C (G76, Gyrotory water bath shaker, New Brunswick Scientific, Edison, USA) in sealed volumetric flasks prior to filtration via a 0.22 µm membrane filter (Whatman Inc., Clifton, USA).

Budesonide, salbutamol sulphate and lactose were crystallised by primary nucleation, using an anti-solvent as a precipitating agent. The heterogeneous nucleation and growth of the crystals onto the glass cover slips precluded the need for any sample preparation of the crystals for AFM investigations.

- **Microscopic surface topography analysis**

All AFM surface topography images were recorded in Tapping Mode operation (TM-AFM). Tetrahedral-tipped silicon-etched cantilevers (OTSP, Digital Instruments) were utilized for imaging. Surface roughness measurements were analyzed over a 2.5µm x 2.5µm area. To quantify the variations in the surface properties of the crystal surfaces, the root-mean-squared surface roughness measurement ( $R_q$ ) and the mean surface roughness ( $R_a$ ) of the height deviations of the surface asperities were computed.

- **Interaction force measurements**

The AFM was housed in an environmental chamber and the ambient conditions maintained at a constant temperature of 25°C ( $\pm 0.2^\circ\text{C}$ ) and relative humidity of 35% RH ( $\pm 3\%$ ). The partial water vapour pressure was controlled via a custom-built perfusion unit coupled to a highly sensitive humidity sensor (Rotronic AG, CH).

Individual force curves ( $n = 4096$ ) were conducted over a  $2.5\mu\text{m} \times 2.5\mu\text{m}$  at a scan rate of 4Hz and a compressive loading of 10nN. These parameters were kept constant throughout the study. Statistical analysis of these data was performed by Fisher's pair wise comparison of one-way ANOVA with 99% confidence limits.

### 3.3. Results

#### 3.3.1. Morphological Characterisation

The macroscopic morphology of the budesonide, salbutamol sulphate and lactose crystals were first identified by scanning electron microscopy. The Miller indices of the dominant growth faces of the crystals obtained were identified using a 3D simulation program (SHAPE V7.0, Shape Software, Tennessee, USA). The 3D crystal structures required the input of the unit cell lattice parameters and the space group symmetry operators. Budesonide crystallises in the orthorhombic crystal system ( $a = 8.550\text{\AA}$ ,  $b = 9.406\text{\AA}$  and  $c = 28.401\text{\AA}$ ), space group  $P2_12_12_1$  [13]. Salbutamol sulphate crystallises in the monoclinic crystal system, ( $a = 28.069\text{\AA}$ ,  $b = 6.183\text{\AA}$ ,  $c = 16.914\text{\AA}$  and  $\beta = 81.19^\circ$ ), space group  $C_c$  [14]. Alpha-lactose monohydrate crystallises in the monoclinic crystal system ( $a = 7.982\text{\AA}$ ,  $b = 21.562\text{\AA}$ ,  $c = 4.824\text{\AA}$  and  $\beta = 109.57^\circ$ ), space group  $P2_1$  [15]. Representative scanning electron micrographs of the dominant growth faces of crystallised budesonide, salbutamol sulphate and lactose are shown in Figure 3.1A, 3.1B and 3.1C respectively. Budesonide crystals displayed an elongated dodecahedral shape in relation to the growth of the dominant  $(01\bar{2})$  and  $(0\bar{1}2)$  Miller indices. Electron micrographs of salbutamol sulphate crystals suggested a needle like morphology dominated by the  $(200)$  face, while the majority of lactose crystals exhibited the well-known tomahawk shape, dominated by the  $(100)$  and  $(1\bar{1}0)$  crystalline faces. The single crystals exhibited highly smooth surface textures.

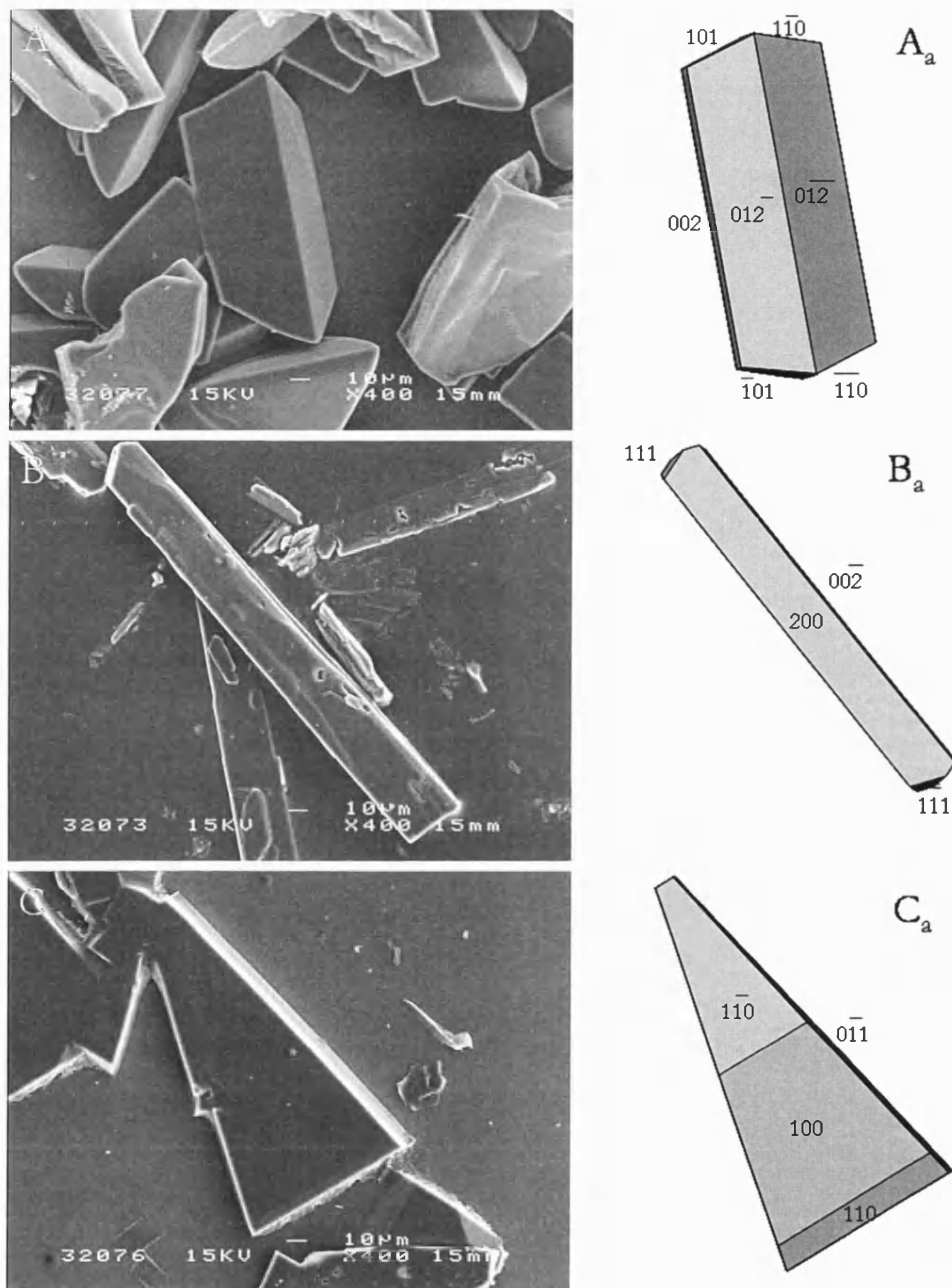


Figure 3- 1: Representative SEM images and corresponding 3D morphologies ( $\alpha$ ) of crystals of budesonide (A), salbutamol sulphate (B) and  $\alpha$ -lactose monohydrate (C).

Representative AFM amplitude images of the dominant single crystal faces of budesonide, salbutamol sulphate and  $\alpha$ -lactose monohydrate are shown in Figure 3.2A, 3.2B and 3.2C, respectively. Topographical AFM images indicated varying degrees of nanometre roughness for the model substrate surfaces. These variations were probably related to differing growth processes and kinetics during crystallisation.

The surface rugosity  $R_a$  (average height from the centre line) and root mean square deviation  $R_q$  (variability of the profile from the centre line) of the three samples are shown in Table 3.1.

The data confirmed the extremely smooth surface morphology of the crystals faces observed by SEM, exhibiting surface roughness measurements well below 5nm. It should be noted that there was no observable modification in surface morphology over large areas ( $>20\mu\text{m}^2$ ) of the crystal faces. Thus, the engineered crystal substrates should provide highly suitable surfaces for quantitative analysis of the force balance in model dry powder formulations.

	budesonide	salbutamol sulphate	$\alpha$ -lactose monohydrate
rugosity (nm)	0.681	2.258	1.837
RMS (nm)	0.872	3.142	2.284

Table 3- 1: Roughness properties of budesonide, salbutamol sulphate and  $\alpha$ -lactose monohydrate.

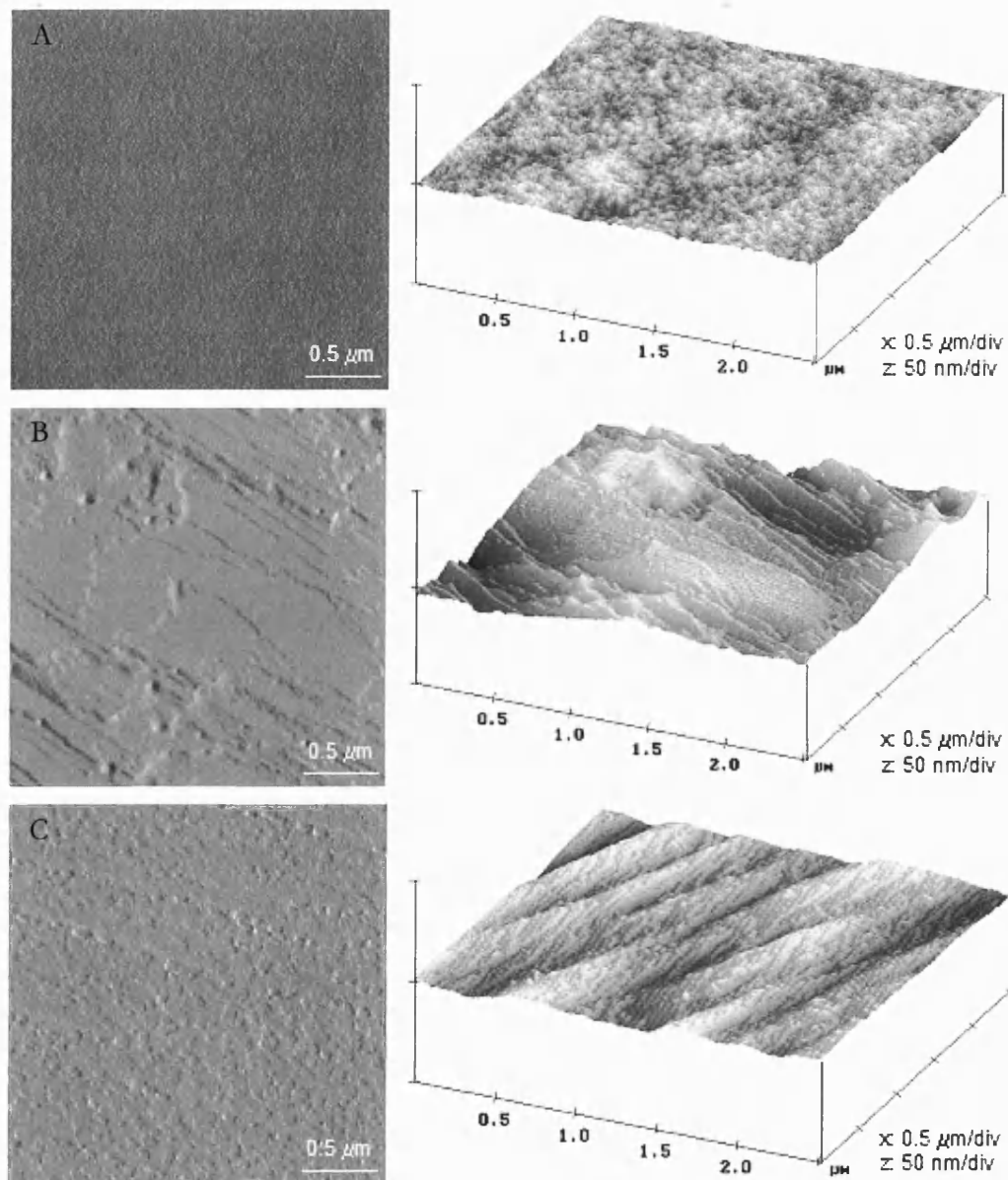


Figure 3- 2: Representative AFM amplitude images of the surface of re-crystallised budesonide (A), salbutamol sulphate (B) and  $\alpha$ -lactose monohydrate (C).



### 3.3.2. Interaction Force Measurements

For consistency, the dominant crystal face of each material was chosen and care was taken to place the probes in the same region on the substrate for each experiment. For all systems, the force distributions could be fitted to a Gaussian distribution, related to the uniformity in contact area between probe and multiple contact points on the substrate surface. Furthermore, the small standard deviation of the distributions confirmed the suitability of the engineered crystal surfaces in producing highly accurate and reproducible data.

The adhesion force of interaction between a series of budesonide probes and  $\alpha$ -lactose monohydrate, salbutamol sulphate and budesonide crystal substrates are shown in Figure 3.3A. The adhesive interaction between budesonide and lactose were significantly higher than with salbutamol sulphate ( $P < 0.01$ ). However, a significant increase and overall dominance of the cohesive interaction was observed for all budesonide probes ( $P < 0.01$ ).

Interaction forces between salbutamol sulphate probes and the dominant crystal faces of  $\alpha$ -lactose monohydrate, salbutamol sulphate and budesonide crystal substrates are shown in Figure 3.3B. In contrast to budesonide interactions, the salbutamol sulphate probes exhibited extremely weak cohesive properties with respect to the adhesive interactions with both  $\alpha$ -lactose monohydrate and budesonide ( $P < 0.01$ ). The adhesive interactions between salbutamol sulphate and lactose were significantly higher than the adhesive salbutamol sulphate-budesonide interaction ( $P < 0.01$ ).

Interaction forces between lactose probes and  $\alpha$ -lactose monohydrate, salbutamol sulphate and budesonide crystal substrates are illustrated in Figure 3.3C. The adhesive interaction between a lactose and salbutamol sulphate were significantly greater than both the cohesive lactose-lactose and adhesive lactose-budesonide interaction ( $P < 0.01$ ). However, the cohesive lactose interactions were significantly greater than the adhesive interactions between lactose and budesonide ( $P < 0.01$ ).

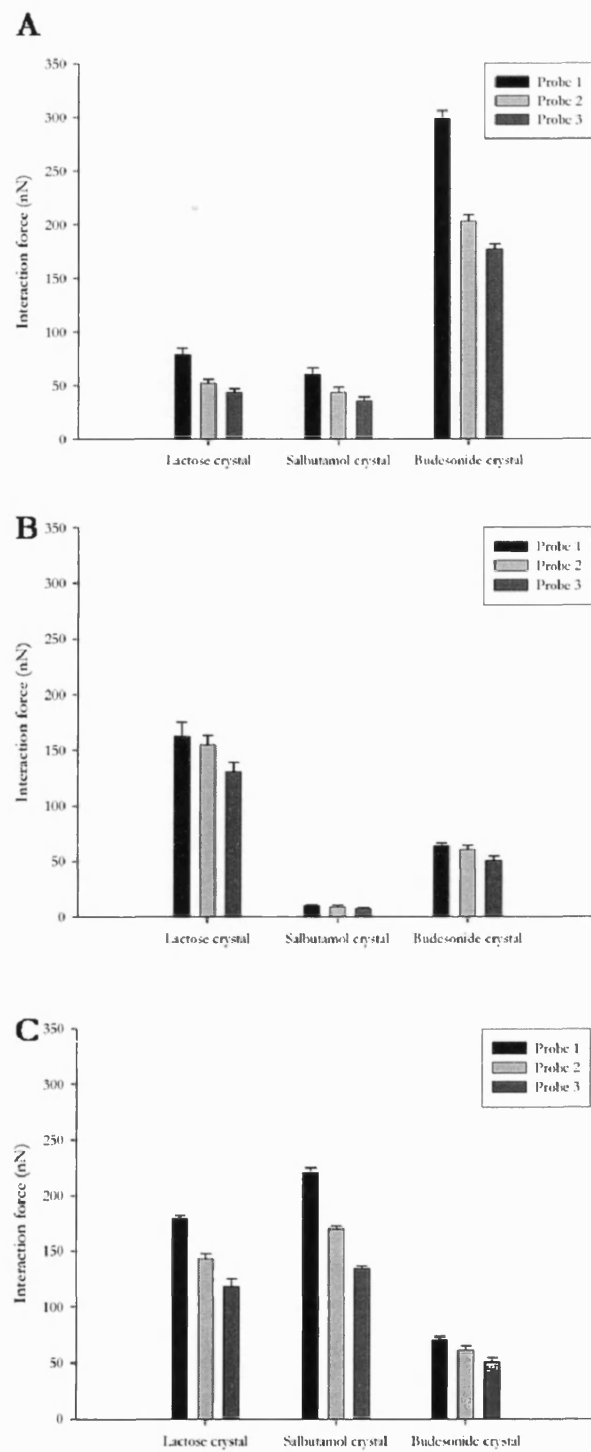


Figure 3- 3: Interaction forces between budesonide (A), salbutamol sulphate (B) and lactose (C) probes and  $\alpha$ -lactose monohydrate, salbutamol sulphate and budesonide crystal substrates.

Since the drug probes were prepared from untreated material, variability in probe geometry was expected. This would result in significant variations in contact area between each probe and the model substrate surface and concomitantly the adhesion force measurements. This variation in contact geometry was highlighted by the variations in adhesion force measurements between each probe and a given substrate. Nevertheless, a relationship between adhesive and cohesive interactions could be obtained by determining the specific variation in interaction between each individual probe and model substrate surfaces.

### **3.4. Discussion**

The balance of inter-particulate forces within dry powder inhaler formulations is critical in the mixing, stability and de-aggregation and dispersion properties of active pharmaceutical ingredients. However, quantitative measurements of these fundamental interactions and their specific role on blending and aerosolisation behaviour have not been fully realised. Such measurements have been limited due to the complex nature of the physico-mechanical interactions and, in particular, the major influence of variations in contact area on particle adhesion. Furthermore, efforts to predict the adhesion forces using theoretical approaches and surface energy measurements have proven unsatisfactory [16, 17]. Theoretical estimates are often several orders of magnitude greater than experimental measurements. The most plausible explanation for this disparity is that the true contact area between contiguous surfaces is significantly less than expected macroscopic dimensions.

In this study, a novel analysis of the AFM colloid probe technique has been utilised to determine the cohesive-adhesive force balances within model dry powder formulations. Controlling the nanoscale morphology of dominant growth faces of drug and excipient crystals substantially reduced the influence of substrate surface roughness on particle adhesion, as described previously [7]. Under controlled environmental conditions, force measurements were observed to be highly reproducible. However, quantification of force measurements was precluded, as it would require normalisation through the determination of the probe-substrate contact area.

In the absence of any significant electrostatic force or upon complete dissipation of the build-up of electrostatic charges from interacting surfaces, the principal forces contributing to particle adhesion are the van der Waals and capillary forces. Various theoretical models, derived from the Hertz approximation [18], have been developed to determine the van der Waals force of interaction. The two most commonly used models are the Johnson-Kendall-Roberts (JKR) [19] and the Deryaguin-Muller-Toporov (DMT) [20] models. The resulting force of adhesion between two spheres is provided in equation [3.1].

$$F_{vdw} = n\pi R^* W_{adh} \quad [3.1]$$

where  $R^*$  is the harmonic mean of the particle radii (also called contact radius),  $W_{adh}$  is the thermodynamic work of adhesion ( $\text{mJ}\cdot\text{m}^{-2}$ ), and  $n$  is a pre-determined constant depending on the selected model ( $n=3/2$  for JKR and  $n=2$  for the DMT).

Capillary forces arise from the dynamic condensation of water molecules onto particle surfaces. If the amount of condensed water is sufficient, a meniscus is formed between the contact points of the adjacent surfaces as liquid is drawn by capillary action around the contact points, inducing an attractive force. Fisher and Israelachvili [21] proposed a method to predict the capillary interaction between two spherical particles that is valid for AFM experiments. The subsequent capillary force equation is shown below:

$$F_c = 4\pi R^* \gamma_L \cos \theta + 4\pi R^* \gamma_{SL} \quad [3.2]$$

where  $\gamma_L$  is the water surface tension,  $\gamma_{SL}$  is the solid-liquid interfacial free energy and  $\theta$  is the measured contact angle of the liquid with the particle surface.

It should be noted that both the thermodynamic work of adhesion  $W_{ad}$  and contact angle are directly dependant on the surface free energies and the interfacial free energy of the interacting surfaces. Furthermore, van der Waals and capillary forces are directly proportional to particle radii, i.e. contact area. Thus, these two factors are of critical importance in the quantification of inter-particle forces.

In order to overcome these limitations, the ratios of adhesive and cohesive balances were compared rather than the separation forces. By combining Eq. [3.1] and Eq. [3.2], this cohesive-adhesive balance between materials A and B can be expressed as:

$$\frac{F_{A-A}}{F_{A-B}} = \frac{R_{A-A}^* (n\pi W_{A-A} + (4\pi\gamma_{water} \cos \theta_{A-A} + 4\pi\gamma_{A-water}))}{R_{A-B}^* (n\pi W_{A-B} + (4\pi\gamma_{water} \cos \theta_{A-B} + 4\pi\gamma_{A-water}))} \quad [3.3]$$

where  $F_{A-A}$  and  $F_{A-B}$  are the cohesive and adhesive forces, respectively. It can be concluded from Eq. [3.3] that with constant environmental conditions, the work of adhesion and contact angle are only dependant on the material physical characteristics. For a colloidal particle interacting with the substrate materials, the only parameters which are susceptible to vary are the contact radii  $R_{A-A}^*$  and  $R_{A-B}^*$ . Assuming the similarity of the two tailored substrate surface contact radii, the cohesion-adhesion ratios for a number of interacting probes of a specific material should theoretically remain constant. Thus, by plotting the measured force of cohesion as a function of the force of adhesion for a number of probes, the force balance within a model formulation could be quantified.

A cohesive-adhesive balance (CAB) graph of a theoretical binary system is illustrated in Figure 3.4. The adhesive force measurements for a number of probes of the interacting materials ( $F_{A-B}$  and  $F_{B-A}$ ) are plotted on the X-axis; the related forces of cohesion ( $F_{A-A}$  and  $F_{B-B}$ ) of the respective probes are plotted on the Y-axis. For equivalent contact geometry, the force data of several probes of a specific material plotted on a CAB-graph should follow a linear fit, resulting from the consistency in the cohesive-adhesive balance ratio ( $F_{A-A}/F_{A-B}$  and  $F_{B-B}/F_{B-A}$ ). The bisecting line corresponds to equilibrium between forces of adhesion and forces of cohesion, which defines two distinctive regions. The relative position of the aligned plots with respect to the bisector is a direct indication of the cohesive-adhesive balance of the interacting material within the binary system. Plots in the lower section indicate a ascendancy of adhesive interactions ( $F_{adh.} > F_{coh.}$ ). Conversely, plots in the upper section of the graph denote a dominance of cohesive properties. Quantitative assessment of the adhesive/cohesive interactions can be directly measured by the linear regression slopes.

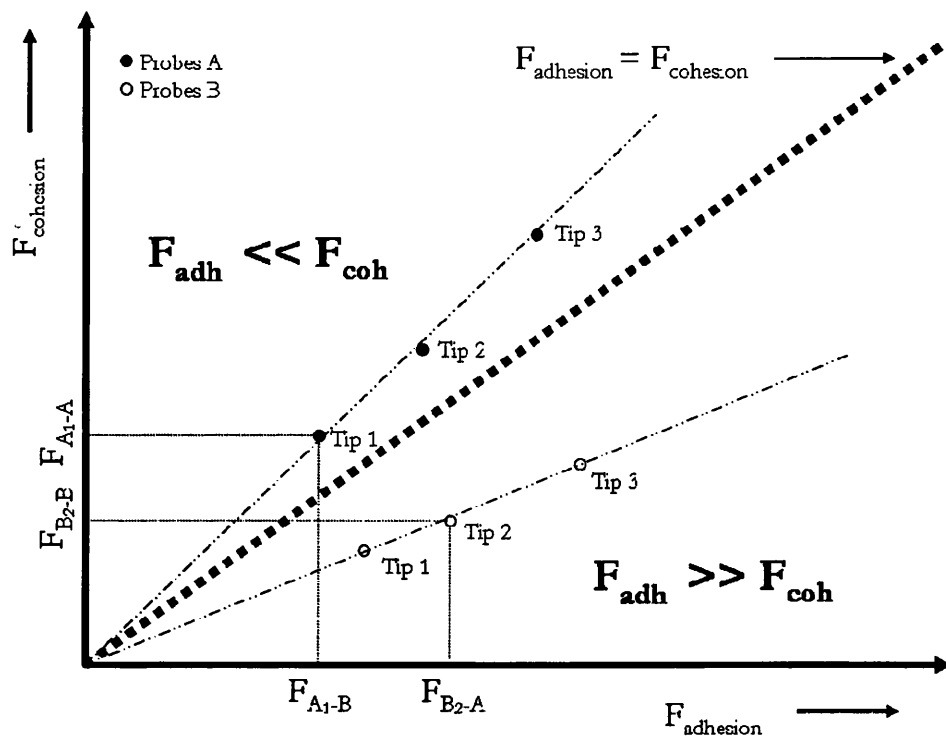


Figure 3- 4: Description of a CAB-graph for a theoretical binary system.

From the force measurements in Figure 3.3, a CAB-graph of a lactose-budesonide system is shown in Figure 3.5. A linear regression was performed for each set of data to verify the consistency of contact area uniformity of probe interaction from one substrate to another. A coefficient of determination ( $R^2$ ) of 0.9910 and 0.9873 for the lactose probes and budesonide probes, respectively, confirmed uniformity in contact area between crystals and the relationship between adhesion and cohesion for the interactive probes. Furthermore, the two plots indicated that for an equivalent contact area, both budesonide and lactose particles experience a greater affinity for cohesive interactions. The measurement of the relative slopes suggested that the budesonide-budesonide interactions are 3.84 fold greater than the adhesive budesonide-lactose interactions, while lactose-lactose interactions are 2.36 fold greater than the adhesive lactose-budesonide interactions. From a formulation perspective, the data suggested that this binary system would exhibit poor blend homogeneity unless a significant amount of shear energy was introduced to overcome the cohesive bonds. Moreover, such a formulation would possibly be subjected to segregation over time due to the very strong budesonide cohesive bonds.

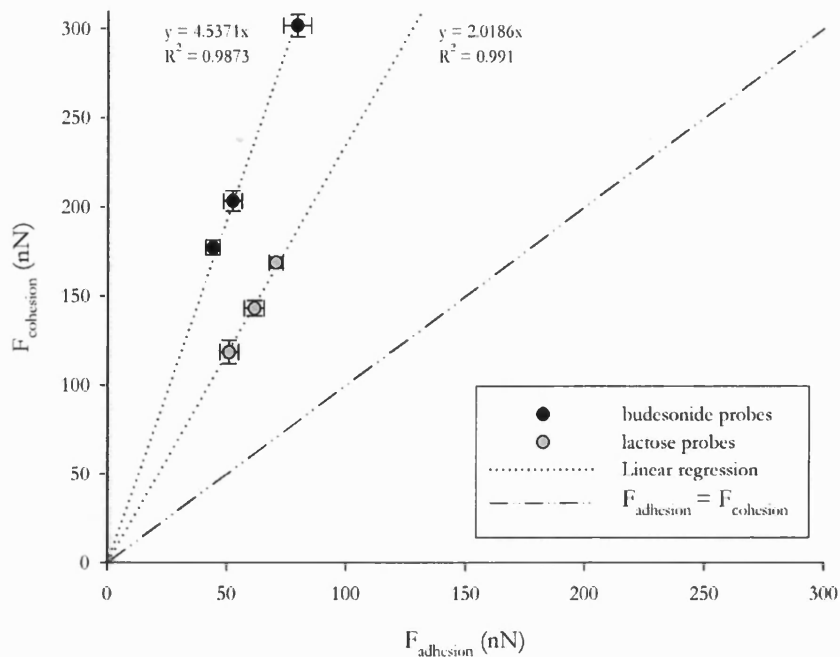


Figure 3- 5: Comparison between forces of cohesion and force of adhesion in a binary lactose/budesonide system.

A CAB-graph generated from the data in Figure 3.3 for a lactose-salbutamol sulphate system is shown in Figure 3.6. The linearity of the data was again validated, with a coefficient of determination of 0.9938 and 0.8537 for the lactose probes and salbutamol sulphate probes, respectively. The relative position of the data below the bisecting line indicated the two materials possess a strong affinity for one another with respect to their cohesive interactions (particularly salbutamol sulphate). The measurement of the slopes indicated that the interaction between salbutamol sulphate and lactose is 16.88 times and 1.22 times greater than the cohesive salbutamol sulphate and lactose interactions, respectively. Upon processing such a powder formulation, the system should not require an excessive amount of energy to generate a homogenous blend with good content uniformity.

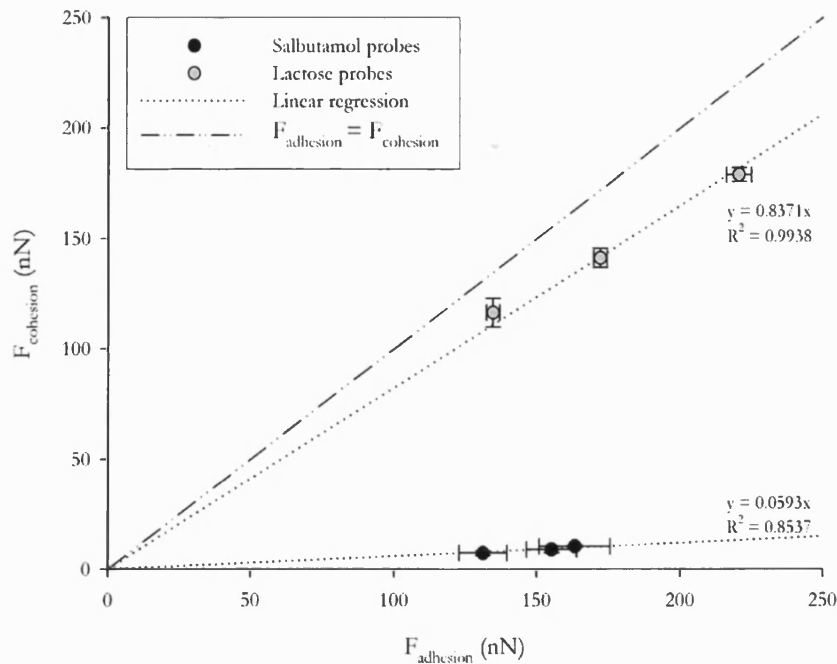


Figure 3- 6: Comparison between forces of cohesion and force of adhesion in a binary lactose/salbutamol sulphate system.

The novel treatment of the AFM data has provided a potentially useful technique in the quantitative determination of the force balance within binary systems. This process, however, may be further expanded to more complex formulations, e.g. combination product formulations, by cross normalising the data. The resulting cohesive-adhesive balance dependencies between salbutamol sulphate, lactose and budesonide are summarised in Table 3.2. The cohesive salbutamol sulphate interactions ratio was set to 1.00 and all the subsequent CAB ratios were calculated relative to this reference ratio. The corresponding matrix provides a complete description of all the various interaction forces within a ternary system. Furthermore, cross normalisation provides a novel means of measuring the hierarchy of the cohesive forces of the materials. The coefficient of proportionality with respect to salbutamol sulphate for lactose and budesonide is 14.13 and 31.76, respectively.



Sample	CAB dependency		
	Salbutamol sulphate <sup>(b)</sup>	$\alpha$ -lactose monohydrate <sup>(b)</sup>	Budesonide <sup>(b)</sup>
Salbutamol sulphate <sup>(a)</sup>	1.00 $\pm$ 0.08	16.88* $\pm$ 0.85	6.59* $\pm$ 0.00
Lactose <sup>(a)</sup>	16.88* $\pm$ 1.06	14.13* $\pm$ 1.06	7.00* $\pm$ 1.6
Budesonide <sup>(a)</sup>	6.59* $\pm$ 0.32	7.00* $\pm$ 1.6	31.76* $\pm$ 1.53

(a): probe; (b): substrate, \* p<0.01

Table 3- 2: Cohesive-adhesive balance dependencies between salbutamol sulphate, lactose and budesonide interaction combinations.

### 3.5. Conclusions

The colloid probe AFM technique has been utilised to measure the characteristics of the inter-particulate forces that govern bulk properties of dry powder formulations. The tailoring of well-defined substrate surfaces minimised intra-variations in the contact area of a colloid probe. This enabled direct characterisation of the adhesive and cohesive interactions within a model dry powder inhaler formulation. Together with the development of a novel cohesive-adhesive balance (CAB) analysis procedure, a quantitative relationship between measurements of the relative interactions within dry powder inhaler formulations was achievable. In combination with bulk techniques, this novel approach may provide a pivotal role in predicting blending, segregation and dispersion characteristics of active pharmaceutical ingredients in dry powder systems.

### 3.6. References

- [1] W. C. Hinds. *Aerosol technology: Properties, Behaviour and measurements of airborne particles*, Wiley, New York, 1999.
- [2] M. C. Korecki and P. J. Stewart. Adhesion of solid particles to solid surface. *A.M.A. Archives of Environmental Health* 1: 13-21 (1987).

- [3] J. N. Staniforth, J. E. Rees, F. K. Lai, and J. A. Hersey. Determination of interparticulate forces in ordered powder mixes. *J. Pharm. Pharmacol.* **33**: 485-490 (1981).
- [4] M. E. Mullin, L. P. Michaels, V. Menon, B. Locke, and M. B. Ranade. Effect of geometry on particle adhesion. *Aerosol Sci. and Tech.* **17**: 105-118 (1992).
- [5] W. A. Ducker, T. J. Senden, and R. M. Pashley. Direct Measurement of Colloidal Forces Using an Atomic Force Microscope. *Nature* **353**: 239-241 (1991).
- [6] E. R. Beach, G. W. Tormoen, J. Drelich, and R. Han. Pull-off force measurements between rough surfaces by atomic force microscopy. *J. Colloid Interface Sci.* **247**: 84-99 (2002).
- [7] R. Price, P. M. Young, S. Edge, and J. N. Staniforth. The influence of relative humidity on particulate interactions in carrier-based dry powder inhaler formulations. *Int. J. Pharm.* **246**: 47-59 (2002).
- [8] U. Sindel and I. Zimmermann. Measurement of interaction forces between individual powder particles using an atomic force microscope. *Powder Technology* **117**: 247-254 (2001).
- [9] J. C. Hooton, C. S. German, S. Allen, M. C. Davies, C. J. Roberts, S. J. B. Tendler, and P. M. Williams. Characterization of particle-interactions by atomic force microscopy: Effect of contact area. *Pharm. Res.* **20**: 508-514 (2003).

- [10] P. G. Royall, D. Q. M. Craig, D. M. Price, M. Reading, and T. J. Lever. An investigation into the use of micro-thermal analysis for the solid state characterisation of an HPMC tablet formulation. *Int. J. Pharm.* **192**: 97-103 (1999).
- [11] L. Mackin, R. Zanon, J. M. Park, K. Foster, H. Opalenik, and M. Demonte. Quantification of low levels (< 10%) of amorphous content in micronised active batches using dynamic vapour sorption and isothermal microcalorimetry. *Int. J. Pharm.* **231**: 227-236 (2002).
- [12] P. Begat, P. M. Young, S. Edge, J. S. Kaerger, and R. Price. The effect of mechanical processing on surface stability of pharmaceutical powders: Visualization by atomic force microscopy. *J. Pharm. Sci.* **92**: 611-620 (2003).
- [13] J. Albertsson, A. Oskarrson, and C. Svensson. X-ray Study of Budesonide: molecular structure and solid solution. *Acta Cryst.* **B34**: 3027-3036 (1978).
- [14] J.-M. Leger, M. Goursolle, and M. Gadret. Structure Cristalline du Sulfate de Salbutamol [tert-butylamino-2 (Hydroxy-4hydroxymethyl-3 phenyl)-1 Ethanol. 1/2 H<sub>2</sub>SO<sub>4</sub>. *Acta. Cryst.* **B34**: 1203-1208 (1978).
- [15] M. Kurimoto, P. Subramony, and R. W. Gurney. Kinetic Stabilization of Biopolymers in Single-Crystal Hosts: green fluorescent Protein in Alpha-Lactose monohydrate. *J. Am. Chem. Soc.* **121**: 6952-6953 (1999).
- [16] D. M. Schaefer, M. Carpenter, R. Reifenberger, L. P. Demejo, and D. S. Rimai. Surface Force Interactions between Micrometer-Size Polystyrene Spheres and Silicon Substrates Using Atomic-Force Techniques. *J. Adhes. Sci. Technol.* **8**: 197-210 (1994).

- [17] D. M. Schaefer, M. Carpenter, B. Gady, R. Reifenberger, L. P. Demejo, and D. S. Rimai. Surface-Roughness and Its Influence on Particle Adhesion Using Atomic-Force Techniques. *J. Adhes. Sci. Technol.* **9**: 1049-1062 (1995).
- [18] H. Hertz. Study on the contact of elastic solid bodies (SLA translations, SLA-57-1164). *Zeitschr. F. Reine Angewandte Mathehmatik* **29**: 156-171 (1881).
- [19] K. L. Jonhson, K. Kendall, and A. D. Roberts. Surface energy and the contact of elastic solids. *Proc. Roy. Soc. London* **324**: 301-303 (1971).
- [20] B. V. Deryaguin, V. M. Müller, and Y. P. Toporov. Effect of contact deformations on the adhesion of particles. *J. Colloid Interface Sci.* **53**: 314-325 (1975).
- [21] L. R. Fisher and J. N. Israelachvili. Direct measurements of the effect of meniscus forces on adhesion: a study of the applicability of macroscopic thermodynamics to microscopic surfaces. *Colloids and Surfaces* **3**: 303-319 (1981).

## Chapter 4

# Influence of the Cohesive-Adhesive Balance on DPI Formulation Behaviour

### 4.1. Introduction

Dry powder inhaler (DPI) formulations are commonly prepared as a binary blend of a coarse carrier, typically  $\alpha$ -lactose monohydrate, and micronised drug [1]. The homogeneity of the blend and the de-aggregation and dispersion properties of the respirable particles upon activation (driven by the patients inspirational energy) are, on a microscopic scale, governed by the resulting cohesive (drug-drug) and adhesive (drug-excipient) interaction forces within the formulation. Excessive adhesive forces may prevent elutriation of the respirable particles from the carrier surfaces, leading to upper airway deposition. Similarly, the presence of strong cohesive forces may increase segregation and agglomerate formation, which could directly affect the fluidisation and dispersion characteristics of the formulation [2, 3]. Numerous studies have investigated the in-vitro deposition characteristics of respirable drug particles from carrier based DPI formulations [4-6]. Many of these studies have indicated that the choice of inhaler device and inspiration flow rate is of critical importance in the fluidisation and aerosol characteristics of a formulation [7-9]. This suggests that the aerodynamic forces, generated within the device, play a crucial role in powder aerosolisation through disruption of the force balances within the formulation.

The aim of this study was to investigate the specific role of the cohesive and adhesive force balances on the de-agglomeration efficiencies and deposition characteristics of drug only (salbutamol sulphate and budesonide) and model drug-lactose formulations via the AFM colloid probe technique in conjunction with CAB-graph analysis procedure.

## 4.2. Methods

General methods of each technique or apparatus used in this study are described in detail in Chapter 2.

- **Preparation of powder formulations**

Drug-lactose blends were prepared by geometrically mixing 1g of drug and 1g of lactose Sorbalac 400 in 100mg increments via a Whirlimixer (Fisons Scientific Apparatus, UK). The resulting blend was further mixed in a Turbula (Glen Creston Ltd, Middlesex, UK) at 46rpm for 30 minutes.

- **Particle size analyses**

The particle size distribution of the 'as supplied' budesonide, salbutamol sulphate and lactose samples were determined by laser light scattering (Mastersizer X, Malvern, UK), using a 300mm lens. Samples were dispersed in cyclohexane and sonicated for 5 minutes prior to analysis (Ultrasonic Bath FS300b, Decon®, UK).

The aerodynamic diameters of budesonide, salbutamol sulphate and lactose samples were determined using an Aerosizer in conjunction with an Aerodisperser (Amherst Process Instruments, Inc., Hadley, MA, USA). Approximately 5mg of powder was introduced into the sample cup of the Aerodisperser. Experiments were carried out at a medium feed rate, with a run time of 180s at both low shear (1psi  $\approx$  6.895 KPa) and high shear forces (5psi  $\approx$  34.474 KPa). This was achieved by varying the pressure drop across the annular gap between the disperser pin and the pin bowl of the Aerodisperser.

- **Content uniformity measurements**

The content uniformity of the salbutamol sulphate-lactose and budesonide-lactose blends was measured by analysing the quantity of active in  $10\text{mg} \pm 0.5\text{mg}$  samples ( $n=10$ ). Drug content was analysed by HPLC. Relative standard deviation between samples was calculated to assess the homogeneity of the different blends.

- ***In vitro* aerosol deposition studies**

To determine the influence of the aerodynamic drag forces on the fluidisation and aerosol characteristics of the cohesive and adhesive formulations, a low and high resistance device were chosen [7]. Various measurements of the internal resistance of dry powder inhaler devices as a function of flow rate have been previously studied [7]. A Turbuhaler<sup>®</sup> (Astra Draco AB, Sweden) was utilised as a high resistance device and a Rotahaler<sup>®</sup> (Glaxo Wellcome, UK) as a low resistance device [10-12]. Approximately 1.5mg of the drug only and carrier formulations was accurately weighed into the metering chamber of the Turbuhaler and 2.5 mg into a gelatine capsule to be loaded into the Rotahaler device.

*In vitro* deposition investigations were performed using a twin-stage liquid impinger (TSI) (Copley, UK). The first and second stages were filled with 7ml and 30ml of mobile phase, respectively. The loaded device was connected to the glass throat of the TSI via a moulded mouthpiece. *In vitro* analysis was performed after each actuation of the device. Each experiment ( $n=3$ ) was performed at  $60\text{L}\cdot\text{min}^{-1}$  flow rate with a 5 second exposure.

## 4.3. Results and Discussion

### 4.3.1. General Physical Characterisation

Representative scanning electron micrographs of the 'as supplied' lactose, salbutamol sulphate, and budesonide are shown in Figure 4.1A, 4.1B and 4.1C, respectively. Each powder sample exhibited variations in particle size, shape and morphology. Electron micrographs suggested that lactose (Sorbalac 400) particles were significantly larger than the active ingredients. The use of smaller lactose particles

(<10 $\mu\text{m}$ ) with respect to more conventional carrier sizes (63-90 $\mu\text{m}$ ) was dictated by the need to minimise the potential influence of larger carrier particles over fluidisation and de-aggregation processes of particle agglomerates. Variations in the degree of agglomeration of the particles were also evident. The salbutamol sulphate particles were assembled as loose agglomerates while the budesonide particles formed highly dense agglomerates.

The particle size measurements of ultrasonically dispersed lactose, salbutamol sulphate and budesonide samples measured by laser scattering are shown in Table 4.1. As each distribution followed a lognormal fit, the average diameter was thus expressed as the 50<sup>th</sup> percentile size ( $d_{50}$ ). In addition, the dispersion of the distribution was characterised by the 16<sup>th</sup> and 84<sup>th</sup> percentiles. Both salbutamol sulphate and budesonide exhibited a median diameter below the respirable size of 5 $\mu\text{m}$  [13]. The median particle diameter of the lactose samples was ca. 10 $\mu\text{m}$ , in accordance with the SEM and suppliers data.

Diameter in ( $\mu\text{m}$ )	Lactose	Salbutamol sulphate	Budesonide
$d_{16}$	$3.00 \pm 0.19$	$2.17 \pm 0.03$	$2.06 \pm 0.02$
$d_{50}$	$9.29 \pm 1.07$	$4.77 \pm 0.13$	$3.75 \pm 0.05$
$d_{84}$	$20.26 \pm 2.36$	$11.58 \pm 1.09$	$6.81 \pm 0.2$

Table 4- 1: Particle size distribution characteristics of lactose Sorbalac 400, micronised salbutamol sulphate and micronised budesonide by laser scattering (mean  $\pm$  SD, n=5).



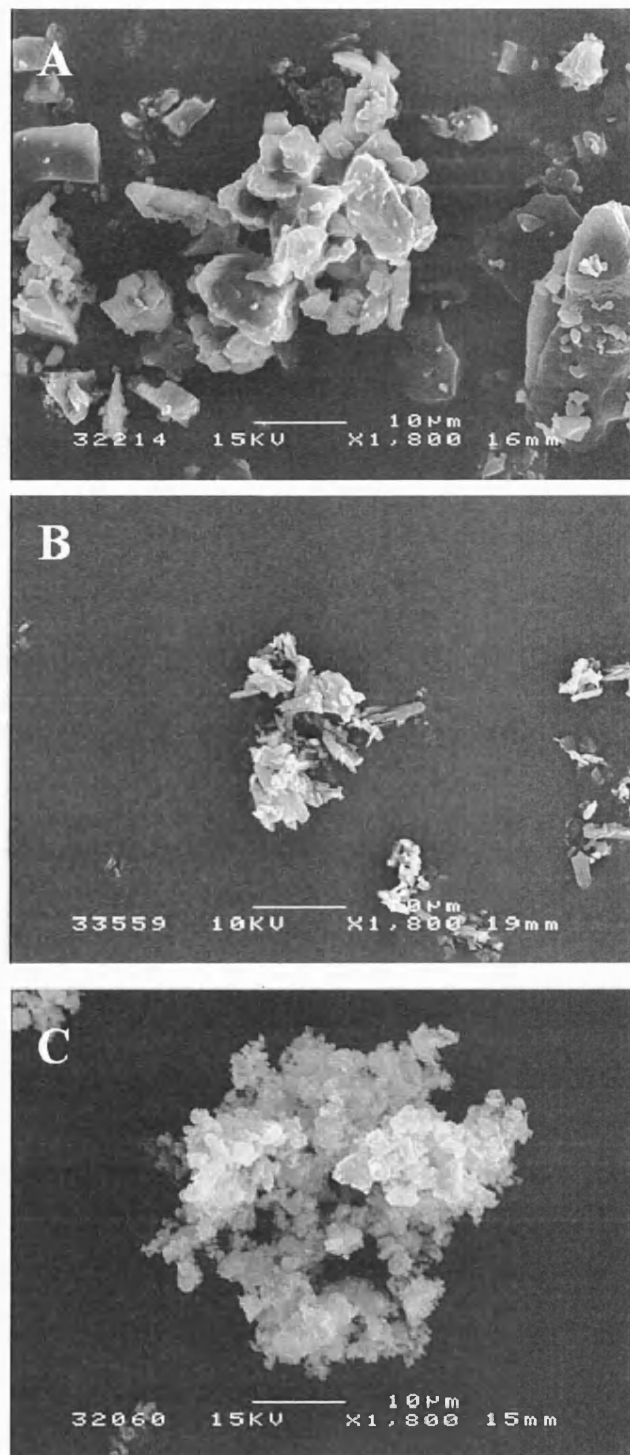


Figure 4- 1: Representative SEM images of ‘as supplied’ lactose Sorbalac 400 (A), salbutamol sulphate (B) and budesonide (C).

### 4.3.2. Influence of Particle Cohesiveness on Powder Behaviour

The aerodynamic particle diameters of micronised lactose, salbutamol sulphate and budesonide at low and high shear forces are summarised in Table 4.2. At high shear forces, the data exhibited relatively narrow lognormal distributions. The median particle diameter of micronised salbutamol sulphate and budesonide were  $2.91\mu\text{m}$  and  $2.63\mu\text{m}$ , respectively. As expected, the aerodynamic diameter of lactose was significantly larger at  $10.54\mu\text{m}$ . The reasonable correlation of these data with ultrasonically dispersed laser scattering measurements suggested complete de-agglomeration of the powder at high shear forces.

At low shear forces, a significant shift in the particle distribution of the time of flight data was observed for both lactose and budesonide (Table 4.2). However, only a very small shift was observed for micronised salbutamol sulphate. The increase in the median aerodynamic diameter and dispersion of the particle size data for lactose and budesonide suggested that the applied low shear force was insufficient to overcome the cohesive bonds within the bulk powders. However, the similarity of the aerodynamic diameter measurements of salbutamol sulphate at low and high shear forces suggested salbutamol sulphate particles can be readily de-agglomerated under shear. Similar changes to particle size distributions of powder samples as a function of shear force have been reported previously [14-17].

Diameter in ( $\mu\text{m}$ )	Lactose		Salbutamol sulphate		Budesonide	
	5 psi	1 psi	5 psi	1 psi	5 psi	1 psi
$d_{15}$	$5.59 \pm 0.37$	$18.35 \pm 3.53$	$1.89 \pm 0.08$	$2.04 \pm 0.40$	$1.63 \pm 0.20$	$20.65 \pm 2.34$
$d_{50}$	$10.54 \pm 0.70$	$29.70 \pm 4.58$	$2.91 \pm 0.30$	$3.58 \pm 0.88$	$2.63 \pm 0.28$	$35.96 \pm 3.12$
$d_{85}$	$14.47 \pm 1.29$	$41.39 \pm 6.1$	$4.32 \pm 0.86$	$5.33 \pm 1.35$	$3.92 \pm 0.40$	$49.18 \pm 3.1$

Table 4- 2: Particle size distribution characteristics of lactose Sorbalac 400, micronised salbutamol sulphate and micronised budesonide by time of flight measurements at high (5psi) and low (1psi) shear forces (mean  $\pm$  SD, n=5).

Further information regarding the possible role of powder cohesiveness on variations in aerodynamic size measurements with shear can be obtained from the difference in the apparent aerodynamic volume. By assuming that the aerodynamic diameters observed for a particular powder at high and low shear are the median particle diameter of the de-agglomerated powder and median diameter of the agglomerated particles, respectively, the agglomerate volume can be expressed as:

$$V_{agglomerate} = n.V_{particle} + \delta_v \quad [4.1]$$

Where  $n$  is the number of particles in the agglomerate, and  $\delta_v$  is the interstitial volume between particles.

Figure 4.2 shows a corresponding plot of the apparent aerodynamic volume ratio (on a logarithmic scale) versus the corresponding cohesive balance dependencies of the powders. The cohesive dependencies of the particles were obtained from the quantitative colloidal AFM measurements undertaken in Chapter 3. A fit of the data indicated that the degree of de-agglomeration decreased exponentially as a function of agglomerate cohesive strength. Thus, the efficiency of de-agglomeration has been dramatically affected by the relative internal cohesive strength of agglomerated particulates and shear force applied. This, in turn, may directly influence the aerosol characteristics and deposition behaviour of an agglomerated system.

The in vitro deposition behaviour of a drug only formulation of micronised salbutamol sulphate delivered via low (Rotahaler<sup>®</sup>) and high (Turbulohaler<sup>®</sup>) internal resistance DPI devices is shown in Figure 4.3A. The emitted dose percentage of the two devices was very high (>80%). This indicated that the pressure drop variations between the two devices, at 60L.min<sup>-1</sup>, had no significant affect on the fluidisation of the micronised salbutamol sulphate particles. However, significant differences between the devices were observed in the amount of the active material collected in the first and the second stages of the TSI ( $p < 0.05$ ). Dispersion using the Rotahaler was rather poor. Similar results were found by other workers [18]. However, the high resistance device significantly increased the fine particle fraction by two fold. Nevertheless, a considerable amount of drug was recovered for both devices in the first stage of the

TSI. This large percentage suggested that micronised salbutamol sulphate did not fully de-aggregate upon aerosolisation. These results were rather surprising considering the relatively low cohesive strength of salbutamol sulphate and the high de-agglomeration efficiency of the particles upon exposure to low shear forces of the Aerodisperser.

The deposition pattern of a drug only formulation containing micronised budesonide from both a Rotahaler<sup>®</sup> and Turbuhaler<sup>®</sup> DPI are shown in figure 4.3B. Although a small increase in the percentage of emitted dose was observed for the Turbuhaler<sup>®</sup> device, a very high percentage of the budesonide remained within the devices upon activation. More significant, however, was the variation in the aerosol characteristics between the two devices. The high resistance device led to a four fold increase in the de-agglomeration efficiency of budesonide with respect to the low resistance inhaler device. This significant increase in the de-agglomeration efficiency of budesonide with increasing airflow resistance may relate to a critical energy requirement of the device in overcoming the highly cohesive nature of budesonide particles.

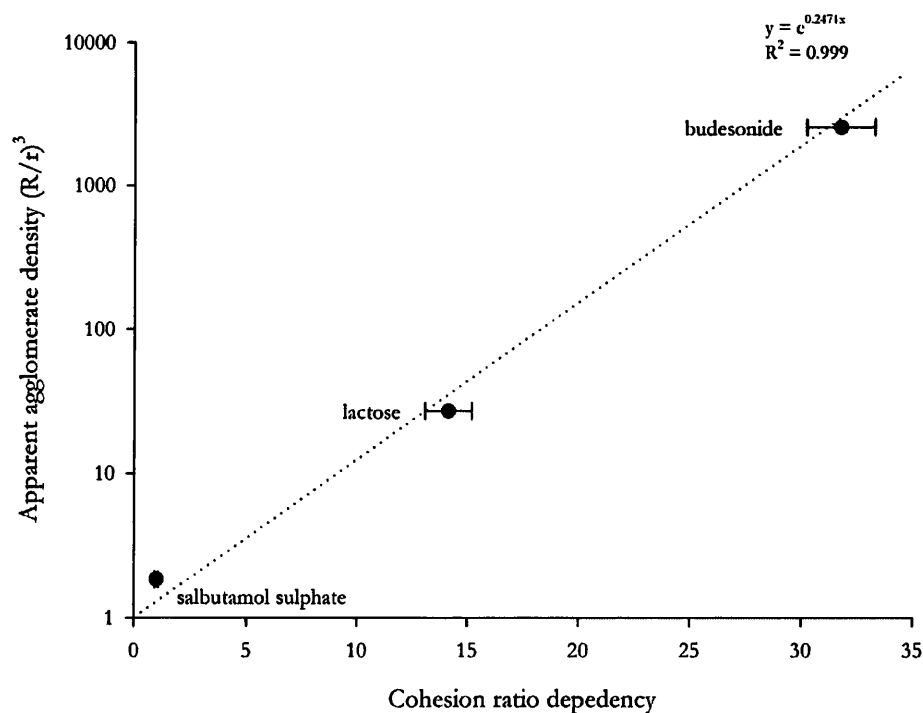


Figure 4- 2: Apparent agglomerate volume versus cohesion ratio dependency of salbutamol sulphate, budesonide and lactose (mean  $\pm$  S.D., n=3).

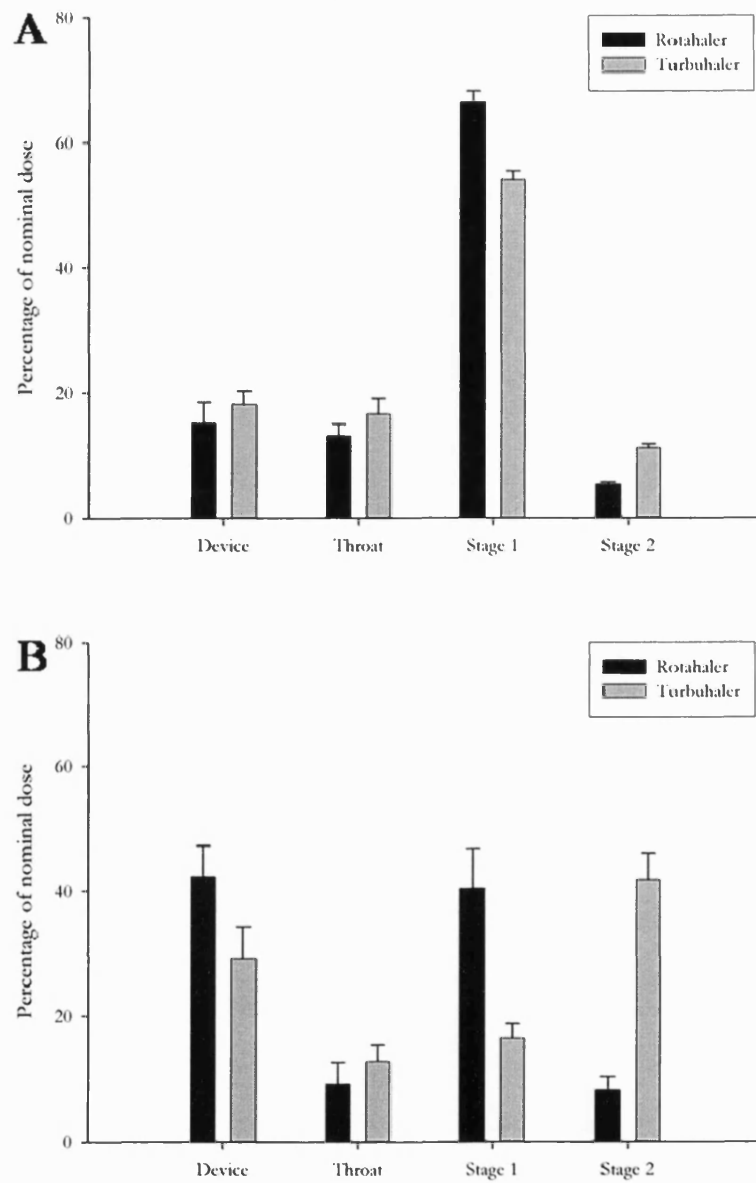


Figure 4- 3: In vitro deposition of salbutamol sulphate (A) and budesonide (B) from a Rotahaler® and a Turbuhaler® DPI (mean  $\pm$  S.D., n=3).

It should be stressed that the in vitro aerosol behaviour of salbutamol sulphate and budesonide particles was unexpected as the aerosolisation patterns of salbutamol were worse than budesonide. These results highlighted the highly complex nature of de-agglomeration and aerosol dispersion mechanisms in the most basic formulations. To further understand this apparent paradoxical behaviour, the stability of agglomerated particles entrained in an air flow was modelled relative to the aerodynamic drag force generated through the device. Assuming a physical system of an object (agglomerate) in an airborne flow, the drag force generated by the displacement of air molecules with respect to the moving object can be expressed as:

$$F_{drag} = C_d \frac{\pi}{8} \rho_{air} \Phi_{agg}^2 v_{flow}^2 \quad [4.2]$$

where  $C_d$  is the drag coefficient, which is dependant upon the ratio of inertial and frictional forces of the agglomerated particles in the airflow,  $\rho_{air}$  is the density of the air,  $\Phi_{agg}$  is the effective diameter of the agglomerate, and  $v_{flow}$  is the airflow velocity. The corresponding initial kinetic energy of the moving object may be expressed as:

$$E_c' = \frac{\pi}{12} \rho_{agg} (\Phi_{agg}')^3 v_{flow}^2 \quad [4.3]$$

where  $\rho_{agg}$  is the density of the agglomerate. Equations [4.2] and [4.3] indicate that the aerodynamic drag force acting on an object and the kinetic energy of a moving object are directly proportional to the square and the cube of its diameter, respectively. As a result, the aerodynamic drag force and kinetic energy differences between a 5 $\mu$ m and a 50 $\mu$ m object at a constant settling velocity would be 10<sup>2</sup> and 10<sup>3</sup>, respectively. This relationship would play a significant role in the de-aggregation and dispersion of agglomerated particles. Thus, despite the significant increase in the cohesive strength of budesonide particles with respect to salbutamol sulphate, the drag force experienced by airborne budesonide aggregates may lead to a higher efficiency in the de-agglomeration and dispersion of respirable particles than for smaller agglomerates with a lower cohesive strength. Furthermore, the substantial increase in kinetic energy of the

larger agglomerates may increase de-aggregation efficiency within the device via impaction (assuming an inelastic collision and no subsequent energy loss).

Hence, it is conceivable that during the de-aggregation and dispersion process, a state can be reached where the internal binding forces of the agglomerate and the drag forces generated within the device reach an equilibrium ( $F_{\text{coh}} = F_{\text{drag}}$ ). This would subsequently lead to the suspension of the elutriation process. The characteristic properties of the metastable aggregate would be directly dependant on the airflow characteristics via the inhaler device and the cohesive properties of the particles within the agglomerate. A schematic representation of the possible aerosol dispersion mechanisms of salbutamol sulphate and budesonide agglomerated particles is therefore illustrated in Figure 4.4.

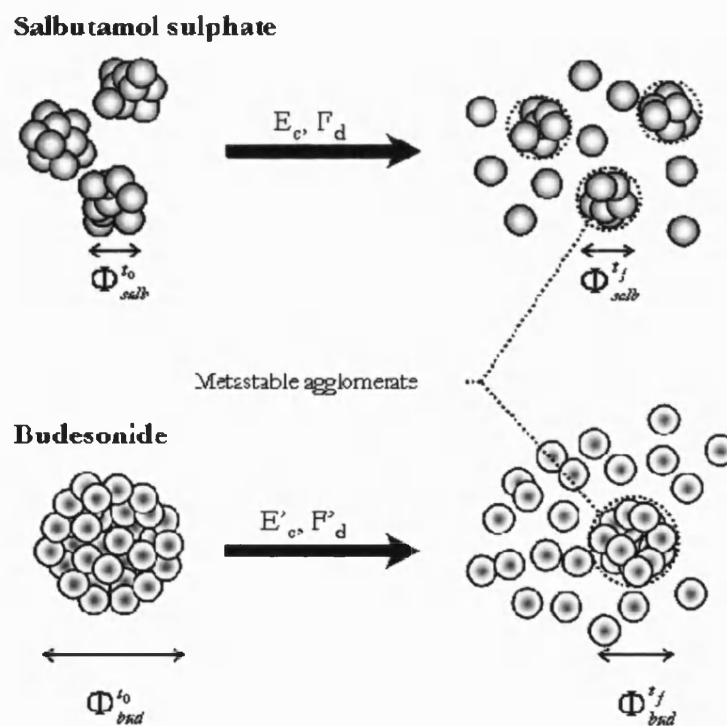


Figure 4- 4: Schematic representation of the possible de-agglomeration and dispersion mechanisms of weakly cohesive (salbutamol sulphate) and highly cohesive (budesonide) particles.

The low cohesive strength of salbutamol sulphate particles, which readily allows aerosolisation and entrainment of relatively small agglomerates, will quickly attain their aerodynamic metastable state, thereby decreasing the degree of respirable particle dispersion. As indicated by in-vitro measurements, this may lead to high emission yet poor fine particle delivery performances. In contrast, highly cohesive budesonide particles require a significantly higher amount of energy to fluidise the aggregated powder, and may lead to the entrainment of larger agglomerates. However, these agglomerates will exhibit greater inertial properties and experience significantly greater aerodynamic drag forces and impact events than smaller agglomerates. This would lead to higher dispersion efficiency and yield to a greater percentage of fine respirable particles, as indicated by in-vitro measurements.

### 4.3.3. Influence of Drug-Excipient Interactions on Formulation Behaviour

Rowe et al. have advanced the efficiency of wet granulation preparation of powders for oral solid dosage forms by judiciously selecting binding agents on the basis of their spreading coefficient ( $\lambda_{12}$ ) [19, 20]. The reduced spreading coefficient is defined as the ratio between the work of adhesion of the substrate and the binder and the work of cohesion of the binder [21]. A similar approach for blending characteristics of carrier-based formulation systems has been applied in this study. The term reduced intermixing coefficient ( $\Lambda_{12}$ ), derived from the reduced spreading coefficient, can be described by the following relationship:

$$\Lambda_{12} = \frac{F_{12}^{ad}}{F_{11}^{co}} = \frac{CAB\ depedency_{12}}{CAB\ depedency_{11}} \quad [4.4]$$

$\Lambda_{12}$ , a dimensionless parameter, corresponds to the force ratio between adhesive interactions ( $F_{12}$ ) and cohesive interactions ( $F_{11}$ ) of two interacting materials.



For carrier based systems, the reduced intermixing coefficient reflects the affinity of the drug (material 1) to interact with the carrier (material 2). Hence, the position of  $\Lambda_{12}$  with respect to unity is a direct indication of the alacrity ( $\Lambda_{12}>1$ ), or the reluctance ( $\Lambda_{12}<1$ ), of the active particles to form an interactive mixture with the carrier particles. The reduced intermixing coefficients between salbutamol sulphate, budesonide and  $\alpha$ -lactose monohydrate were consequently calculated from the quantitative cohesive-adhesive balance dependencies obtained from Chapter 3 and are given in table 4.3. A clear distinction between salbutamol sulphate and budesonide (materials 1) was observable with  $\alpha$ -lactose monohydrate (material 2). The disparity in the reduced intermixing coefficients of salbutamol sulphate ( $\Lambda_{12}=16.88$ ) and budesonide ( $\Lambda_{12}=0.22$ ) strongly suggests that agglomerated salbutamol sulphate particles can be easily displaced to form an interactive mixture within a carrier based formulation, whereas budesonide would require an intensive mixing process to form a metastable carrier based formulation.

Sample	Reduced intermixing coefficient ( $\Lambda_{12}$ )		
	Salbutamol Sulphate <sup>(b)</sup>	Lactose <sup>(b)</sup>	Budesonide <sup>(b)</sup>
Salbutamol sulphate <sup>(a)</sup>	-	16.88 ± 0.91	6.59 ± 0.21
Lactose <sup>(a)</sup>	1.19 ± 0.42	-	0.5 ± 0.31
Budesonide <sup>(a)</sup>	0.21 ± 0.13	0.22 ± 0.21	-

(a): material 1, (b): material 2

Table 4- 3: Reduced intermixing coefficient of salbutamol sulphate, budesonide and lactose (mean ± S.D., n=3).

To highlight the influence of the intermixing coefficient on the blending characteristics of salbutamol sulphate and budesonide carrier based formulation, scanning electron microscopy and drug content uniformity analyses of the blends were investigated. Representative scanning electron micrographs of salbutamol sulphate–lactose and budesonide-lactose are shown in Figures 4.5A and 4.5B, respectively.

The electron micrographs suggested a uniform distribution of highly dispersed salbutamol sulphate particles over the lactose surface. In contrast, budesonide particles appeared to remain agglomerated and unevenly spread over the lactose carrier. Predictably, dose content uniformity analysis revealed a relative standard deviation of 4.2% for salbutamol sulphate and 28.1% for budesonide. These observations both suggested good correlation between the reduced intermixing coefficient and the characteristics of the respective carrier based formulations. In addition to providing pertinent information regarding the blending characteristics of carrier formulations, the reduced intermixing coefficient may also provide an insight into the stability and aerosol characteristics of such systems.

The aerosol delivery properties of salbutamol sulphate and budesonide carrier-based formulations from both a Rotahaler<sup>®</sup> and Turbuhaler<sup>®</sup> DPI are shown in figures 4.6A and 4.6B, respectively. The emission efficiency of salbutamol sulphate-lactose formulations was very similar to the drug only formulation, with no significant differences between the two devices. Significant changes in the fine particle delivery behaviour were, however, measured between the two systems. The significant decrease in stage 1 deposition ( $p < 0.05$ ) for a carrier based formulation led to an increase in stage 2 deposition ( $p < 0.05$ ), resulting in a net increase in fine particle fraction delivery. The co-processing of budesonide with  $\alpha$ -lactose monohydrate resulted in a significant decrease in stage 1 deposition and an associated improvement in fine particle delivery performance via a Rotahaler<sup>®</sup> device ( $p < 0.05$ ). No significant variations between drug only and carrier based formulations were measured with a high resistance Turbuhaler<sup>®</sup> inhaler.

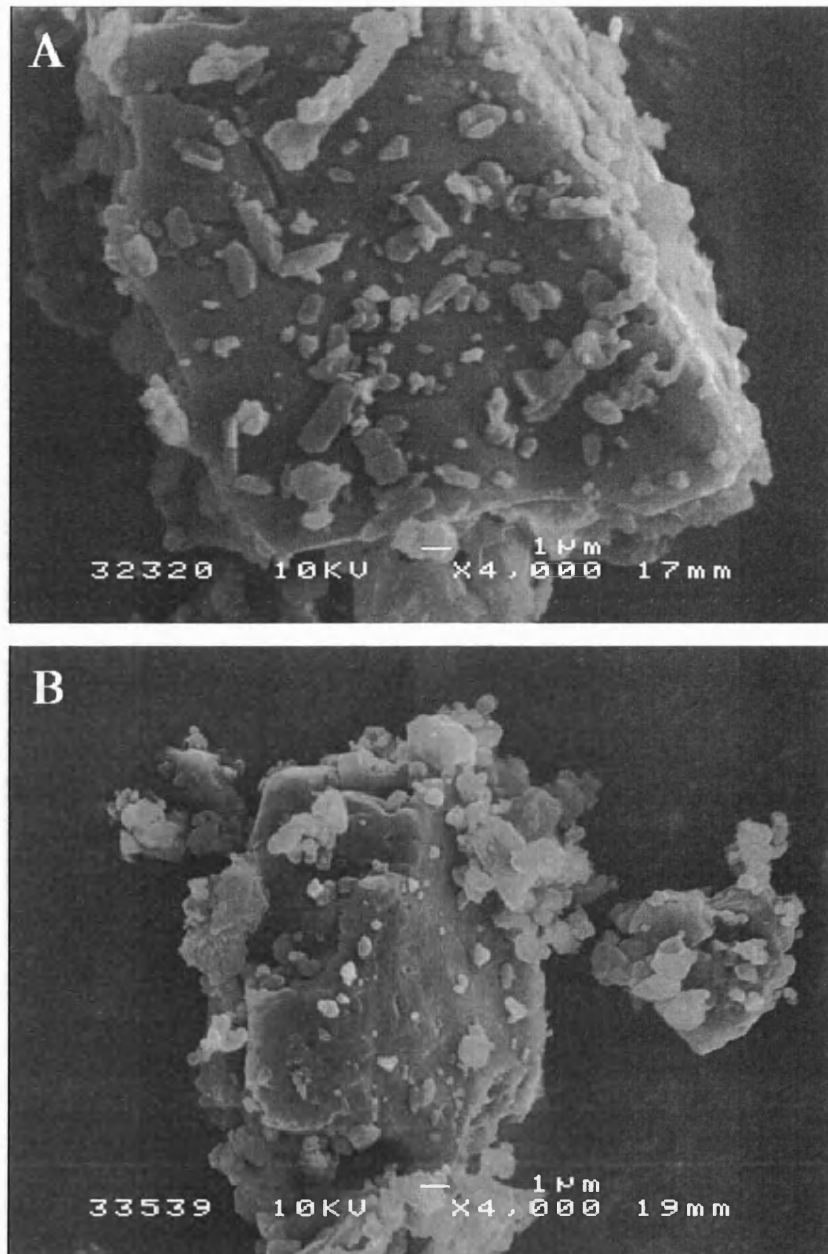


Figure 4- 5: Representative micrographs of blends of salbutamol sulphate-lactose (A), and budesonide-lactose (B).

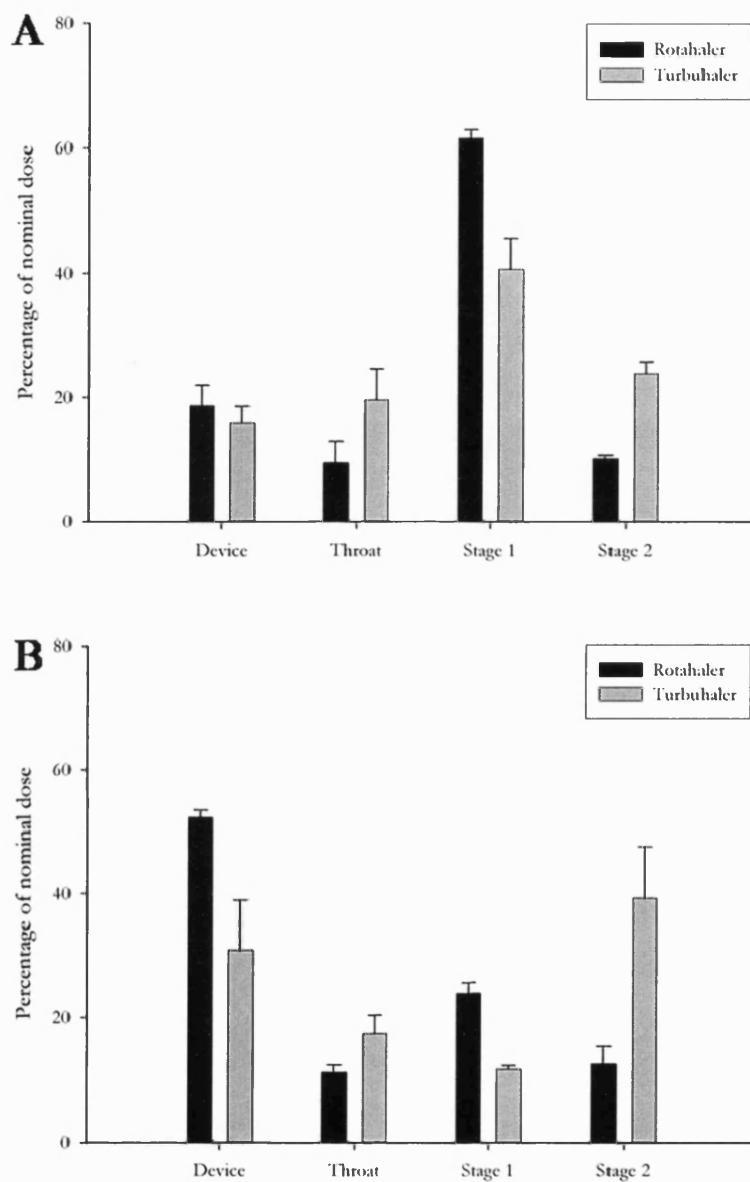


Figure 4- 6: *In vitro* deposition of salbutamol sulphate-lactose (A) and budesonide-lactose (B) carrier-based formulation from a Rotahaler<sup>®</sup> and a Turbuhaler<sup>®</sup> DPI (mean  $\pm$  S.D., n=3).

A summary table of the deposition percentages of the drug only and carrier-based formulations are shown in Table 4.4. The high reduced intermixing coefficient between salbutamol sulphate and lactose suggested that salbutamol sulphate particles would interactively mix with  $\alpha$ -lactose monohydrate. Thus, the de-aggregation and dispersion behaviour of the salbutamol sulphate particles should be dominated by the drug-excipient interactions. *In vitro* measurements indicated, however, that the performance of the carrier-based formulation remained mediocre. This may be attributed to the excessive adhesive forces leading to an incomplete detachment of the salbutamol sulphate from the carrier. This may subsequently lead to a substantial amount of active material deposition in the throat and stage 1. The high emission efficiency of the carrier-based formulation was possibly a result of the high affinity of salbutamol to the carrier. Meanwhile, the increase in the fine particle performance of the carrier-based formulation may relate to the higher aerodynamic drag force experienced by the particulates adhering to the excipient particle surface. This behaviour was corroborated by the improvement in drug detachment at higher shear forces when the Turbuhaler was used. The measurements further supported the requirement for the formation of stable agglomerate of critical dimensions to induce a significant aerodynamic drag force within the device to disperse the respirable particles. The dimensions and aerodynamic properties of the fine carrier particles may, therefore, have a significant affect on the dispersion energy of the adhering drug particles. The colloidal AFM measurements also indicate that modifying the adhesive-cohesive force balance may enhance the efficiency of dispersion. For a salbutamol sulphate formulation this may be achieved by lowering the interfacial energy of interaction between drug and excipient, leading to adhesive forces which would nonetheless remain stronger than the drug cohesive forces.

Formulation	<sup>(a)</sup> Rotahaler <sup>®</sup>		<sup>(b)</sup> Turbuhaler <sup>®</sup>	
	FPF (%)	Emission (%)	FPF (%)	Emission (%)
Salbutamol sulphate	6.2 ± 0.6	84.9 ± 3.4	13.7 ± 0.5	81.9 ± 2.1
Salbutamol + Lactose	12.6 ± 1.2	81.3 ± 3.3	28.4 ± 1.5	84.2 ± 2.7
Budesonide	14.4 ± 4.9	57.7 ± 5.0	63.4 ± 3.4	64.8 ± 4.6
Budesonide + Lactose	26.3 ± 6.2	47.7 ± 1.2	58.9 ± 7.1	66.3 ± 8.0

(a): Rotahaler<sup>®</sup>, 0.68 kPa pressure drop at 60 L.min<sup>-1</sup>.

(b): Turbuhaler<sup>®</sup>, 8.5 kPa pressure drop at 60 L.min<sup>-1</sup>.

Table 4- 4: Fine particle fraction and emission efficiency of salbutamol sulphate and budesonide carrier-based formulations from a Rotahaler<sup>®</sup> and Turbuhaler<sup>®</sup> DPI (mean ± S.D., n=3).

The reduced intermixing coefficient between budesonide and lactose suggested that budesonide particles would not interactively mix with  $\alpha$ -lactose monohydrate. These findings were supported by electron micrographs, content uniformity measurements and *in vitro* profiles of the drug only and carrier based formulation. The instability of budesonide particles in a carrier based formulation was corroborated by the low emission efficiency and the reduction in fine particle fraction delivery of carrier based budesonide formulations under high shear. This suggested that an increase in the aerodynamic drag coefficient resulted in the rapid separation of the budesonide agglomerates from the lactose surface, introducing a similar dispersion mechanism as for the cohesive drug only formulation. It would therefore appear that the drug-drug interaction forces are the predominant factor in the delivery characteristics of highly cohesive drug systems. Optimisation of such dry powder formulations would require passivation of the excessive cohesive bonds through controlled modifications of the interfacial energetics.

## 4.4. Conclusions

The influence of the cohesive and adhesive dependencies of salbutamol sulphate and budesonide particles in model dry powder formulations was investigated. A surprising relationship between particle cohesive strength and de-agglomeration efficiencies of drug only formulations was observed. A possible explanation for the dramatic variation in the fluidisation and aerosolisation properties between low and high cohesive particles was modelled on the relationship between cohesion, metastable agglomerate size and the resulting aerodynamic mechanisms acting on the fluidised agglomerates such as drag forces and impaction/collisions. The addition of a fine particle lactose carrier influenced the drug deposition patterns in different ways depending on the relative cohesive and adhesive force balance within the formulation. The use of the colloid AFM technique together with the novel development of CAB-graph system provides a novel pre-formulation tool for predicting the likely behaviour of a dry powder formulation and a possible means of interpreting the possible de-aggregation and dispersion mechanisms of carrier-based formulations.

## 4.5. References

- [1] J. H. Bell, P. S. Hartley, and J. S. Cox. Dry Powder Aerosol I: A New Powder Inhalation Device. *J. Pharm. Sci.* **60**: 1559-1563 (1971).
- [2] P. R. Byron. Some Future Perspectives for Unit Dose Inhalation Aerosols. *Drug Dev. Ind. Pharm.* **12**: 993-1015 (1986).
- [3] A. J. Hickey, N. M. Concession, N. M. Van Oort, and R. M. Platz. Factors influencing the dispersion of dry powders as aerosols. *Pharm. Tech.* **8**: 58-82 (1994).
- [4] M. T. Vidgren, P. A. Vidgren, P. Uotila, and J. Paronen. In vitro inhalation of disodium cromoglycate powders using two dosage forms. *Acta. Pharm. Fenn.* **97**: 187-195 (1988).

- [5] H. Larhrib, X. M. Zeng, G. P. Martin, C. Marriott, and J. Pritchard. The use of different grades of lactose as a carrier for aerosolised salbutamol sulphate. *Int. J. Pharm.* **191**: 1-14 (1999).
- [6] X. M. Zeng, G. P. Martin, S. K. Tee, and C. Marriott. The role of fine particle lactose on the dispersion and deaggregation of salbutamol sulphate in an air stream in vitro. *Int. J. Pharm.* **176**: 99-110 (1998).
- [7] A. H. De boer, I. Winter, and C. F. Lerk. Inhalation characteristics and their effects on in vitro drug delivery from dry powder inhalers part 1. Inhalation characteristics, work of breathing and volunteers' preference in dependence of the inhaler resistance. *Int. J. Pharm.* **130**: 231-244 (1996).
- [8] G. Pitcairn, G. Lughetti, P. Ventura, and S. Newman. A Comparison of the Lung Deposition of Salbutamol Inhaled from a New Dry Powder Inhaler, at 2 Inhaled Flow-Rates. *Int. J. Pharm.* **102**: 11-18 (1994).
- [9] X. M. Zeng, G. P. Martin, C. Marriott, and J. Pritchard. The influence of carrier morphology on drug delivery by dry powder inhalers. *International Journal of Pharmaceutics* **200**: 93-106 (2000).
- [10] K. Osterman, A. M. Norborg, and E. Sthal. A Multiple Dose Inhaler (Turbuhaler) Compared With A Conventional Aerosol. *Allergy* **44**: 294-297 (1989).
- [11] A. R. Clark. Medical Aerosol Inhalers - Past, Present, and Future. *Aerosol Sci. and Tech.* **22**: 374-391 (1995).
- [12] G. M. Pover, A. K. Browning, B. M. Mullinger, A. G. Butler, and C. H. Dash. A New Dry Powder Inhaler. *Practitioner* **226**: 565-567 (1982).
- [13] D. Ganderton and N. M. Kassem. *Advances in Pharmaceutical sciences.*, Academic Press, London, 1992.



- [14] N. Laitinen and A. M. Juppo. Measurement of pharmaceutical particles using a time-of-flight particle sizer. *Eur. J. Pharm. Biopharm.* **55**: 93-98 (2003).
- [15] H. Harris and D. A. V. Morton. Powder DIspersibility Testing, *Drug Delivery to the Lungs XIV*, London, 2003.
- [16] P. York and M. Hanna. Particle engineering by supercritical fluid technologies for powder inhalation drug delivery, *Respiratory Drug Delivery*, Phoenix, 1996.
- [17] B. Y. Shekunov, J. C. Feeley, and A. H. L. Chow. Aerosolisation behaviour of micronised and supercritical-processed powders. *J. Aerosol Sci.* **34**: 553-568 (2003).
- [18] N. Y. K. Chew, D. F. Bagster, and H. K. Chan. Effect of particle size, air flow and inhaler device on the aerosolisation of disodium cromoglycate powders. *Int. J. Pharm.* **206**: 75-83 (2000).
- [19] R. C. Rowe. Binder Substrate Interactions in Granulation - a Theoretical Approach Based on Surface Free-Energy and Polarity. *Int. J. Pharm.* **52**: 149-154 (1989).
- [20] R. C. Rowe. Surface Free-Energy and Polarity Effects in the Granulation of a Model System. *Int. J. Pharm.* **53**: 75-78 (1989).
- [21] R. C. Rowe. Polar Non-Polar Interactions in the Granulation of Organic Substrates with Polymer Binding-Agents. *Int. J. Pharm.* **56**: 117-124 (1989).

## **Chapter 5**

# **The Use of Force Control Agents in Model Salbutamol Sulphate DPI Formulations**

### **5.1. Introduction**

The co-processing of carrier particles with low surface free energy materials has been reported as a possible means of increasing the aerosolisation efficiencies of dry powder inhaler formulations [1-3]. The predominant role of these agents is to modify the interfacial properties of the excipient particles to decrease drug-excipient adhesion. To optimise the efficiency of a carrier based formulation, the force control agent must be specifically introduced into the dry powder formulation to selectively target the particle interactions to be modified.

In this study, the FCA was mechanically fused via a highly intensive Mechanofusion system, with the aim of achieving a nanometre thick coating of a guest material with a host component in the formulation [4]. This approach for inhalation powders was recently developed by Staniforth et al [5]. In contrast to other low energetic mixing or even conventional intensive mixing, this dry coating process is designed to provide a relatively complete ultra thin coating onto the host particles via the application of a combination of high shear and compression forces. A schematic representation of the possible effect of increasing shear on particle coating is shown in Figure 5.1.

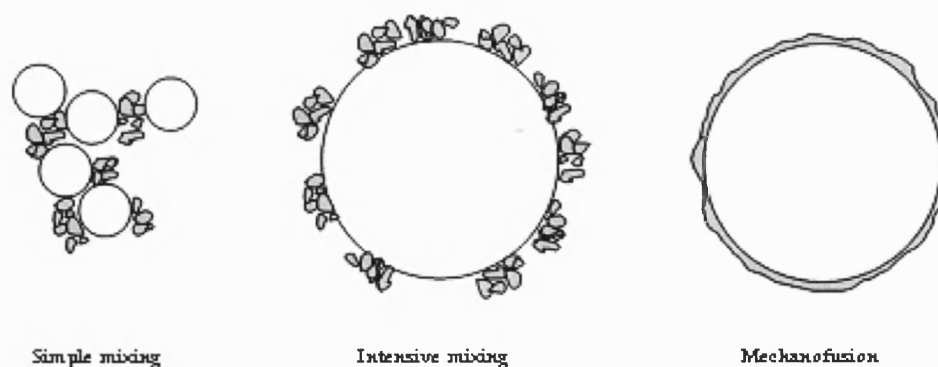


Figure 5- 1: Schematic representation of mechanofusion particle mixing mechanisms.

Succinctly, a Mechanofusion mixer is composed of a large rotor with one or more rounded blades revolving in a steel vessel at very high speed (up to 8000rpm). The gap size between the rotor blades and the vessel wall as well as the angular velocity can be adjusted in order to vary the processing energy delivered to the powder blend. As a result, the particles experience very high shear forces as they are compressed between the inner drum wall and the rotor.

The aim of this study was to investigate the specific influence of force control agents (leucine, lecithin and magnesium stearate) on the interfacial properties of a salbutamol sulphate-lactose dry powder inhaler formulation. The influence of the FCAs on the cohesive and adhesive force balance was directly assessed via an AFM colloid probe technique in conjunction with CAB-graph analysis procedure (Chapter 3). By quantifying the cohesive-adhesive balances in a dry powder formulation, this technique can be directly utilised to highlight their specific effect on formulation behaviour and delivery characteristics (Chapter 4). The in-vitro deposition profile of the model salbutamol sulphate formulations was investigated to elucidate any correlation between the cohesive and adhesive nature of the modified formulations with their aerosol delivery performance.

## 5.2. Methods

General methods of each technique or apparatus used in this study are described in detail in Chapter 2.

- **Preparation of powder formulations**

Powder mixing was achieved in two successive steps involving different energetic processes. Pre-blends of salbutamol sulphate and FCA (5% w/w) or lactose and FCA (5% w/w) were prepared using a Mechanofusion system (Hosokawa-Alpine, Augsburg, Germany). Powders to be processed were sealed into the Mechanofusion system core. A cold-water circulation provided the regulation of the internal vessel temperature using an incorporated water jacket. Samples were mixed at 5000rpm for 10 minutes to achieve the required process intensity and mechanically fuse the FCA to the host particles.

The formulations were subsequently prepared by geometrically mixing 1g of pre-blend and 1g of either lactose or drug depending on the nature of the pre-blend in 100mg increments via a Whirlimixer (Fisons Scientific Apparatus, Loughborough, UK). The resulting mixture was further mixed in a Turbula (Glen Creston Ltd, Middlesex, UK) at 46rpm for 30 minutes.

This blend design was not intended to reflect any commercially available or relevant DPI powder formulation. The use of Sorbalac 400 lactose particles ( $d_{50} < 10\mu\text{m}$ ) with respect to more conventional carrier sizes (63-90 $\mu\text{m}$ ) was dictated by the need to minimise the potential influence of larger carrier particles over fluidisation and de-aggregation processes of particle agglomerates [6, 7]. This formulation was selected solely to suit the objectives of the study of the cohesive-adhesive balance between drug and lactose components.

- **Contact angle measurements**

The sessile drop technique was used to determine the surface free energy of the powders. Compact surfaces of the powder samples were prepared for analysis. Contact angle measurements were performed using a Goniometer (Ramé-hart Inc.,

New Jersey, USA). Diiodomethane was used as an apolar liquid while ethylene glycol and glycol were used as polar liquids.

- **Interaction force measurements**

The AFM was housed in an environmental chamber and the ambient conditions maintained at a constant temperature of 25°C ( $\pm 0.2^\circ\text{C}$ ) and relative humidity of 35% RH ( $\pm 3\%$ ). The partial water vapour pressure was controlled via a custom-built perfusion unit coupled with a highly sensitive humidity sensor (Rotronic AG, CH). Individual force curves ( $n = 4096$ ) were conducted over a  $2.5\mu\text{m} \times 2.5\mu\text{m}$  at a scan rate of 4Hz and a compressive loading of 10nN. These parameters were kept constant throughout the study. Statistical analysis of these data was performed by Fisher's pair wise comparison of one-way ANOVA with 99% confidence limits.

- **Cohesive-adhesive balance (CAB) graph analysis**

The wealth of information from AFM measurements of the interparticulate forces was analysed using a recently developed cohesive-adhesive balance procedure. Detailed information regarding the CAB graph analysis is described in Chapter 3.

- **Content uniformity measurements**

The content uniformity of the salbutamol sulphate-lactose blends was measured by analysing the quantity of active in  $10\text{mg} \pm 0.5\text{mg}$  samples ( $n=10$ ). Drug content was analysed by HPLC. Relative standard deviation between samples was calculated to assess the homogeneity of the different blends.

- ***In vitro* aerosol deposition studies**

Approximately 10 mg of the carrier formulations was accurately weighed into a gelatine capsule to be loaded into a Monohaler<sup>®</sup> device (Miat SpA, Milan, Italy). *In vitro* deposition investigations were performed using a next generation impactor (NGI) (Copley Scientific, Nottingham, UK). The loaded device was connected to the throat of the NGI via a moulded mouthpiece. *In vitro* analysis was performed after each actuation of the device. Each experiment ( $n=3$ ) was performed at  $60\text{L}\cdot\text{min}^{-1}$  flow rate with a 5 second exposure. Each NGI plate was rinsed with mobile phase and the subsequent solution was collected in a 50ml volumetric flask.

### 5.3. Results and Discussion

Previous studies have emphasized the relative strength of the adhesive salbutamol sulphate-lactose adhesive forces with respect to salbutamol sulphate cohesive forces (Chapter 3). The initial part of the present study was to quantify possible variations in cohesive and adhesive bonds via the introduction of a force control agent. This was achieved by first conditioning the lactose with various force control agents using a Mechanofusion system, prior to mixing with the drug.

The CAB-graph obtained for a salbutamol sulphate-lactose binary system (with the use of compact substrates) is shown in Figure 5.2. The relative position of the data below the bisecting line indicated a stronger affinity between salbutamol sulphate and lactose than their cohesive forces. This suggested a predisposition for an interactive blend. However, the quantitative measurement of the relative strength of the cohesive-adhesive ratio indicated that the adhesive salbutamol sulphate-lactose interaction was approximately six times greater ( $\Lambda_{12}=6.25$ ) than the cohesive salbutamol sulphate bond.

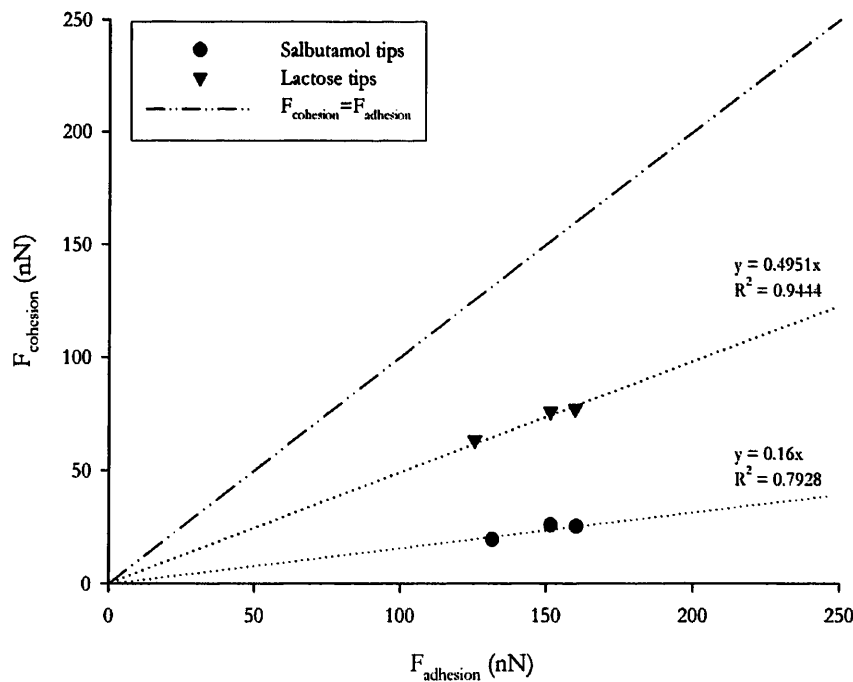


Figure 5- 2: CAB-graph of a salbutamol sulphate lactose binary system .

It should be highlighted that the previous assessments (Chapter 3) performed with model crystal substrates revealed a salbutamol sulphate-lactose reduced intermixing coefficient of 16.88 (Chapter 4). This disparity may be explained by the inevitable increase in surface roughness by using compressed powder substrates in contrast to smooth crystalline substrates. This would be anticipated to have a considerable effect on relative contact area and influence both van der Waals forces and capillary forces [8, 9]. Nevertheless, both studies revealed a consequent adhesively led system, suggesting that a significant amount of energy would be required to overcome the adhesive interaction for efficient dispersion of the drug from a lactose surface. Thus, the introduction of an FCA was intended to advantageously lower the adhesive interactions between drug and excipient to facilitate the detachment of the drug particles from the carrier upon aerosolisation provided that an adhesive led system was maintained.

### 5.3.1. Model Formulations with Conditioned Lactose

The CAB-graphs obtained for the interaction of salbutamol sulphate probes and lactose probes where the lactose particles have been conditioned with leucine, lecithin and MgST are shown in Figures 5.3, 5.4 and 5.5, respectively. As expected, the addition of FCAs significantly modified the salbutamol-lactose interactions. In all cases, the introduction of the ternary agent significantly reduced the adhesive interactions of the salbutamol probe with the various modified lactose substrates. However, particle adhesion decreased to such an extent that the reduced intermixing coefficient ( $F_{\text{drug-lactose}}/F_{\text{drug-drug}}$ ), calculated from the gradient of the CAB plots, was below 1 (Table 5.3). This shift moved the CAB system to one synonymous of a cohesive led system. The conditioning of lactose with MgST resulted in the lowest intermixing coefficient value ( $\Lambda_{12}=0.61$ ) while the addition of leucine and lecithin reduced the intermixing coefficient to 0.96 and 0.88, respectively. Thus, the pre-conditioning of lactose particles with leucine, lecithin or MgST transformed a system which was dominated by the adhesive drug-lactose forces into a cohesive system. Such lowering of the interactions between drug and excipient via the introduction of the FCAs may possibly lead to an unstable formulation, and subjected to undesirable segregation.

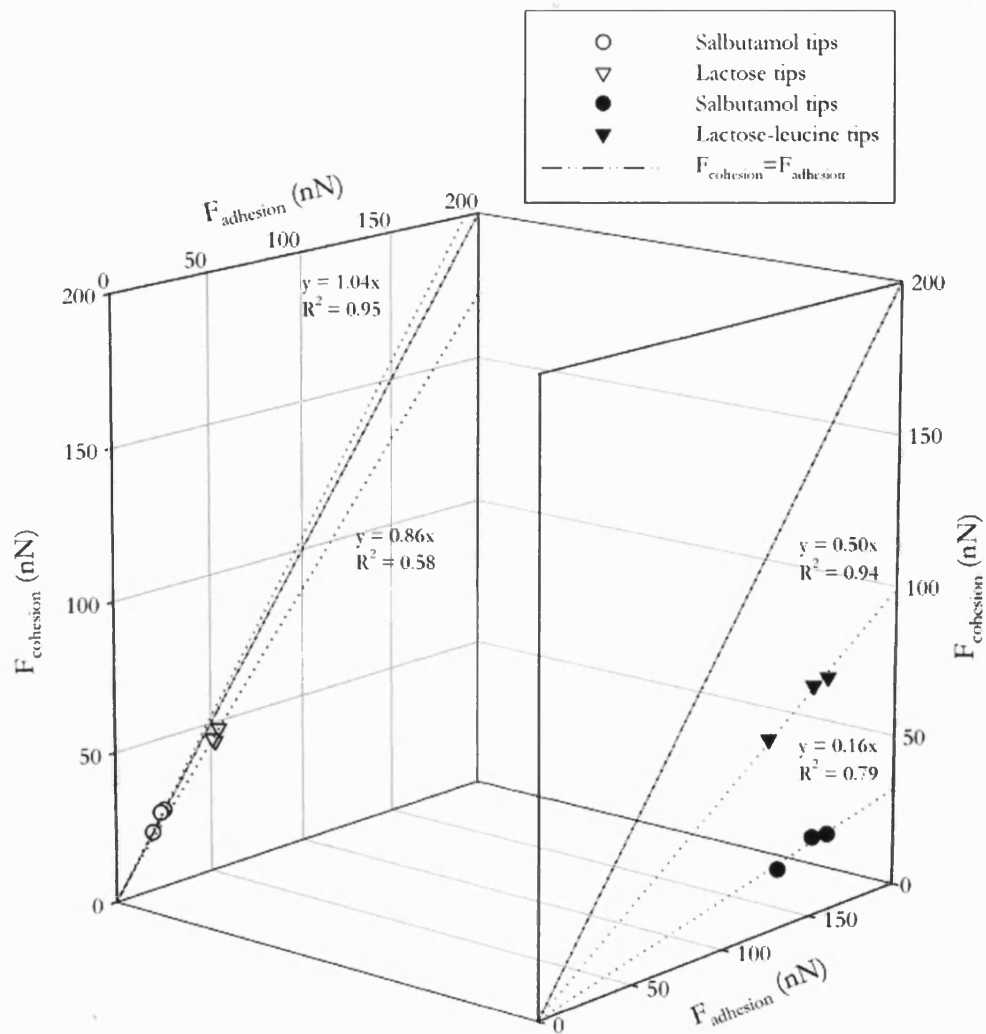


Figure 5- 3: Influence of the mechanofusion of lactose with leucine on the cohesive-adhesive balances of a salbutamol sulphate-lactose system.



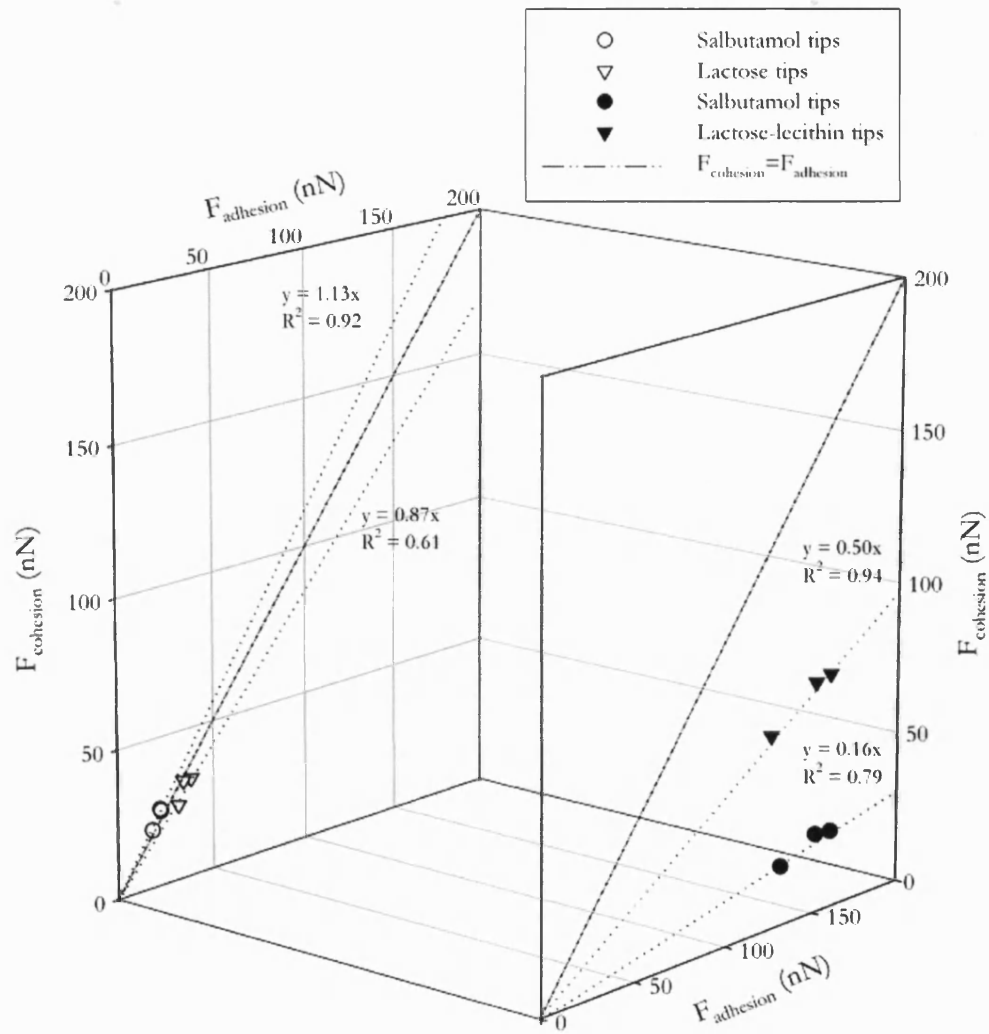


Figure 5- 4: Influence of the mechanofusion of lactose with lecithin on the cohesive-adhesive balances of a salbutamol sulphate-lactose system.

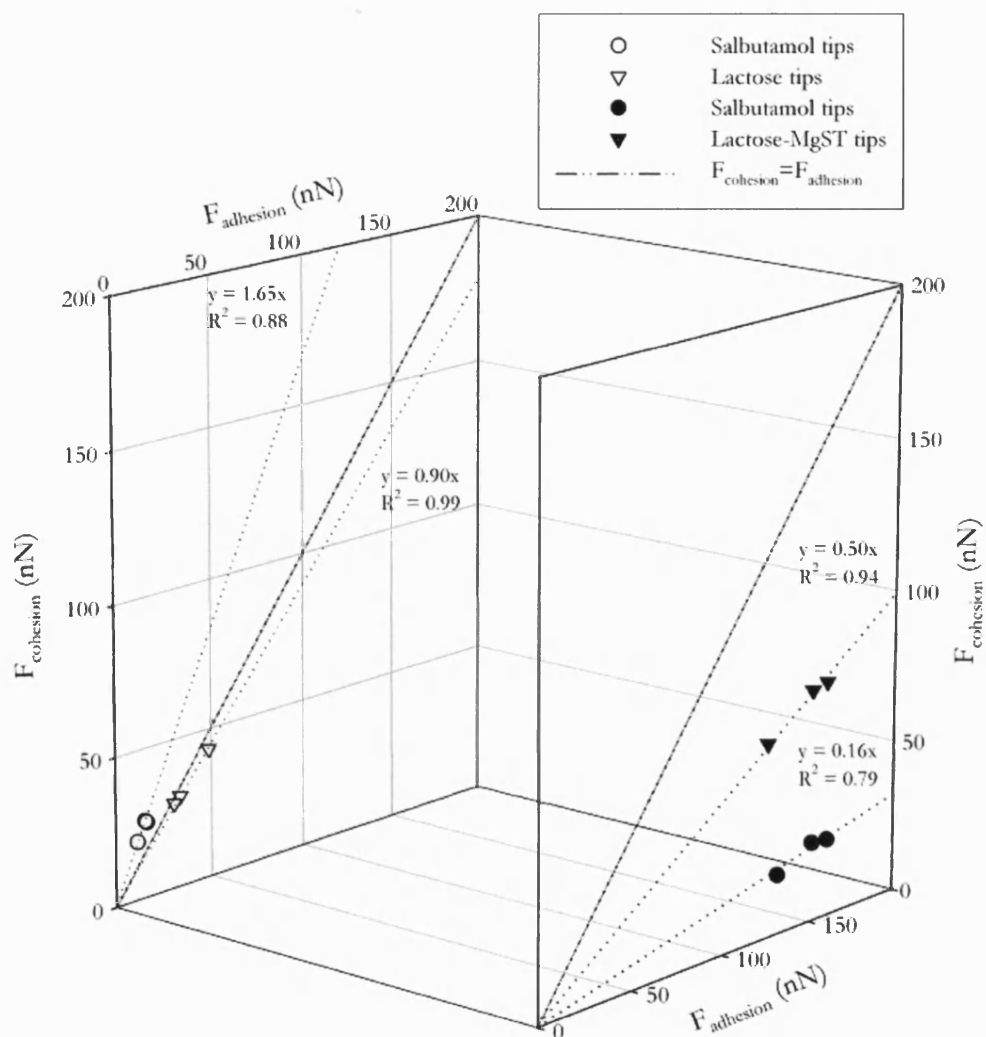


Figure 5- 5: Influence of the mechanofusion of lactose with lecithin on the cohesive-adhesive balances of a salbutamol sulphate-lactose system.

Contact angle measurements were performed on compact surfaces of mechanofused lactose with leucine, lecithin and MgST. The resulting contact angles obtained with diiodomethane, ethylene glycol and ultra pure water are shown in Table 5.1. Using the van Oss-Chaudhury-Good (VCG) thermodynamic approach [10], described in more detail in Chapter 2, the surface energy contributions and resulting Gibbs interfacial free energy of cohesion of mechanofused lactose with leucine, lecithin and MgST are summarised in Table 5.2.

Sample	Contact angle ( $\theta$ )		
	Diiodomethane	Ethylene glycol	U.P. water
Sorbalac 400 + Leucine	52.00 $\pm$ 1.00	44.33 $\pm$ 3.51	14.67 $\pm$ 2.52
Sorbalac 400 + Lecithin	60.00 $\pm$ 3.61	11.67 $\pm$ 0.58	8.67 $\pm$ 1.53
Sorbalac 400 + MgST	62.00 $\pm$ 1.00	81.00 $\pm$ 2.00	87.33 $\pm$ 5.86

Table 5- 1: Contact angle measurements of mechanofused lactose with FCAs.

Sample	$\gamma^{LW}$	$\gamma^+$	$\gamma^-$	$\gamma^{tot}$	$\Delta G^{tot}$
Sorbalac 400 + Leucine	33.15	0.18	85.48	40.42	-82.01
Sorbalac 400 + Lecithin	28.58	1.09	69.67	45.99	-91.98
Sorbalac 400 + MgST	27.42	0.59	12.43	32.79	-76.41

Table 5- 2: Surface energy contributions and resulting Gibbs interfacial free energy of interaction of mechanofused lactose with FCAs (All units are in  $\text{mJ}\cdot\text{m}^{-2}$ ).

As anticipated, the inclusion of FCAs with the lactose greatly decreased the total surface free energy of the coated particles in comparison to the 'as supplied' Sorbalac 400 (Chapter 2). The dispersive contribution ( $\gamma^{LW}$ ) decreased from  $48.51\text{mJ}\cdot\text{m}^{-2}$  for the untreated material to  $33.15\text{mJ}\cdot\text{m}^{-2}$  when mechanofused with leucine,  $28.58\text{mJ}\cdot\text{m}^{-2}$  when mechanofused with lecithin and  $27.42\text{mJ}\cdot\text{m}^{-2}$  when mechanofused with MgST. These results were very close to the pure FCAs, being  $27.23\text{mJ}\cdot\text{m}^{-2}$ ,  $23.07\text{mJ}\cdot\text{m}^{-2}$  and  $23.06\text{mJ}\cdot\text{m}^{-2}$  for leucine, lecithin and MgST, respectively. The resulting total surface free energy of the mechanofused materials, calculated from the van der Waals and polar contributions, significantly decreased from  $52.28\text{mJ}\cdot\text{m}^{-2}$  for the untreated material to  $40.42\text{mJ}\cdot\text{m}^{-2}$  when mechanofused with leucine,  $45.99\text{mJ}\cdot\text{m}^{-2}$  when mechanofused with lecithin and  $32.79\text{mJ}\cdot\text{m}^{-2}$  when mechanofused with MgST. The interfacial Gibbs free energy of cohesion of the three mechanofused samples, calculated from VCG theory, indicated a significant decrease in particle-particle interaction via the inclusion of leucine, lecithin or MgST. These data were in good accordance with the force ratios obtained via CAB graphs analyses. They also supported the premise that the pre-conditioning of lactose particles with leucine, lecithin or MgST may possibly lead to an unstable formulation, subjected to undesirable segregation.

Representative SEM images of formulations of salbutamol sulphate mixed with lactose-leucine, lactose-lecithin and lactose-MgST conditioned particles are shown in Figures 5.6A, 5.6B and 5.6C, respectively. As anticipated from the intermixing coefficient measurements, scanning electron micrographs highlighted a high degree of drug segregation via the introduction of the FCAs. A very limited adhesive interaction was apparent between agglomerated salbutamol sulphate particles and conditioned lactose-leucine (Figure 5.6A). However, large quantities of drug particles were present as loose agglomerates. This segregation was even more pronounced for lecithin (Figure 5.6B) and MgST (Figure 5.6C) conditioned lactose particles. Virtually no interaction was observed between drug and the conditioned lactose surfaces, which resulted in the formation of large drug agglomerates. Interestingly, the mechanofused Sorbalac 400 lactose particles appeared to be smoother after pre-conditioning with leucine, lecithin or magnesium stearate, compared to the 'as supplied' Sorbalac (Chapter 4). This suggested a smooth continuous coating of the FCAs over the surface of the lactose particles.

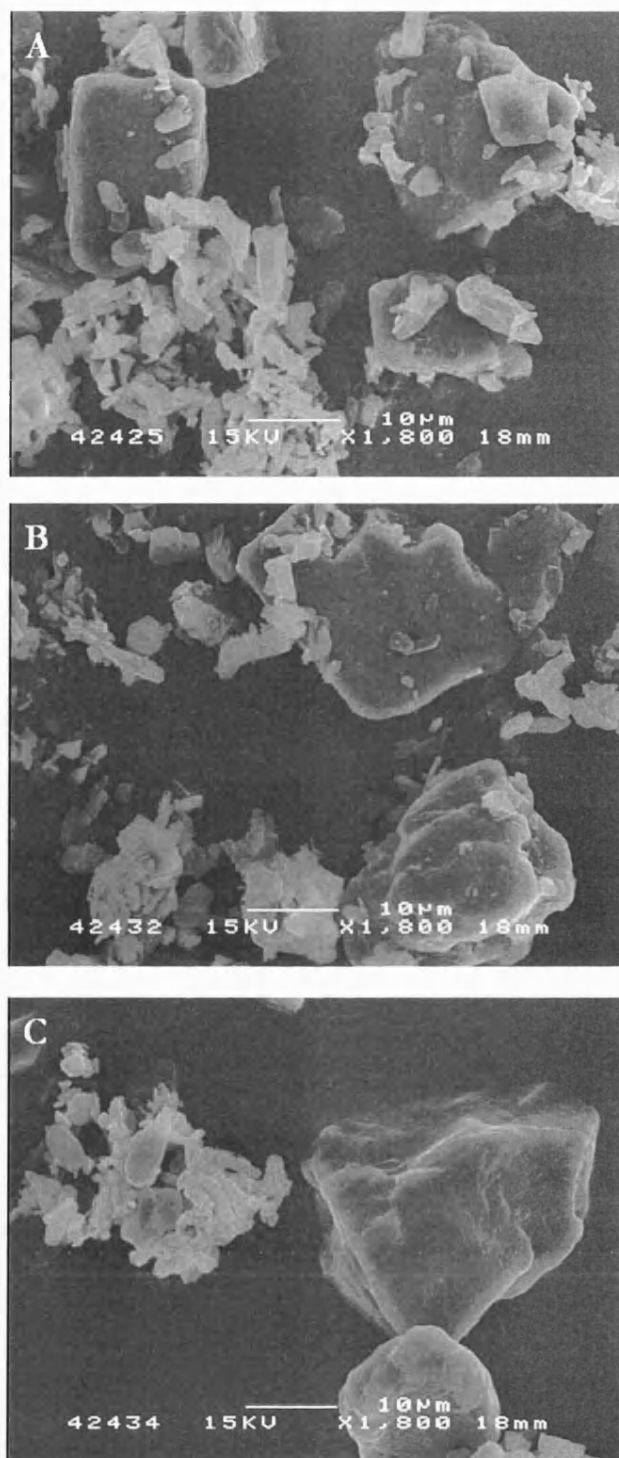


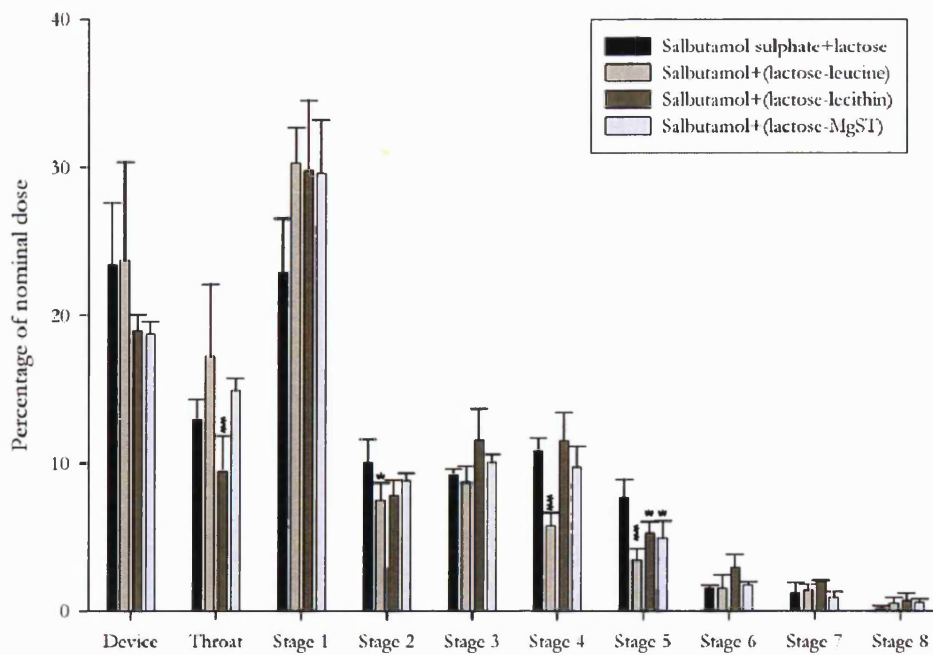
Figure 5- 6: Representative scanning electron micrographs of ternary mixtures of salbutamol sulphate and lactose pre-conditioned with leucine (A), lecithin (B) and magnesium stearate (C).

As anticipated, dose content uniformity measurements revealed an increase in the relative standard deviation of salbutamol sulphate of each blend (Table 5.3). The RSD of 4.2% for micronised salbutamol sulphate mixed with lactose increased to 8.92% with the conditioning of lactose with leucine, 9.31% for lactose-lecithin and 15.51% for lactose-MgST. These observations suggested good correlation between the reduction of the intermixing coefficients, which were significantly below 1, and the content uniformity measurements of salbutamol sulphate in the corresponding carrier-based formulations.

The de-agglomeration and dispersion behaviour of the salbutamol sulphate particles from the model carrier based formulations are shown in Figure 5.7. The emitted dose of the salbutamol sulphate-lactose formulation via the low resistance Monohaler<sup>®</sup> device was quite high (76.57%). However, a significant percentage of the drug was recovered in the throat and the first stage of the NGI apparatus. These results were in accordance with the previous *in vitro* study conducted with a Rotahaler<sup>®</sup> and Turbuhaler<sup>®</sup> DPI devices (Chapter 4). This study suggested that the observed deposition pattern was due to the limited detachment of the drug from the carrier upon actuation caused by the highly adhesive salbutamol sulphate-lactose interactions.

Conditioning	Mixing	Reduced intermixing coefficient ( $\Lambda_{12}$ )	Content uniformity (% RSD)
Mechanofusion, 10 min @ 5200 rpm	Turbula, 30 min@ 46 rpm		
Salbutamol sulphate (non treated)	Sorbalac 400	6.25	4.20
Sorbalac 400 + Leucine	Salbutamol sulphate	0.96	8.92
Sorbalac 400 + Lecithin	Salbutamol sulphate	0.88	9.31
Sorbalac 400 + MgST	Salbutamol sulphate	0.61	15.51

Table 5- 3: Mixing sequences of salbutamol sulphate carrier-based formulations with conditioned lactose and reduced intermixing coefficients and content uniformities.



\*  $p < 0.05$ , \*\*  $p < 0.01$ , \*\*\*  $p < 0.001$ : significant difference compared to without force control agent by ANOVA one-way.

Figure 5- 7: In-vitro deposition of salbutamol sulphate carrier-based formulations with conditioned lactose (mean  $\pm$  S.D.,  $n=3$ ).

The mechanical fusion of leucine with lactose resulted in a similar drug emission efficiency to the conventional blend. However, the amount of salbutamol sulphate recovered in the first stage of the NGI significantly increased with respect to the non coated lactose blend. The coating of lactose with either lecithin or MgST slightly reduced the device retention of the active ingredient from 23.43% to 18.73% and 18.99%, respectively. Although the interactions between drug and coated lactose surfaces were significantly decreased, a large amount of drug was still recovered on the upper stage of the in vitro apparatus.

These results were consistent with the assessment from the CAB-graphs. The CAB analysis indicated that the energy of interaction between the drug and coated lactose would reduce to such an extent that the adhesively led salbutamol sulphate-lactose formulation would shift to an unfavourable cohesive system. The aerosolisation

performances of the modified lactose carrier-based formulations may not have improved since the dramatic shift in the force balance was shown to lead to poor blend homogeneity and the potential for significant segregation between drug and carrier particles.

### **5.3.2. Model Formulations with Conditioned Salbutamol Sulphate**

The conditioning of excipient particles with a FCA modified the adhesive interaction between drug-carrier and excipient-excipient interactions. In contrast, the processing of the micronised drug particles with the FCA would alter both the cohesive (drug-drug) and adhesive (drug-lactose) interactions. To further investigate the possibility of selectively modifying both these interactions within a carrier based formulation, the drug was mechanofused with the FCAs.

The CAB-graphs obtained for the interaction between conditioned salbutamol sulphate with leucine, lecithin or MgST and lactose are shown in Figures 5.8, 5.9 and 5.10, respectively. The balance remained adhesive for all three systems, although the drug-lactose forces decreased by more than a half of its original value. The conditioning of salbutamol sulphate with leucine, lecithin and MgST led to an intermixing coefficient of 1.89, 2.13 and 1.52, respectively. These mixtures would therefore be expected to form homogenous interactive blends with advantageously weak drug-lactose interactions.

Concomitantly, the force balance of lactose interactions transformed from an adhesive to a cohesive led system. Nevertheless, it can be speculated that this shift should not greatly affect the formulation properties as this change of behaviour is predominately due to a decrease in the adhesive (drug-lactose) forces and not due to an increase of the lactose cohesive bonds.



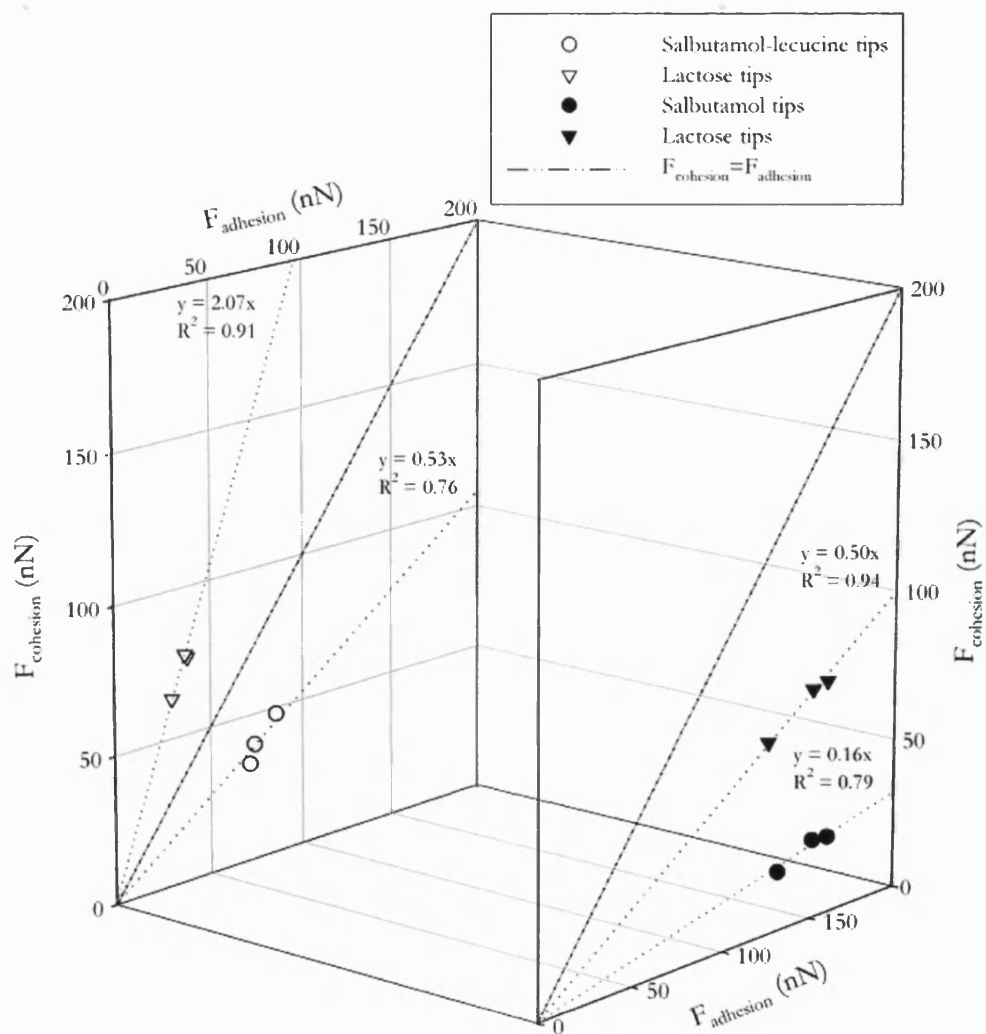


Figure 5- 8: Influence of the mechanofusion of salbutamol sulphate with leucine on the cohesive-adhesive balances of a salbutamol sulphate-lactose system.

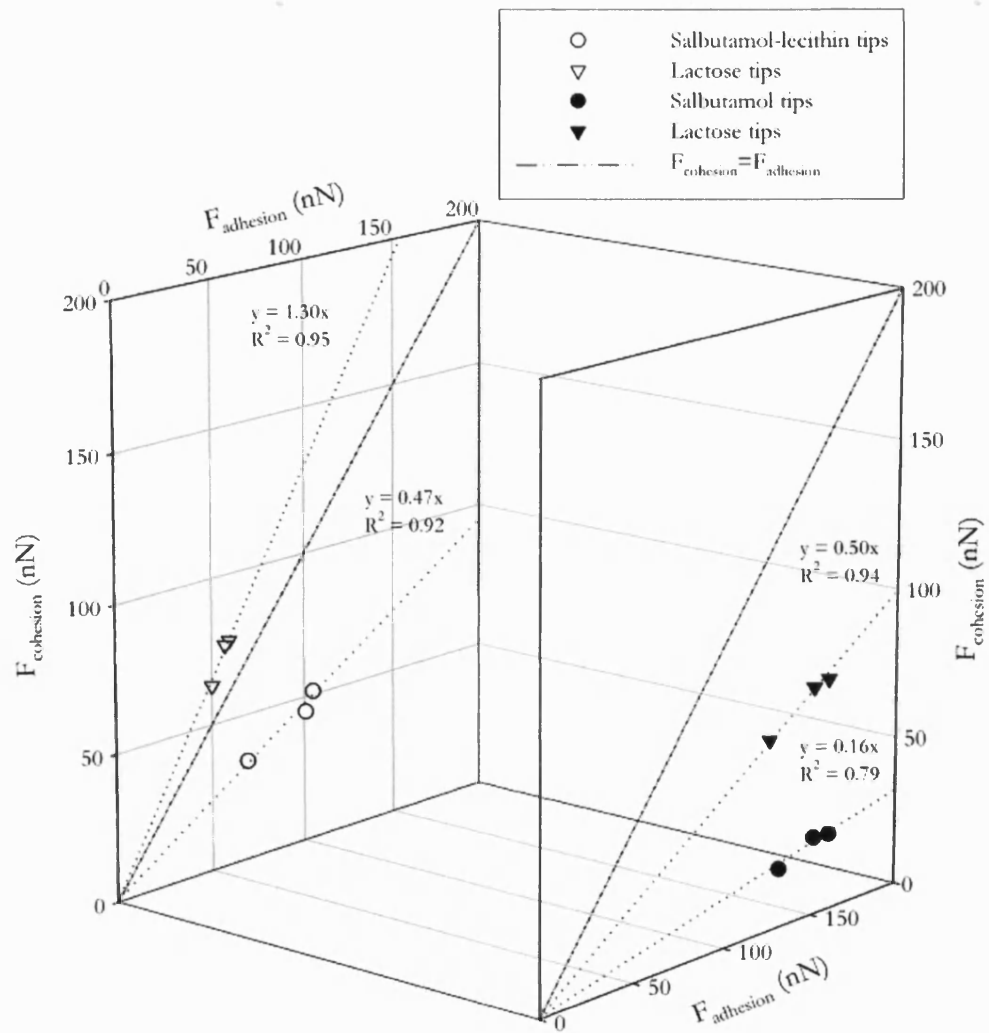


Figure 5- 9: Influence of the mechanofusion of salbutamol sulphate with lecithin on the cohesive-adhesive balances of a salbutamol sulphate-lactose system.

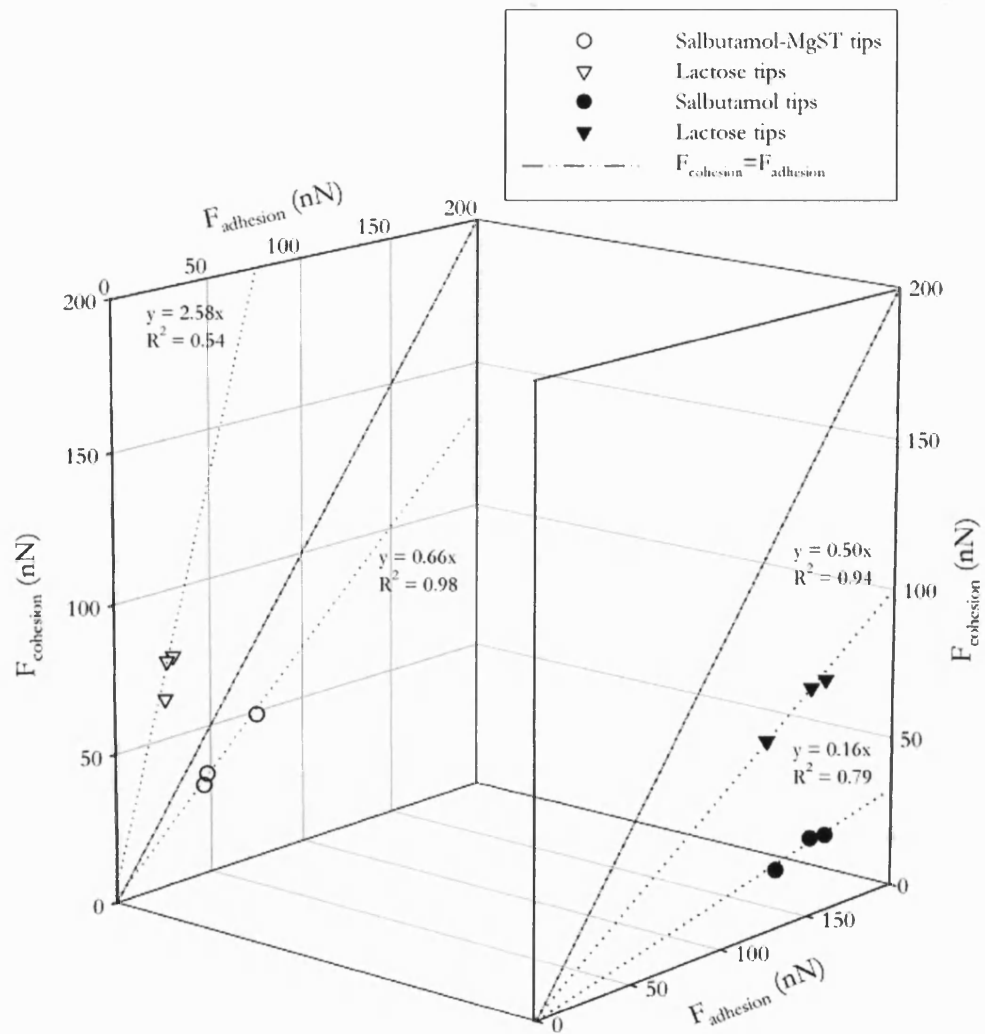


Figure 5- 10: Influence of the mechanofusion of salbutamol sulphate with lecithin on the cohesive-adhesive balances of a salbutamol sulphate-lactose system.

As for the mechanofused lactose samples, contact angle measurements were performed on compact surfaces of mechanofused salbutamol sulphate with leucine, lecithin and MgST. contact angles obtained with diiodomethane, ethylene glycol and ultra pure water are shown in Table 5.4. The surface energy contributions and resulting interfacial Gibbs free energy of cohesion of mechanofused salbutamol sulphate particles are expressed in Table 5.5.

Sample	Contact angle ( $\theta$ )		
	Diiodomethane	Ethylene glycol	U.P. water
Salbutamol + Leucine	$30.67 \pm 1.53$	$18.33 \pm 0.76$	$25.83 \pm 1.89$
Salbutamol + Lecithin	$60.00 \pm 1.00$	$12.00 \pm 2.00$	$12.67 \pm 2.08$
Salbutamol + MgST	$55.00 \pm 1.00$	$61.00 \pm 2.65$	$57.67 \pm 1.53$

Table 5- 4: Contact angle measurements of mechanofused salbutamol sulphate with leucine, lecithin and MgST.

Sample	$\gamma^{LW}$	$\gamma^+$	$\gamma^-$	$\gamma^{tot}$	$\Delta G^{tot}$
Salbutamol + Leucine	39.61	0.15	59.44	45.42	-90.98
Salbutamol + Lecithin	28.57	1.12	67.83	46.03	-92.09
Salbutamol + MgST	31.45	0.28	40.72	37.88	-75.42

Table 5- 5: Surface energy contributions and resulting interfacial Gibbs free energy of cohesion of mechanofused salbutamol sulphate with FCAs (in  $\text{mJ}\cdot\text{m}^{-2}$ ).

The introduction of the FCAs significantly decreased the surface energy contributions of the coated particles in comparison to the 'as supplied' micronised drug (Chapter 2). The dispersive contributions decreased from  $43.94\text{mJ}\cdot\text{m}^{-2}$  for the untreated material to  $39.61\text{mJ}\cdot\text{m}^{-2}$  when mechanofused with leucine,  $28.57\text{mJ}\cdot\text{m}^{-2}$  when mechanofused with lecithin and  $31.45\text{mJ}\cdot\text{m}^{-2}$  when mechanofused with MgST. It is important to note, however, that the polar contributions of the mechanofused samples, although less than the micronised drug, remained substantial. As a result, total surface free energy and corresponding Gibbs free energy were higher than anticipated from CAB graphs analyses. These discrepancies may have arisen from the smaller size of the drug particles and resulting increase in specific surface area with respect to the Sorbalac 400 particles (Chapter 4). The mechanofusion of the same amount of FCA with the drug may have therefore resulted in a thinner and more permeable coating. This may have contributed to partial adsorption of the liquids upon contact angle measurements and resulted in limited but direct interaction between liquids and drug particles.

Representative scanning electron micrographs of the lactose particles blended with conditioned salbutamol sulphate-leucine, salbutamol sulphate-lecithin, and salbutamol sulphate-MgST are shown in Figures 5.11A, 5.11B and 5.11C, respectively. In contrast to the ternary mixture of drug and conditioned lactose shown in Figure 5.6, the conditioned drug particles strongly interacted with the lactose particles for all three FCAs. This suggested an effective adhesive disposition, in agreement with the CAB data analyses.

The corresponding content uniformity measurements of the ternary mixtures reflected an adhesive led system with low relative standard deviations for lactose mixed with salbutamol sulphate-leucine (2.92%), salbutamol sulphate-lecithin (3.00%) and salbutamol sulphate-MgST (3.62%) conditioned particles (Table 5.6). These observations suggested good correlation between the reduced intermixing coefficients and the characteristics of the respective carrier-based formulations. Such formulations would be expected to be stable during handling and storage, and may lead to a greater de-agglomeration and dispersion efficiency of the respirable particles.

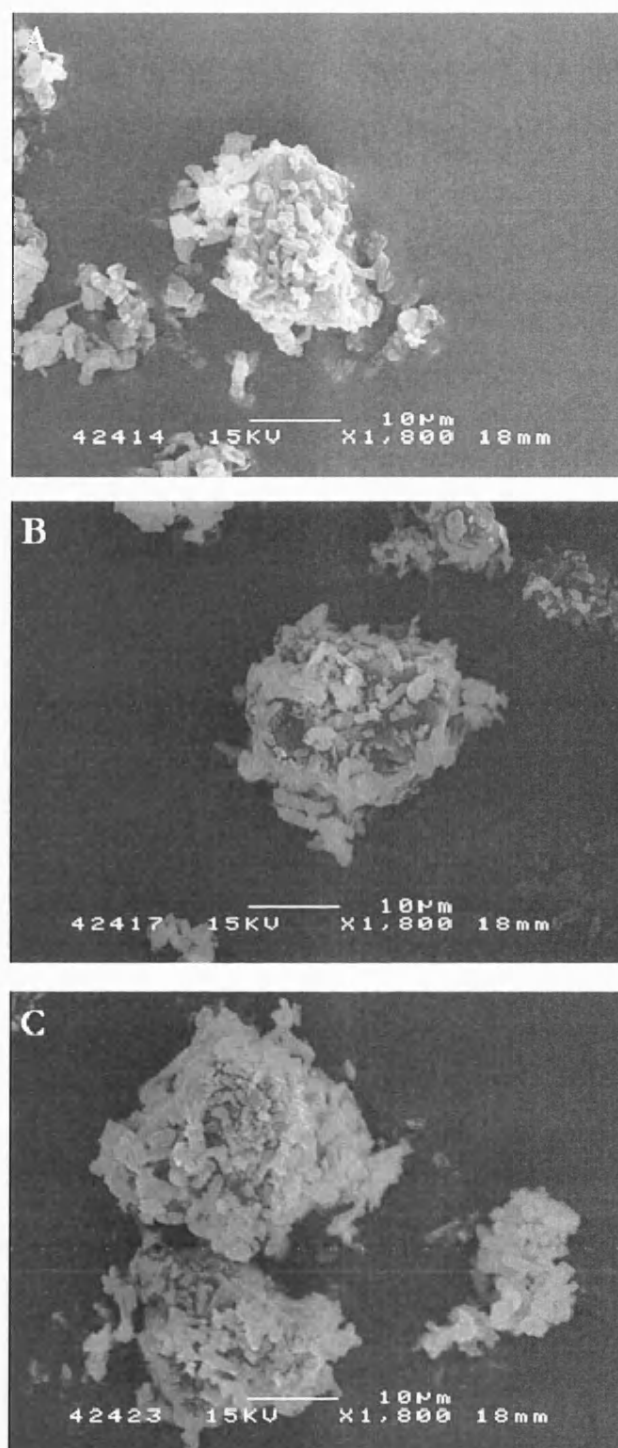
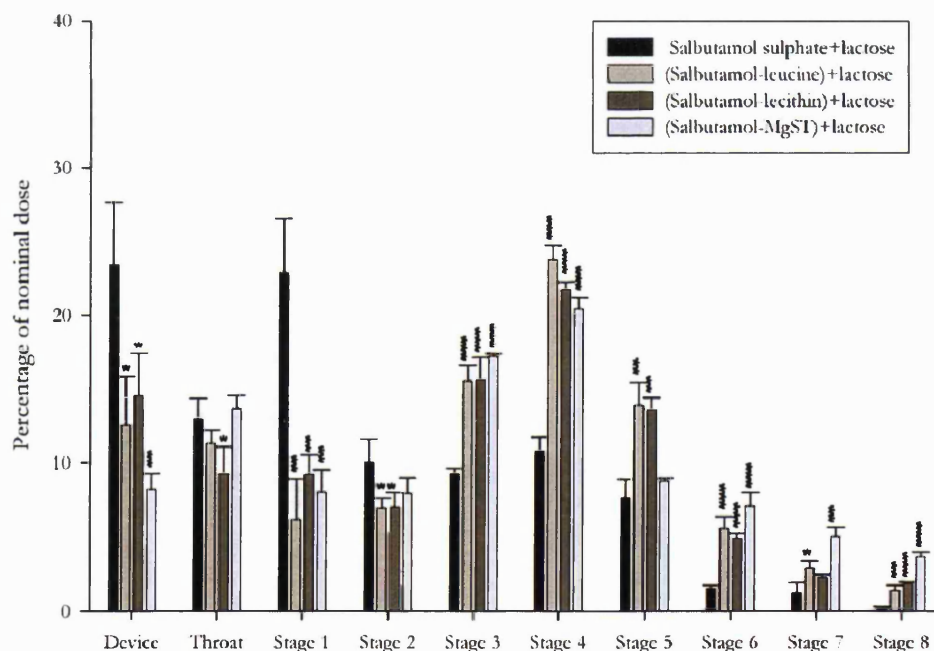


Figure 5- 11: Representative scanning electron micrographs of ternary mixtures of lactose and salbutamol sulphate pre-conditioned with leucine (A), lecithin (B) and magnesium stearate (C).

Conditioning	Mixing	Reduced intermixing coefficient ( $\Delta_{12}$ )	Content uniformity (% RSD)
Mechanofusion, 10 min @ 5200 rpm	Turbula, 30 min @ 46 rpm		
Salbutamol sulphate (non treated)	Sorbalac 400	6.25	4.20
Salbutamol sulphate + Leucine	Sorbalac 400	1.89	2.92
Salbutamol sulphate + Lecithin	Sorbalac 400	2.13	3.00
Salbutamol sulphate + MgST	Sorbalac 400	1.52	3.62

Table 5- 6: Mixing sequences of salbutamol sulphate carrier-based formulations with conditioned drug and reduced intermixing coefficients and content uniformities.

The in-vitro deposition profiles of formulation of Sorbalac 400 mixed with micronised salbutamol sulphate and Sorbalac 400 mixed with salbutamol sulphate conditioned with leucine, lecithin and MgST are shown in Figure 5.12.



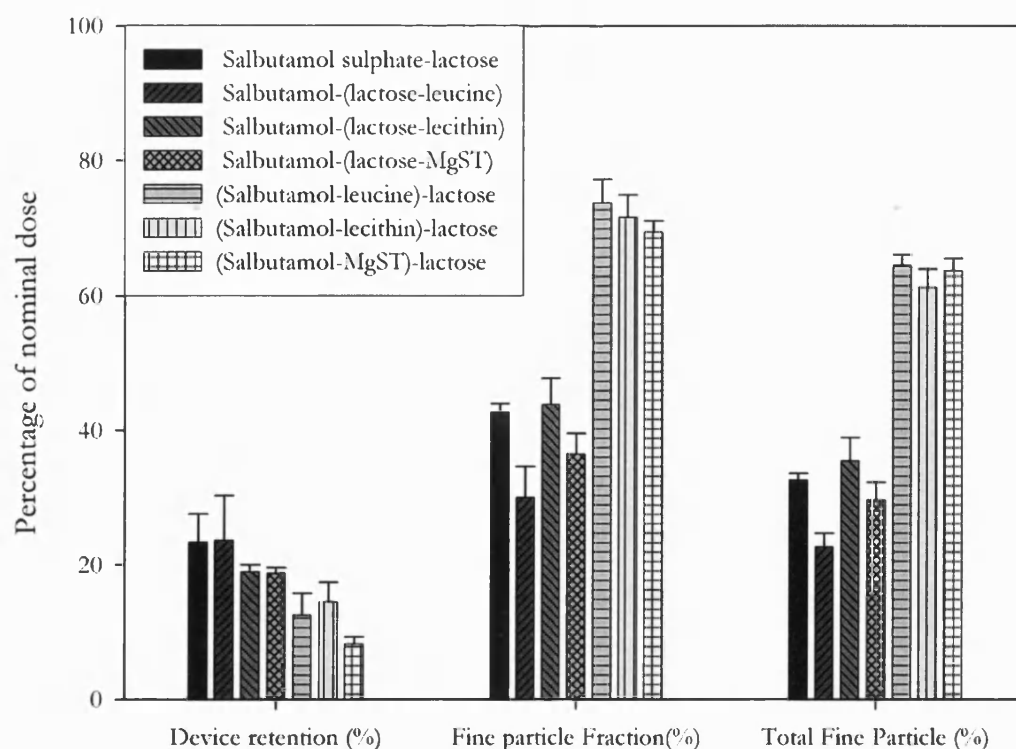
p<0.05, \*\* p<0.01, \*\*\* p<0.001: significant difference compared to without force control agent by ANOVA one-way.

Figure 5- 12: In-vitro deposition of carrier-based formulations with conditioned salbutamol sulphate (mean  $\pm$  S.D., n=3).

The mechanofused salbutamol sulphate particles resulted in a significant decrease in device retention from 23.42% for the FCA free formulation to 12.51% with leucine, 14.52% with lecithin and 8.23% with MgST. These results suggested a lubrication effect of the FCA and subsequent reduction in interaction between the powder bed and the capsule, while the formulation conserved its metastability as suggested by the CAB analyses. More dramatic was the significant decrease of the percentage of drug deposited in the first stage (cut off diameter  $\approx 8.06\mu\text{m}$ ) of the NGI apparatus. Stage 1 deposition decreased from 22.89% to 6.16% for the conditioning of salbutamol sulphate with leucine, to 9.20% for salbutamol sulphate-lecithin and 7.99% for salbutamol sulphate-MgST. This indicated a greater de-agglomeration efficiency of the coated salbutamol sulphate particles in the carrier based formulations, which was further highlighted by the increase deposition of the active ingredient in the lower stages of the in vitro apparatus.

A summary of the device retention, fine particle fraction (% respirable particle of the emitted dose) and total fine particle fraction (% respirable particle from total recovered dose) of the salbutamol sulphate carrier-based formulations is shown in Figure 5.13. A clear pattern of formulation performance was observed depending on whether the force control agent was fused either with the drug or the lactose. Formulations with pre-conditioned drug, in contrast to conditioned lactose, offered the best drug delivery performances. It is suggested that the conservation of an adhesive system for the pre-conditioned drug particles directly led to the increased de-aggregation performance. Meanwhile, the selective decrease of the drug-lactose interfacial interaction for conditioned lactose particles led to a dominant cohesive (drug-drug) system, which resulted in poor blend homogeneity and poor fluidisation. The highest %FPF of the emitted dose was obtained for formulations with leucine and lecithin coating salbutamol sulphate particles (73.72% and 71.87%, respectively). The low drug retention of salbutamol sulphate-MgST conditioned particles (8.23% device retention) contributed to deliver an equivalent total fine particle dose as for leucine and lecithin (64.43% for leucine, 61.41% for lecithin and 63.79% for MgST). These data clearly indicated that the characteristic properties of carrier based formulations can be controllably enhanced by judicious selection of the interparticulate interactions to be modified by the introduction of the FCAs.





\*  $p < 0.05$ , \*\*  $p < 0.01$ , \*\*\*  $p < 0.001$ : significant difference compared to without force control agent by ANOVA one-way.

Figure 5- 13: Fine particle fraction and emission efficiency of salbutamol sulphate carrier-based formulations (mean  $\pm$  S.D.,  $n=3$ ).

## 5.4. Conclusions

The influence of force control agents on the properties and performances of model salbutamol sulphate carrier based formulations was investigated. The cohesive and adhesive dependencies were controlled by conditioning either the drug or the carrier before mixing in order to create selective modifications of the inter-particle interactions within the dry powder formulation. The colloid probe AFM technique together with the novel cohesive-adhesive balance (CAB) analysis procedure was utilised to measure the variations in inter-particle forces of the ternary blends. The predictive CAB-graph indicated radical modifications in the behaviour of the formulation dependant on whether the FCAs were conditioned with the drug or the lactose. The content uniformity measurements and drug deposition patterns of the

various ternary mixtures were in good accordance with predictions of the CAB assessment of the colloid probe AFM measurements.

## 5.5. References

- [1] J. N. Staniforth. Pre-formulation aspects of dry powder aerosols., *Respiratory Drug Delivery V*, 1996.
- [2] J. N. Staniforth. Improvement in dry powder inhaler performance: surface passivation effects. *Proceedings of Drug Delivery to the Lungs VII* 86-89 (1996).
- [3] P. Begat, M. Green, D. A. V. Morton, A. Whittock, and J. N. Staniforth. PowderHale: A Novel High Performance Dry Powder Inhaler Formulation Technology for Targeted and Systemic Drug Delivery. *Drug Delivery to the Lung XII* 119 (2001).
- [4] R. Pfeffer, R. N. Dave, D. G. Wei, and M. Ramlakhan. Synthesis of engineered particulates with tailored properties using dry particle coating. *Powder Technol.* **117**: 40-67 (2001).
- [5] J. N. Staniforth and D. A. V. Morton. Powder Technology Research Leading to Improvements in Inhaler Products. *Powder Science and Engineering* **34**: 60-64 (2002).
- [6] X. M. Zeng, G. P. Martin, C. Marriott, and J. Pritchard. The effects of carrier size and morphology on the dispersion of salbutamol sulphate after aerosolization at different flow rates. *J. Pharm. Pharmacol.* **52**: 1211-1221 (2000).
- [7] X. M. Zeng, K. H. Pandhal, and G. P. Martin. The influence of lactose carrier on the content homogeneity and dispersibility of beclomethasone dipropionate from dry powder aerosols. *Int. J. Pharm.* **197**: 41-52 (2000).

- [8] R. Price, P. M. Young, S. Edge, and J. N. Staniforth. The influence of relative humidity on particulate interactions in carrier-based dry powder inhaler formulations. *Int. J. Pharm.* **246**: 47-59 (2002).
- [9] J. C. Hooton, C. S. German, S. Allen, M. C. Davies, C. J. Roberts, S. J. B. Tendler, and P. M. Williams. An atomic force microscopy study of the effect of nanoscale contact geometry and surface chemistry on the adhesion of pharmaceutical particles. *Pharm. Res.* **21**: 953-961 (2004).
- [10] C. J. van Oss, M. K. Chaudhury, and R. J. Good. Interfacial Lifshitz-van der Waals and polar interactions in macroscopic systems. *Chem. Rev.* **86**: 927-941 (1988).

## Chapter 6

# The Use of Force Control Agents in Model Budesonide DPI Formulations

### 6.1. Introduction

Chapter 3 highlighted the increased cohesive properties of micronised budesonide particles with respect to its adhesive interaction with the dominant growth face of  $\alpha$ -lactose monohydrate particles, as measured by the quantitative CAB-graph analyses of AFM data. Further work, which was presented in Chapter 4, investigated the behaviour of a mixture of lactose Sorbalac 400 and budesonide. The formulation exhibited poor content uniformity and visual observations by scanning electron microscopy implied a highly segregated system. These findings in conjunction with in vitro studies suggested a mechanism in which the presence of large and dense agglomerates of budesonide may significantly increase the deaggregation efficiencies of the active ingredient. The influence of the carrier would hence be relatively inconsequential as the drug agglomerates would readily fluidise upon actuation, resulting in similar aerosolisation properties as the drug-only formulation. It was therefore suggested that delivery characteristics of DPI formulations of highly cohesive drug systems were predominantly governed by the drug-drug interaction forces. As the lactose cohesive bonds would only play a minor role in the overall formulation behaviour, optimisation of such dry powder formulations would require passivation of the excessive cohesive bonds to create a more interactive drug-lactose system.

The use of a force control agent (FCA) in conjunction with a mixing procedure capable of producing effective nano-layer coating, presented in Chapter 5, have shown to strongly affect de-agglomeration and entrainment properties of model lactose-salbutamol sulphate DPI formulations. For that purpose, the Mechanofusion system was used to ensure an efficient coating of the drug to be conditioned with the force control agent. The shear forces involved in the Mechanofusion process may provide the necessary energy to break up the cohesive drug agglomerates. While the host particles (FCAs) interact with the guest particles to create a more homogeneous blend, the compression forces may then complete the fusion of the guest onto the host by solid sintering. The conditioning of budesonide particles with ternary agents in lowering the surface energy of interaction may, therefore, dramatically affect their cohesive behaviour. The drug mixture could exhibit a greater affinity to the lactose carrier, leading to a more homogenous formulation that may in turn improve the stability and aerosolisation properties of budesonide.

The study was carried out with three force control agents (leucine, lecithin and magnesium stearate). Cohesive and adhesive force balances were assessed via the AFM colloid probe technique together with CAB-graph analysis. Aerosol drug deposition of the budesonide formulations was assessed by in-vitro measurements.

## 6.2. Methods

General methods of each technique or apparatus used in this study are described in detail in Chapter 2.

- **Preparation of powder formulations**

Powder mixing was achieved in two successive steps involving different energetic processes. Pre-blends of budesonide and FCA (5% w/w) or lactose and FCA (5% w/w) were prepared using a Mechanofusion system. (Hosokawa-Alpine, Augsburg, Germany). Powders to be processed were sealed into the Mechanofusion system core. A cold-water circulation assured the regulation of the internal vessel temperature using an incorporated water jacket. Samples were mixed at 5000rpm for 10 minutes to achieve the required process intensity and mechanically fuse the

FCA to the host particles. The formulations were subsequently prepared by geometrically mixing 1g of pre-blend and 1g of either lactose or drug depending on the nature of the pre-blend in 100mg increments via a Whirlimixer (Fisons Scientific Apparatus, Loughborough, UK). The resulting mixture was further mixed in a Turbula (Glen Creston Ltd, Middlesex, UK) at 46rpm for 30 minutes.

- **Contact angle measurements**

The sessile drop technique was used on tablets of the samples to be analysed. Analyses were performed using a Goniometer (Ramé-hart Inc., New Jersey, USA). Diiodomethane was used as an apolar liquid whereas ethylene glycol and glycol were used as polar liquids.

- **Interaction force measurements**

The AFM was housed in an environmental chamber and the ambient conditions maintained at a constant temperature of 25°C ( $\pm 0.2^\circ\text{C}$ ) and relative humidity of 35% RH ( $\pm 3\%$ ), The partial water vapour pressure was controlled via a custom-built perfusion unit coupled to a highly sensitive humidity sensor (Rotronic AG, CH). Individual force curves ( $n = 4096$ ) were conducted over a  $2.5\mu\text{m} \times 2.5\mu\text{m}$  at a scan rate of 4Hz and a compressive loading of 10nN. These parameters were kept constant throughout the study. Statistical analysis of these data was performed by Fisher's pair wise comparison of one-way ANOVA with 99% confidence limits.

- **Content uniformity measurements**

The content uniformity of the conditioned budesonide-lactose blends was measured by analysing the quantity of active in  $10\text{mg} \pm 0.5\text{mg}$  samples. Drug content was analysed by HPLC. Relative standard deviation between samples was calculated to assess the homogeneity of the different blends.

- ***In vitro* aerosol deposition studies**

Approximately 10 mg of the carrier formulations was accurately weighed into a gelatine capsule to be loaded into a Monohaler<sup>®</sup> device (Miat SpA, Milan, Italy). *In vitro* deposition investigations were performed using a next generation impactor (NGI) (Copley Scientific, Nottingham, UK). The loaded device was connected to

the throat of the NGI via a moulded mouthpiece. *In-vitro* analysis was performed after each actuation of the device. Each experiment ( $n=3$ ) was performed at  $60\text{L}\cdot\text{min}^{-1}$  flow rate with a 5 second exposure. Each NGI plate was rinsed with the mobile phase and the subsequent solution was collected in a 50ml volumetric flask.

### 6.3. Results and Discussion

A CAB-graph of a budesonide-lactose binary system (with the use of compressed tablet substrates) is shown in Figure 6.1. As expected, the AFM data indicated strongly cohesive budesonide interactions. The resulting reduced intermixing coefficient of 0.33 calculated from the slope coefficient of the budesonide probes strongly suggested the probable reluctance of the drug to form an interactive mixture with the lactose. The CAB analysis clearly suggested the need to lower the budesonide-budesonide interactions to convert a cohesive drug-drug system into an adhesive drug-carrier structure in optimising the possible benefits of a stable carrier-based formulation.

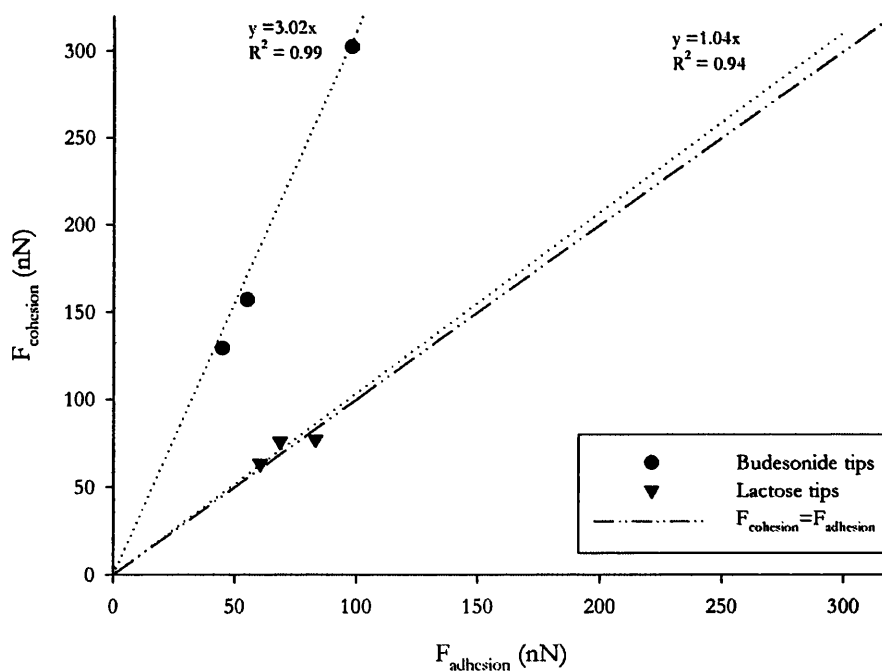


Figure 6- 1: CAB-graph of a budesonide lactose binary system

### 6.3.1. Model Formulations with Conditioned Budesonide

CAB-graphs obtained for lactose probes and probes of budesonide conditioned with leucine, lecithin and MgST are shown in Figure 6.2, 6.3 and 6.4, respectively. The pre-conditioning of budesonide by mechanofusion with the FCAs significantly reduced the budesonide-budesonide interactions, as illustrated by the sharp drop of circle plot groups in the respective figures. The position of the coated drug probes (○) with respect to the bisector when compared to the micronised drug probes (●) indicated that an adhesive drug system had successfully been achieved.

The corresponding reduced intermixing coefficients (Table 6.3) exhibited values higher than 1, ergo indicative of an adhesive system. Budesonide particles coated with leucine exhibited a  $\Lambda_{12}$  of 1.33. The use of lecithin and magnesium stearate seemed to have the additional effect of concurrently decreasing the adhesive lactose-budesonide interactions, contributing to create a weaker adhesively led system. This resulted in the higher reduced intermixing coefficients of 1.43 and 1.96 for budesonide particles mechanofused with lecithin and magnesium stearate, respectively. Assuming that the coverage of the ternary agents over the drug particles is uniform, it would be expected that conditioned budesonide would display an enhanced carrier affinity and exhibit better formulation homogeneity.

Concomitantly, the force balance of lactose interactions transformed from an adhesive to a cohesive led system. Nevertheless, it can be speculated that this shift should not greatly affect the formulation properties as this change of behaviour is predominately due to a decrease in the adhesive (drug-lactose) forces and not due to an increase of the lactose cohesive bonds.



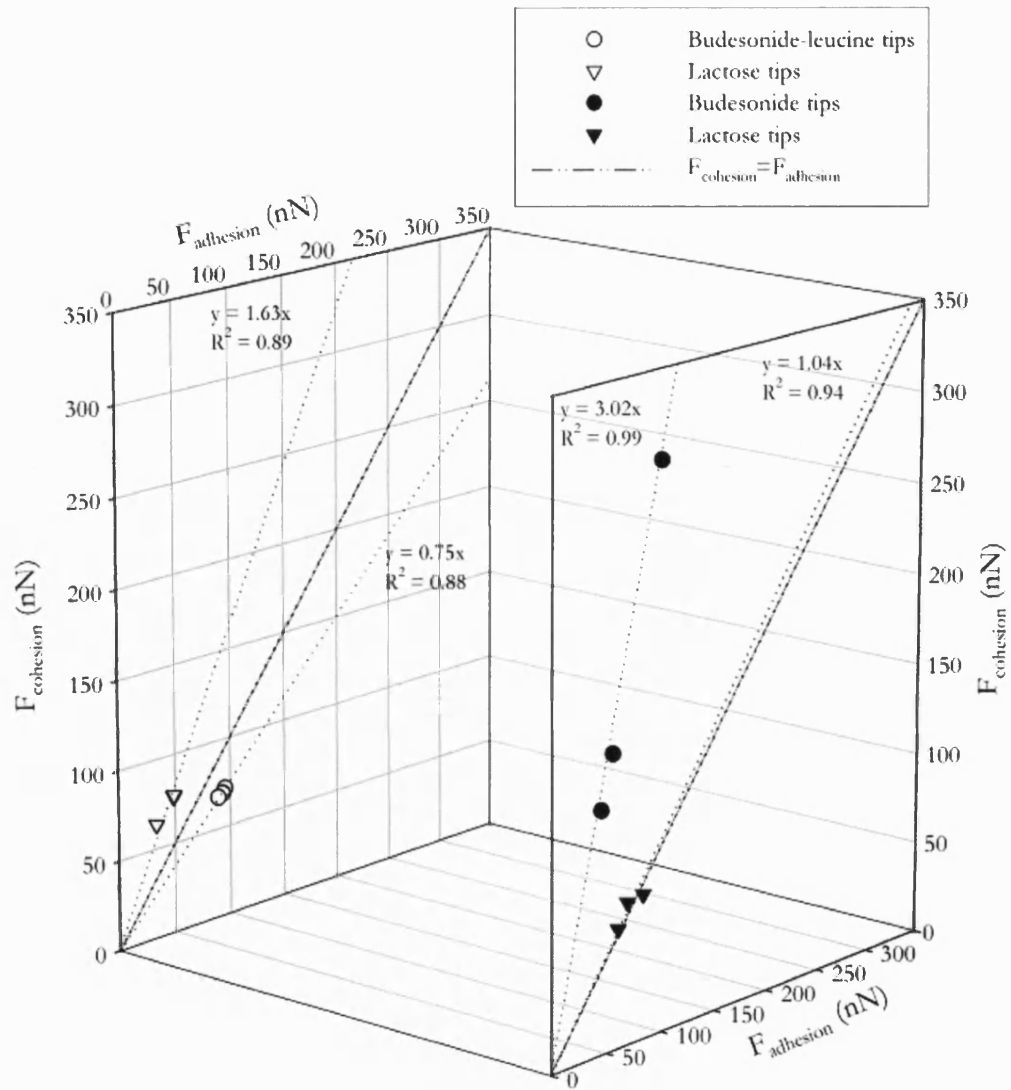


Figure 6- 2: Influence of the coating of budesonide with leucine on the cohesive-adhesive balances of a budesonide-lactose system.

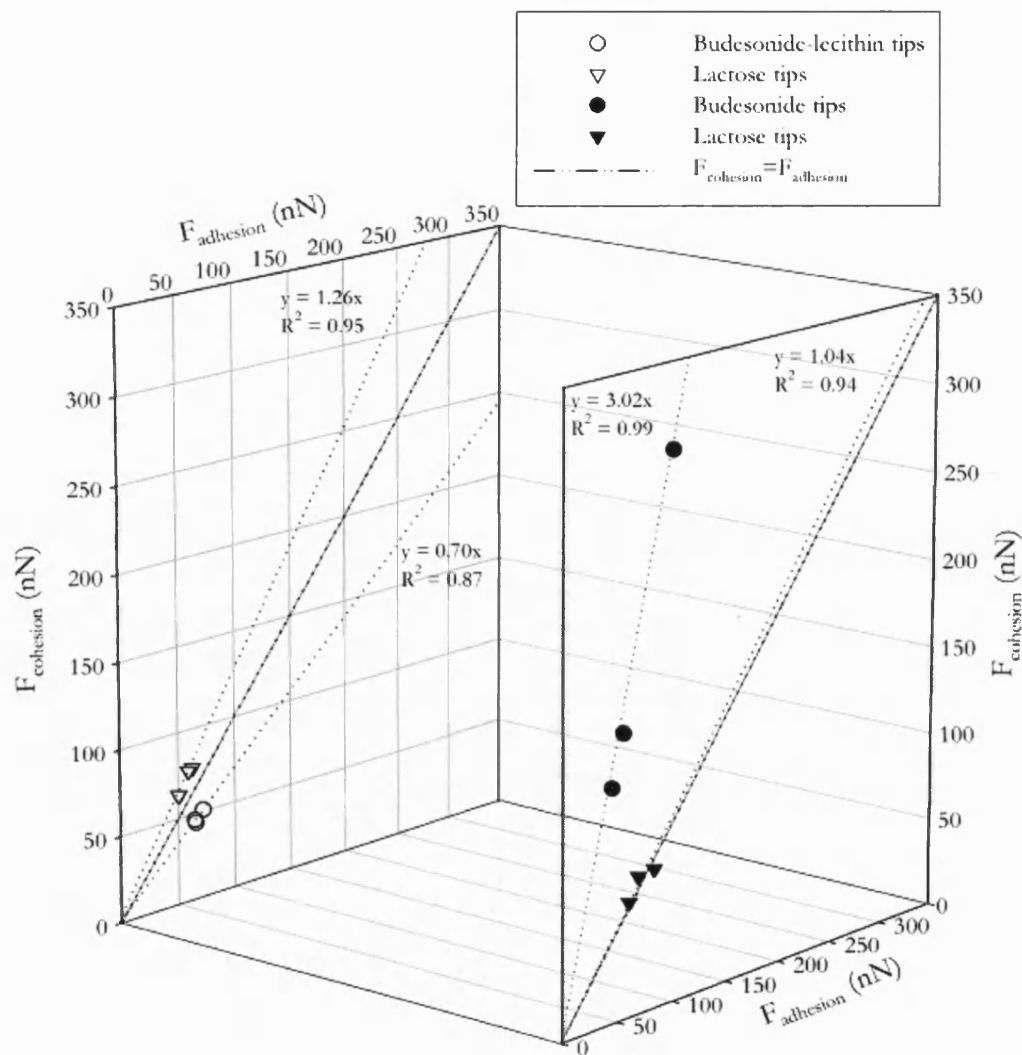


Figure 6- 3: Influence of the coating of budesonide with lecithin on the cohesive-adhesive balances of a budesonide-lactose system.

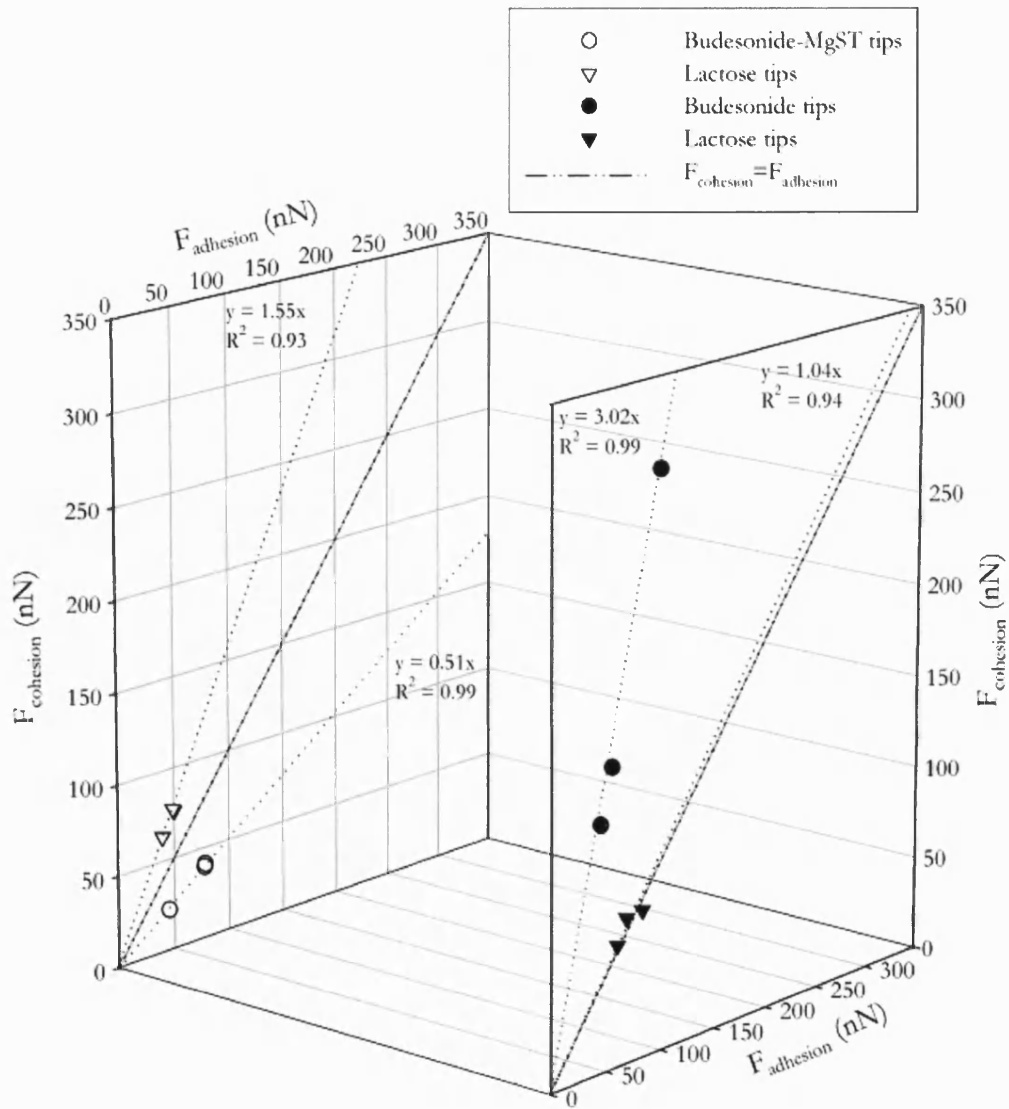


Figure 6- 4: Influence of the coating of budesonide with magnesium stearate on the cohesive-adhesive balances of a budesonide-lactose system.

Contact angle measurements were performed on compact surfaces of mechanofused budesonide with leucine, lecithin and MgST to assess their surface free energies. The resulting contact angles obtained with diiodomethane, ethylene glycol and ultra pure water are shown in Table 6.1. Using the van Oss-Chaudhury-Good (VCG) thermodynamic approach, described in more detail in Chapter 2, the surface energy contributions and resulting Gibbs interfacial free energy of cohesion of mechanofused lactose with leucine, lecithin and MgST are summarised in Table 6.2. Contact angle measurements of micronised budesonide particles indicated a dispersive surface free energy ( $\gamma^{LW}$ ) of  $50.40\text{mJ}\cdot\text{m}^{-2}$ , and a total surface free energy ( $\gamma^{\text{tot}}$ ) of  $78.74\text{mJ}\cdot\text{m}^{-2}$ . The interfacial free energy of the cohesive interaction was calculated as  $157.51\text{mJ}\cdot\text{m}^{-2}$ . The inclusion of FCA clearly reduced the surface energy of the drug particles, thereby decreasing the drug cohesiveness. Although the dispersive contributions of the mechanofused powders remained significant with respect to the corresponding pure FCA (Chapter 2), the interfacial Gibbs free energy of cohesion decreased by more than a third for all three samples. This indicated effective force modification upon conditioning the drug with leucine, lecithin or MgST.

Sample	Contact angle ( $\theta$ )		
	Diiodomethane	Ethylene glycol	U.P. water
Budesonide + Leucine	$32 \pm 1.00$	$47.33 \pm 1.15$	$34.67 \pm 0.58$
Budesonide + Lecithin	$46.00 \pm 2.65$	$38.00 \pm 2.65$	$18.67 \pm 2.08$
Budesonide+ MgST	$41.00 \pm 3.46$	$55.00 \pm 1.73$	$88.33 \pm 2.89$

Table 6- 1: Contact angle measurements of mechanofused budesonide with leucine, lecithin and MgST.

Sample	$\gamma^{LW}$	$\gamma^+$	$\gamma^-$	$\gamma^{\text{tot}}$	$\Delta G^{\text{tot}}$
Budesonide + Leucine	41.08	0.22	56.75	48.16	-96.39
Budesonide + Lecithin	36.46	0.07	75.62	40.72	-82.23
Budesonide+ MgST	39.08	0.12	1.81	39.92	-80.01

Table 6- 2: Surface energy contributions and resulting interfacial Gibbs free energy of cohesion of mechanofused budesonide with FCAs (in  $\text{mJ}\cdot\text{m}^{-2}$ ).

To assess the influence of FCAs on the physical properties of a budesonide-lactose blend, the ternary powder samples were characterised by scanning electron microscopy. Representative scanning electron micrographs of formulations of lactose mixed with mechanofused budesonide-leucine, budesonide-lecithin, and budesonide-MgST are shown in Figure 6.5A, 6.5B and 6.5C, respectively. Corroborating with the CAB predictions, SEM micrographs illustrated an enhanced affinity between the drug and the lactose. In the presence of the FCAs, the budesonide particles preferentially adhered to the lactose surface rather than forming individual agglomerates. These observations were in great contrast to previous work investigating the formulation homogeneities of binary mixtures of micronised budesonide and lactose (Chapter 4). In the absence of a force control agent, the presence of dense agglomerates of drug particles located on the lactose surfaces suggested an inhomogeneous blend.

Dose content uniformity analysis revealed a dramatic variation in the homogeneity of the budesonide formulation upon the introduction of FCAs (Table 6.3). While the content uniformity of a budesonide-lactose system showed an RSD of 9.54%, formulations containing pre-conditioned drug exhibited significantly lower content uniformities of 3.57, 3.53 and 2.37 for budesonide-leucine, budesonide-lecithin, and budesonide-MgST, respectively. These results were in good accordance with the corresponding intermixing coefficients calculated from the CAB-graphs for each of the ternary samples, suggesting that powder homogeneity increases as a function of  $\Lambda_{12}$ . These changes in formulation behaviour may hopefully contribute to enhance the aerosolisation properties of budesonide and improve in vitro performance.

Conditioning	Mixing	Reduced intermixing coefficient ( $\Lambda_{12}$ )	Content uniformity (% RSD)
Mechanofusion, 10 min @ 5200 rpm	Turbula, 30 min @ 46 rpm		
Budesonide (non conditioned)	Sorbalac 400	0.33	9.54
Budesonide + Leucine	Sorbalac 400	1.33	3.57
Budesonide + Lecithin	Sorbalac 400	1.43	3.52
Budesonide + MgST	Sorbalac 400	1.96	2.37

Table 6- 3: Mixing sequences of budesonide carrier-based formulations with conditioned budesonide and reduced intermixing coefficients and content uniformities.

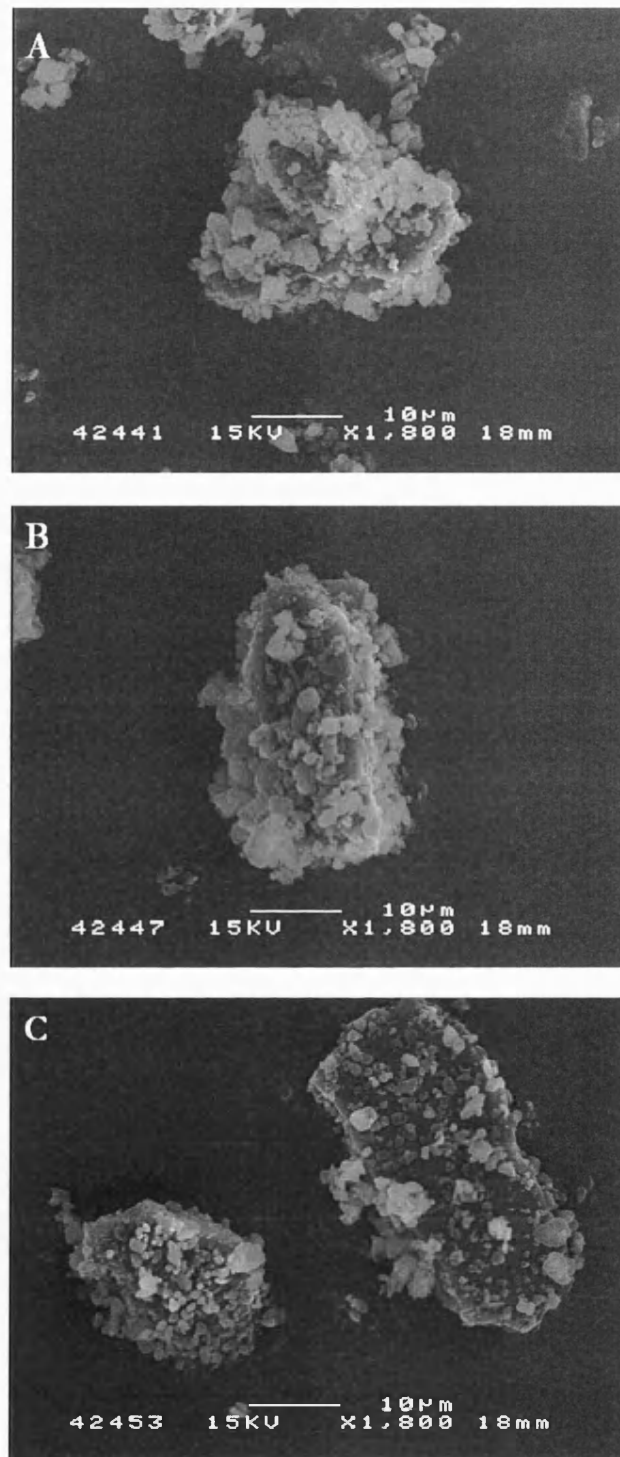
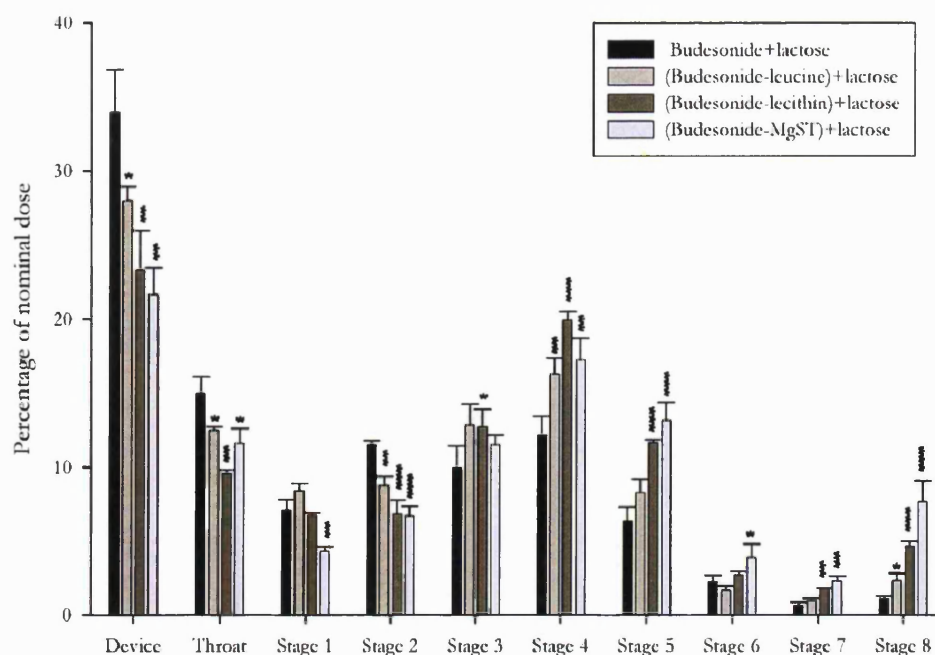


Figure 6- 5: Representative scanning electron micrographs of ternary mixtures of lactose and budesonide pre-conditioned with leucine (A), lecithin (B) and MgST (C).

The aerosol delivery properties of the budesonide carrier-based formulations are shown in figure 6.6. In vitro tests performed with micronised budesonide revealed high device retention (35%), a significant amount of drug in the throat (15%) and a considerable percentage evenly recovered from the 2<sup>nd</sup> to the 5<sup>th</sup> stage ( $\approx 40\%$ ). No more than 5% of active ingredient was recovered in the lower stages. Mechanofusing the budesonide with leucine contributed to a small but significant decrease in the amount of drug recovered from both the device and the throat (28% and 12.5%, respectively). This reduction in the upper stages subsequently transferred to increase deposition in the lower stages of the NGI and more especially the 3<sup>rd</sup> and 4<sup>th</sup> stage (12.9% and 16.3%).

Conditioning the drug with lecithin resulted in a significant improvement in drug emission from the device (23.32%) as well as the throat (9.59%). These results suggested that the budesonide particles were successfully de-agglomerated and were interacting with the lactose to form a more stable powder blend. The amount of drug recovered in the 2<sup>nd</sup> stage of the NGI was significantly lower than without FCA (6.82%). This led to a concomitant increase in drug deposition in stage 3 (12.76%) and stage 4, 5 and 8 (19.96%, 11.69% and 4.66%, respectively). These results suggested that the drug was more effectively detached from the carrier and that the magnitude of the conditioned drug cohesive forces allowed sufficient de-agglomeration to reach the lower stages of the impactor.

The addition of MgST provided the best performances, with a device retention of just 22%. The low amount of drug recovered in the throat and especially the first and second stage (11.63% and 4.3%, respectively) suggested efficient drug detachment from the carrier. Little was recovered in stage 3 (11.52%) and stage 4 (17.24%) when compared to drug coated with lecithin, but was significantly higher than non-treated budesonide (9.96% and 12.17%, respectively). The differences in the de-aggregation and dispersion behaviour of conditioned drug particles directly relate to high drug fractions in the lowest stages (stages 5, 6, 7 and 8), suggesting a very efficient drug dispersion.



\*  $p < 0.05$ , \*\*  $p < 0.01$ , \*\*\*  $p < 0.001$ : significant difference compared to without force control agent by ANOVA one-way.

Figure 6- 6: In-vitro deposition of budesonide carrier-based formulations with conditioned budesonide (mean  $\pm$  S.D.,  $n=3$ ).

### 6.3.2. Model Formulations with Conditioned Lactose

Pre-conditioning the lactose particles with a FCA should in theory only affect the budesonide-lactose adhesive bonds and the lactose cohesive bonds. Given the nature of the initial interactions occurring in a budesonide-lactose binary system, no improvements in formulation performances would be expected as the overall powder behaviour would still be dictated by the high cohesive drug-drug interactions. Nonetheless, experiments were repeated with the lactose pre-conditioned with a ternary agent in order to highlight the specific effects of the use of a selective mixing procedure.



The whole matrix of interactions between budesonide and lactose mechanofused with force control agents was first assessed by atomic force microscopy. The resulting CAB-graphs with leucine, lecithin and MgST as force control agents are shown in Figure 6.7, 6.8 and 6.9, respectively. As expected, the addition of the ternary agents further reinforced the cohesively led systems. The initial reduced intermixing coefficient of 0.33 between micronised budesonide and lactose further decreased to 0.26, 0.25 and 0.27 upon mechanofusing the lactose with leucine, lecithin and MgST, respectively (Table 6-4).

Surface energy properties of lactose particles mechanofused with leucine, lecithin and MgST have already been investigated in Chapter 5. It was found that, predictably, the inclusion of FCAs with the lactose greatly decreased the surface energy contributions of the coated particles in comparison to the as supplied Sorbalac 400 (Chapter 2). It was therefore anticipated from both surface energy data and CAB graph analyses that decreasing the lactose-lactose and lactose-budesonide interactions particles with the inclusion of leucine, lecithin or MgST may further destabilise the powder formulations.

Conditioning	Mixing	Reduced intermixing coefficient ( $\Lambda_{12}$ )	Content uniformity (% RSD)
Mechanofusion, 10 min @ 5200 rpm	Turbula, 30 min @ 46 rpm		
Sorbalac 400 (non conditioned)	Budesonide	0.33	9.54
Sorbalac 400 + Leucine	Budesonide	0.26	7.27
Sorbalac 400 + Lecithin	Budesonide	0.25	7.37
Sorbalac 400 + MgST	Budesonide	0.27	9.65

Table 6- 4: Mixing sequences of budesonide carrier-based formulations with conditioned lactose and reduced intermixing coefficients and content uniformities.

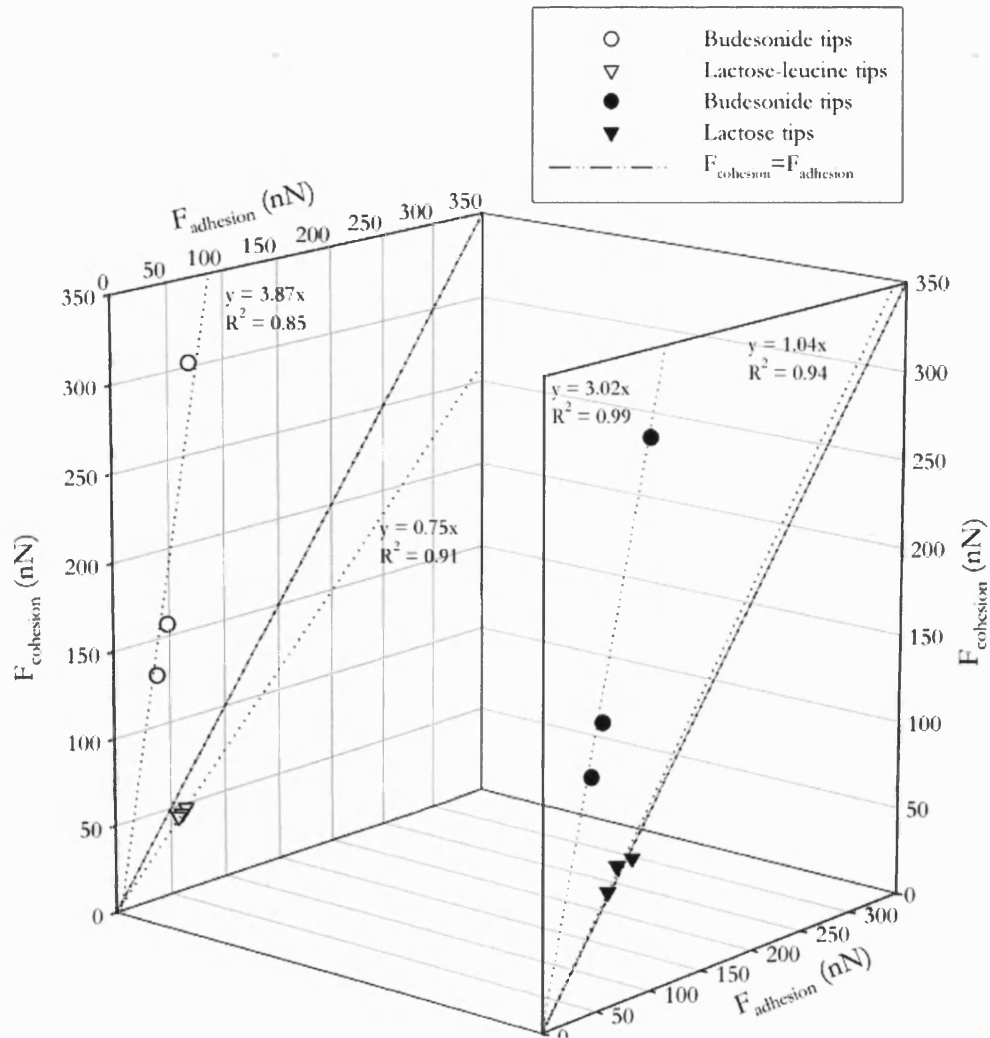


Figure 6- 7: Influence of the coating of lactose with leucine on the cohesive-adhesive balances of a budesonide-lactose system.

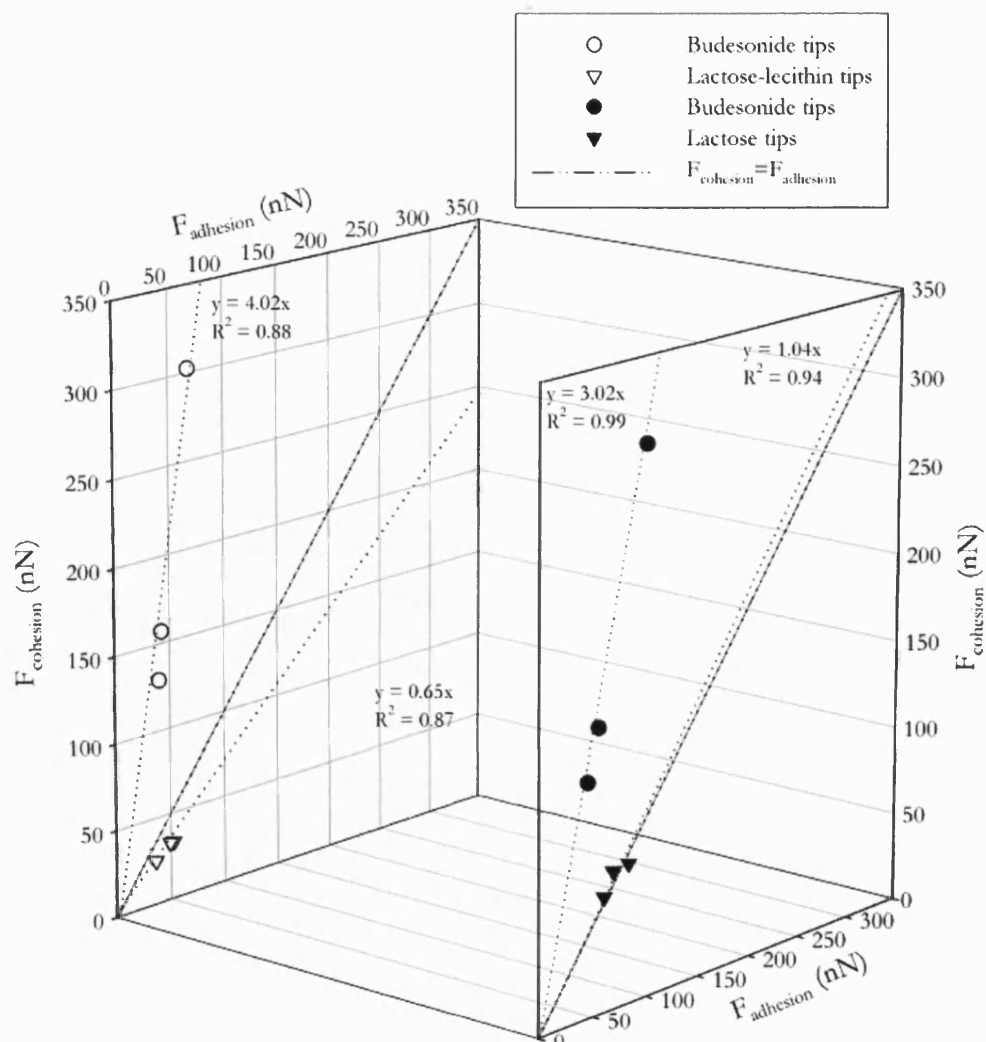


Figure 6- 8: Influence of the coating of lactose with lecithin on the cohesive-adhesive balances of a budesonide-lactose system.

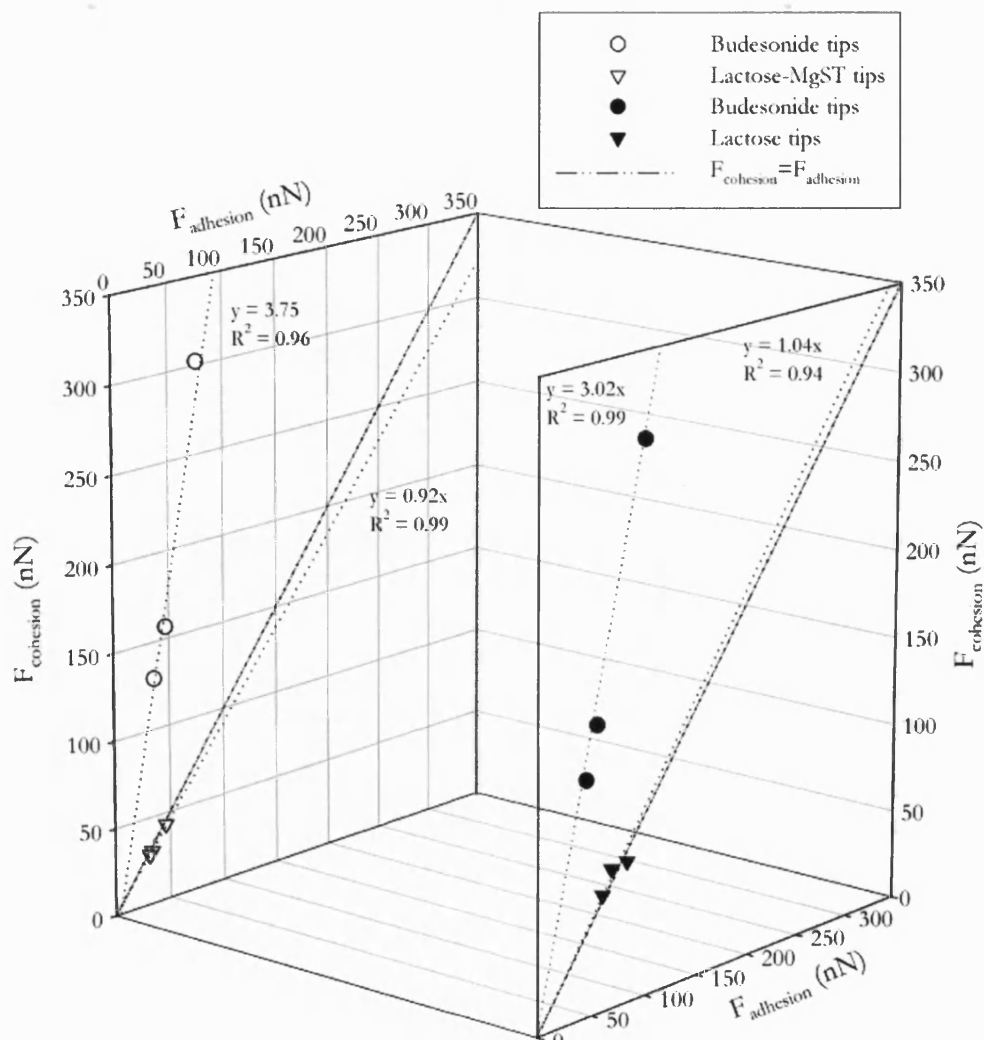
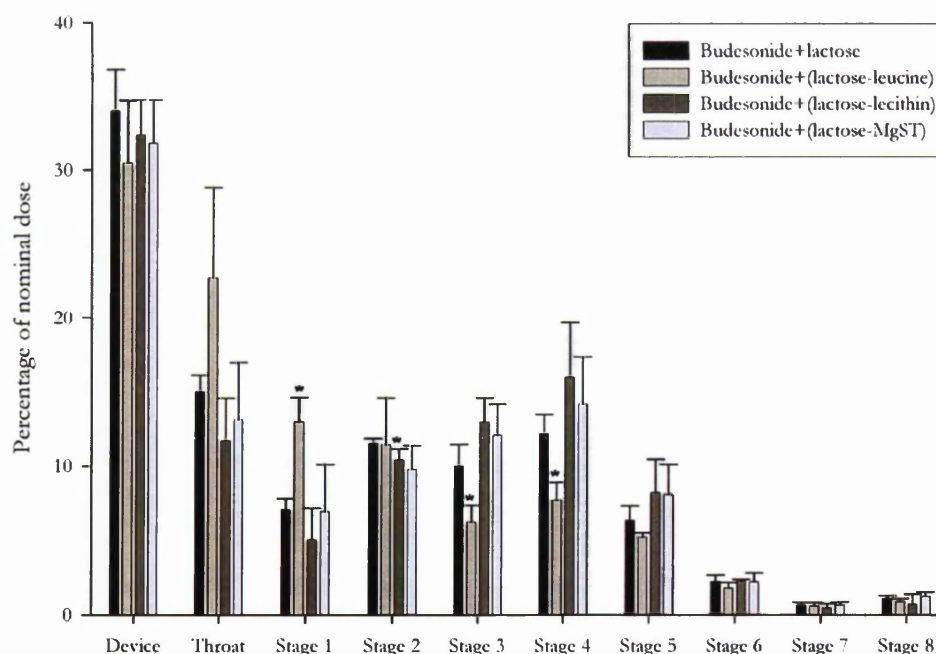


Figure 6- 9: Influence of the coating of lactose with magnesium stearate on the cohesive-adhesive balances of a budesonide-lactose system.

Representative scanning electron micrographs of formulations of budesonide blended with mechanofused lactose-leucine, lactose-lecithin, and lactose-MgST are shown in Figure 6.10A, 6.10B and 6.10C, respectively. In contrast to mechanofused drug formulations, scanning electron micrographs of mechanofused lactose formulations showed extremely segregated systems. The pre-treated lactose particle surfaces virtually precluded any drug adhesion. Moreover, large agglomerates of budesonide of more than  $30\mu\text{m}$  in size were visible. Corresponding content uniformities, shown in Table 6.4, were unsurprisingly high, synonymous of inhomogeneous formulations, with a relative standard deviation of 7.27%, 7.37% and 9.65% for the formulations of budesonide and lactose mechanofused with leucine, lecithin and MgST, respectively.

The aerosol delivery properties of the various formulations of budesonide and mechanofused lactose-FCA formulations are shown in figure 6.11. The drug distribution patterns of pure lactose, and lactose mechanofused with leucine, lecithin and magnesium stearate were generally statistically analogous. This indicated the relative invariance in the relative cohesive-adhesive balances of the ternary formulations, and subsequent similarity in formulation aerosolisation behaviour.



\*  $p < 0.05$ , \*\*  $p < 0.01$ , \*\*\*  $p < 0.001$ : significant difference compared to without force control agent by ANOVA one-way.

Figure 6- 10: In-vitro deposition of budesonide carrier-based formulations with conditioned lactose (mean  $\pm$  S.D.,  $n=3$ ).

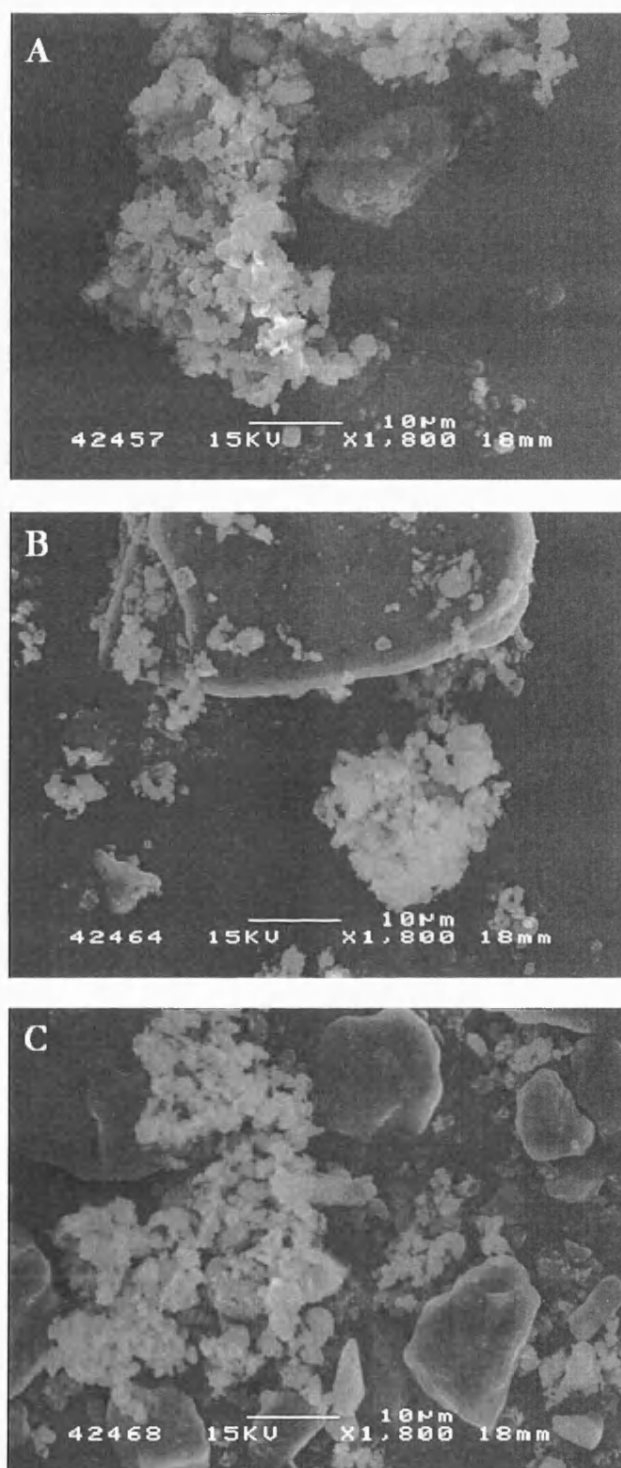
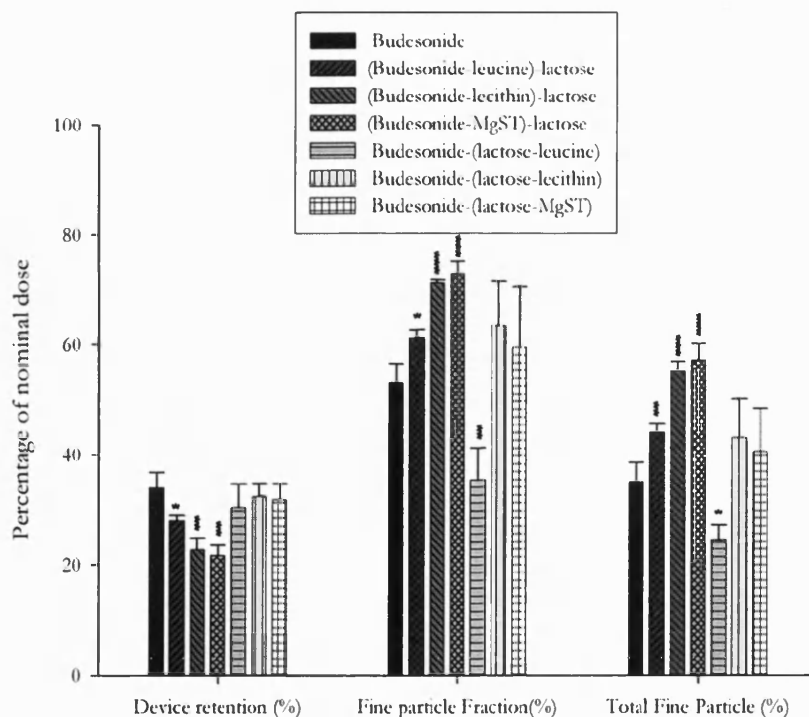


Figure 6- 11: Representative scanning electron micrographs of ternary mixtures of budesonide and lactose pre-conditioned with leucine (A), lecithin (B) and magnesium stearate (C).

A summary of the device retention, fine particle fraction (% respirable particle from emitted dose) and total fine particle fraction (% respirable particle from initial dose) of the various budesonide carrier-based formulations is illustrated in Figure 6.12. An unambiguous distinction in formulation behaviour was observable, indicative of a selective mixing. Combining the carrier with a FCA did not contribute to significant variations when compared to untreated lactose in device retention, %FPF or %TFP as was expected from CAB-graphs predictions. Since altering the lactose physico-chemical properties predominantly affected the already mediocre carrier-drug interactions, the formulations generally behaved as a function of their unchanged budesonide cohesive interparticulate forces.



p<0.05, \*\* p<0.01, \*\*\* p<0.001: significant difference compared to budesonide without force control agent by ANOVA one-way.

Figure 6- 12: Fine particle fraction and emission efficiency of budesonide carrier-based formulations (mean  $\pm$  S.D., n=3).

The inclusion of a FCA with the budesonide and subsequent modification of the drug cohesiveness resulted in major formulation improvements when compared to a binary system of micronised budesonide and lactose. Mechanofusing budesonide with leucine decreased the drug device retention of the formulation by 17.64% while increasing the %FPF by 16.5%. Conditioning the drug with lecithin resulted in a notable decrease in device retention by 33.2% and a resulting %FPF increase by 38.6%. The most effective FCA was MgST, which led to a 36.29% reduction in device retention and corresponding increase in %FPF by 36% with respect to the budesonide-lactose binary formulation. As the fine particle fraction only indicates the efficiency of delivery of the respirable particles which are emitted from the device, it does not reflect any changes in actual respirable fraction from the loaded dose. Since a significant increase in drug emission was observed with the various conditioned-drug formulations, the effects of FCAs were even more noticeable by comparing the total fine particle fractions. This showed overall improvement of 26.8%, 64.26% and 59.1%, for budesonide mechanofused with leucine, lecithin and MgST, respectively with respect to pure micronised drug.

## **6.4. Conclusions**

The influence of modifying the interfacial properties of a highly cohesive drug (budesonide) in a model carrier based formulation was studied. Drugs surface energetics was lowered using a ternary agent to facilitate interactions with the carrier. This was achieved by first coating the drug with a force control agent using a high energetic process (Mechanofusion) followed with a low energetic process (Turbula) to mix the conditioned drug with the carrier. Controlling the interaction forces led to dramatic changes both on a microscopic level (van der Waals forces) and on a macroscopic level (formulation homogeneity). A distinct improvement in the budesonide formulation performances was subsequently obtained upon conditioning the drug particles. The specific role of targeting the interfacial interactions on formulation behaviour was further exemplified by investigating the influence of modifying adhesive interactions by conditioning the surfaces of the excipient particles.



## Chapter 7

# Optimisation of the Fluidisation and Aerosolisation of Drug Only Formulations

### 7.1. Introduction

The majority of dry powder inhaler (DPI) formulations are developed as carrier-based mixtures. Among the various excipient candidates, suitable for these solid dosage forms,  $\alpha$ -lactose monohydrate is industrially preferred because of it is generally regarded as a safe excipient [1, 2]. However, specific conditions relating to formulation incompatibilities or patient pathologies may preclude the use of lactose as a carrier. For instance, various compounds including formoterol, several corticosteroids, peptides or proteins, may interact with the reducing sugar function of the lactose, inducing undesired chemical reaction [3]. In this reaction, known as the Maillard reaction, the reactive carbonyl group of the sugar interact with the nucleophilic amino group [4]. In addition, patients suffering from lactase-deficiency or exhibiting allergenicity to protein contaminants (often found as sub-products of lactose) have developed various degree of lactose intolerance [5]. In such circumstances, alternative DPI formulation preparations will be required. These may involve the use of alternative non-reducing carbohydrates or the possible development of a drug only formulation.

The continued development of carrier-free formulations are of utmost interest as the use of undiluted drug would yield to a smaller amount of powder to be dispensed and may concomitantly lead to the engineering of more ergonomic DPI devices. In addition, typical issues encountered with carrier-based formulations such as blending

homogeneity or powder segregation would no longer be relevant. However, respirable sized particles are notoriously difficult to fluidise due to their cohesive nature [6]. Moreover, the filling of small quantities of highly cohesive materials may be practically difficult, eventually compromising the accuracy of pre-metered and device metered formulations. In order to possibly overcome these poor re-dispersion tendencies and device filling issues, drug particles would need to be specifically engineered or processed to display suitable flowing characteristics.

A common DPI approach is to spheronize the micronised drug, which may be achieved with a little amount of a suitable solvent to form uniformly sized agglomerates. This technique is often referred as pelletization [7]. A study revealed that specific pelletized powders of disodium cromoglycate (DSCG) performed equally if not better than corresponding carrier based formulations [5]. In such systems, the pellet form confers an adequate size to improve flowability of the cohesive drug particles. However, the various processes used to pelletise micronised particles can lead to an increase in particle-particle forces. Consequently, greater energy would be required to de-agglomerate and disperse the respirable drug particles for lung deposition. The energy requirements are provided by the shear and impaction forces generated by the patient inspiratory air flow through the DPI device. To increase the de-aggregation efficiencies of agglomerated based formulations, the resistance of these devices need to be high. The balance between agglomerate strength (filling, handling) and re-dispersion efficiency is therefore critical.

Another approach to improve the flowability and dispersibility of fine drug particle is to reduce their intrinsic cohesiveness. This paradigm however implies the need to significantly optimise the physical and chemical properties of the active ingredient. Current techniques used to modify their physico-chemical properties involve the manufacture of more uniform respirable particles by particle engineering technologies, hitherto mainly achieved by spray drying or supercritical fluid precipitation techniques [8, 9]. However, the metastable nature of amorphous particles produced via spray-drying processes often raises stability issues and has precluded their wider use in dry powder formulations [10, 11]. Supercritical fluid (SCF) precipitation methods have been shown to produce highly crystalline particles, exhibiting lower surface free

energies and increased stability in comparison to the conventionally micronised products [12]. However, particles produced by SCF techniques can exhibit smooth and planar crystal faces, which may result in a significant increase in the contact area of contiguous surfaces. Previous studies have emphasised the potential influence of contact area upon resulting force magnitude between particles [13]. Despite the reduction in interfacial surface free energy, the net particle adhesion may therefore be increased and reduce powder flowability [9, 14].

Recently, the introduction of force control agents (FCA) was considered as a possible means of decreasing inter-particulate interactions of micron sized drug particles [15]. The primary role of these low surface free energy materials is to modify the interfacial chemistry of the guest particles in reducing their intrinsic cohesion. Effective coating of the active ingredient was obtained using a Mechanofusion system. This approach was first developed for inhalation powders by Staniforth et al [16]. This highly energetic dry coating process is designed to mechanically fuse the FCA onto the drug by solid sintering, thereby forming complete nano-structured layers around the guest particles [17]. Previous studies have shown that the mechanical fusion of a force control agent significantly reduced the cohesive interactions of inhalable particles (Chapter 5 and 6).

The objectives of the present study were to examine the variations in drug properties and their performance upon the introduction of a force control agent. Salbutamol sulphate and budesonide, two active ingredients frequently administered via the inhalation route, were selected for their contrasting hydrophilic and hydrophobic properties [18]. Leucine, lecithin and magnesium stearate, recognized for having lamellar “surface-active” properties, were employed as force control agents. Their anticipated anti-adherent and/or anti-friction properties were intended to contribute to improve the flow and dispersion properties to the fine drug particles.

## **7.2. Methods**

General methods of each technique or apparatus used in this study are described in detail in Chapter 2.

- **Preparation of powder formulations**

Blends of the drugs and force control agents (5% w/w) were prepared using a Mechanofusion system (Hosokawa-Alpine, Augsburg, Germany). Powders to be processed were sealed into the Mechanofusion system core. A cold-water circulation assured the regulation of the internal vessel temperature using an incorporated water jacket. Samples were blended for 10 minutes to mechanically fuse the FCA to the micronised drug.

- **Laser diffraction analyses**

Experiments were performed using a laser diffraction particle sizer (Spraytech, Malvern Instruments, Malvern, UK) at three different flow rates of 30, 60 and 90L.min<sup>-1</sup>. Approximately 10 mg of each sample was accurately weighted and delivered via a Monohaler<sup>®</sup> directly into the Spraytech inhalation cell. Test duration was set at 5000ms with an acquisition frequency of 2500Hz. Each experiment was performed in triplicates. After each shot, device and capsule were washed in the appropriate mobile phase, and the solutions were analysed by UV spectrometry to quantify the related emitted dose.

- ***In vitro* aerosol deposition studies**

Approximately 10 mg of the formulations was accurately weighed into a gelatine capsule to be loaded into a Monohaler<sup>®</sup> device (Miat SpA, Milan, Italy). *In-vitro* deposition investigations were performed using a next generation impactor (NGI) (Copley Scientific, Nottingham, UK). The loaded device was connected to the throat of the NGI via a moulded mouthpiece. *In-vitro* analysis was performed after each actuation of the device. Each experiment (n=3) was performed at 60L.min<sup>-1</sup> flow rate with a 5 second exposure. Each NGI plate was rinsed with mobile phase and the subsequent solution was collected in a 50ml volumetric flask. Statistical analysis of the data was performed using one-way ANOVA. The levels of significance are indicated in the legend of the respective graphs.

## **7.3. Results**

The inter-particulate forces of micron-sized drug are of crucial importance in the de-agglomeration and dispersion properties of active pharmaceutical ingredients. In order to influence these cohesive bonds, force control agents (FCA) were blended in small quantities (5% w/w) with two different drugs, salbutamol sulphate and budesonide. To proficiently assess the influence of the FCAs on the drug cohesive forces and their subsequent variability in formulation performances, the general appearance of the powders were inspected by scanning electron microscopy. Aerosol deposition studies were characterised by in-vitro measurements and laser diffraction measurements, with the objective of obtaining a greater fundamental understanding of the complex mechanisms of powder aerosolisation and de-agglomeration.

### **7.3.1. General Powder Morphology**

Representative scanning electron micrographs of salbutamol formulations (Figure 7.1A-D) and budesonide formulations (Figure 7.2A-D) provided a useful insight into the influence of the various FCA over the degree of drug particle agglomeration. While SEM picture of micronised salbutamol sulphate suggested the presence of loose agglomerates, the inclusion of either leucine or lecithin appeared to be responsible for a slight increase in agglomerate number and size. In contrast, salbutamol particles coated with magnesium stearate appeared well dispersed as individual particles. Although powders were inspected over a wide area, reliability and consistency of such subjective examination should be treated with caution. It is suggested that the slight increase in agglomerate size and frequency may result from the competing granulation influences in the process against cohesive reduction resulting from the FCA coating. In comparison, budesonide, which is reputed to be a more cohesive material [18, 19], was unsurprisingly present in large and dense agglomerates as illustrated in Figure 2A. The mechanofusion of budesonide with leucine did not seem to improve the system as shown in Figure 2B, which suggested a considerably aggregated powder composition. Similar explanations to those indicated above are proposed. SEM micrographs of budesonide mechanofused with lecithin and magnesium stearate both indicated that the majority of particles were completely dispersed, with very few agglomerates.

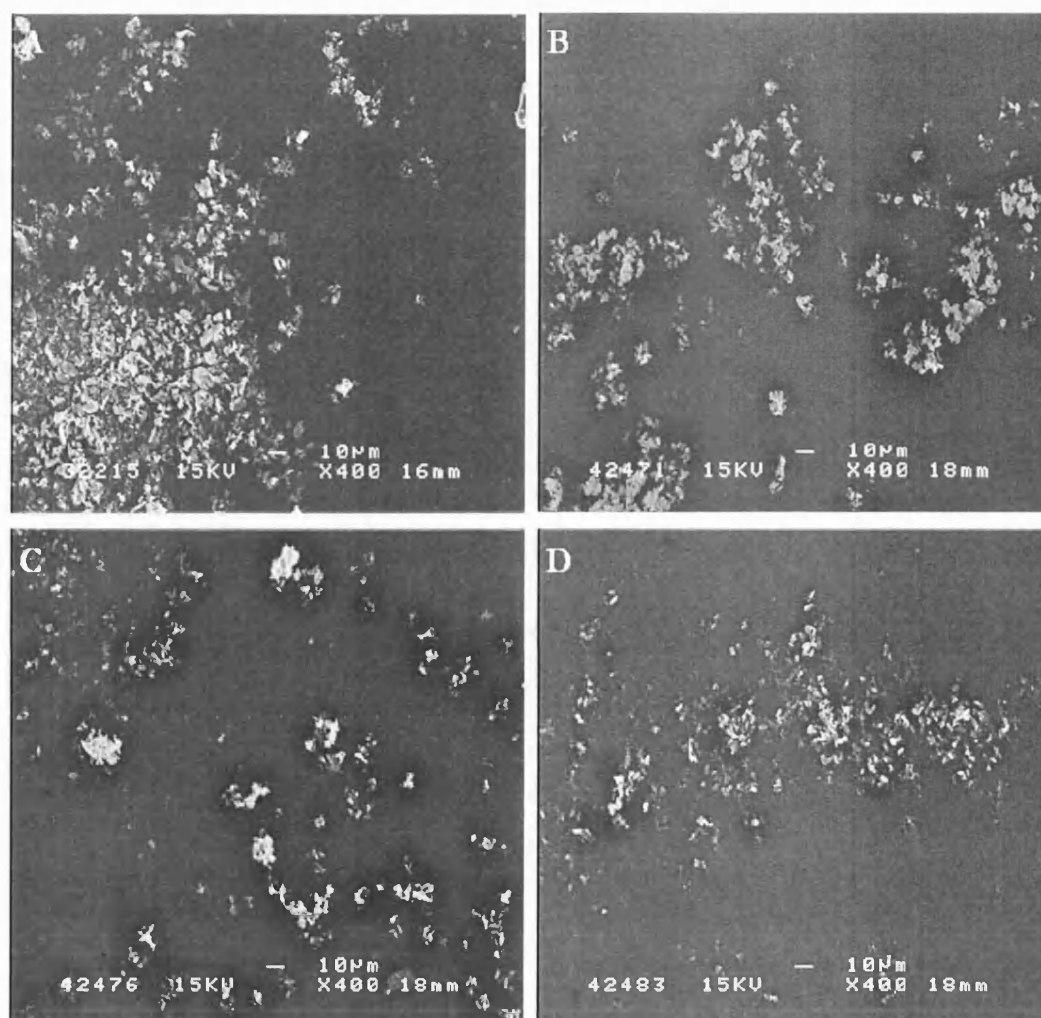


Figure 7- 1: Scanning electron micrographs of unprocessed salbutamol sulphate (A) and salbutamol sulphate mechanofused with leucine (B), lecithin (C) and MgST (D).

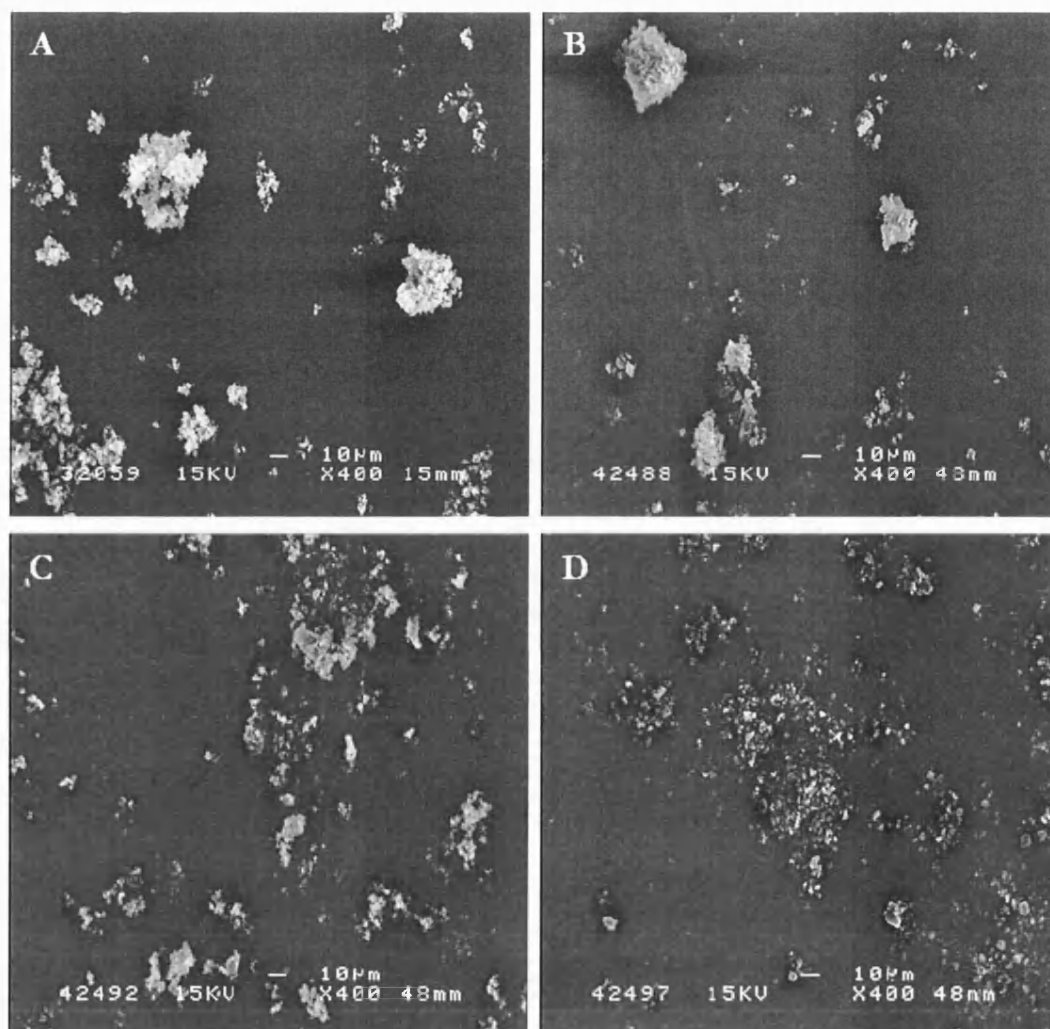


Figure 7- 2: Scanning electron micrographs of unprocessed budesonide (A) and budesonide mechanofused with leucine (B), lecithin (C) and MgST (D).

### 7.3.2. *In Vitro* Aerosol Deposition Studies

In vitro deposition studies of micronised salbutamol sulphate and blends of the drug mechanofused with leucine, lecithin and MgST are shown in Figure 7.3. Micronised salbutamol sulphate powder bed re-suspended well, with the lowest relative device retention of 17%. However, a large amount of material was found in the first stage of the NGI (46.79 %) and little was collected past the 4<sup>th</sup> stage. The inclusion of leucine or lecithin with salbutamol sulphate contributed to a significant increase in drug device retention (26.75% and 25.28%, respectively). No significant variations were however observed for magnesium stearate (19.4%). A very substantial drop in the amount of drug collected in stage 1 was however observed for all of the three FCAs, with a subsequent statistical increase in drug deposition in the lower stages. The addition of lecithin significantly improved the drug performances, although more than 10% was recovered in the first stage of the NGI. Drug conditioned with magnesium stearate was predominately recovered from the 3<sup>rd</sup> and 4<sup>th</sup> stages ( $\approx 50\%$  between the two stages), in addition to a reasonable amount collected between stage 5 and 7.

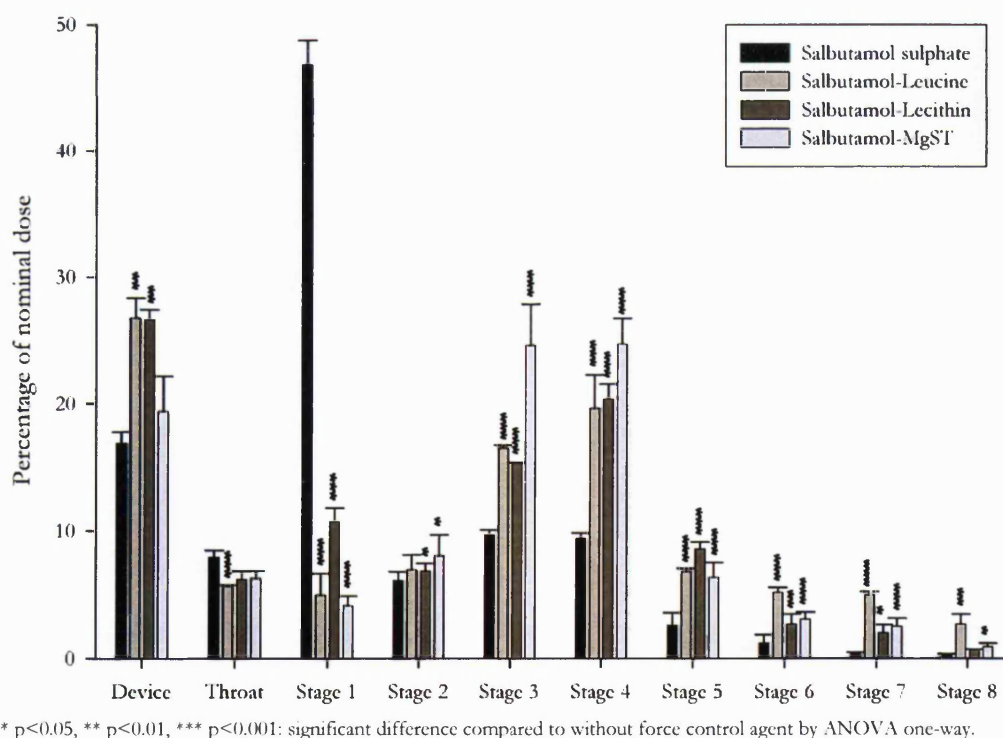
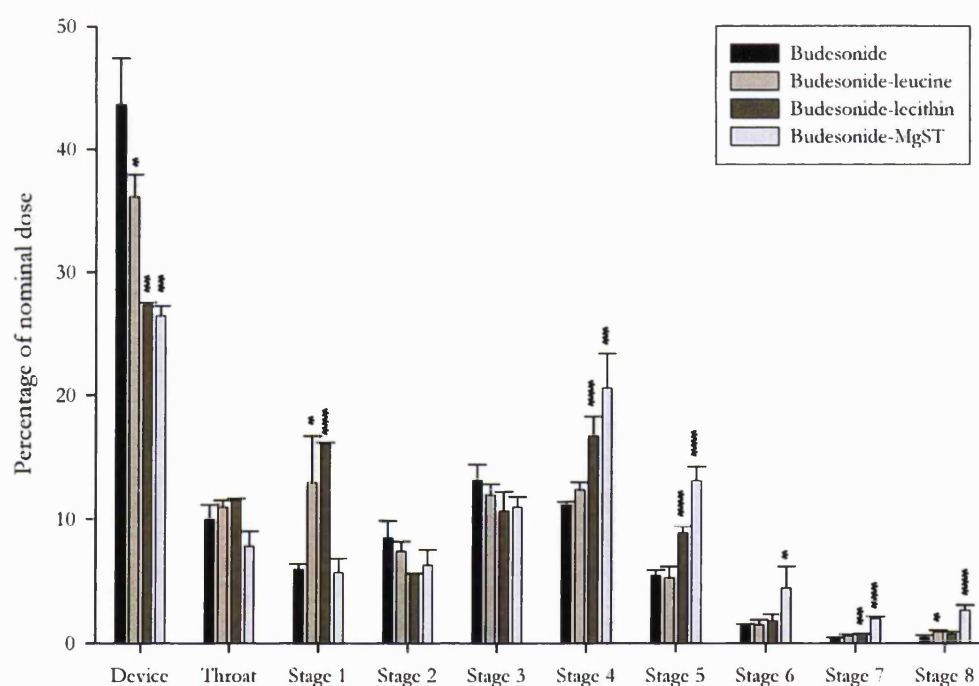


Figure 7- 3: In-vitro deposition of micronised salbutamol sulphate and FCAs formulations (mean  $\pm$  S.D., n=3).



*In vitro* deposition studies of micronised budesonide and drug mechanofused with FCAs are shown in Figure 7.4. Micronised budesonide exhibited significantly high device retention (43.2%), while the emitted drug deposited relatively evenly from the throat to the 5<sup>th</sup> stage. Little was recovered in the NGI lower stages. The processing of budesonide with leucine resulted in similar drug deposition patterns to micronised budesonide, despite a slight reduction in device retention (36.15%) and an increase in drug recovery in stage 1 (12.96%). Significant reductions in device drug recovery (27.47%) and drug deposition in the first stage of the NGI were however observed when the budesonide particles were coated with lecithin compared to micronised drug. An improvement in powder dispersion was nonetheless discernable, with a higher amount of drug recovered in the 4<sup>th</sup> and 5<sup>th</sup> stages (16.72% and 8.89%, respectively). Formulation containing MgST exhibited remarkable fluidisation and dispersion aptitudes. A significant reduction in device retention (26.46%) was observed. However, the amount of drug recovered in the first stage (5.68%) was similar to the micronised budesonide sample (5.95%), yielding to a large increase in drug deposition in stage 4 and 5 (20.60% and 13.09%, respectively) as well as the lower stages of the NGI.



p<0.05, \*\* p<0.01, \*\*\* p<0.001: significant difference compared to without force control agent by ANOVA one-way.

Figure 7- 4: In-vitro deposition of micronised budesonide and FCAs formulations (mean  $\pm$  S.D., n=3).

### 7.3.3. Laser Diffraction Analyses

The Spraytech apparatus can provide a complete particle distribution of an aerosol cloud passing through a laser beam every 2ms for the 5000ms of device actuation. It was felt to be irrelevant and unrepresentative for this study to present a particle distribution summary over the duration of the aerosolisation process since each data report to the powder state at a specific time segment. The Spraytech method was instead used to characterise the rate of particle emission and to generate a general distribution pattern of each formulation upon activation. Moreover, experiments were performed at three different flow rates in order to compare the effects of changing shear forces and impaction energy on the aerosolisation and re-dispersion properties of each formulation. Volume concentrations of the emitted dose, corresponding to particle count, which was recorded every 2ms, and was plotted cumulatively for each sample.

Resulting cumulative distributions of salbutamol sulphate-based formulations delivered via a Monohaler<sup>®</sup> DPI device at 30, 60 and 90L.min<sup>-1</sup> are shown in Figure 7.5A, 7.5B and 7.5C, respectively. At low flow rate (30L.min<sup>-1</sup>), the emission of the micronised salbutamol sulphate particles seemed continuous and regular throughout the whole actuation time. No significant variations in emission patterns were visible between micronised and conditioned salbutamol sulphate with the exception of the MgST-coated drug, which appeared to be emitted slightly faster. Increasing the shear forces by raising the flow rate to 60L.min<sup>-1</sup> unsurprisingly decreased the total emission time of micronised salbutamol sulphate. The conditioning of the drug with leucine did not contribute to significant changes. The addition of either lecithin or MgST, in contrast, resulted in a shorter emission time, suggesting that the conditioned particles were fluidised more effectively, subsequently passing through the inhalation cell more rapidly. Raising the flow rate to 90L.min<sup>-1</sup> further increased the discrepancies observed. At this flow rate, a clear gradient in emission rate was observable from micronised salbutamol sulphate, to leucine-mechanofused, lecithin-mechanofused and finally MgST-mechanofused, which again emitted the fastest from the device.

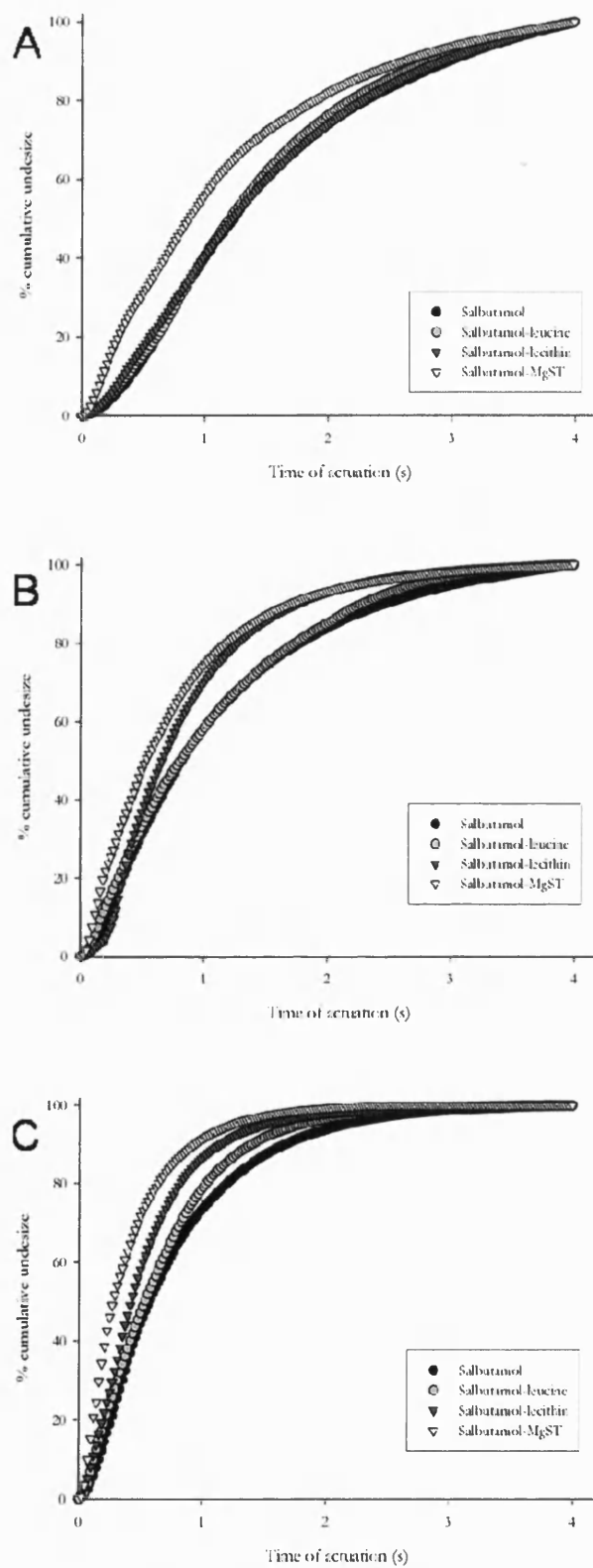


Figure 7- 5 Cumulative salbutamol sulphate formulation emissions as a function of actuation time at a flow rate of 30L.min<sup>-1</sup> (A), 60L.min<sup>-1</sup> (B), and 90L.min<sup>-1</sup> (C).

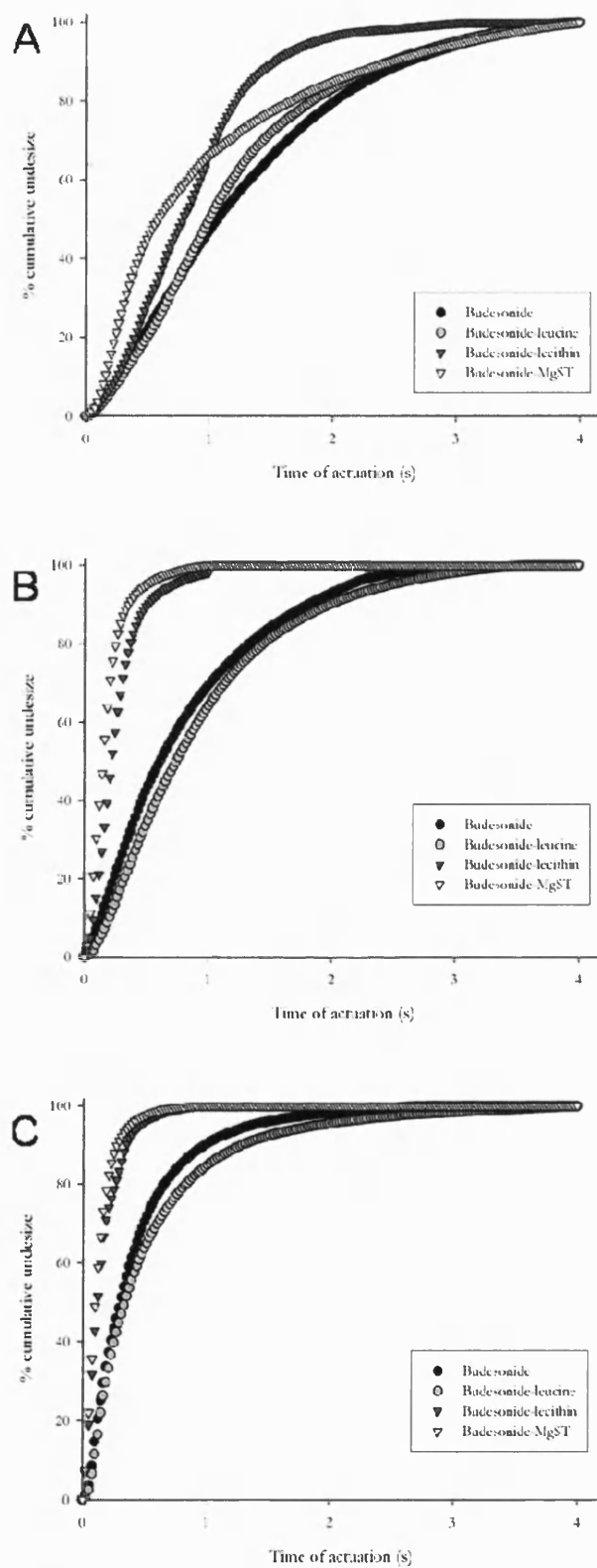


Figure 7- 6: Cumulative budesonide formulation emissions as a function of actuation time at a flow rate of 30L.min<sup>-1</sup> (A), 60L.min<sup>-1</sup> (B), and 90L.min<sup>-1</sup> (C).

The cumulative distributions of budesonide-based formulations delivered via a Monohaler® DPI device at 30, 60 and 90L.min<sup>-1</sup> are shown in Figures 7.6A, 7.6B and 7.6C, respectively. Similar patterns were observable between micronised budesonide and drug mechanofused with leucine, lecithin or MgST. However, these patterns were more pronounced. While the processing of leucine with budesonide resulted in a similar emission pattern to the pure drug for all three flow rates, the addition of lecithin and MgST contributed to a considerable change in drug emission rate even at 30L.min<sup>-1</sup>. By increasing the shear forces (60L.min<sup>-1</sup> and 90L.min<sup>-1</sup>), the pharmaceutical compositions containing either lecithin or magnesium stearate were more rapidly discharged from the device. In fact the entire emitted drug passed through the Spraytech inhalation cell in the first second of the device actuation, in contrast to 2-3 seconds observed for the other cases. These observations again suggested a very effective fluidisation of the powder bed and consequent rapid aerosolisation process.

Concurrent measurements of the device and capsule retention allowed the location of the non emitted drug. These data are shown in table 7.1. With the exception of magnesium stearate, the processing of salbutamol sulphate with lecithin and leucine yielded an increase in device retention, whether at low or high flow rate. Conversely, a reduction in device retention was observed when the budesonide particles were treated with the FCAs. The results obtained at 60L.min<sup>-1</sup> were in good accordance with in-vitro drug deposition tests performed at an identical flow rate.

While device retention of the micronised salbutamol only slightly decreased upon increasing the flow rate, a more noticeable drop was observed for the conditioned materials. Interestingly, the amount of drug recovered in the capsules remained analogous for each mechanofused sample while the amount of drug recovered in the device significantly decreased. These results suggested that the energy delivered to the bulk powder beds at low flow rate was sufficient to fluidise and remove the drug particles from the capsule. Under such flow conditions, however, the shear forces within the device may be unable to efficiently de-aggregate the cohesive particles, which may consequently lead to increased impaction and sedimentation of drug within the device, and, thus higher device retention. At higher flow rates, however, the air stream characteristics seemed sufficient to entrain and disperse the particles.

	30 L.min <sup>-1</sup>		
	Recovered dose		Device retention (%)
	in device (µg)	in capsule (µg)	
Salbutamol sulphate	6.27 ± 2.7	15.76 ± 3.33	22.03 ± 4.21
Salbutamol leucine	24.16 ± 3.218	16.91 ± 0.85	41.06 ± 2.35
Salbutamol lecithin	24.97 ± 2.06	13.25 ± 6.89	38.22 ± 7.18
Salbutamol MgST	33.10 ± 5.46	7.02 ± 0.70	40.12 ± 5.75
Budesonide	33.14 ± 3.76	12.59 ± 3.01	45.73 ± 5.17
Budesonide leucine	30.17 ± 1.49	8.27 ± 0.83	38.44 ± 1.71
Budesonide lecithin	24.01 ± 1.17	9.17 ± 0.86	33.17 ± 2.02
Budesonide MgST	19.3 ± 2.67	8.99 ± 1.15	38.30 ± 3.41

	60 L.min <sup>-1</sup>		
	Recovered dose		Device retention (%)
	in device (µg)	in capsule (µg)	
Salbutamol sulphate	10.62 ± 2.00	8.79 ± 2.36	19.40 ± 0.93
Salbutamol leucine	11.85 ± 2.99	16.26 ± 2.55	28.11 ± 1.13
Salbutamol lecithin	15.24 ± 2.81	9.63 ± 2.5	24.86 ± 0.66
Salbutamol MgST	12.82 ± 0.39	5.93 ± 0.78	18.75 ± 1.14
Budesonide	25.93 ± 5.56	13.11 ± 2.37	39.05 ± 5.45
Budesonide leucine	24.38 ± 2.00	9.09 ± 1.79	33.46 ± 3.65
Budesonide lecithin	20.69 ± 0.20	8.99 ± 2.23	29.68 ± 2.03
Budesonide MgST	14.10 ± 0.62	7.73 ± .95	21.83 ± 1.55

	90 L.min <sup>-1</sup>		
	Recovered dose		Device retention (%)
	in device (µg)	in capsule (µg)	
Salbutamol sulphate	9.17 ± 1.59	4.63 ± 0.91	13.80 ± 2.49
Salbutamol leucine	6.88 ± 1.36	10.24 ± 1.19	17.12 ± 1.79
Salbutamol lecithin	7.93 ± 0.63	8.30 ± 2.76	16.23 ± 3.03
Salbutamol MgST	6.25 ± 0.34	3.90 ± 0.22	10.14 ± 0.51
Budesonide	15.73 ± 2.05	7.80 ± 1.00	23.53 ± 2.74
Budesonide leucine	18.91 ± 0.91	9.11 ± 0.59	28.02 ± 0.60
Budesonide lecithin	18.01 ± 1.74	8.00 ± 1.34	26.01 ± 2.27
Budesonide MgST	13.63 ± 2.24	6.77 ± 0.32	20.40 ± 1.98

Table 7- 1: Summary of recovered dose in device and capsule, and subsequent device retention for salbutamol and budesonide formulations at 30, 60 and 90L.min<sup>-1</sup>.

The inclusion of FCAs with budesonide contributed to a decrease in device retention when compared to the micronised active ingredient. Moreover, the reduction in device retention observed with increasing the flow rate was related to a decrease in wall deposition within the device. This suggested that the conditioned powder was more effectively entrained in the air stream. Of particular interest was the improvement in the emission of micronised budesonide particles at  $60\text{L}\cdot\text{min}^{-1}$  and  $90\text{L}\cdot\text{min}^{-1}$ . The increase in flow rate led to a two-fold decrease in device retention. The emission of the sample of budesonide mechanofused with MgST, on the other hand, remained independent of the flow rate at  $60\text{L}\cdot\text{min}^{-1}$  and  $90\text{L}\cdot\text{min}^{-1}$ . A two fold decrease in device retention drop was however observed between  $30\text{L}\cdot\text{min}^{-1}$  and  $60\text{L}\cdot\text{min}^{-1}$ . This strongly suggested that the high cohesion between the budesonide particles had effectively been lowered through the conditioning process with magnesium stearate.

## 7.4. Discussion

The fluidisation and dispersion properties of pure salbutamol sulphate and budesonide have been investigated in a previous study [19]. The results showed differing patterns depending on the intrinsic cohesiveness of the drug particles. It was suggested that de-aggregation efficiency of a DPI formulation critically relies on the balance between the internal strength of the agglomerated particles and the aerodynamic diameter (size) of fluidised agglomerates. It was shown that low cohesive materials (e.g. salbutamol sulphate) tend to form small agglomerates, which are difficult to efficiently de-aggregate with the drag forces and kinetic energies generated via passive DPI device. In contrast, highly cohesive materials (e.g. budesonide) tend to form larger airborne agglomerates, which are consequently subjected to greater kinetic energy and drag forces within a DPI device. This was shown to contribute to a more efficient de-agglomeration process than the low cohesive material. However, the strong cohesive forces may form a stable powder bed, which may prevent efficient entrainment upon actuation. In order to assess these mechanistic processes, a particle sizing apparatus operating on airborne powders was used to provide information into the fluidisation, de-aggregation and dispersion properties of particles with modified cohesive behaviour.

Using the Spraytech analyses, a dynamic study of the particle cloud profiles was performed for each formulation sample at 30, 60 and 90L.min<sup>-1</sup>. The plume duration for the various samples were assessed from the cumulative undersize distributions by identifying the time at which 10% ( $t_{10}$ ), 50% ( $t_{50}$ ) and 90% ( $t_{90}$ ) of the sample dose has passed through the Spraytech inhalation cell. In addition, the effective emitted dose of each formulation was calculated from the measurement of the weighted dose and the recovered drug after each Spraytech experiment. These values were associated to the  $t_{90}$  to describe the actual density of the airborne particle clouds. Resulting emission time span and plume density of salbutamol sulphate and budesonide formulations are illustrated in Figure 7.7 and 7.8, respectively.

At 30L.min<sup>-1</sup>, the discharge of micronised salbutamol sulphate and co-processed salbutamol formulations were similar, as 90% of the samples were emitted between 2.6s and 3s. The long window of particle emission resulted in low cloud densities around 2000 $\mu\text{g.s}^{-1}$ . An incremental increase in the flow rate from 30 to 90L.min<sup>-1</sup> gradually reduced the plume duration for each of the four salbutamol samples. Since the emitted dose increased as a function of flow rate (Table 1), the subsequent cloud density progressively increased from 5000 $\mu\text{g.s}^{-1}$  for micronised salbutamol sulphate to 8000 $\mu\text{g.s}^{-1}$  for the MgST-conditioned salbutamol sulphate.

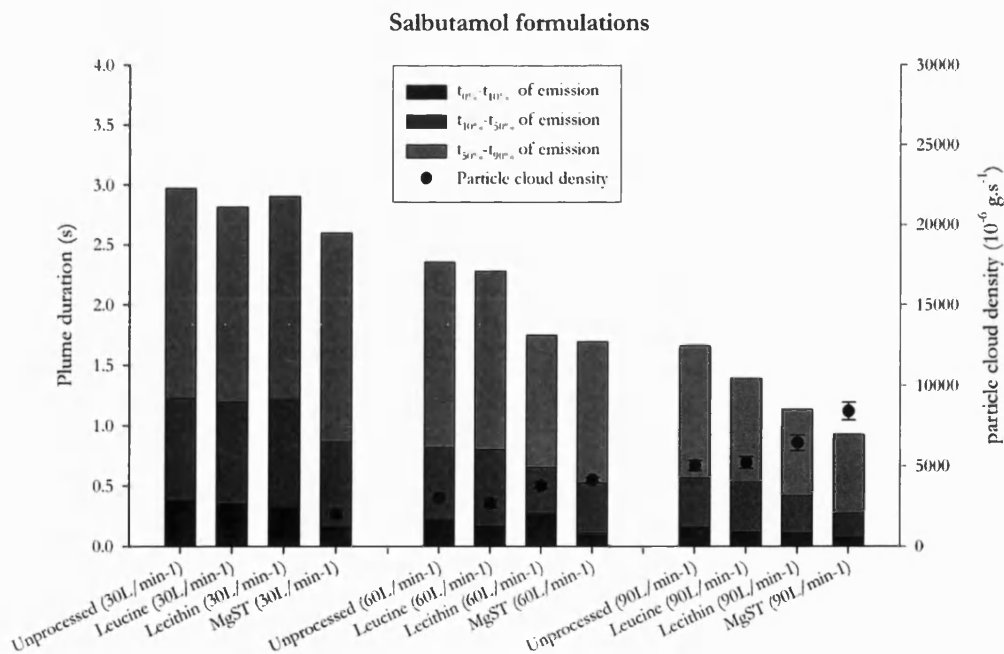


Figure 7- 7: Plume duration and density of salbutamol sulphate formulations.



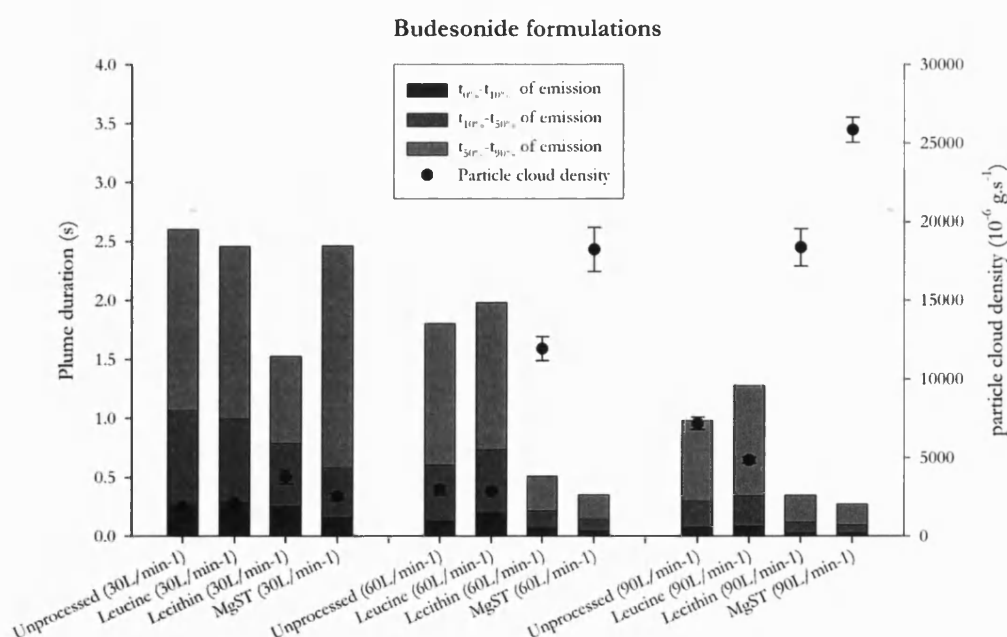


Figure 7- 8: Plume duration and density of budesonide formulations.

At identical flow rates, the budesonide formulations generally passed through the Spraytech cell faster than the salbutamol formulations. At  $30\text{L}\cdot\text{min}^{-1}$ , the 50<sup>th</sup> percentile of emission time was attained in about 1s for micronised budesonide, with a decreasing gradient from leucine-mechanofused, lecithin-mechanofused to MgST-mechanofused. Surprisingly, budesonide fused with MgST fully emitted in approximately 2.5s when it was anticipated that this sample would re-suspend the fastest. At this stage, it is not clear why such incongruity was observed other than a potential experimental variability occurring at low flow rate. At higher flow rate, however, the choice of force control agent dramatically affected the rate of particle emission. The  $t_{50}$  of micronised budesonide and budesonide-leucine was reached after 0.6 seconds of device actuation at  $60\text{L}\cdot\text{min}^{-1}$ , for an overall cloud density of  $2900\mu\text{g}\cdot\text{s}^{-1}$ . In the meantime, the whole emitted dose of the budesonide samples treated with either lecithin or MgST was released in 0.5s. Due to this very short time of emission, cloud densities greatly increased from an average  $2900\mu\text{g}\cdot\text{s}^{-1}$  for the untreated material to  $12,000\mu\text{g}\cdot\text{s}^{-1}$  and  $18,000\mu\text{g}\cdot\text{s}^{-1}$  for the lecithin and MgST coated materials, respectively. Increasing the flow rate to  $90\text{L}\cdot\text{min}^{-1}$  further accentuated this discrepancy. As the budesonide samples were discharged faster and in greater quantity, the measured cloud densities of lecithin

and MgST-based compositions reached very high concentrations of  $18,000\mu\text{g}\cdot\text{s}^{-1}$  and  $26,000\mu\text{g}\cdot\text{s}^{-1}$ , respectively. In fact, lecithin and magnesium stearate had a similar effect on the plume duration for both drugs, although to different extents. Their anti-adherent or anti-friction aptitudes seemed to generate a greater degree of flowability. This resulted in more efficient fluidisation and entrainment from the capsule and device. Such characteristics would undoubtedly have serious implications on the re-dispersion behaviour of the materials and resulting lung delivery efficiency.

Inter-particulate forces of ternary blends composed of a drug, a force control agent (leucine, lecithin and MgST) and fine lactose were investigated previously for salbutamol sulphate (Chapter 5) and budesonide (Chapter 6) using the colloid probe AFM technique together with the novel cohesive-adhesive balance (CAB) analysis procedure. From these data, it was possible to deduce the variations in drug cohesion upon the introduction of the FCAs. It is important to stress, however, that experiments were performed with compacted tablet substrates, leading to notable variation in surface roughness and consequent higher variability in interaction force measurements. A summary of the inferred ratios of cohesion for salbutamol sulphate and budesonide formulations is shown in Table 2.

	% Ratio of cohesion ( $f_{\text{coh. conditioned drug}}/f_{\text{coh. micronised drug}}$ )	
	Salbutamol-sulphate	Budesonide
Micronised drug	100	100
Drug-Leucine	$78.23 \pm 3.55$	$16.14 \pm 2.87$
Drug-Lecithin	$94.67 \pm 2.08$	$19.54 \pm 1.75$
Drug-MgST	$75.95 \pm 2.57$	$11.45 \pm 1.84$

Table 7- 2: Variations in drug cohesiveness by co-processing drug and force control agent by mechanofusion.

Results suggested that conditioning salbutamol sulphate with leucine or MgST caused a decrease in interaction forces of 21.77% and 24.05%, respectively. The influence of the conditioning of the salbutamol sulphate particles with lecithin was not so evident, with a slight decrease of 5.63%. The affect of conditioning more cohesive material such as budesonide with the force control agents were more apparent with a dramatic drop of more than 80% in particle interaction forces. However, these percentages should be interpreted carefully as they are calculated relatively to the initial cohesive force measurements of the micronised drugs. According to these data, binding strengths of both micronised salbutamol sulphate and budesonide significantly decreased when coated with a force control agent via mechanofusion.

In order to relate the reduction in blend cohesiveness to aerosol performances, a summary of the device retention, fine particle fraction (% respirable particle of the emitted dose) and total fine particle fraction (% respirable particle from total recovered dose) of the salbutamol sulphate and budesonide blends is shown in Figure 7.9 and 7.10, respectively.

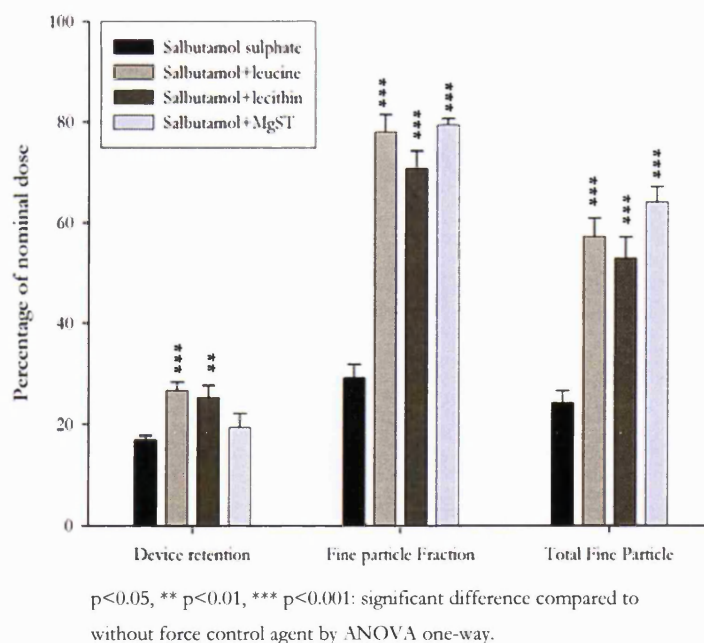


Figure 7- 9: Fine particle fraction and emission efficiency of salbutamol sulphate formulations (mean  $\pm$  S.D., n=3).

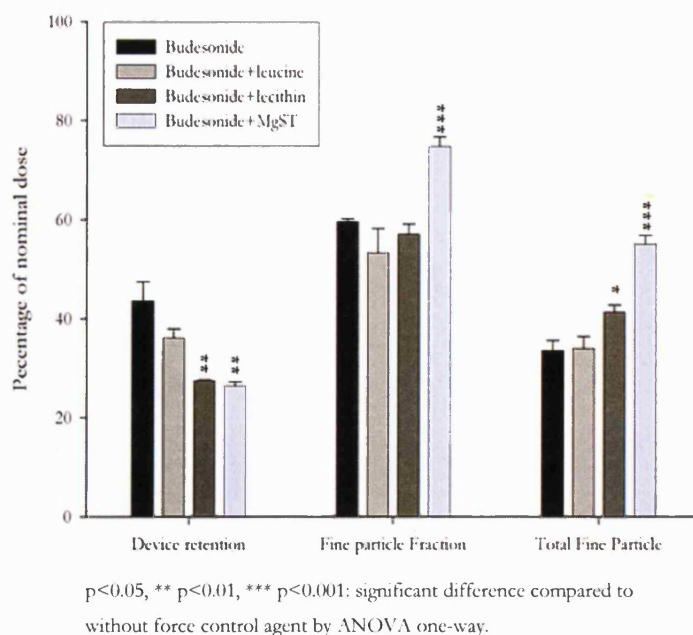


Figure 7- 10: Fine particle fraction and emission efficiency of budesonide formulations (mean  $\pm$  S.D., n=3).

A clear change in the salbutamol sulphate delivery performance was observed as a result of the drug conditioning with FCAs and the subsequent reduction in particle cohesiveness. The device retention slightly increased for the salbutamol sulphate mechanofused with leucine lecithin or MgST (26.75%, 25.28% and 19.40%, respectively) when compared to pure salbutamol sulphate (16.91%). These results were analogous to the results obtained in Table 1 for the Spraytech analyses. It is suggested that the loss in kinetic energy for an individual particle compared to an agglomerated system may explain the slight reduction in the percentage of emission. More striking, however, was the increase in %FPF by mechanofusing the salbutamol sulphate with the FCAs. The fine particle fraction increased from 29.18% to 78.03% for the conditioning of salbutamol sulphate with leucine, 70.79% for salbutamol sulphate-lecithin and 79.42% for salbutamol sulphate-MgST. It is suggested that for these conditioned particles, the salbutamol bonds weaken to such an extent that the powder bed was more effectively fluidised and dispersed upon actuation, therefore contributing to this convincing increase in aerosol performances. Consequently, the

respirable fraction of the total dose increased from 24.26% to 57.19% for the conditioning of salbutamol sulphate with leucine, 52.94% for salbutamol sulphate-lecithin and 64.03% for salbutamol sulphate-MgST.

Noticeable variations in aerosol performances were also discerned for the conditioned budesonide blends (Figure 9B). The device retention decreased from 43.18% to 36.25% for the conditioning of budesonide with leucine, 28.25% for budesonide-lecithin and 26.46% for budesonide-MgST. These results were again in good accordance with the Spraytech analyses at 60Lmin. This enhanced particle emission was expected from the ratios of cohesion previously mentioned since the FCAs contributed to reduce the drug particle cohesiveness. As the powder bed strength weakened, the conditioned drug particles became more sensitive to the drag forces generated upon patient actuation ensuring more effective fluidisation and re-dispersion. The highest %FPF of the emitted dose was obtained for formulations budesonide particles coated with MgST (74.80%). The addition of either leucine or lecithin did not contribute to improve the %FPF and led to similar values than for pure budesonide (~60%). This was corroborated with SEM micrographs of the conditioned budesonide particles with leucine and lecithin, which suggested that the processed particles formed agglomerates.

It should be noted that as the ratio of cohesion decreases as a result of conditioning the drug particles, so does the size of the airborne agglomerates. This raises the issue of the conflicting mechanisms of reduction in drag forces and impaction energy acting on the agglomerates concomitant to the reduction in agglomerate binding strength. This may explain that no major increase in %FPF such as observed with the conditioned salbutamol sulphate blends occurred with the conditioned budesonide blends. Nevertheless, due to an increase in percentage in particle emission, the conditioning of budesonide with either lecithin or MgST contributed to significantly improve the total fine particle fraction (38.74% and 55.01%, respectively).

## 7.5. Conclusions

Force control agents (leucine, lecithin and magnesium stearate) were used to modify the physico-chemical properties of two model respirable drugs (salbutamol sulphate and budesonide). Powders were co-processed using a Mechanofusion system whereby high shear forces ensured a nanometre thick coating of the specific components of the formulation.

Particle size analyses performed on the airborne powders using a Spraytech system revealed dramatic variations in rate of particle emission, upon device actuation, between treated and untreated drug particles. The anti-adherent or anti-friction aptitudes of the FCAs seemed to generate increased flowability of the pharmaceutical materials, especially with the addition of lecithin or MgST. A considerable time reduction in powder bed fluidisation and increased entrainment efficiency was observed.

In-vitro measurements performed on both treated and untreated salbutamol sulphate revealed striking improvements in aerosol deposition by mechanofusing an FCA with the drug particles. By physically disrupting the drug interparticulate interactions, the formulatory procedure led to a critical state in drug cohesiveness that allowed more effective de-agglomeration. For budesonide, although no variation was observed in %FPF, a net decrease in device retention due to a reduction in powder bed strength contributed to significantly increase the drug respirable fraction.

In summary, an improved de-agglomeration and entrainment of both drugs was achieved by selecting a force control agent in conjunction with a mixing procedure capable of producing effective nano-layer coating.

## 7.6. References

- [1] M. P. Timsina, G. P. Martin, C. Marriott, D. Ganderton, and M. Yianneskis. Drug-delivery to the respiratory tract using Dry Powder Inhalers. *Int. J. Pharm.* **01**: 1-13 (1994).
- [2] P. Baldrick and D. G. Bamford. A toxicological review of lactose to support clinical administration by inhalation. *Food Chem. Toxicol.* **35**: 719-733 (1997).
- [3] J. S. Patton and R. M. Platz. Pulmonary delivery of peptides and proteins for systemic action. *Adv. Drug Deliv. Rev.* **8**: 179-228 (1992).
- [4] J. M. Ames. Control of the Maillard reaction in food systems. *Trends Food Sci. Tech.* **1**: 150-154 (1990).
- [5] A. M. Edwards and A. Chambers. Comparison of a Lactose-Free Formulation of Sodium Cromoglycate and Sodium Cromoglycate Plus Lactose in the Treatment of Asthma. *Curr. Med. Res. Opin.* **11**: 283-292 (1989).
- [6] A. J. Hickey, N. M. Concession, N. M. Van Oort, and R. M. Platz. Factors influencing the dispersion of dry powders as aerosols. *Pharm. Tech.* **8**: 58-82 (1994).
- [7] M. J. Clarke, M. J. Tobyn, and J. N. Staniforth. The formulation of powder inhalation systems containing a high mass of nedocromil sodium trihydrate. *J. Pharm. Sci.* **90**: 213-223 (2001).
- [8] J. Broadhead, S. K. Edmont Rouan, and C. T. Rhodes. The spray drying of pharmaceuticals. *Drug Dev. Ind. Pharm.* **18**: 1169-1206 (1992).
- [9] P. York. Strategies for particle design using supercritical fluid technology. *Pharm. Sci. Techn. T.* **2**: 430-440 (1999).

- [10] L. Yu. Amorphous pharmaceutical solids: preparation, characterization and stabilization. *Adv. Drug Deliv. Rev.* **48**: 27-42 (2001).
- [11] A. Columbano, G. Buckton, and P. Wikeley. A study of the crystallisation of amorphous salbutamol sulphate using water vapour sorption and near infrared spectroscopy. *Int. J. Pharm.* **237**: 171-178 (2002).
- [12] J. C. Feeley, B. Y. Shekunov, A. H. L. Chow, and P. York. Surface and aerodynamic characteristics of particles for inhalation produced using supercritical fluid technology., *Drug Delivery to the Lung XI*, London, 2000.
- [13] E. R. Beach, G. W. Tormoen, J. Drelich, and R. Han. Pull-off force measurements between rough surfaces by atomic force microscopy. *J. Colloid Interface Sci.* **247**: 84-99 (2002).
- [14] H. Schiavone, S. Palakodaty, A. R. Clark, P. York, and S. T. Tzannis. Evaluation of SCF-engineered particle-based lactose blends in passive dry powder inhalers. *Int. J. Pharm.* **281**: 55-66 (2004).
- [15] P. Begat, M. Green, D. A. V. Morton, A. Whittock, and J. N. Staniforth. PowderHale: A Novel High Performance Dry Powder Inhaler Formulation Technology for Targeted and Systemic Drug Delivery. *Drug Delivery to the Lung XII* 119 (2001).
- [16] J. N. Staniforth and D. A. V. Morton. Powder Technology Research Leading to Improvements in Inhaler Products. *Powder Science and Engineering* **34**: 60-64 (2002).
- [17] R. Pfeffer, R. N. Dave, D. G. Wei, and M. Ramlakhan. Synthesis of engineered particulates with tailored properties using dry particle coating. *Powder Technol.* **117**: 40-67 (2001).



- [18] P. Begat, D. A. V. Morton, J. N. Staniforth, and R. Price. The cohesive-adhesive balances in dry powder inhaler formulations I: Direct quantification by atomic force microscopy. *Pharm. Res.* **21**: 1591-1597 (2004).
- [19] P. Begat, D. A. V. Morton, J. N. Staniforth, and R. Price. The cohesive-adhesive balances in dry powder inhaler formulations II: Influence on fine particle delivery characteristics. *Pharm. Res.* **21**: 1826-1833 (2004).

# Chapter 8

## General Conclusions

### 8.1. Introduction

The development of efficient powder aerosols for inhalation therapy demands the formulation of drug as a simple or compound powder which disaggregates into an aerosol containing a large fraction of respirable particles to reach the deep lung. The efficiency of particle aerosolisation and de-agglomeration rests on a critical balance of two competing physical mechanisms. The intrinsic short-ranged forces acting between the solid particles contribute to the metastable agglomeration of the powder formulation and its stability during storing and handling. Conversely, the aerodynamic forces generated by the patient's inspiration through the device provide the necessary energy required to yield effective de-agglomeration and produce respirable particles. The prediction and control of the interparticulate forces in dry powder inhaler (DPI) formulations for inhalation are therefore of uppermost importance in the improvement of drug delivery performances.

The first aim of this study was to develop a novel technique capable of quantifying the degree of interaction between the various components of a given dry powder formulation. From this knowledge, model formulations were tested in terms of their flowability, dispersibility and aerosolisation with the purpose of relating the formulation behaviour to its inherent balance of interactive forces. Finally, the selective introduction of force control agents (FCA) to reduce specific inter-particulate interactions within a DPI formulation was investigated as a possible means of improving drug delivery to the lung.

## 8.2. Summary

The inter-particulate forces between two drugs, salbutamol sulphate and budesonide, and lactose were assessed by colloid probe AFM technique. The tailoring of well-defined substrate surfaces by crystallisation minimised intra-variations in the contact area of a colloid probe. This enabled direct quantification of the relative adhesive-cohesive contributions within a model dry powder inhaler formulation. From this knowledge, a novel cohesive-adhesive balance (CAB) analysis procedure was developed in order to predict formulation characteristics and behaviour from its relative interactive force ratios. A clear hierarchy in interaction forces observed between various materials. The CAB graph analyses anticipated that the formulation of budesonide with a lactose carrier would largely be governed by the relatively strong cohesiveness of the drug whilst the formulation of salbutamol with lactose would principally hinge on the adhesive forces between the two compounds.

Aerodynamic particle analyses together with aerosol deposition studies performed on pure micronised salbutamol sulphate and micronised budesonide provided a plausible explanation in the fluidisation and aerosolisation properties between low and high cohesive particles, modelled on the relationship between cohesion, metastable agglomerate size and the resulting aerodynamic mechanisms acting on the fluidised agglomerates such as drag forces and impaction/collisions. It is suggested that during the de-aggregation and dispersion process, the internal binding forces of the agglomerate and the drag forces generated within the device reach equilibrium. This subsequently would lead to the suspension of the elutriation process. The characteristic properties of the metastable aggregates would be directly dependant on the airflow characteristics via the inhaler device and the cohesive properties of the agglomerated particles.

The formulation of these drugs with a fine particle lactose carrier generally contributed to a better emission from the device, principally due to the aerodynamic properties of the carrier particles. However, the relative strong adhesion between salbutamol sulphate and lactose measured from the CAB graph analyses precluded an effective drug particle detachment. Therefore, notwithstanding exemplary low device retention,

the overall performances of the carrier-based formulation were disappointing since most of the drug particles remained attached to the carrier and did not reach a respirable size. In contrast, the highly cohesive nature of budesonide resulted in an unstable carrier based formulation. The mediocre affinity between drug and carrier resulted in the rapid separation of the budesonide agglomerates from the lactose surface, introducing a similar dispersion mechanism as for the cohesive drug only formulation.

In order to improve dry powder formulation delivery characteristics, the influence of force control agents (FCAs) on the properties and performances of model carrier-based formulations was investigated. Three FCAs were chosen for their low surface energetic properties: leucine, lecithin and magnesium stearate. The cohesive and adhesive dependencies were controlled by conditioning either the drug or the carrier with an FCA before mixing in order to create selective modifications of the interparticulate interactions within the dry powder formulation. This was achieved by first using a high energetic process (Mechanofusion) following a low energetic process (Turbula blending). Controlling the interaction forces led to dramatic changes both on a microscopic level (van der Waals forces) and on a macroscopic level (formulation homogeneity and aerosolisation patterns). Radical modifications in the behaviour of the formulation were dependant on whether the FCAs were first conditioned with the drug or the lactose. This influence was predicted by the CAB-graph analyses and confirmed experimentally via in-vitro deposition studies. A distinct improvement in the salbutamol sulphate and budesonide formulation performances (emission and aerosolisation) was obtained when a weak adhesive system was obtained.

Alternatively, the same conditioning procedure was performed on pure micronised salbutamol sulphate and budesonide to investigate the effect of modifying the physico-chemical properties of the drugs on their flowability, dispersibility and aerosolisation characteristics. Results indicated that the introduction of FCAs dramatically reduced particle emission time, suggesting a very effective fluidisation of the powder bed and consequent rapid aerosolisation. Accordingly, *in vitro* studies revealed net improvements in aerosol deposition patterns by mechanofusing an FCA with the drug particles.

### 8.3. Future Work

It has been shown that controlled crystallisation of model substrates for AFM studies provided the opportunity to directly quantify the interaction forces between a single particle and the crystal substrate. However, the 3-D arrangement of the molecules in the crystal lattice resulted in specific chemical groups being exposed at the surface of the crystal faces. Further investigations into the potential discrepancies in interactions between two materials upon the choice of crystal face for AFM analyses are required.

Notwithstanding, only  $\alpha$ -lactose monohydrate was considered as a carrier in this study. Further CAB graph and complementary *in vitro* analyses should focus on the use of alternative excipients as a choice of carrier to help in determining the best suitable candidate for a specific active agent.

Additionally, a more complex matrix of active agent, carrier and fines should be investigated from both a microscopic (CAB assessment) and macroscopic approach (fluidisation and aerosolisation properties). The concomitant use of carrier and fines differing in their chemical nature could provide a desirable synergetic effect in producing effective dry powder formulations for inhalation.